Functional characterization of MuSK, receptor tyrosine kinase required for the formation and the maintenance of nerve-muscle synapses.
In vivo and *in vitro* approaches.
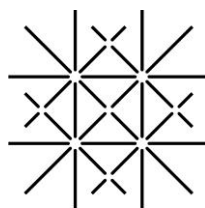
INAUGURALDISSERTATION

zur
Erlangung der Würde eines Doktors der Philosophie
vorgelegt der
Philosophisch-Naturwissenschaftlichen Fakultät
der Universität Basel

von

Marcin Maj

aus Skawina, Polen
Basel, 2008

UNI
BASEL

Genehmigt von der Philosophisch-Naturwissenschaftlichen Fakultät auf Antrag von:

Prof. Dr. Markus A. Rüegg
Dissertationsleitung

PD Dr. Thomas Meier
Koreferat

Prof. Dr. Martin Spiess
Vorsitz

Basel, den 16. April 2008

Prof. Dr. Hans Peter Hauri
Dekan der Philosophisch-Naturwissenschaftlichen Fakultät

While the sun hangs in the sky and the desert has sand
While the waves crash in the sea and meet the land
While there's a wind and the stars and the rainbow
Till the mountains crumble into the plain (...)

(...) We'll keep on trying
Tread that fine line
We'll keep on trying
Till the end of time (...)

(...) If there's a God or any kind of justice under the sky
If there's a point, if there's a reason to live or die
If there's an answer to the questions we feel bound to ask (...)

(...) We'll keep on trying
Tread that fine line
We'll keep on trying
Till the end of time (...)

(…)And whatever will be, will be…

(Innuendo by Queen, 1991)

I'm still alive
Must have been a miracle
It's been a hell of ride
Destination still unknown
It's a fact of life (...)

(...) I'm a runaway train on broken track
I'm a ticker on a bomb, you can't turn back this time
That's right
I got away with it all and I'm still alive
Let the end of the world come tumbling down
I'll be the last man standing on the ground
As long as I got blood rush trough my veins
I'm still alive (...)

(Alive by Michael Lee Aday – Meatloaf –, 2006)

All this work is dedicated to

Kasia, Grzegorz and my Parents

TABLE OF CONTENTS

SUMMARY

The developing neuromuscular junction (NMJ) serves as one of the best model systems for studying synapse formation since changes in shape, size, and molecular composition can be followed with high spatial and temporal resolution.

Formation of the NMJ depends on coordinated interactions between nerve terminals and muscle fibres [1] and requires reciprocal signals from both cells to efficiently regulate all the events taking place during its development. This includes synapse-specific gene expression, generation of action potentials and stabilization events leading to the formation of a sophisticated apparatus which ensures that the muscle fibre is provided with trophic factors as well as electrical stimuli. The receptor tyrosine kinase MuSK and its natural ligand, a neuron-specific isoform of the extracellular matrix molecule agrin, are considered to play a fundamental role in the formation and maintenance of the NMJ. In cultured myotubes, MuSK is activated by neural agrin, and this causes its phosphorylation and results in the formation of AChRs clusters on the cell surface [2-5].

The present study discusses different approaches to understand better the mechanisms of how the NMJ is formed and maintained.

In the first project, we addressed the question of MuSK – neural agrin interaction and the necessity for an additional component of the agrin receptor complex. We generated transgenic mice overexpressing MuSK or neural mini-agrin as well as both proteins throughout the entire muscle fibre. We found evidence that in muscle cells MuSK is sufficient to respond to neural agrin with no necessity of any additional co-receptor protein. We also show that Dok-7, a MuSK adaptor protein, limits the formation of ectopic postsynaptic like structures in innervated muscle. From this, we conclude that it is very likely that in muscle cells MuSK serves as a functional receptor for neural agrin.

The second project refers to the regulation of the NMJ formation. We found that signal transduction downstream of agrin involves the mitogen-activated protein kinase (MAPK) pathway, particularly ERK1/2 and JNK. It involves MuSK signaling, requires Dok-7 and is ErbB-independent. We also show that MAPK phosphatase-1, MKP-1, plays a crucial regulatory role in formation of the nerve-muscle connection.

Results of the third project describe that a miniaturized form of agrin is able to fully rescue perinatal death of agrin-deficient mice, and that this function does not depend on local deposition of agrin at synapses. Moreover, we show that acetylcholine together with neural agrin stabilizes the postsynaptic structures at the NMJ.

The function of agrin in CNS was our main interest in the fourth project. Using

agrin-deficient mice with a transgenic reconstitution of the expression of neural agrin by motor neurons, we found that in the brain, agrin is localized to the excitatory synapses. Lack of agrin resulted in a strong reduction of synaptic structures in the cerebral cortex coinciding with the attenuation of the frequency of miniature postsynaptic currents. Additionally we found that muscle specific kinase MuSK is also expressed in the brain, thus possibly involved in the formation of the nerve-nerve connections. Finally, we show that agrin function involves MAP kinase signaling.

TABLE OF ABBREVIATIONS

Ach	Acetylcholine
AChE	Acetylcholine esterase
AChR	Acetylcholine Receptor
Btx	α-Bungarotoxin
Cdc42	Cell division cycle 42 (GTP binding protein)
CNS	Central Nervous System
CRD	Cysteine Rich Domain
CRE	cAMP Responsive Element
Dok-7	Docking Protein 7 (phosphotyrosine binding protein)
ErbB	Receptor Tyrosine Kinase for neuregulins
GABP	Growth Associated Binding Protein
Ig	Immunoglobin
MASC	Myotube Specific Accessory Component
MU	Motor Unit
MuSK	Muscle Specific Kinase
N-CAM	Neural Cell Adhesion Molecule
NMJ	Neuromuscular Junction
PAK1	P21-activated kinase
PH	Pleckstrin Homology Domain
PTB	Phosphotyrosine Binding Domain
Rac1	ras-related C3 botulinum toxin substrate 1 (GTP binding protein)
RATL	Rapsyn Associated Transmmbrane Linker
RTK	Receptor Tyrosine Kinase
TKD	Tyrosine Kinase Domain

CHAPTER I

GENERAL INTRODUCTION

1.   THE SYNAPSE

In every living organism, sophisticated and highly efficient mechanisms are required to enable communication between cells. In case of neuronal cells, such communication is made possible by synapses, the functional contacts between neurons. The term "synapse" was introduced at the turn of the 20th century by Charles Sherrington to describe a specialized zone of contact at which one neuron communicates with another. The meaning of the word "synapse" comes from its Greek derivative "synaptein" ("syn" - "together", "haptein" - "to fasten") [6]. Two different types of synapses, electrical and chemical, have been found in neurons based on their mechanism of transmission. At electrical synapses, current flows through gap junctions, which are specialized membrane channels that connect two cells. In contrast to this, chemical synapses enable cell-to-cell communication via the secretion of neurotransmitters, the chemical agents released by the presynaptic neurons to produce secondary current flow in postsynaptic neurons by activating specific receptor molecules [7]. Chemical synapses exist also outside the central nervous system. For example, axons of the autonomic nervous system innervate glands, smooth muscles and hearth. It is also true for skeletal muscle where chemical synapses occur between axons of motor neurons of the spinal cord and muscle fibres (Fig.1) within the functional structures, called motor units (MU), representing the close connection between neurons and muscle.

1.1 MOTOR UNIT

The motor unit (MU) represents the smallest part of a muscle which can be activated selectively by the central nervous system and is defined as a motor neuron together with all the muscle fibres that it innervates [8] (Fig 1). MUs are considered to be the basic functional units of the neuromotor system. They can vary widely in size, having innervation ratios (i.e., the number of muscle fibres per motor neuron) ranging from a few fibres per motor neuron in some extraocular muscles to thousands of fibres per motor neuron in some large limb muscles. In muscles from normal animals, the fibres within a MU show relatively similar, although not identical, biochemical and histochemical properties [9]. Several schemes have been developed for classifying MUs into distinct groups or type based on additional physiological properties. According the presence or absence of decline in force output during low-frequency tetanization as well as relative resistance to fatigue during a normal stimulation, the motor units have been classified into FF units (fast twitch, fatigable), FR units (fast twitch, fatigue resistant) and S units (slow twitch) [10, 11]. It is worthy to mention that one motor neuron can innervate from 1 to over 2000 muscle fibres, but each muscle fibre receives inputs from only one motor neuron [7]. An important anatomical and functional part of the MU is a synapse formed in the place of contact of motor neuron and muscle fibre, called neuromuscular junction (NMJ), which has many of the structural features of the chemical synapses in the central nervous system [12].
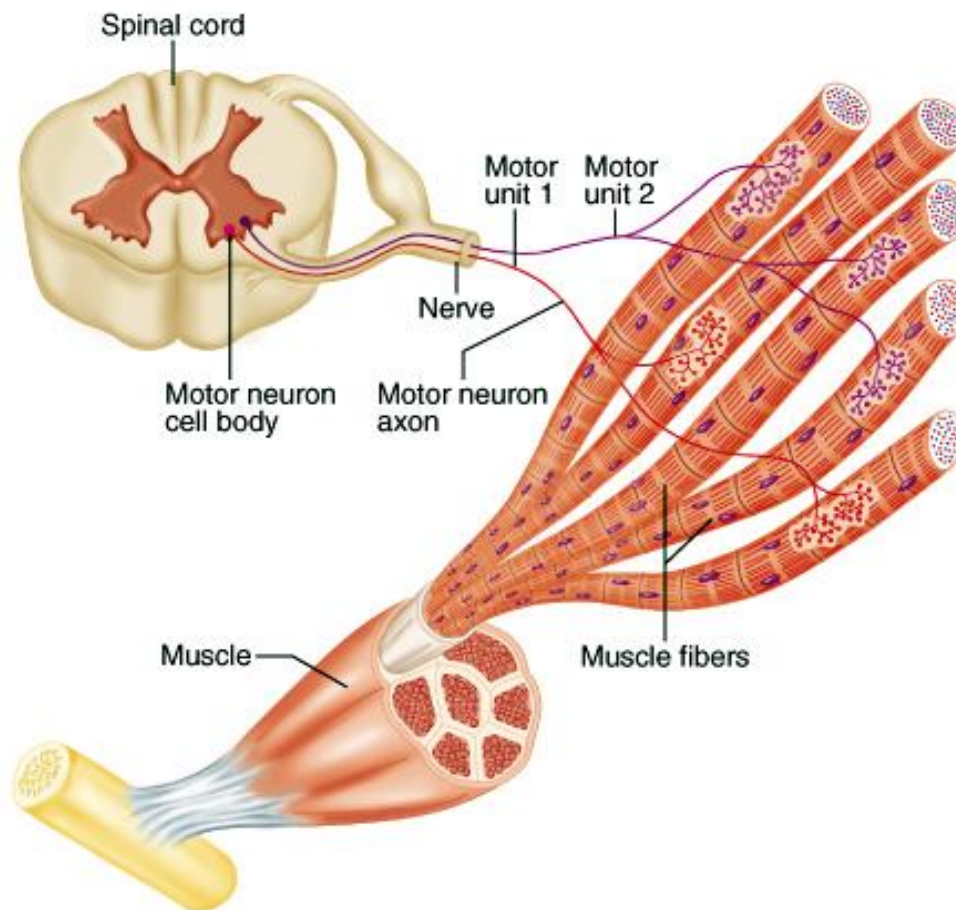
Figure 1 │A motor unit

Muscle fibres are innervated by motor neurons whose cell bodies are located in the spinal cord. Their axons leave the spinal cord and are distributed to the motor nerves. Each motor axon branches several times and innervates many muscle fibres. One nerve ending innervates one muscle fibre. The combination of a single motor neuron and all the muscle fibres it innervates is called a motor unit (MU). (from B. Cummings, 2001; available in internet: http://www.etsu.edu/cpah/hsci/forsman/Histology%20of%20musclefor%20web_files/image015.jpg)

1.2 NEUROMUSCULAR JUNCTION

The neuromuscular junction (NMJ), a synapse formed between motor neuron and muscle fibre, is a complex structure that allows the efficient communication between those two cells (Fig.1 and Fig.2). Its formation and activity ensures muscle fibres to be provided with trophic factors as well as electrical impulses (via the chemical neurotransmitter, acetylcholine) that generates a muscle action potential. Thanks to its unique anatomical properties, the NMJ is a very useful model system for studying synapse formation and maintenance.

Three cell types are involved in the formation and maintenance of the NMJ; motor neurons, muscle fibres and Schwann cells. Synaptic portions of all three cells are highly specialized, containing high concentrations of organelles and molecules found also at low concentrations extrasynaptically and this is one of the cardinal features of the NMJ structure. Looking closely, the following main elements can be distinguished within the NMJ: the presynaptic region containing the nerve terminal, the synaptic cleft and the postsynaptic surface, which is a part of muscle fibre [13] (Fig.2).

The motor nerve terminal is specialized for neurotransmitter release. It contains a large numbers of 50-nm-wide synaptic vesicles filled with a neurotransmitter, acetylcholine, as well as numerous mitochondria providing the energy for synthesis and release of neurotransmitter. The terminal is polarized, with most of the vesicles clustered in the half-terminal that faces the muscle fibre, and most of its mitochondria in the half-terminal beneath the Schwann cell. Many of the vesicles are further focused at dense patches on the presynaptic membrane, called active zone, at which vesicles fuse with the

membrane to release their contents into the synaptic cleft [14].

The postsynaptic membrane is specialized to respond rapidly and reliably to neurotransmitter released from the overlying nerve terminal. The characteristic ultrastructural features of the postsynaptic muscle membrane is its local immersion into shallow gutters beneath the nerve terminal, and then subsequent invagination into ∼1-µm-deep folds that open directly opposite to the presynaptic active zones. Many types of molecules including nicotinic receptors for acetylcholine (AChRs), ion channels and cell adhesion molecules playing their roles at the NMJ, are selectively localized to individual parts of the postsynaptic folds. AChRs together with rapsyn (a 43-kDa, AChR-associated protein) are mainly localized to the crests and partway down the sides of the folds (in concentration higher than 10,000 molecules per $µm^2$), whereas for example, sodium channels and the neural cell adhesion molecule (N-CAM) are concentrated in the depths of folds [15, 16]. This kind of molecular arrangement at the NMJ is likely to be important to warrant sufficient synaptic transmission [17].

The synaptic cleft is a space of ∼50 nm that separates nerve terminal and muscle fibre plasma membranes. It is comprised of basal lamina, which unsheathes each muscle fibre, passes through the synaptic cleft and extends into the junctional folds. It may also bind receptors on adjacent cell membrane surfaces, providing a means of cell adhesion and signaling among NMJ components [18]. The major components of muscle basal lamina are similar to those of basal laminae throughout the body — collagen IV, laminins, nidogen, and heparan sulfate proteoglycans. However, synaptic and extrasynaptic portions of the basal lamina can differ in their isoform composition. Synaptic basal lamina contains also additional, distinct molecules including a collagen-tailed form of acetylcholinesterase a set of glycoconjugates, as well as signaling molecules (agrin and neuregulin) [19, 20].

Synapsin-I, II
Rab 3a
Rabphilin 3a
Cysteine string
        protein
SV2
Synaptobrevin
Synaptotagmin
Synaptophysin
Vesicular ACh
    transporter
Acetylcholine

S-100
N-CAM
Schwann Cell
Nerve
Terminal

Choline acetyltransferase

α CGRP

Laminin-α2,α4,α5,β2,γ1
Collagen IV-α3,α4,α5
AChE-T, Q
Agrin
Neuregulin
GalNAcβ-X

Muscle
Fiber

Rim
K$^+$ channels
Ca^{++} channels
Syntaxin
SNAP 25

Rapsyn
Utrophin
αDystrobrevin-1
β2-Syntrophin

N-CAM
Na channels

Ankyrin
Dystrophin
αDystrobrevin-2
Syntrophin-α1,β1

AChR-α,β,δ,ε
Integrin α7A,B,β1
Dystroglycan α,β
Sarcoglycan-α,β,γ,δ
MuSK
ErbB2,3,4
GalNAc transferase

Figure 2 │ Neuromuscular junction

A neuromuscular junction (NMJ) is the synapse formed at the place of connection of a motor neuron and a muscle fibre. NMJ is analogous to the synapse formed between two neurons and consists of pre- and postsynaptic parts that are separated by synaptic cleft. A nerve fibre divides into many terminal branches; each terminal ends on a region of muscle fibre called the end plate. Upon stimulation by a nerve impulse, the terminal releases the chemical neurotransmitter acetylcholine from synaptic vesicles. Acetylcholine then binds to the AChR, opens it, and sodium ions flow through the muscle fibre plasma membrane. This initiates the end-plate potential, the electrical event that leads to contraction of the muscle fibre.

(adapted from Sanes and Lichtman, Ann Rev Neurosci, 1999)

1.2.1   DEVELOPMENT OF NMJ

For the proper development of the NMJ, synchronized cooperation of different cell types, which must reach the appropriate place in appropriate time and developmental stage, is necessary. It requires also a series of reciprocal inductive interactions between the motor neuron and the muscle cell that culminate in the precise juxtaposition of a highly specialized presynaptic nerve terminal with a complex postsynaptic endplate on the muscle surface

Muscle fibres are multinucleated cells derived from mesodermal precursor cells that acquire a myogenic identity in the dermatomyotomal portion of the somites [21]. Committed myogenic cells migrate to sites where muscles will form. There they divide, and their postmitotic progeny differentiates into myoblasts. The myoblasts align into "straps," then fuse to form myotubes. Upon fusion, expression of a large number of genes that encode many contractile and signaling molecules is activated [22].

Motor neurons arise in the ventral portion of the neural tube from multipotent progenitors that also give raise to interneurons and glial cells [23]. Motor axons exit the central nervous system through ventral roots or cranial nerves and then run long distances through peripheral nerves to muscles. Motor axons reach target muscles as myoblasts are fusing to form myotubes. When a motor neuron enters a muscle, it loses its myelin sheath and splits into many terminal branches to innervate tens to hundreds of muscle fibres [24] (Fig. 3). These terminal branches run along the myofibres to end at the NMJ. Once the motor axon's growth cone contacts a newly formed myotube, synaptic transmission commences quickly. Initially, however, the efficacy of transmission is extremely low, reflecting the absence of both pre- and postsynaptic specializations. Over a period of about a week, a fully functional (but still immature) synapse forms in which both nerve and muscle are greatly transformed [24] (Fig.3).

Schwann cells, the glia of the peripheral nervous system, are derivatives of the neural crest, which arises from the dorsal margin of the neural tube. While motor neurons and muscle fibres are involved in the formation of pre- and postsynaptic site, respectively, the role of Schwann cells is to form a cap in close apposition to the nerve terminal. With the cap, NMJs can be properly protected, insulated from the environment and provided with trophic factors [24]. Schwann cells play also an important role in the induction of nerve terminal sprouting following partial denervation and it is likely that they also influence the remodeling of the presynaptic nerve terminal during aging [25].

Neuromuscular synaptic transmission is fast and reliable. An action potential in the motor axon always causes an action potential in the muscle cell it innervates. It is partially

thanks to the existence of structural specializations at the NMJ. Its most important specialization is the size. The NMJ is one of largest synapses in the organism. In addition, postsynaptic terminals contain, as mentioned before, a series of shallow folds. Together with the presence of a large number of active zones in the presynaptic nerve ending it ensures that many of neurotransmitter molecules can be focally released onto a large surface of a highly sensitive postsynaptic membrane [12].
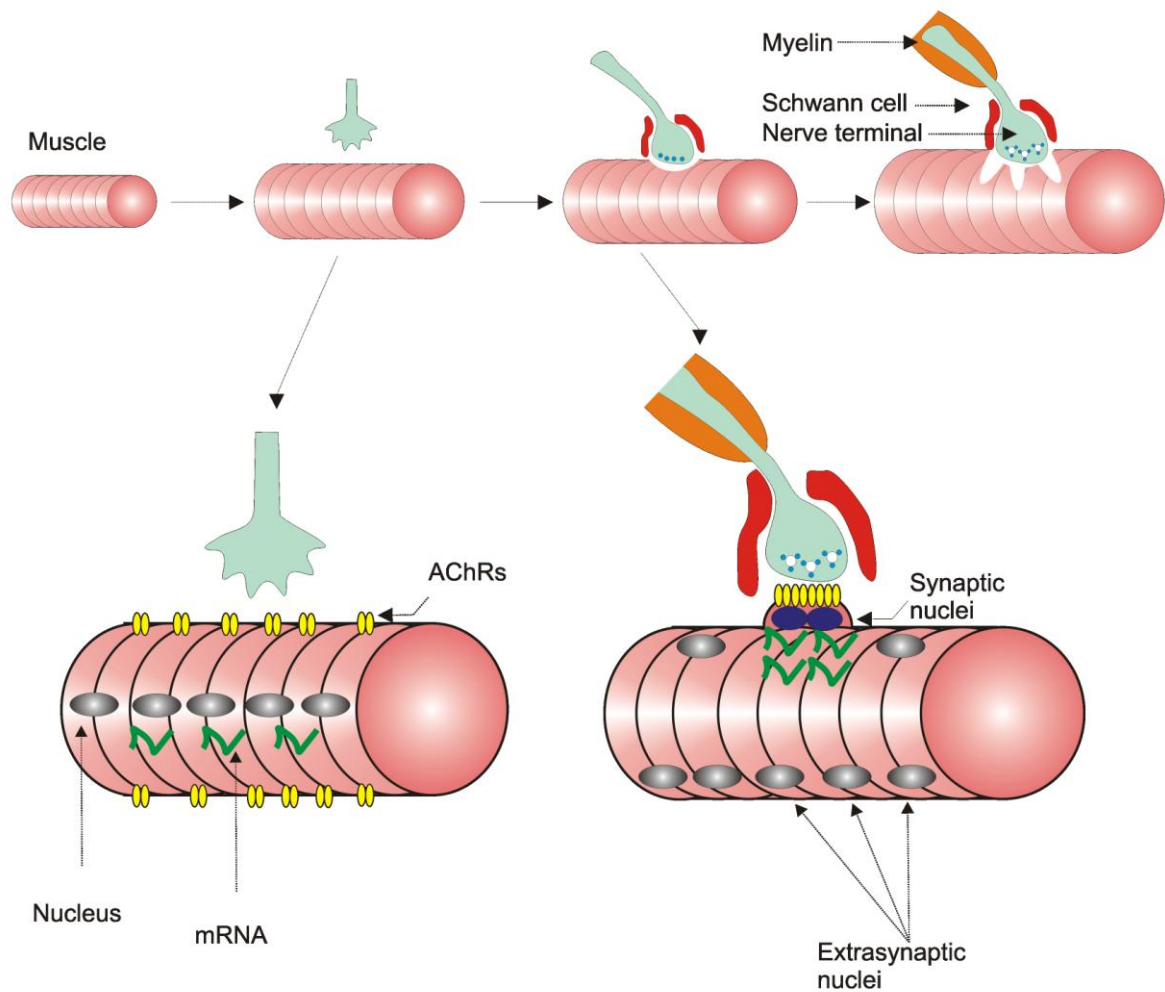
Figure 3 │ Development of neuromuscular junction

(Upper part) The motor axon approaches a newly formed myotube. At the area of contact, the axon differentiates into a motor nerve terminal that is specialized for transmitter release. Schwann cell processes cap the terminal and the muscle forms a complex postsynaptic apparatus.

(Lower part) Acetylcholine receptors (AChRs) are initially present at a moderate level throughout the myotube surface. In adult muscle, by contrast, AChRs are mainly and highly concentrated in the postsynaptic membrane but not extrasynaptically. This clustering involves both redistribution of AChR proteins, and localized synaptic synthesis of AChRs. The local synthesis results from enhanced transcription of AChR genes by subsynaptic nuclei and by repression of extrasynaptic nuclei.

(adapted from Sanes and Lichtman, Nat Rev Neurosci, 2001)

1.3   SIGNALLING AT THE NMJ, MOLECULES

1.3.1   MUSCLE SPECIFIC KINASE MuSK

1.3.1.1   IDENTIFICATION

MuSK (**Mu**scle **S**pecific **K**inase) is a receptor tyrosine kinase (RTK), which plays a crucial role in the formation and maintenance of the NMJ. MuSK has been identified and described for the first time by Valenzuela and collaborators in 1995. In their studies, authors searched for RTKs, that are selectively expressed in skeletal muscle and that are up-regulated upon denervation, based on the idea that denervation could induce the re-expression of RTKs important during embryogenesis as well as of those involved in NMJ plasticity. Initially, MuSK, was found to be expressed exclusively in skeletal muscle [26]; however the subsequent studies have shown MuSK to be present also in the central nervous system, suggesting its possible role in the formation of neuron-neuron connections [27-29].

1.3.1.2   STRUCTURE

The mouse MuSK gene consists of at least 15 exons distributed over 90 kb on chromosome 4 [26]. Several transcriptional start sites have been identified within the MuSK promoter region. The one closest to the coding sequence (designated as nucleotide 1) is thymidine 51 upstream of the translation start site. Transcription may also start at –42 guanosine, –60 cytidine, –89 adenosine and –114 adenosine [30]. In addition, many regulatory elements were found in the MuSK 5'-flanking region. Kim and collaborators have identified four E-box elements, the sequences known to be involved in differentiation-dependent gene expression [30]. Secondly, N-box regulatory elements – sequences involved in synapse-specific gene expression at the NMJ – were also identified in the MuSK promoter region [31]. Finally, a cyclic AMP response element (CRE)-like regulatory element has also been found within MuSK promoter region and described to have an inhibitory influence on MuSK expression [30]. Presence of multiple transcription start sites as well as different regulatory sequences in the MuSK promoter region implies the possibility of controlling of MuSK expression by several regulatory systems.
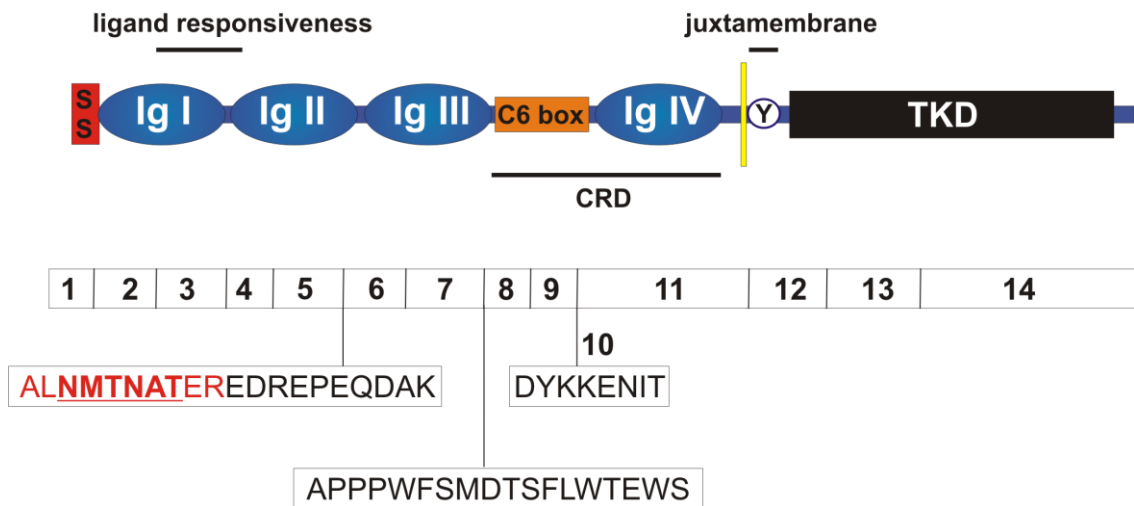
Figure 4 │Structure and exon organization of muscle specific kinase (MuSK)

SS – signal sequence; IgI-IV – immunoglobulin like domains; C6 box – 6 conserved cysteine residues; CRD – cysteine rich domain; Y – juxtamembrane tyrosine residue; TKD – tyrosine kinase domain, NMTNAT – two putative N-glycosylation sites

MuSK mRNA undergoes alternative splicing. Accordingly, distinct cDNAs were isolated encoding slightly different versions of MuSK extracellular domain (Fig. 4). The splice versions differ by the presence or absence of one, two or three different insertions (a 10 amino acid insertion, a 15 amino acid insertion and an 8 amino acid insertion) in the ectodomain. Localizations of exons encoding for the 8 and 10 amino acid splice inserts are conserved in mouse MuSK when compared to human and their sequences display high percentage of identity [26, 32]. No rat or human counterpart for the 15 amino acid exon has been published so far, but in mouse MuSK this sequence is inserted precisely at a splice site reported previously by Hesser and collaborators for a MuSK variant lacking the entire third Ig-like domain [32, 33]. This splice variant of MuSK is the result of elimination of two exons. Interestingly, the MuSK molecule is still fully functional even if the whole third Ig-like domain is missing [33].

Mature MuSK is composed of 860 - 893 amino acids with a predicted (isotopically averaged) molecular weight of 95.6 – 99.6 kDa depending on the splice variant. This includes a signal peptide, an ectodomain, a transmembrane and a cytoplasmic region. The extracellular portion of MuSK consists of four immunoglobulin-like (Ig-like) domains with a C6 box (region with six filogenetically conserved cysteine residues) between the third and the fourth Ig-like domain [26] (Fig. 4). Closer analysis of the sequence containing the C6 box together with the fourth Ig-like domain of MuSK resulted with identification of cysteine-rich domain (CRD), a pattern of ten cysteine residues which is characteristic for Wnt receptors; and is taught to bind Wnt proteins [34-36].

Usually, the extracellular part of receptors serves as the ligand-binding site. It has also been shown for MuSK that the sequence in or near the first Ig-like domain is required for ligand responsiveness [37]. Moreover, the individual residues in this domain (methionine 48, leucine 83, and isoleucine 96) have been identified as critical for ligand-stimulated MuSK activation [38]. The intracellular part of MuSK is composed of twelve subdomains characteristic for functional tyrosine kinases [26].

1.3.1.3   EXPRESSION

MuSK was found to be expressed expressed at low levels in proliferating myoblasts and its expression is induced upon their differentiation and fusion [26]. During development of muscle, as myoblasts fused already to form primary myotubes, MuSK expression remains at high levels throughout the entire muscle fibre and is dramatically down regulated after innervation. In the adult muscle, MuSK mRNA is locally transcribed by and concentrated around subsynaptic nuclei (group of nuclei positioned underneath the NMJ) similarly to other "synaptic genes" (e.g. AChR subunit genes). In comparison to this, extrasynaptic nuclei do not express MuSK as well as the other "synaptic genes". Similarly to AChR, MuSK expression at both mRNA and protein level increases after denervation or blockage of electrical activity [26]. Following denervation, MuSK transcripts become widely detectable in the entire muscle fibre and restriction of transcription of the MuSK gene only to subsynaptic nuclei is abolished. After re-innervation (3 weeks after sciatic nerve crush) MuSK expression is again localized to subsynaptic nuclei [26, 39].

At the NMJ, MuSK co-localizes with AChRs, which are known to be confined to the postsynaptic membrane of the NMJ. This is also true during development of the NMJ where MuSK is associated at the motor endplate with the earliest observable AChR clusters (E14-15) and these two molecules co-distribute throughout the entire development of the NMJ. Co-localization of MuSK and AChRs was also confirmed by *in vitro* experiments showing that MuSK and AChRs can be clustered on the surface of rat primary myotubes after and without application of the endogenous MuSK activator - neural agrin [39].

1.3.1.4   ACTIVITY / ACTIVATION

Ligand-induced dimerization is an essential step in the activation process of RTKs and in many cases is sufficient to activate them [40, 41]. Also MuSK requires homodimerization to be fully functional. After that, the tyrosine residues within the kinase domain become phosphorylated and the signal can be transduced.

The extracellular part of MuSK contains 19 tyrosine residues, 17 of which are contained within the kinase domain and 2 within the juxtamembrane region. The juxtamembrane tyrosine residue (Y553 in mice) as well as 3 out of 17 tyrosine residues (Y576, Y750 and Y755) included in the kinase domain region, called "activation loop tyrosines" are critical for ligand-induced MuSK activation. Mutation of the juxtamembrane tyrosine residue completely abolishes the kinase activity of MuSK and clustering of AChRs on the surface of muscle fibres, a visible sign of MuSK activation in muscle. Mutations of the activation loop tyrosines result also in complete or partial failure of MuSK signaling properties [42]. Interestingly, activation of MuSK by neural agrin *in vivo* in comparison to its self-activation caused by overexpression in heterologous cells *in vitro* involves most probably the same set of tyrosine residues including the juxtamembrane as well as two out of three activation loop tyrosine residues [43]. Recently, it has been described that not only tyrosine but also serine residues (S680 and S697), which are conserved between species and are substrates for Casein Kinase 2α, play a regulatory role in MuSK activity-induced AChR clustering [44].

1.3.2   AGRIN

Agrin is a heparan sulfate proteoglycan with a predicted molecular weight of ~220 kDa (400-600 kDa after glycosylation) that is synthesized by motor neurons, transported in motor axons, and released at synaptic sites, where it organizes postsynaptic differentiation [1, 45, 46]. It was first identified by McMahan and collaborators from Torpedo Californica electric organ basing on its activity to induce AChR clusters on the surface of myotubes [47, 48]. The mature protein of agrin contains multiple domains, most of which are also found in other basal lamina proteins [49, 50]. Signal sequence (SS) together with an amino (N)-terminal agrin domain (NtA), characteristic for the agrin isoform that is localized to the NMJ, allow it to be properly released and bound to the basal lamina. The N-terminal region includes also nine cysteine-rich follistatin-like domains (FS) likewise two Laminin EGF-like domains (LE). A number of glycosylation sites are distributed throughout the protein. The amino-terminal part of agrin is highly glycosylated at serine/threonine (S/T) glycosylation and glycosaminoglycan attachment sites (Fig. 5). These regions are also involved in binding to neural-cell adhesion molecule (NCAM) and heparin-binding growth factors. The C-terminal portion of agrin is characterized by four EGF-like (EG) repeats and three laminin G-like (LG) domains [51].
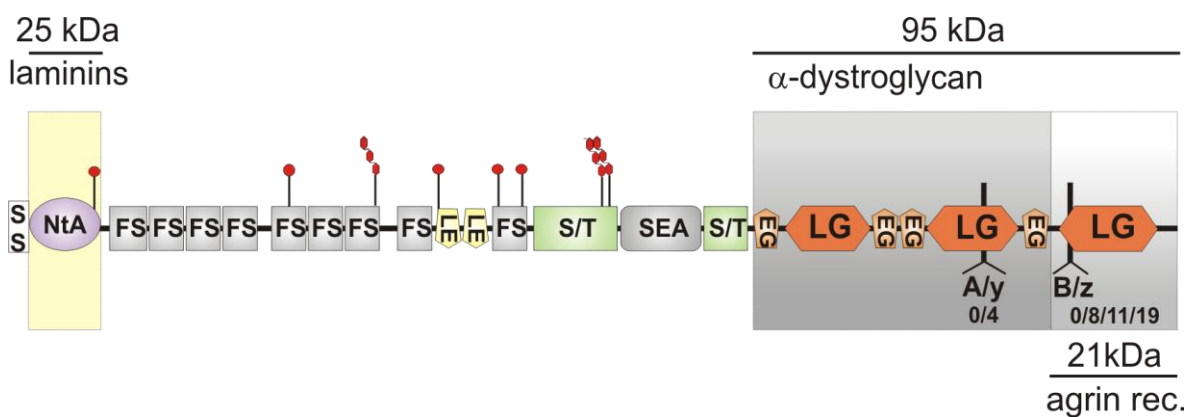
Figure 5 │ Structure of agrin

SS – Signal sequence; NtA – amino (N)-terminal agrin domain; FS – cysteine-rich follistatin-like domains; LE – Laminin EGF-like domains; S/T – serine/threonine glycosylation and glycosaminoglycan attachment sites; LG – laminin G-like domains; EG – EGF-like repeats
(adapted from Bezakova and Ruegg, Nat Rev Mol cell Biol, 2003)

In addition to motor neurons and CNS neurons, agrin is expressed widely in the several tissues including muscle, lung, kidney, glia cells [47, 52-55]. Nevertheless, only agrin synthesized and released by motor neurons, having an 8, 11 or 19 amino acid splice insert in the C terminus and called "neural agrin" has been shown to activate MuSK *in vitro* as well as to play a role in NMJ formation and maintenance. In contrast, "muscle agrin" (without given splice insertions) shows none of those properties [56-58]. The ability of neural agrin to activate MuSK is restricted to a 21-kDa, C-terminal part that has been shown to be sufficient for induction of MuSK phosphorylation as well as AChRs aggregation [57, 59]. This part of agrin molecule also is supposed to contain binding sites for still unidentified "agrin receptor" [60].

1.3.3   Dok-7

Dok-7 is a member of the Dok protein family (Dok-1 – Dok-7) which consists of a group of cytosolic proteins that contain a phosphotyrosine binding (PTB) domain and have been shown to bind directly to phosphorylated tyrosine residues contained within an NPXY motif of intracellular portion of many receptor tyrosine kinases (TrkB, TrkC, IGFR,) [61, 62]. Dok-7 has been identified and cloned by Okada by searching for a previously unidentified member of the Dok-family, which could play a role in NMJ formation. Mature Dok-7 protein consists of 504 amino acids with a molecular weight of 55kDa. Like other members of the family, Dok-7 has pleckstrin-homology (PH) and phosphotyrosine binding (PTB) domains in the N-terminal portion and Src homology 2 (SH2) domain target motifs in the C-terminal region [63]. Analysis of mRNA coding for Dok-7 as well as immunostainings showed that Dok-7 is preferentially expressed in skeletal muscle and heart but not in liver or spleen. In mature muscle, Dok-7 is selectively expressed by subsynaptic nuclei and localizes to the postsynaptic side of the NMJ. Dok-7 has also been shown to bind directly to juxtamembrane tyrosine residue of MuSK in a phosphorylation-dependent manner *in vitro*. This binding results in a strong increase of MuSK phosphorylation [63]. Moreover, overexpression of Dok-7 in C2C12 myotubes induces the formation of AChR clusters similar to those observed after neural agrin-induced MuSK activation. Therefore, Dok-7 is considered to be an essential muscle-intrinsic activator of MuSK.

This conclusion is also supported by the finding that mice lacking Dok-7 (Dok-7$^{-/-}$) show marked disruption of neuromuscular synaptogenesis. Similar to mice lacking MuSK or agrin, Dok-7$^{-/-}$ mice are immobile and die shortly after birth due to respiratory failure. Severe defects can be also observed in neuromuscular transmission in the skeletal muscles of those mice. Consistently, Dok-7$^{-/-}$ mice do not form AChR clusters in the end-plate area of the diaphragm muscle [63]. Thus, proper neuromuscular synaptogenesis requires Dok-7 within the skeletal muscle and Dok-7 dysfunction is involved in the pathogenesis of NMJ disorders [64-66].

The discovery of Dok-7 put more light on agrin-MuSK signalling. First, Dok-7 expression; similarly to MuSK, is induced upon the fusion of myoblasts to myotubes. Second, co-expression of Dok-7 and MuSK in non-muscle cells results in MuSK activation and in case of muscle cells, in the formation of AChR clusters. Third, Dok-7 binds directly to MuSK juxtamembrane tyrosine residue, which is known to be important for MuSK activation [42]. Fourth, the phenotype of Dok-7 deficient mice is very similar to those observed for MuSK or agrin mutants suggesting involvement in the same signalling

pathway. Therefore, Dok-7 seems to be a good candidate molecule to play an important regulatory role in activity status of MuSK.
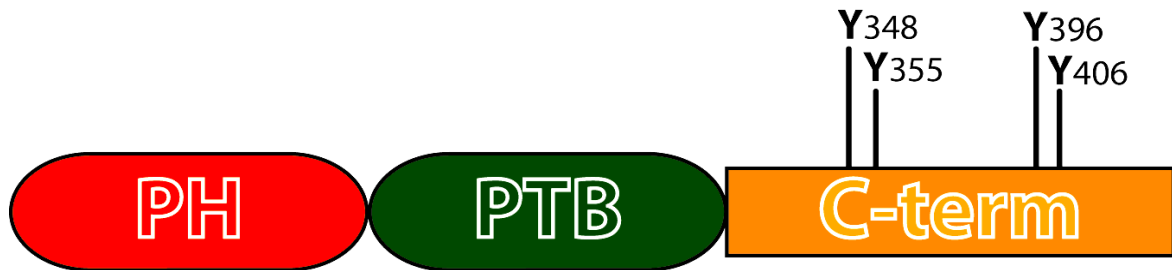
Figure 6 │ Structure of Dok-7

PH - pleckstrin-homology domain (8-108 amino acid); PTB - phosphotyrosine binding domain (109-204 amino acid); Y348, 355, 396, 406 – C terminus tyrosine residues which become phosphorylated after MuSK activation

1.4   MuSK/AGRIN SIGNALING CASCADE

In cultured myotubes neural agrin activates MuSK and induces its rapid and long-lasting phosphorylation [58]. This activation results in few hours in the formation of AChR clusters on the surface of myotubes. The formation of AChR clusters depends on MuSK expression since none of the clusters is formed in MuSK knockout myotubes [2]. Many signaling molecules have been shown to participate in this phenomenon and to influence the agrin/MuSK-dependent formation of AChR clusters on the surface of muscle cells. The one that is boosting agrin/MuSK signaling cascade is MuSK adaptor protein Dok-7.

Rac1 and Cdc42, Rho GTPases playing mainly roles in is the regulation of actin cytoskeletal structures in the cell, were also shown to take a part in the agrin/MuSK signalling. Activity of both Cdc42 and Rac1 is elevated in muscle cells in response to agrin stimulation [31, 67]. Additionally, agrin-induced increase in the selective binding of activated Rac and Cdc42 to a Rac/Cdc42-binding domain derived from PAK1, a downstream effector molecule that is thought to link Rac1 activation to actin polymerization was also described [68-71]. Interestingly, PAK1 interacts with MuSK through its binding to Dishevelled1 (Dvl1). Agrin acting through MuSK activates PAK1, and this activation requires Dvl1. On the other hand, inhibition of PAK1 activity attenuates AChR clustering [72]. Agrin-induced activation of Rac1 and Cdc42 depends also on phosphoinositide 3-kinase (PI3-K), since muscle cells treated with specific PI3-K inhibitors are unable to form full-size AChR clusters in response to agrin and phosphorylation of β-subunit of AChR is also reduced. Moreover, agrin-induced activation of Rac and Cdc42 is impaired in the presence of PI3-K inhibitors [67]. The importance of other signalling molecules has been also studied in agrin/MuSK-mediated AChR clustering process. There is evidence that *in vitro* agrin activates Src family kinases that are associated with the AChRs. The activation occurs downstream of MuSK, requires rapsyn, and correlates closely with agrin-induced AChRs clustering [73]. All the conformational changes including MuSK activation, formation of protein complex and downstream signal transduction lead, in turn, to activation of expression of the NMJ-specific genes. This local synthesis comes from enhanced transcription of those genes by subsynaptic nuclei and by repression of extrasynaptic nuclei.

Several transcription factors contribute in driving synapse specific gene expression. One of them called GABP (**GA - b**inding **p**rotein) belongs to Ets family of transcription factors [74]. The DNA sequence -CCGGAA - known as N-box found within MuSK and many other NMJ-specific genes serves as a GABP binding site. GABP

consists of 2 subunits. The 58 kDa GABP α subunit binds DNA through its Ets domain, while the 43 kDa GABP β subunit does not contact DNA but contains ankyrin repeats that mediate its interaction with GABP α, thus strengthening the interaction of the α subunit with DNA [75]. GABP regulates synapse-specific gene expression at the NMJ and is required for the formation and proper function of postsynaptic apparatus. In muscle cells neural agrin-mediated activation of the AChRε subunit promoter is abolished by the inhibition of GABP function. Moreover, agrin-induced aggregation of AChRs as well as aggregation of acetylcholine esterase and utrophin, two additional components of the postsynaptic apparatus is strongly reduced. Thus, GABP is required for the formation of a functional postsynaptic apparatus [76 582]. Interestingly, GABPα is expressed broadly throughout the entire muscle fibres with only a minor enrichment in the subsynaptic domain [74]. Additionally, GABP deficient mice survive to adulthood without any overt signs of muscle weakness or motor behavioural phenotypes to be expected from mice with severely compromised subsynaptic gene expression. Moreover, no changes in the level or pattern of subsynaptic gene expression at NMJs can be observed in these mice [77]. This, in turn, argues against a major role for *GABP* in the regulation of subsynaptically restricted gene expression.

Recently, another ETS transcription factor, Erm, was described for its importance in regulating the gene expression at the NMJ. Erm is expressed selectively from subsynaptic nuclei and its mutation in mice leads to severe downregulation of many genes with normally enriched subsynaptic expression (MuSK, AChR δ and ε subunits, DuSP4). Moreover, Erm mutant mice display an expansion of the muscle central domain in which acetylcholine receptor (AChR) clusters accumulate, show gradual fragmentation of AChR clusters, and exhibit symptoms of muscle weakness mimicking congenital myasthenic syndrome (CMS). This findings show Erm to be an upstream regulator of a transcriptional program selective to subsynaptic nuclei at the NMJ and underscore the importance of transcriptional control of local synaptic protein accumulation [78].

1.5   MuSK - AN AGRIN RECEPTOR?

MuSK and neural agrin are supposed to act within the same signaling pathway. Both agrin and MuSK knockout (KO) mice show very similar but distinguishable phenotypes. They die at birth due to respiratory failure caused by improper innervation of the diaphragm. However, "prepatterned" AChR clusters (formed prior to innervation and being likely a result of MuSK self activation) are entirely absent in skeletal muscle of MuSK mutant mice, whereas, though infrequent, can be detected in agrin mutant mice [3]. Neuromuscular synapses do not form in both agrin and MuSK deficient mice, suggesting that agrin activating MuSK can induce signaling cascades responsible for all the aspects of synapse formation, including organization of the postsynaptic membrane, synapse-specific transcription, and presynaptic differentiation [79]. It is also known for MuSK that when it is expressed on the surfaces of non-muscle (HEK) cells, is able to selectively inhibit the growth of peripheral motor neurites but not those formed by retinal ganglion cells. This effect can be reversed by application of antibodies raised against either the extracellular portion of MuSK or agrin suggesting the involvement a MuSK/agrin signaling complex on the cell surface of the cell [80]

Interestingly, MuSK can be activated with neural agrin only in mature myotubes but not in myoblasts or when force expressed in other non-differentiated cells (myoblasts, HEK293, COS) Moreover, *in vitro* agrin can be chemically cross-linked with MuSK, but it seems not to bind to MuSK ectodomain directly [58]. These observations raised the hypothesis that MuSK could serve only as part of a fully functional agrin receptor. Thus, another activity, specific for mature myotubes, was postulated and was called myotube specific accessory component (MASC) [58]. In principle, the additional myotube-specific activity/activities could be a co-receptor [81], a co-ligand [82, 83] or a post-translational modification [84]. So far, none of them has been substantiated by experimental evidence.

In the last decade, many efforts have been put to elucidate the problem of neural agrin-induced MuSK activation. The studies of several groups were focused mainly on finding the molecule which could act as a missing part of the functional agrin receptor and then to be able to fulfill "MASC hypothesis". Unfortunately, all described MuSK interacting proteins including Dok-7 [63], Geranylgeranyltransferase I [85], Abl kinase [86], AChE [87], Dishevelled I [72], Magi-1C [88], 14-3-3γ [89], Src, Fyn [90] proved to be more or less important for the formation and maintenance of NMJ. However, none of these molecules has proved to be the long-sought MASC molecule. Majority of these described MuSK interacting proteins bind to the intracellular part of MuSK. Moreover, their activity mostly

depended on activation of MuSK with neural agrin. On the other hand, several molecules on the myotube surface are capable of interacting with agrin including alpha-dystroglycan, considered at that time as a functional agrin receptor [91, 92], integrins [93], HB-GAM/pleiotropin [94], heparan sulfate proteoglycans, N-CAM [95] and laminins [96]. Several of these have been implicated in AChR clustering based on studies in cultured myotubes but none has been shown to be critical for postsynaptic differentiation *in vivo*. Nevertheless, MuSK is now emerged as the best candidate for the agrin receptor, even though it has not been shown so far that it binds agrin directly.
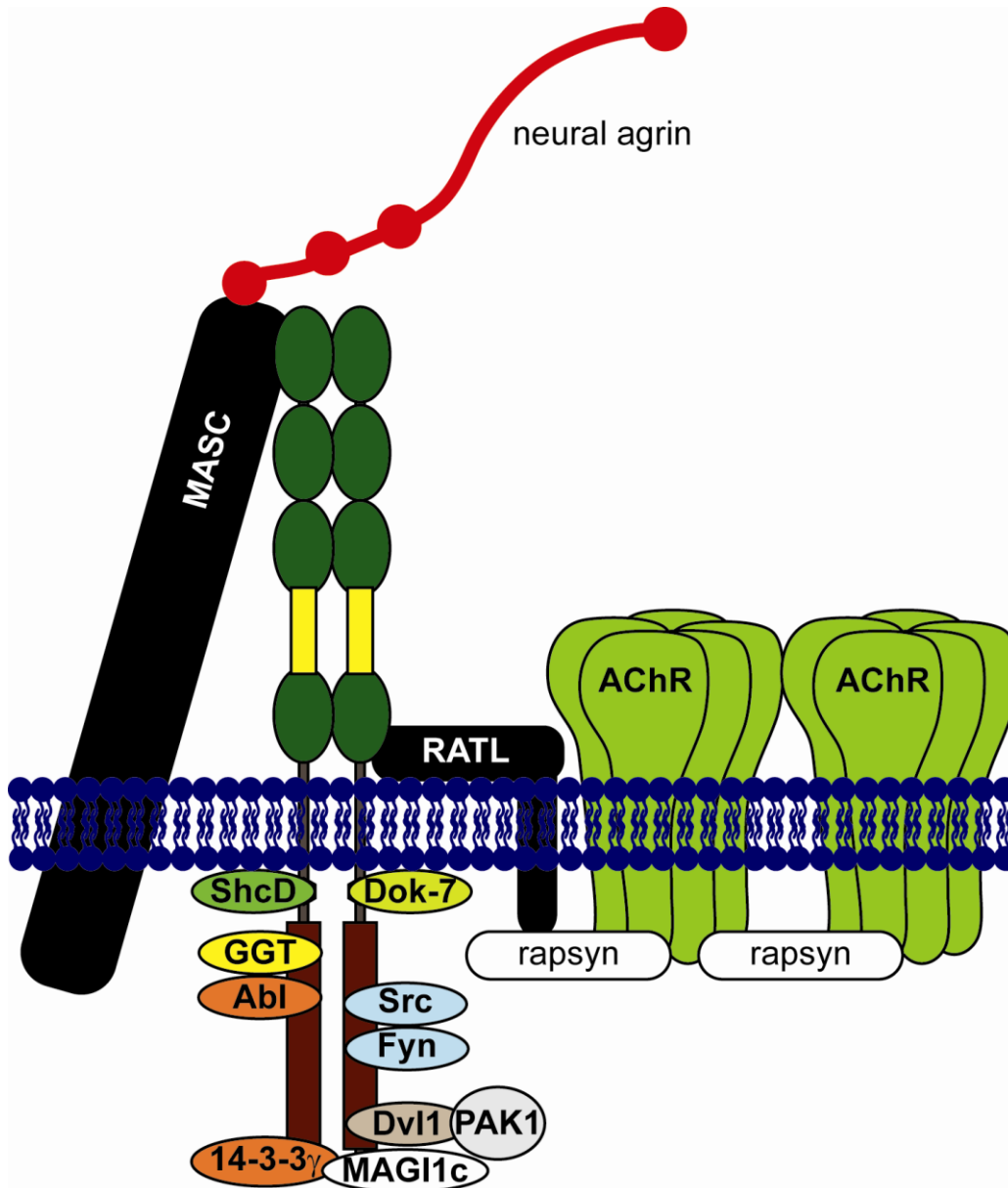
Figure 7 │ Model of the MuSK complex

Neural agrin interacting with MuSK leads to its phosphorylation and recruitment of adaptor proteins. Formation of such protein complex allows downstream signal transduction resulting in specific gene expression as well as AChR clustering process

MASC Myotube Associated Specificity Component (hypothetical), RATL - Rapsyn Accessory Transmembrane Linker (hypothetical), Dvl1 – Dishevelled 1, MAGI-1C – membrane-associated guanylate kinase with inverted domain organization,, Fyn, Src – nonreceptor tyrosine kinases, GGT – Geranylgeranyltransferase I, ShcD - Shc family adaptor protein D/4

(adapted from Strochlic L., Bioessays 2005)

2   GOAL OF THESIS

The neural agrin – MuSK signaling pathway is considered as the most important for the formation and the maintenance of the NMJ. However, the mechanism by which neural agrin activates MuSK remains poorly understood. It is also not completely elucidated how agrin-induced MuSK activation leads to the formation of the postsynaptic apparatus and which regulatory proteins are involved in this process.

In this study, we focused on how neural agrin activates MuSK. We addressed the question of whether the putative agrin co-receptor protein (MASC) indeed exists. We hypothesized that in muscle cells interaction of MuSK and neural agrin can occur directly with and that a muscle-specific, cytoplasmic protein could then represent the MASC phenomenon. Additionally, we studied signalling events which are activated downstream of MuSK and can have a regulatory impact on the formation and the maintenance of the NMJ. Finally we describe the mechanisms that stabilize newly formed postsynaptic structures at the NMJ.

CHAPTER II

RESULTS

The following chapter includes manuscripts of the original papers which have already been published or are about to be submitted to scientific journals. The author of the thesis contributed in preparation of those publications during the PhD study.

MuSK alone is sufficient to respond to neural agrin in muscle cells

Marcin Maj, Shuo Lin, Markus A. Ruegg

Biozentrum, University of Basel, CH-4056 Basel, Switzerland;

1.1 ABSTRACT

In developing muscle, neural agrin activates muscle specific kinase (MuSK) and this, in turn, results in clustering of acetylcholine receptors and the formation of the postsynaptic apparatus. However, the mechanism of how neural agrin activates MuSK remains poorly understood. To elucidate the problem of MuSK/neural agrin interaction, we examined transgenic mice overexpressing MuSK or a miniaturized form of neural agrin or both proteins throughout the entire muscle fibre. We find that mice transgenic for either MuSK or neural miniagrin produce only few ectopic AChR clusters localized mostly to the terminal parts of muscle fibre. Interestingly, denervation of MuSK transgenic mice resulted in formation of such a clusters in entire muscle fibre. In contrast to single transgenic mice, the mice transgenic for both proteins display high number of ectopic postsynaptic sites present throughout the entire muscle fibre. Moreover, the same phenotype can be observed in innervated muscle of MuSK transgenic mice with additionally introduced expression of MuSK adaptor protein Dok-7. We conclude that in muscle cells MuSK alone is sufficient to respond to neural agrin stimulation and that Dok-7 seems to be the missing activity component linking neural agrin-activated MuSK to AChRs clustering process. Thus, in muscle cells MuSK is the functional receptor for neural agrin.

1.2 INTRODUCTION

The receptor tyrosine kinase MuSK and its ligand, neural form of agrin are the main organizing molecules at the mammalian neuromuscular junction (NMJ). Both proteins are involved in formation and maintenance of the NMJ since no functional pre- and postsynapses are formed in neither MuSK nor agrin knockout mice [2, 97].

In vitro, neural agrin induces rapid and long lasting phosphorylation of MuSK leading to clustering of AChRs on the cell surface [58]. Juxtamembrane tyrosine residue (Y553 in mice) of MuSK is known to play a crucial role in this process, since myotubes expressing an Y553F MuSK mutant fail to cluster AChRs in response to agrin application. Moreover, the Y553F MuSK mutant does not respond to neural agrin stimulation *in vitro* [42]. The mechanism of MuSK-agrin interaction remains poorly understood. There are no data showing a direct binding of neural agrin to MuSK. Additionally, the activation of MuSK by neural agrin takes place only in mature myotubes but not in myoblasts or other non-muscle cells [58]. Based on these observations, an additional component called MASC (Myotube Associated Specificity Component) has been postulated to act as an agrin co-receptor [58]. However, its existence has not been substantiated by experimental evidence.

An essential step in the activation process of every receptor tyrosine kinase (RTK) is dimerization of two receptor molecules [40, 41]. This status can be achieved upon ligand binding or in a ligand-independent manner, by overexpression of RTK [98]. The receptor becomes then phosphorylated and this allows binding of downstream adaptor proteins and activation of signal transduction. This is also true for MuSK, and in case of both ligand- and overexpression-induced activation of MuSK involves similar tyrosine residues, including one of the juxtamembrane and two out of three tyrosines within the activation loop [43].

Recently, a phosphotyrosine binding adaptor protein, Dok-7 has been identified as a downstream component of MuSK, that is crucial for its activation as well as clustering of AChRs [63]. This work showed that Dok-7 is a muscle specific protein, whose expression; similarly to MuSK, is induced upon the fusion of myoblasts to myotubes. Second, co-expression of Dok-7 and MuSK in non-muscle cells results in MuSK activation. In case of muscle cells, the formation of AChR clusters can be also observed [63]. Third, Dok-7 binds directly to MuSK juxtamembrane tyrosine residue, which is known for its importance in MuSK activation [42, 63]. Fourth, similarly to mice lacking MuSK, no AChR clusters are formed in Dok-7 deficient mice [63]. Taking together, Dok-7 seems to be a good candidate

for being MASC, even though it does not fulfil all the criteria that have been postulated for this phenomenon before [58].

In this study, using transgenic mice we were trying to elucidate whether existence of MASC, an additional co-receptor protein is necessary for agrin-induced MuSK activation. We tested the hypothesis that in muscle cells MuSK and neural agrin can bind occur directly with no need of any additional component and that the MASC could be then by a muscle-specific, cytoplasmic regulatory protein. Here we show that in muscle cells MuSK alone is sufficient for driving agrin-induced signalling cascade. Moreover, we show Dok-7 as a linking neural agrin-activated MuSK to AChRs clustering process and postulate that Dok-7 could be a MASC equivalent.

1.3 MATERIALS AND METHODS

01. Transgenic mice

The pBS KS+ expression vector with 1.3 kb fragment of Muscle Creatine Kinase (MCK) promoter region subcloned upstream and poly adenylation sequence subcloned downstream of the modified multiple cloning site has been used. The vector was digested with EcoRV and full length mice Nsk2 (mice MuSK) - TAP tag fusion protein cDNA was subcloned into this site. Then the construct was excised using PacI restriction enzyme and injected into mouse oocytes. Transgenic lines were identified by PCR and Western blot analysis. Two transgenic lines with different expression level have been generated. The line expressing highest amount of MuSK-TAP tag fusion protein and called MuSK-tg was chosen and used in all the experiments and subsequent cross breeding with other transgenic mice lines.

02. Sciatic nerve dissection

Wild type (WT) and MuSK-tg mice were anesthetized by intraperitoneal injection of Ketamine and Xylazine, 90 mg and 21 mg per kg body weight respectively. The left sciatic nerve was identified and lifted. Then, a 1 cm segment of the sciatic nerve was excised, and the distal and proximal nerve stumps were separated to prevent nerve regeneration. The surgical incisions were closed and the animals were returned to their cages. 10 days after the surgery the mice have been taken to the subsequent steps of experiment.

03. Dok-7 electroporation

WT and MuSK-tg mice were anesthetized by intraperitoneal injection of Ketamine and Xylazine, 90 mg and 21 mg per kg body weight respectively. The left soleus muscle was exposed and 15 µg of pCINeo-Dok-7-myc and 7 µg of construct expressing green fluorescent protein containing a nuclear localization signal (NLS-GFP), in a total volume of 10 µl of 0.9% NaCl were injected, followed by electroporation using an ECM 830 electroporation system (BTX, Holliston, MA) as described previously [5]. Control animals have been injected with 15 µg of pCINeo and 7 µg of NLS-GFP. At 2 months after electroporation the muscles were dissected and AChR clusters were visualized by Btx staining.

04. Staining with α-bungarotoxin

Mice were sacrificed by cervical dislocation and soleus, EDL and diaphragm muscle were quickly removed. The muscles were mounted on the Sylgard 184 (Dow Corning) coated Petri dishes, washed 3 times in PBS and injected with 250 µl of rhodamine-conjugated α-bungarotoxin 1 µg / ml (Btx). After 15 min. of incubation muscles were washed 3 times with PBS and fixed with 2% paraformaldehyde (pH – 7.4) in PBS. Then the muscles were again washed 3 times with PBS and thin muscle bundles were dissected under a microscope.

05. RNA extraction, reverse transcription and PCR reactions

Total RNA was extracted from 50 mg of mouse soleus, EDL or gastrocnemius muscle. 1 ml of TRI reagent (Sigma) was added to the tissue and homogenization was performed using Fast Prep FP120 apparatus (Savant, Hicksville, NY). Residual proteins were extracted by addition 100 µl of chloroform. Total RNA was precipitated with isopropanol, washed with ice-cold 75 % ethanol and re-centrifuged at 4 °C for 5 min at 7500 x g. The RNA pellet was air-dried and dissolved in 80 µl of nuclease free water (Ambion). Single-stranded cDNA was prepared from 5 µg of total RNA using SuperScript™ II Reverse Transcriptase (Invitrogen) according to supplier's instruction. The Real Time PCR reactions were carried out using Abi Prism 7000 Sequence Detection System (Applied Biosystems) and Power SYBR Green PCR Master Mix reagent (Applied Biosystems)

PCR reactions were carried out with use of the following primer sets: GAPDH (Sense – 5'CATCGTGGAAGGGCTCATGAC3', Antisense – 5'CTTGGCAGCACCAGTGGATG3'), TAP-tag (Sense: 5'GGCGTCTCAGCAGCCAACCG3', Antisense: 5'CGGCTTCATCGTGTTGCGC3'), AChR alpha1 subunit (Sense: 5'CCACCTATGGGCTTTCACTC3', Antisense: 5'CCATCACCATGGCAACATAC3', AChR epsilon subunit (Sense: 5'CTGTGAACTTTGTGGGTGAG3', Antisense: 5'GGAGATCAGGAACTTGGTTG3'), AChR gamma subunit (Sense: 5'GGAGAAGCTAGAGAATGGTCC3', Antisense: 5'CCCACTGACAAAGTGACTCTGC'), Dok-7 (Sense: 5'GCCTCCAGCTTTCTTTTTGT', Antisense: 5'CTCACTGTGTGGTCGCTCA3'), MuSK (Sense: 5'CTGGATCAAGGGGGACAAT3', Antisense: 5'GTCGACCTAACTTTTGCCTTT3')

06. Cloning of Dok-7 cDNA

Mouse gastrocnemius muscle cDNA has been used as a template for cloning of the full length Dok-7. PCR reaction was performed using a Long Expand Polymerase PCR system with the forward primer 5'-CCGCTCGAGATGACCGAGGCAGCGC-3' and the reverse primer 5'-CTAGTCTAGAGGGAGGGGAGGGGGCTTTAC-3' (use of this primer

excluded stop codon of Dok-7). 1535 bp product was then purified and subcloned into pCiNeo expressing vector (Promega). Then, 5 x myc tag sequence was subcloned in the C terminus following by sequencing and examination of protein expression.

07. Stable cell lines generation

HEK-293 cells were maintained in Dulbecco's modified Eagle's medium (DMEM) (PAA) supplemented with 10 % foetal calf serum (PAA) as well as L-glutamine (GIBCO), sodium pyruvate, penicillin and streptomycin (Sigma). The cells were transfected with pCi-Neo expressing vector containing cDNA encoding for full length mouse MuSK using jetPEI transfection reagent (Qbiogene) or lipofectamine 2000 transfection reagent (Invitrogen) according to the manufacturer's instructions. At 48 h after transfection the cells were trypsinized and transferred to 150 mm cell culture dishes. Then the clones were selected by growth in complete medium containing G418 (600 µg / ml) for about 2 weeks. Isolated clones were then cultured, expanded and examined for expression of transfected cDNAs.

08. Transient transfections

HEK-293 cells were maintained in Dulbecco's modified Eagle's medium (DMEM) supplemented with 10 % foetal calf serum as well as L-glutamine, sodium pyruvate, penicillin and streptomycin. The cells were transfected with pCi-Neo expressing vector containing cDNA encoding for full length mouse Dok-7-myc using Lipofectamine 2000 transfection reagent (Invitrogen) according to the manufacturer's instructions. 24 h after transfection the cells have been subjected for further assays.

09. Immunoprecipitations.

The cells were washed two times with ice cold serum free DMEM (PAA) and then lysed in cold lysis buffer [20 mM HEPES, pH - 7.5, 150 mM NaCl, 1 mM EDTA, protease inhibitor cocktail 1:50 (Upstate), phosphatase inhibitor cocktail II 1:50 (Sigma)]. Cell lysates were incubated on ice for 30 min and centrifuged (20000 g for 15 min. at 4 °C) to remove cell debris. Cleared lysates were incubated for 1 h at 4 °C with antibodies directed against the extracellular portion of MuSK and then 50 µl of 50 % protein A-sepharose beads suspension (GE Healthcare) was added and the lysates were incubated for 2 h at 4 °C. After centrifugation (3000 g for 5 min. at 4 °C), the beads were washed 3 times with ice cold lysis buffer, and bound proteins were then eluted with 2xSDS sample buffer.

11. Western blot

Lysates or immunocomplexes after immunoprecipitation were subjected to SDS-PAGE and then transferred to nitrocellulose membranes (Schleicher&Schuell, Keene, NH). Nitrocellulose blots were incubated for 3 h in blocking buffer [5 % Bovine Serum Albumin (PAA) in PBS / 0.1 % Tween (PBST)] at room temperature (RT). 3 % TOP Block (VWR) in PBST has been used for blocking in case of application of anti-phosphotyrosine antibodies. The blots were then incubated in blocking buffer containing specific primary antibodies overnight at 4 °C. After washing three times for 15 min with washing buffer (the same composition as blocking buffer), the blots were incubated with horseradish peroxidase-conjugated secondary antibodies for 45 min at RT followed by washing three times for 15 min with washing buffer. Immunoreactive bands were visualized with chemiluminescence reagents kit (GE Healthcare).

1.4   RESULTS

AChR clusters formed in MuSK and neural agrin transgenic mice

In innervated muscle fibre, MuSK is mainly expressed by subsynaptic nuclei and localized to the NMJ [26]. MuSK deficient mice die at birth [2], and this restricts the ability to examine MuSK signalling *in vivo* to embryonic stages. Thus, to obtain an experimental setup for studying MuSK signalling in the adult, innervated muscle, we generated transgenic mice expressing full-length MuSK throughout the entire muscle fibre. To distinguish the transgene protein from endogenous MuSK, it was tagged c-terminally with a tandem affinity protein (TAP) tag **(Fig. 1A).** The expression of MuSK was driven by a 1.3 kb fragment of the muscle creatine kinase (MCK) promoter region. Since MCK gene is expressed by myonuclei of the whole muscle fibre [99], we expected the same expression pattern also for our transgenic MuSK. Indeed, RT-PCR analysis showed that levels of MuSK mRNA were highly increased in MuSK transgenic (MuSK-tg) mice compared to WT littermates and that the transcript of transgenic MuSK could be detected at embryonic day 13 (E13) **(Fig. 1B).** Using specific antibodies against extracellular portion of MuSK as well as for the TAP-tag (anti Protein A) we detected transgenic MuSK to be present at the NMJ as well as in extrasynaptic parts of muscles fibre **(Fig. 1C,D)** and to be localized to the plasma membrane **(not shown).** This finding differs from those published before showing that MuSK can be localized only to the NMJ despite the presence MuSK mRNA in the entire muscle fibre [100]. The differences in the levels of MuSK-tg expression in particular muscles were also observed **(Fig. 1G)**, corresponding to the different activity of MCK promoter in those muscles [101].

Overexpression of MuSK in entire muscle fibre resulted in the formation of ectopic AChR clusters **(Fig. 1E)**, however, not in the number expected according to the expression level of MuSK-tg. Curiously, the ectopic AChR clusters formed primarily in the terminal parts of muscle fibre **(Fig. 1E, squares)**. Moreover, the number of AChR clusters did not correlate with the level of MuSK-tg expression in a particular muscle and was higher in soleus than in EDL muscle **(Fig. 1F)**.

To examine whether MuSK-tg was also phosphorylated in extrasynaptic regions of muscle fibre, where neural agrin released by the innervating motor neuron is not present, we separated synaptic and extrasynaptic parts of the soleus and EDL muscle and examined for MuSK-tg phosphorylation. Using the phosphotyrosine specific antibody (4G10) we detected phosphorylated MuSK in both synaptic and non-synaptic regions of

soleus and EDL muscles **(Fig. 1G).** Surprisingly, the levels of MuSK-tg and phosphorylated form were higher in synaptic parts of those muscles **(Fig. 1G)** suggesting an existence of synapse-specific stabilization phenomenon.

Similar results were obtained when another transgenic line, overexpressing neural miniagrin (c-magB/z8-tg), was examined. The neural miniagrin construct used for generation of that line (N25C21B8) represents the smallest part of agrin which is able to activate MuSK [59] as well as to induce AChR phosphorylation and aggregation *in vitro* [102]. It is the fusion protein consisting of NtA domain and LG3 domain containing an 8 amino acid splice insert **(Fig. 1A)** Overexpression of c-magB/z8-tg also induces formation of ectopic AChR clusters; however, the number of AChR clusters was much higher than in MuSK-tg mice **(Fig. 1E,F)**. AChR clusters formed in muscles of those mice are also mainly localized to terminal portions of muscle fibre. Likewise in MuSK-tg mice soleus muscle was found to be more responsive to overexpression of neural miniagrin what resulted in formation of higher number of clusters **(Fig. 1E,F)**.
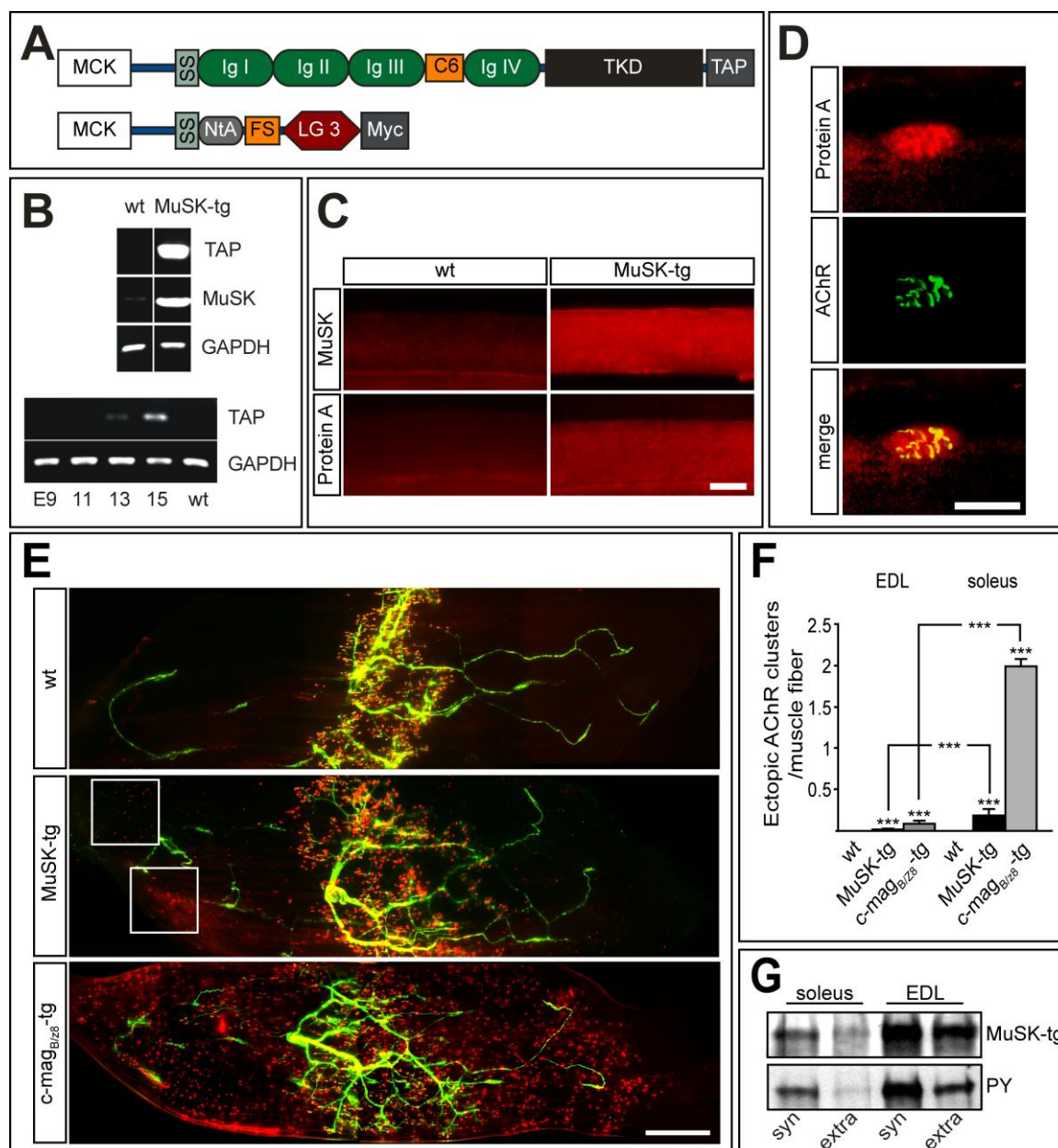
Fig. 1 Ectopic AChR clusters are formed in both MuSK (MuSK-tg) and neural miniagrin (c-magB/z8-tg) transgenic mice

(A)   Expression constructs used for generation of transgenic mice lines.

(B)   Expression of MuSK-tg in calf muscle measured with PCR. **Upper panel:** MuSK
mRNA detected with primers recognizing MuSK as well as TAP tag sequences. **Lower panel:** expression of MuSK-tg starts at embryonic day 13 (E13). PCR reaction was performed with primers recognizing TAP tag sequence.

(C,D)   Expression of MuSK-tg is observed throughout the entire muscle fibre. The pictures show immunostainings with anti-MuSK and anti-protein A antibody to detect MuSK-tg at the NMJ **(D)** and throughout the muscle fibre **(C)** The scale bar is 25 μm

(continued on the next page)

(E)   The whole soleus muscles of wt, MuSK-tg/YFP and c-magB/z8-tg/YFP mice are shown stained with rhodamine conjugated α-bungarotoxin (btx) to visualize AChR receptors (red). The peripheral nerve is shown as green. Preferential localization of ectopic AChR clusters in MuSK-tg mice is indicated with squares. Scale bar is 1mm

(F)   Evaluation of the ectopic AChR clustering phenomenon in MuSK-tg and c-magB/z8-tg transgenic mice. Soleus and EDL muscles of wt, MuSK-tg and c-magB/z8-tg mice have been dissected into single layer bundles and ectopic AChR clusters were counted. The data comes from three animals of each group and represents mean ± S.D.

(G)   Expression of phosphorylation of transgenic MuSK in sub- and extrasynaptic regions of soleus and EDL muscles of MuSK-tg mice. 400 μg of total muscle homogenate was subjected to immuonoprecipitation.

NMJ shape is changed in c-magB/z8-tg and MuSK-tg mice

Both c-magB/z8-tg and MuSK-tg transgenic mice do not show any overt phenotype but closer examination showed the presence of some abnormalities in the final shape of the postsynaptic part of the NMJ of these mice. Staining for AChRs showed that overexpression of MuSK or neural miniagrin caused a substantial fragmentation of the postsynaptic part of the NMJ in both soleus and EDL muscles. Potsynapses of MuSK-tg and c-magB/z8-tg mice did not form a pretzel-like shape characteristic for the mature NMJ but consisted of a number of small parts **(Fig. 2A)**. NMJ fragmentation was observed to be more severe in c-magB/z8-tg than in MuSK-tg mice **(Fig. 2A,C)**. Endplates of c-magB/z8-tg mice represented a big number of small fragments, whereas those observed in MuSK-tg animals formed as a circle-like structure **(Fig. 2A,C)**. Mature, pretzel-like shape of postsynaptic part of the NMJ is also characterized by presence of branching phenomenon [17]. We also observed that the number of branching points (the places within the postsynaptic site, where one AChR dense branch at the NMJ originates with two independent branches) was markedly reduced. **(Fig. 2A,B)**
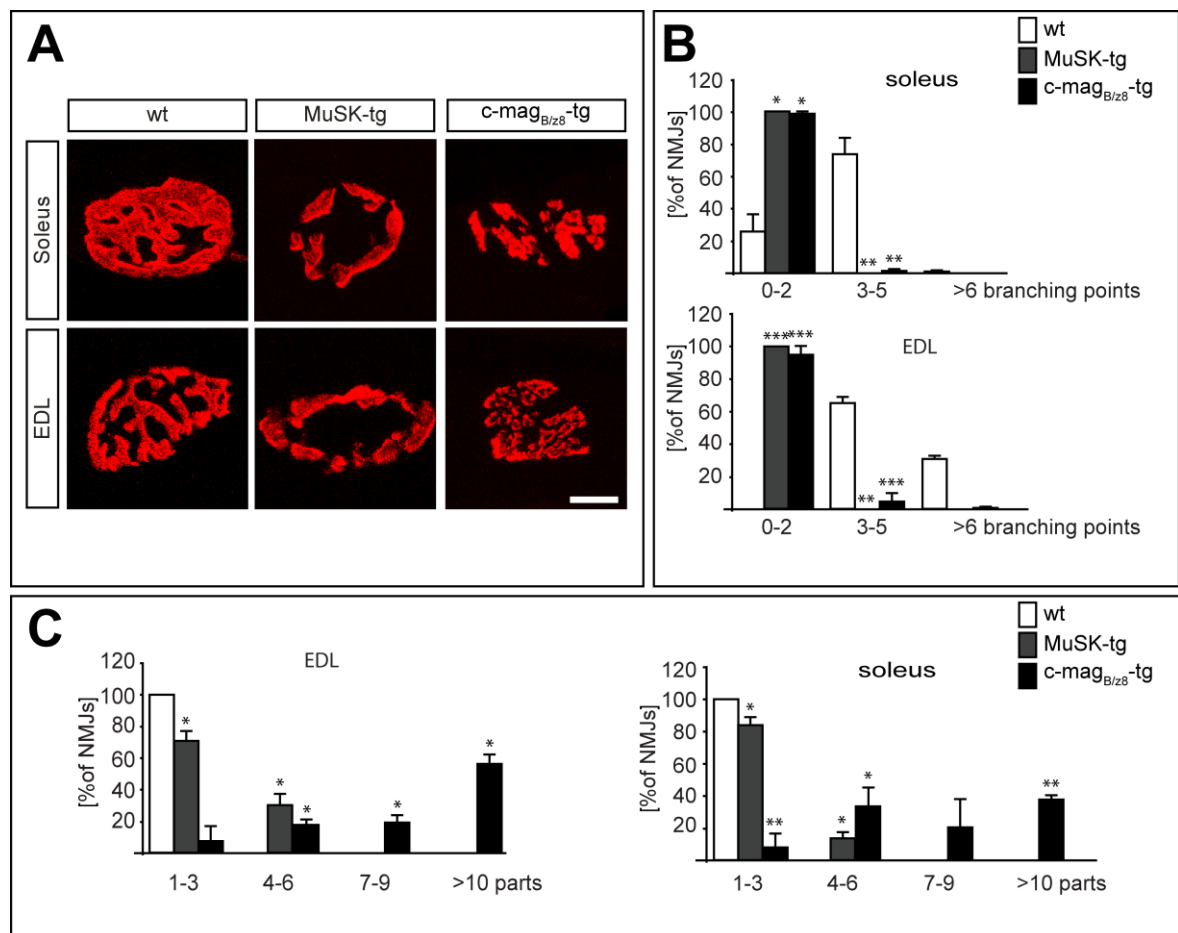
Fig. 2 NMJ shape is changed in MuSK-tg and c-magB/z8-tg transgenic mice

(A)   Soleus and EDL muscles of MuSK-tg and c-magB/z8-tg transgenic mice were stained with Btx and the shape of postsynaptic parts of the NMJ was evaluated. The pictures show robust fragmentation and reduction of branching in both soleus and EDL muscles of MuSK-tg and c-magB/z8-tg transgenic mice. The scale bar is 10 μm

(B,C)   Quantification. Branching points **(B)** and fragments that the NMJs consisted of **(C)** were counted and classified into groups of 0-2, 3-5, 6 and more (>6) for NMJ branching reduction, and 1-3, 4-6, 7-9, 10 and more (>10) for NMJ fragmentation. Data comes from 150-200 NMJ of 3 animals per experimental group and represents mean ± S.D.

Denervation induces the formation of AChR clusters in MuSK-tg mice

In innervated muscle, transcription of synaptic proteins is restricted to a subset of nuclei localized underneath NMJ [1, 103]. After denervation, many of those genes including MuSK, AChR alpha subunit, rapsyn become re-expressed by nuclei throughout the entire muscle fibre [26, 104, 105].To test whether lack of electrical activity would also induce the expression of other components required for AChR clustering process, we denervated the hindleg of wt and MuSK-tg mice by sciatic nerve transsection. Ten days after denervation, we found an high number of AChR clusters formed along the entire muscle of MuSK-tg but not WT mice **(Fig. 3A)**, where the AChR clusters were formed very occasionally in soleus but not EDL muscle **(Fig. 3A, arrow)**. The number of AChR clusters differed between the muscles according to the MuSK-tg expression level and was higher in EDL than in soleus muscle **(Fig. 3A,B)**. The level of mRNA for alpha and gamma subunit of AChR, which are known to be up-regulated after denervation [105], remained unchanged between WT and MuSK-tg denervated muscles **(Fig. 3D,E)**. Nevertheless, it was obvious that denervation also induced the expression of other protein(s) linking the activated MuSK to AChR clustering process. Interestingly, Dok-7 mRNA level was elevated in denervated muscle, both soleus and EDL **(Fig. 3C)**.
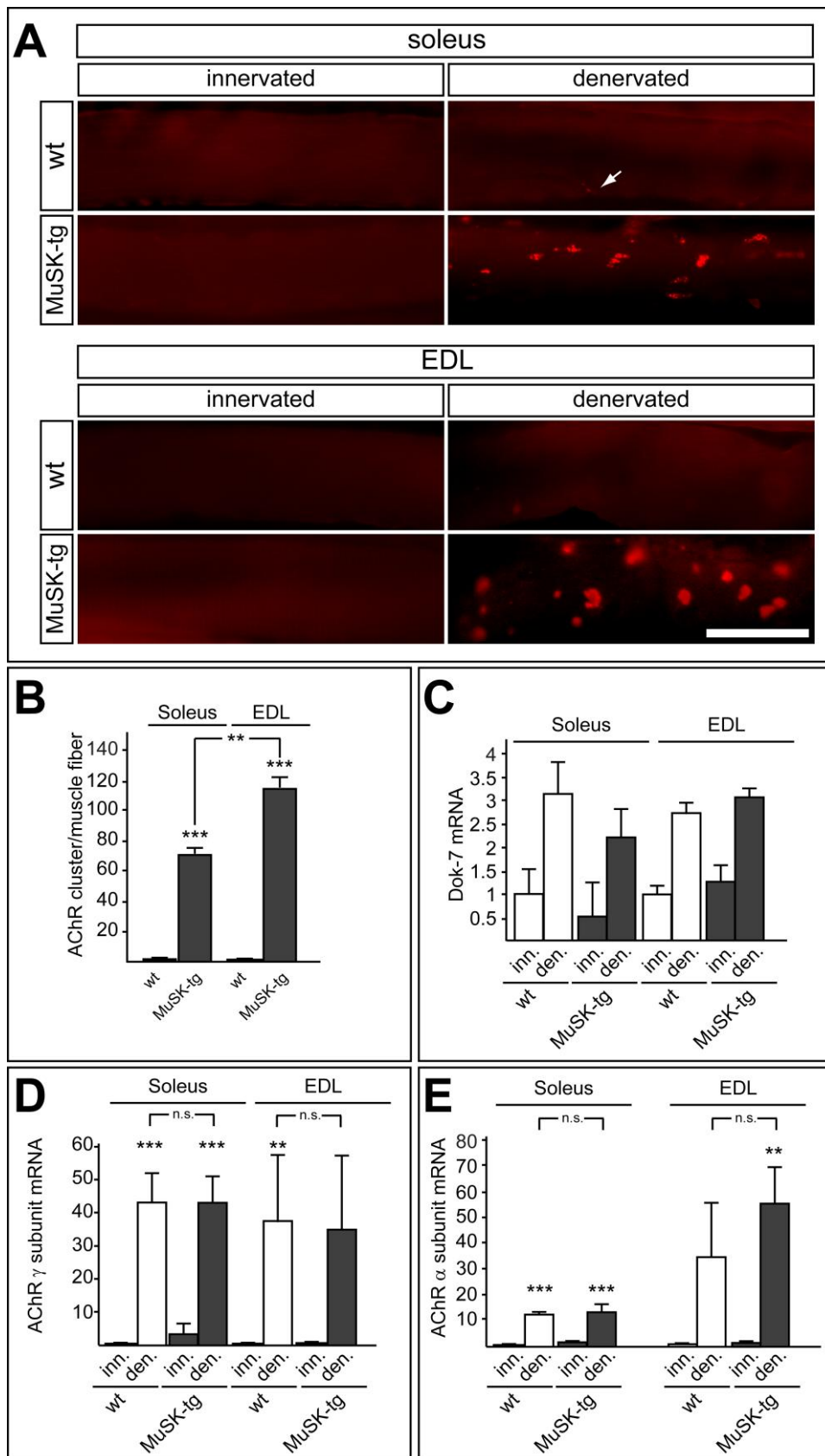
Fig. 3 Denervation induces formation of ectopic AChR clusters in MuSK-tg mice

(A)   AChRs were visualized by staining with btx. In both soleus and EDL muscle, high number of AChR clusters was observed in MuSK-tg mice. In wt mice only few such clusters could be visualized in soleus muscle (indicated by an arrow). Scale bar is 25 μm

(B)   Evaluation of the ectopic AChR clustering in denervated wt and MuSK-tg muscles. Soleus and EDL muscles of wt, MuSK-tg were stained with Btx and dissected into bundles containing a single layer of muscle fibres. Ectopic AChR clusters were counted and are presented as number of AChR cluster per muscle fibre. The data comes from three animals of each group and represents mean ± S.E.M.

(C)   Denervation induces expression of Dok-7 in wt and MuSK-tg muscles. Data is shown as mean of relative mRNA level ± S.D.

(D,E)   Expression of α and γ subunits of AChR is not changed in MuSK-tg soleus and EDL denervated muscle when compared with wt. Data is shown as mean of relative mRNA level ± S.D.

Fig. 3 Denervation induces formation of ectopic AChR clusters in MuSK-tg mice

Many ectopic AChR clusters formed in MuSK/ c-magB/z8 double transgenic mice

Formation of the NMJ depends mainly on neural agrin released from the nerve terminal activating MuSK [106]. Interaction between MuSK and neural agrin is required to induce the clustering of AChRs and other synapse specific proteins on the muscle surface. To test whether MuSK and neural agrin could be sufficient for the formation of the postsynaptic structures we mated MuSK-tg mice with c-magB/z8-tg to generate MuSK/c-magB/z8 double transgenic mice (MADT).

MADT mice were born in the expected number and as newborns did not differ from their WT littermates. At the age of 4 weeks, an overt phenotype became, however, visible. They lost weight, showed signs of muscle fibrillation and developed kyphosis **(Fig. 4A, arrow)**. Having problems with walking and breathing they eventually died because of respiratory failure at the age of 6-8 weeks. Closer examination of muscles of these mice showed formation of many postsynapse-like structures along the entire muscle fibre **(Fig. 4D)**, some of them being apposed by a nerve terminal **(Fig. 4E, arrows)** but most remaining non-innervated **(Fig. 4E, arrowheads)**. This phenotype has been observed in both soleus and EDL **(Fig. 4D)** muscles as well as in diaphragm **(Fig. 4E)**. Moreover, in soleus muscle and diaphragm, the presynaptic nerve endings had sprouted along the entire length of the muscle fibres **(Fig. 4D,E)**.

We were also interested whether co-expression of MuSK and neural agrin, without any additional component, would be sufficient for activation of the synapse-specific gene expression throughout the entire muscle fibre. Indeed, examination of AChR subunit composition in MADT mice showed induction of both alpha and epsilon subunit mRNA in soleus and EDL muscles **(Fig. 4B)**. Additionally, AChR gamma subunit mRNA level was increased in soleus but not EDL muscle **(Fig. 4B)**. It is in agreement with the observation that the nerve sprouting has been observed in diaphragm and soleus muscle but not in EDL **(Fig. 4D,E)**. We also checked the expression levels of Dok-7 and found mRNA for Dok-7 to be elevated in MADT mice **(Fig. 4C)**. Interestingly, we found also higher accumulation of MuSK transgene in extrasynaptic portions of muscle fibre of MADT when compared to MuSK-tg mice **(Fig. 4F)**.
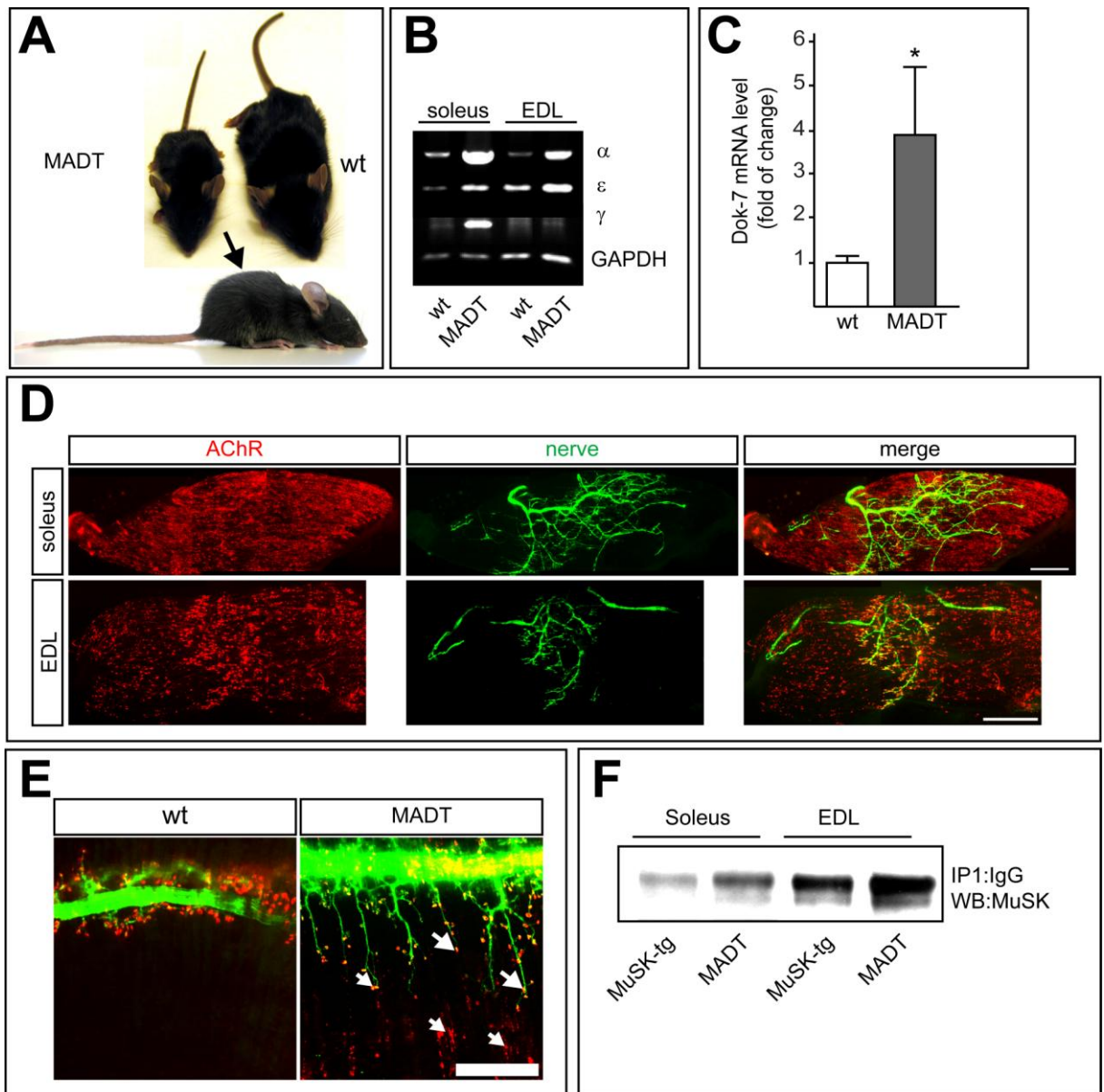
Fig. 4 Severe abnormalities in muscle function in MuSK/c-magB/z8-tg double transgenic mice (MADT).

(A)   6 week-old MADT mice together with its wt littermate. Loss of weight and progressive kyphosis (indicated by arrow) can be observed.

(B)   Synapse-specific gene expression is activated in muscles of MADT mice. The levels of AChR subunits are shown to be elevated in soleus and EDL muscles.

(C)   Dok-7 expression is elevated in MADT mice. Calf muscle of wt and MADT mice has been subjected to RNA extraction followed by reverse transcription and real time PCR. Data is shown as mean of relative mRNA level ± S.D.

(continued on the next page)

(D,E)   Soleus and EDL muscles and diaphragm of 6 weeks-old MADT mice. Overexpression with MuSK together with neural agrin resulted in the formation of high number of ectopic AChR clusters throughout the entire muscle fibre. The nerve endings of the soleus muscle and diaphragm left the postsynaptic places and sprouted along the muscle fibre (B,D). A non innervated synapse-like structures can be observed in soleus and EDL muscles (E arrows) Scale bars D: 1000 μm, E: 500 μm

(F)   MuSK is stabilized in muscles of MADT mice. 200 μg of total muscle homogenate was subjected to immunoprecipitation.

Dok-7 limits formation of AChR clusters in innervated muscle

To avoid the problem of early agrin-induced MuSK activation we generated another transgenic mice line by mating MuSK-tg mice with the mice in which expression of neural miniagrin is regulated by TET OFF expression system. In these animals, expression of transgenic neural agrin can be activated at any time point by withdrawal of antibiotic, Doxycycline, from drinking water

Doxycycline (50 μg / ml) was added to drinking water (containing 4% sucrose) of parents as well as newborn mice. At six weeks after birth transgenic expression of neural agrin was induced by withdrawal of antibiotic doxycycline. Control animals were treated with doxycycline through the entire duration of the experiment. We started our examinations at eight weeks after antibiotic withdrawal. Overexpression of neural agrin in adult MuSK-tg mice resulted also in formation of ectopic AChR clusters. Interestingly, the clusters were formed only in the region surrounding the NMJ **(Fig.5A)**, but not in the entire muscle fibre, where both agrin and MuSK expression was detected using specific antibodies **(not shown)**. This phenotype could be better visible in EDL than in soleus muscle probably due to higher expression level of transgene proteins. None of such a phenotype has been observed in both soleus and EDL muscles of control animals (not shown). Thus, this data strongly suggests that another, (NMJ-specific) factor prevents the formation of additional ectopic postsynaptic sites in innervated muscle.

We were then interested, whether Dok-7, known to act downstream from MuSK [63], could be such a limiting factor. To test this we electroporated soleus muscle of wt and MuSK-tg mice with constructs expressing full length Dok-7-myc and GFP containing nuclear localization signal (NLS-GFP). Control animals received empty vector together with the one containing NLS-GFP. Two months after electroporation, the mice were sacrificed and AChR clusters visualized. Indeed, coexpression of MuSK and Dok-7 caused formation of high number of AChR clusters along the entire muscle fibre **(Fig. 5B)**. Such a phenotype was observed only when MuSK and Dok-7 were co-expressed but not in case of only Dok-7 (wt mice) overexpression. Terminally formed ectopic clusters **(presented in Fig. 1E)** were also visible in MuSK-tg after empty vector electroporation **(not shown)**. This data shows that Dok-7 equally with MuSK and neural agrin is limiting the formation of ectopic AChR clusters in innervated muscle. Moreover, Dok-7 seems to act as a component linking activated MuSK to AChR clusters formation.
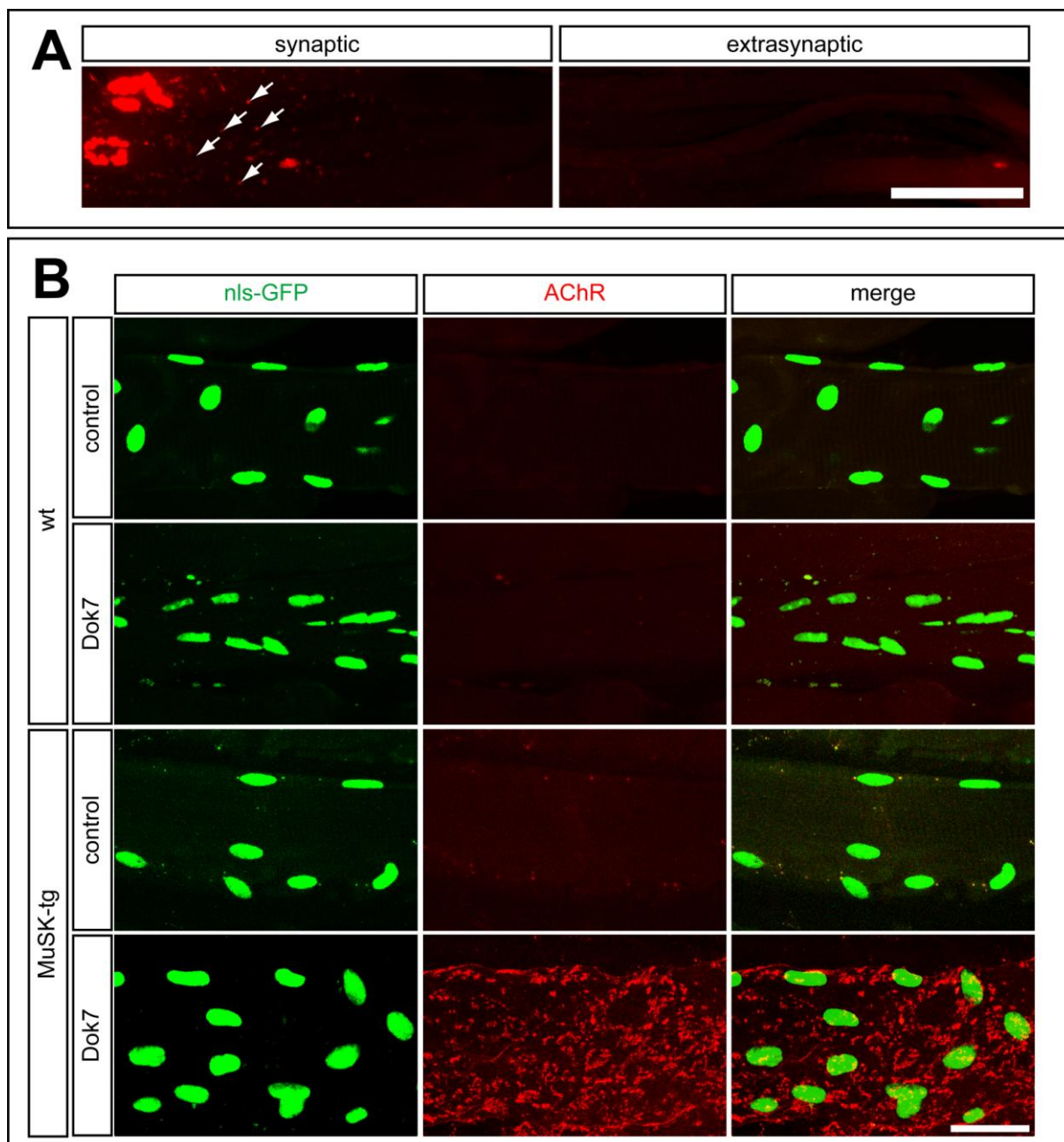
Fig. 5 Dok-7 limits formation of AChR clusters in innervated muscles of MuSK-tg mice

(A) Overexpression of neural agrin in adult (6 weeks old) MuSK-tg mice induces formation of ectopic AChR clusters in synaptic **(indicated with arrows)**, but not in extrasynaptic regions of muscle fibre. Pictures present synaptic and extrasynaptic portions of EDL muscle of MuSK-tg mice. AChRs are visualized with Btx staining 8 weeks after withdrawal of Doxycycline. Scale bar is 50 μm

(continued on the next page)

(B)   Co-expression of MuSK and Dok-7 induces formation of AChR clusters along the entire muscle fibre. Dok-7 and NLS GFP cDNAs were electroporated into soleus muscle of wt and MuSK-tg mice. Two months later, the muscles were removed and AChRs were visualized by staining with Btx. NLS GFP positive nuclei are shown as green, AChRs as red. Scale bar is 25 μm

1.5   DISCUSSION

In present work we focussed on neural agrin-induced activation of muscle specific tyrosine kinase MuSK in muscle cells. We found that in muscle cells MuSK alone might be sufficient to respond to neural miniagrin with no need of any co-receptor protein and that MuSK and Dok-7 are sufficient to drive the formation of ectopic postsynaptic sites in innervated muscle fibre.

In both MuSK-tg and c-magB/z8-tg mice ectopic AChR clusters, although not frequent, are mainly localized to the terminal portions of muscle fibre at the regions of formation of the myotendinous junctions (MTJ). There is evidence that proteins known to be expressed in innervated muscle selectively at the NMJ can also be found in the MTJ regions. It seems to be the truth for AChE [107] and AChRs [108], possibly involved in muscle repair processes [109], alpha7beta1 integrin, localized peripherally around fibres and enriched at myotendinous (MTJ) and neuromuscular (NMJ) junctions [110, 111]. Since none of AChR clusters can be observed in both MuSK and Dok-7 deficient mice [2, 63], it is then very likely that those two proteins as well as other components of agrin/MuSK signalling pathway are also expressed at MTJs. Moreover, the distal regions of muscle fibre correspond to its youngest parts where myoblasts fuse to the muscle endings [112] and expression of both MuSK and Dok-7 is known to be induced upon fusion of myoblasts to myotubes *in vitro* [26, 63].

The ectopic AChR clusters observed in innervated and denervated MuSK-tg mice represent presumably a result of MuSK self-activation. Such neural agrin-independent MuSK activity has already been observed during development. At E18.5 AChRs are clustered in the central region of muscle lacking motor axons [79]. This state is probably achieved by strong, local overexpression of MuSK and the additional components required for AChRs clustering in developing muscle. Secondly, lack of electrical activity is known to induce the expression of genes known to be involved in several stages of muscle development such as MuSK, AChR subunits or rapsyn [26, 104, 105] and Dok-7, but it seems that much more of MuSK is necessary to achieve the prepatterning phenomenon taking place during development. Thus, denervation reflects the developmental stages of the muscle more in qualitative than quantitative manner.

The formation of only few AChR clusters in MuSK-tg mice can be overcome by its co-expression with neural miniagrin. Since miniagrin used to generate those mice represents only a small ~40 kDa fragment of the mature agrin protein (400-600 kDa), which is still able to activate MuSK [59] and induce AChR phosphorylation and clustering

in vitro [102], the influence of all the glycosylation processes which agrin undergoes posttranslationally [113, 114] as well as binding to α-dystroglycan [92, 115] can be excluded. We then conclude that phenomenon observed in those mice, interestingly coinciding with increased expression of Dok-7, might be the result of direct agrin/MuSK interaction. Thus, MuSK together with neural agrin is able to drive the NMJ-specific signalling cascade with no need of any co-receptor protein, but Dok-7 is necessary to link activated MuSK with AChRs clustering process.

Different responses to overexpression of MuSK together with neural miniagrin observed in soleus muscle or diaphragm in comparison to EDL muscle can be explained by affiliation of those muscles to different groups, according to the spatio-temporal shape of NMJ formation. Both diaphragm and soleus muscle belong to group with so called DeSyn properties. In contrast EDL represents FaSyn muscle class. FaSyn and DeSyn muscles show distinct patterns of synapse assembly as well as response to paralysis or denervation in the adult [116].

Overexpression of neural agrin in adult MuSK-tg mice resulted in formation of ectopic AChR clusters only in the region surrounding the NMJ but not throughout the entire muscle fibre where both transgenes were detected. This is unexpected and implies involvement of another, NMJ- specific, protein/s limiting formation of ectopic postsynapses in innervated muscles. Dok-7 seems to be a good candidate, and co-expression of MuSK and Dok-7 in innervated muscle resulted in formation of many ectopic AChR clusters along the entire muscle fibre.

The way of how Dok-7 contributes to linking activated MuSK to the AChR clustering remains still not clear. Its domain architecture strongly suggests the involvement in PI3 kinase signalling cascade. First, by binding to the juxtamembrane tyrosine residue with its phosphotyrosine binding (PTB) domain, Dok-7 causes a strong boosting of agrin-induced MuSK activation and keeps MuSK phosphorylation state relatively high [63]. Second, mature protein of Dok-7 contains also pleckstrin homology (PH) domain, [63] and it is well known than PI3 signalling events cause relocalization of the proteins containing PH domains and target them to the plasma membrane, where they interact with phosphoinositides [117-119]. Involvement PI3 kinase in this process has been described for several RTKs (e.g. EGFR, Insulin receptor). [120, 121] and such a receptor activity-induced membrane targeting seems to be the common phenomenon for the Dok family and has been observed also for other Dok family members [122, 123]. Third, clustering of AChRs requires reorganization of the cytoskeleton and Rac and Cdc42 are the key regulatory molecules that link surface receptors to the organization of the actin cytoskeleton [124, 125]. Additionally, PI3 kinase acts through Rac and Cdc42 during agrin-induced acetylcholine receptor clustering and application of PI3 inhibitors substantially impairs length of agrin-induced AChR clusters as well as activity of Rac and

Cdc42 *in vitro* [67]. It is then very likely that Dok-7 might be the missing signalling component in PI3 kinase signalling pathway, in which through activation of Rac/Cdc42.

The other possibility could be a stabilization of activated MuSK dimers to the plasma membrane allowing the formation of a scaffold for the recruitment of the other members of the cluster (e.g. AChRs, rapsyn). In our experiments we were able to immunoprecipitate more MuSK transgenic protein from synaptic regions of MuSK-tg mice compared to extrasynaptic parts. On the other hand, much more MuSK transgene can be detected in extrasynaptic portions of MADT mice, rich in ectopic AChR clusters. Since, MCK gene is expressed by myonuclei throughout the entire fibre [99] and all the transgenic proteins are expressed throughout the entire muscle fibre relatively equally, it is then likely that Dok-7, found to be localized to the ectopic AChR clusters *in vitro* [63] stabilizes MuSK to the postsynaptic plasma membrane.

1.5 REFERENCES

(for Chapter I and Maj et al. From Chapter II)

1.   Sanes, J.R. and J.W. Lichtman, *Induction, assembly, maturation and maintenance of a postsynaptic apparatus.* Nature reviews, 2001. **2**(11): p. 791-805.

2.   DeChiara, T.M., et al., *The receptor tyrosine kinase MuSK is required for neuromuscular junction formation in vivo.* Cell, 1996. **85**(4): p. 501-12.

3.   Gautam, M., et al., *Distinct phenotypes of mutant mice lacking agrin, MuSK, or rapsyn.* Brain research, 1999. **114**(2): p. 171-8.

4.   Hesser, B.A., O. Henschel, and V. Witzemann, *Synapse disassembly and formation of new synapses in postnatal muscle upon conditional inactivation of MuSK.* Molecular and cellular neurosciences, 2006. **31**(3): p. 470-80.

5.   Kong, X.C., P. Barzaghi, and M.A. Ruegg, *Inhibition of synapse assembly in mammalian muscle in vivo by RNA interference.* EMBO reports, 2004. **5**(2): p. 183-8.

6.   Sherrington, C.S.i.V.L., 1897). *A Text-Book of Physiology 7th edn (ed. Foster, M.).* 1897.

7.   Purves D, A.G.J., Fitzpatrick D., Hall W.C., *Neuroscience Chapter 5 (synaptic transmission).* 2004.

8.   English, A.W. and S.L. Wolf, *The motor unit. Anatomy and physiology.* Phys Ther, 1982. **62**(12): p. 1763-72.

9.   Enoka, R.M., *Morphological features and activation patterns of motor units.* J Clin Neurophysiol, 1995. **12**(6): p. 538-59.

10. Burke, R.E., *Revisiting the notion of 'motor unit types'.* Prog Brain Res, 1999. **123**: p. 167-75.

11. McDonagh, J.C., et al., *Tetrapartite classification of motor units of cat tibialis posterior.* J Neurophysiol, 1980. **44**(4): p. 696-712.

12. Bear M.F., C.B.W., Paradiso M.A., *Neuroscience, Exploring the brain.* 2006.

13. Engel A.G., F.-A.C., *Myology: Basic and Clinical.* 1994. **1**: p. 261– 302.

14. Yee, V.C., et al., *Regional heterogeneity in the distal motor axon: three zones with distinctive intrinsic components.* J Neurocytol, 1988. **17**(5): p. 649-56.

15.   Covault, J. and J.R. Sanes, *Distribution of N-CAM in synaptic and extrasynaptic portions of developing and adult skeletal muscle.* J Cell Biol, 1986. **102**(3): p. 716-30.

16.   Flucher, B.E. and M.P. Daniels, *Distribution of Na+ channels and ankyrin in neuromuscular junctions is complementary to that of acetylcholine receptors and the 43 kd protein.* Neuron, 1989. **3**(2): p. 163-75.

17.   Wood, S.J. and C.R. Slater, *The contribution of postsynaptic folds to the safety factor for neuromuscular transmission in rat fast- and slow-twitch muscles.* J Physiol, 1997. **500 (Pt 1)**: p. 165-76.

18.   Rauvala, H. and H.B. Peng, *HB-GAM (heparin-binding growth-associated molecule) and heparin-type glycans in the development and plasticity of neuron-target contacts.* Prog Neurobiol, 1997. **52**(2): p. 127-44.

19.   Krejci, E., et al., *The mammalian gene of acetylcholinesterase-associated collagen.* J Biol Chem, 1997. **272**(36): p. 22840-7.

20.   Scott LJ, B.F., Sanes JR., *A synapse-specific carbohydrate at the neuromuscular junction: association with both acetylcholinesterase and a glycolipid.* J Neuroscience, 1988. **8**(3): p. 932-944.

21.   Brand-Saberi, B., et al., *The formation of somite compartments in the avian embryo.* Int J Dev Biol, 1996. **40**(1): p. 411-20.

22.   Ontell, M., M.P. Ontell, and M. Buckingham, *Muscle-specific gene expression during myogenesis in the mouse.* Microsc Res Tech, 1995. **30**(5): p. 354-65.

23.   Leber, S.M., S.M. Breedlove, and J.R. Sanes, *Lineage, arrangement, and death of clonally related motoneurons in chick spinal cord.* J Neurosci, 1990. **10**(7): p. 2451-62.

24.   Sanes, J.R. and J.W. Lichtman, *Development of the vertebrate neuromuscular junction.* Annu Rev Neurosci, 1999. **22**: p. 389-442.

25.   Son, Y.J., J.T. Trachtenberg, and W.J. Thompson, *Schwann cells induce and guide sprouting and reinnervation of neuromuscular junctions.* Trends Neurosci, 1996. **19**(7): p. 280-5.

26.   Valenzuela, D.M., et al., *Receptor tyrosine kinase specific for the skeletal muscle lineage: expression in embryonic muscle, at the neuromuscular junction, and after injury.* Neuron, 1995. **15**(3): p. 573-84.

27.   Cheusova, T., et al., *Identification of developmentally regulated expression of MuSK in astrocytes of the rodent retina.* Journal of neurochemistry, 2006. **99**(2): p. 450-7.

28.   Garcia-Osta, A., et al., *MuSK expressed in the brain mediates cholinergic responses, synaptic plasticity, and memory formation.* The Journal of neuroscience, 2006. **26**(30): p. 7919-32.

29.   Ksiazek, I., et al., *Synapse loss in cortex of agrin-deficient mice after genetic rescue of perinatal death.* The Journal of neuroscience, 2007. **27**(27): p. 7183-95.

30.   Kim, C.H., W.C. Xiong, and L. Mei, *Regulation of MuSK expression by a novel signaling pathway.* The Journal of biological chemistry, 2003. **278**(40): p. 38522-7.

31.   Lacazette, E., et al., *A novel pathway for MuSK to induce key genes in neuromuscular synapse formation.* The Journal of cell biology, 2003. **161**(4): p. 727-36.

32.   Kuehn, R., S.A. Eckler, and M. Gautam, *Multiple alternatively spliced transcripts of the receptor tyrosine kinase MuSK are expressed in muscle.* Gene, 2005. **360**(2): p. 83-91.

33.   Hesser, B.A., A. Sander, and V. Witzemann, *Identification and characterization of a novel splice variant of MuSK.* FEBS letters, 1999. **442**(2-3): p. 133-7.

34.   Bhanot, P., et al., *A new member of the frizzled family from Drosophila functions as a Wingless receptor.* Nature, 1996. **382**(6588): p. 225-30.

35.   Masiakowski, P. and G.D. Yancopoulos, *The Wnt receptor CRD domain is also found in MuSK and related orphan receptor tyrosine kinases.* Curr Biol, 1998. **8**(12): p. R407.

36.   Saldanha, J., J. Singh, and D. Mahadevan, *Identification of a Frizzled-like cysteine rich domain in the extracellular region of developmental receptor tyrosine kinases.* Protein science, 1998. **7**(7): p. 1632-5.

37.   Zhou, H., et al., *Distinct domains of MuSK mediate its abilities to induce and to associate with postsynaptic specializations.* The Journal of cell biology, 1999. **146**(5): p. 1133-46.

38.   Stiegler, A.L., S.J. Burden, and S.R. Hubbard, *Crystal structure of the agrin-responsive immunoglobulin-like domains 1 and 2 of the receptor tyrosine kinase MuSK.* Journal of molecular biology, 2006. **364**(3): p. 424-33.

39.   Bowen, D.C., et al., *Localization and regulation of MuSK at the neuromuscular junction.* Developmental biology, 1998. **199**(2): p. 309-19.

40.   Heldin, C.H., *Dimerization of cell surface receptors in signal transduction.* Cell, 1995. **80**(2): p. 213-23.

41.   Schlessinger, J. and A. Ullrich, *Growth factor signaling by receptor tyrosine kinases.* Neuron, 1992. **9**(3): p. 383-91.

42.   Herbst, R. and S.J. Burden, *The juxtamembrane region of MuSK has a critical role in agrin-mediated signaling.* The EMBO journal, 2000. **19**(1): p. 67-77.

43.   Watty, A., et al., *The in vitro and in vivo phosphotyrosine map of activated MuSK.* Proceedings of the National Academy of Sciences of the United States of America, 2000. **97**(9): p. 4585-90.

44.   Cheusova, T., et al., *Casein kinase 2-dependent serine phosphorylation of MuSK regulates acetylcholine receptor aggregation at the neuromuscular junction.* Genes & development, 2006. **20**(13): p. 1800-16.

45.   McMahan, U.J., *The agrin hypothesis.* Cold Spring Harb Symp Quant Biol, 1990. **55**: p. 407-18.

46.   Ruegg, M.A. and J.L. Bixby, *Agrin orchestrates synaptic differentiation at the vertebrate neuromuscular junction.* Trends in neurosciences, 1998. **21**(1): p. 22-7.

47.   Godfrey, E.W., et al., *Components of Torpedo electric organ and muscle that cause aggregation of acetylcholine receptors on cultured muscle cells.* J Cell Biol, 1984. **99**(2): p. 615-27.

48.   Nitkin, R.M., et al., *Molecular components of the synaptic basal lamina that direct differentiation of regenerating neuromuscular junctions.* Cold Spring Harb Symp Quant Biol, 1983. **48 Pt 2**: p. 653-65.

49.   Campanelli, J.T., et al., *Agrin mediates cell contact-induced acetylcholine receptor clustering.* Cell, 1991. **67**(5): p. 909-16.

50.   McMahan, U.J., et al., *Agrin isoforms and their role in synaptogenesis.* Curr Opin Cell Biol, 1992. **4**(5): p. 869-74.

51.   Bezakova, G. and M.A. Ruegg, *New insights into the roles of agrin.* Nature reviews, 2003. **4**(4): p. 295-308.

52.   Hoch, W., et al., *Developmental regulation of highly active alternatively spliced forms of agrin.* Neuron, 1993. **11**(3): p. 479-90.

53.   O'Connor, L.T., et al., *Localization and alternative splicing of agrin mRNA in adult rat brain: transcripts encoding isoforms that aggregate acetylcholine receptors are not restricted to cholinergic regions.* J Neurosci, 1994. **14**(3 Pt 1): p. 1141-52.

54.   Ruegg, M.A., et al., *The agrin gene codes for a family of basal lamina proteins that differ in function and distribution.* Neuron, 1992. **8**(4): p. 691-9.

55.   Yang, J.F., et al., *Schwann cells express active agrin and enhance aggregation of acetylcholine receptors on muscle fibers.* J Neurosci, 2001. **21**(24): p. 9572-84.

56.   Burgess, R.W., et al., *Alternatively spliced isoforms of nerve- and muscle-derived agrin: their roles at the neuromuscular junction.* Neuron, 1999. **23**(1): p. 33-44.

57.   Gesemann, M., A.J. Denzer, and M.A. Ruegg, *Acetylcholine receptor-aggregating activity of agrin isoforms and mapping of the active site.* J Cell Biol, 1995. **128**(4): p. 625-36.

58.   Glass, D.J., et al., *Agrin acts via a MuSK receptor complex.* Cell, 1996. **85**(4): p. 513-23.

59.   Scotton, P., et al., *Activation of muscle-specific receptor tyrosine kinase and binding to dystroglycan are regulated by alternative mRNA splicing of agrin.* The Journal of biological chemistry, 2006. **281**(48): p. 36835-45.

60.   Gesemann, M., et al., *Alternative splicing of agrin alters its binding to heparin, dystroglycan, and the putative agrin receptor.* Neuron, 1996. **16**(4): p. 755-67.

61.   Shi, L., et al., *Dok5 is substrate of TrkB and TrkC receptors and involved in neurotrophin induced MAPK activation.* Cellular signalling, 2006. **18**(11): p. 1995-2003.

62.   Zhang, Y., et al., *Molecular basis of distinct interactions between Dok1 PTB domain and tyrosine-phosphorylated EGF receptor.* J Mol Biol, 2004. **343**(4): p. 1147-55.

63.   Okada, K., et al., *The muscle protein Dok-7 is essential for neuromuscular synaptogenesis.* Science (New York, N.Y, 2006. **312**(5781): p. 1802-5.

64.   Beeson, D., et al., *Dok-7 mutations underlie a neuromuscular junction synaptopathy.* Science (New York, N.Y, 2006. **313**(5795): p. 1975-8.

65.   Muller, J.S., et al., *Phenotypical spectrum of DOK7 mutations in congenital myasthenic syndromes.* Brain, 2007. **130**(Pt 6): p. 1497-506.

66.   Palace, J., et al., *Clinical features of the DOK7 neuromuscular junction synaptopathy.* Brain, 2007.

67.   Nizhynska, V., R. Neumueller, and R. Herbst, *Phosphoinositide 3-kinase acts through RAC and Cdc42 during agrin-induced acetylcholine receptor clustering.* Developmental neurobiology, 2007. **67**(8): p. 1047-58.

68.   Manser, E., et al., *A brain serine/threonine protein kinase activated by Cdc42 and Rac1.* Nature, 1994. **367**(6458): p. 40-6.

69.   Sander, E.E., et al., *Matrix-dependent Tiam1/Rac signaling in epithelial cells promotes either cell-cell adhesion or cell migration and is regulated by phosphatidylinositol 3-kinase.* J Cell Biol, 1998. **143**(5): p. 1385-98.

70.   Sells, M.A., J.T. Boyd, and J. Chernoff, *p21-activated kinase 1 (Pak1) regulates cell motility in mammalian fibroblasts.* J Cell Biol, 1999. **145**(4): p. 837-49.

71.   Weston, C., et al., *Agrin-induced acetylcholine receptor clustering is mediated by the small guanosine triphosphatases Rac and Cdc42.* J Cell Biol, 2000. **150**(1): p. 205-12.

72.   Luo, Z.G., et al., *Regulation of AChR clustering by Dishevelled interacting with MuSK and PAK1.* Neuron, 2002. **35**(3): p. 489-505.

73.   Mittaud, P., et al., *Agrin-induced activation of acetylcholine receptor-bound Src family kinases requires Rapsyn and correlates with acetylcholine receptor clustering.* The Journal of biological chemistry, 2001. **276**(17): p. 14505-13.

74. Schaeffer, L., et al., *Implication of a multisubunit Ets-related transcription factor in synaptic expression of the nicotinic acetylcholine receptor.* Embo J, 1998. **17**(11): p. 3078-90.

75. Batchelor, A.H., et al., *The structure of GABPalpha/beta: an ETS domain- ankyrin repeat heterodimer bound to DNA.* Science, 1998. **279**(5353): p. 1037-41.

76. Briguet, A. and M.A. Ruegg, *The Ets transcription factor GABP is required for postsynaptic differentiation in vivo.* J Neurosci, 2000. **20**(16): p. 5989-96.

77. Jaworski, A., C.L. Smith, and S.J. Burden, *GA-binding protein is dispensable for neuromuscular synapse formation and synapse-specific gene expression.* Mol Cell Biol, 2007. **27**(13): p. 5040-6.

78. Hippenmeyer, S., et al., *ETS transcription factor Erm controls subsynaptic gene expression in skeletal muscles.* Neuron, 2007. **55**(5): p. 726-40.

79. Yang, X., et al., *Patterning of muscle acetylcholine receptor gene expression in the absence of motor innervation.* Neuron, 2001. **30**(2): p. 399-410.

80. Dimitropoulou, A. and J.L. Bixby, *Motor neurite outgrowth is selectively inhibited by cell surface MuSK and agrin.* Molecular and cellular neurosciences, 2005. **28**(2): p. 292-302.

81. Jing, S., et al., *GDNF-induced activation of the ret protein tyrosine kinase is mediated by GDNFR-alpha, a novel receptor for GDNF.* Cell, 1996. **85**(7): p. 1113-24.

82. Klagsbrun, M. and A. Baird, *A dual receptor system is required for basic fibroblast growth factor activity.* Cell, 1991. **67**(2): p. 229-31.

83. Lopez-Casillas, F., et al., *Structure and expression of the membrane proteoglycan betaglycan, a component of the TGF-beta receptor system.* Cell, 1991. **67**(4): p. 785-95.

84. Binari, R.C., et al., *Genetic evidence that heparin-like glycosaminoglycans are involved in wingless signaling.* Development, 1997. **124**(13): p. 2623-32.

85. Luo, Z.G., et al., *Implication of geranylgeranyltransferase I in synapse formation.* Neuron, 2003. **40**(4): p. 703-17.

86. Finn, A.J., G. Feng, and A.M. Pendergast, *Postsynaptic requirement for Abl kinases in assembly of the neuromuscular junction.* Nature neuroscience, 2003. **6**(7): p. 717-23.

87. Cartaud, A., et al., *MuSK is required for anchoring acetylcholinesterase at the neuromuscular junction.* The Journal of cell biology, 2004. **165**(4): p. 505-15.

88. Strochlic, L., et al., *MAGI-1c: a synaptic MAGUK interacting with muSK at the vertebrate neuromuscular junction.* The Journal of cell biology, 2001. **153**(5): p. 1127-32.

89.   Strochlic, L., et al., *14-3-3 gamma associates with muscle specific kinase and regulates synaptic gene transcription at vertebrate neuromuscular synapse.* Proceedings of the National Academy of Sciences of the United States of America, 2004. **101**(52): p. 18189-94.

90.   Mohamed, A.S., et al., *Src-class kinases act within the agrin/MuSK pathway to regulate acetylcholine receptor phosphorylation, cytoskeletal anchoring, and clustering.* The Journal of neuroscience, 2001. **21**(11): p. 3806-18.

91.   Bowe, M.A., et al., *Identification and purification of an agrin receptor from Torpedo postsynaptic membranes: a heteromeric complex related to the dystroglycans.* Neuron, 1994. **12**(5): p. 1173-80.

92.   Gee, S.H., et al., *Dystroglycan-alpha, a dystrophin-associated glycoprotein, is a functional agrin receptor.* Cell, 1994. **77**(5): p. 675-86.

93.   Martin, P.T. and J.R. Sanes, *Integrins mediate adhesion to agrin and modulate agrin signaling.* Development, 1997. **124**(19): p. 3909-17.

94.   Daggett, D.F., et al., *The role of an agrin-growth factor interaction in ACh receptor clustering.* Mol Cell Neurosci, 1996. **8**(4): p. 272-85.

95.   Storms, S.D., et al., *NCAM-mediated adhesion of transfected cells to agrin.* Cell Adhes Commun, 1996. **3**(6): p. 497-509.

96.   Denzer, A.J., et al., *Agrin binds to the nerve-muscle basal lamina via laminin.* J Cell Biol, 1997. **137**(3): p. 671-83.

97.   Gautam, M., et al., *Defective neuromuscular synaptogenesis in agrin-deficient mutant mice.* Cell, 1996. **85**(4): p. 525-35.

98.   Penuel, E., R.W. Akita, and M.X. Sliwkowski, *Identification of a region within the ErbB2/HER2 intracellular domain that is necessary for ligand-independent association.* The Journal of biological chemistry, 2002. **277**(32): p. 28468-73.

99.   Tang, J., S.A. Jo, and S.J. Burden, *Separate pathways for synapse-specific and electrical activity-dependent gene expression in skeletal muscle.* Development (Cambridge, England), 1994. **120**(7): p. 1799-804.

100.   Herbst, R., E. Avetisova, and S.J. Burden, *Restoration of synapse formation in Musk mutant mice expressing a Musk/Trk chimeric receptor.* Development (Cambridge, England), 2002. **129**(23): p. 5449-60.

101.   Lyons, G.E., et al., *Developmental regulation of creatine kinase gene expression by myogenic factors in embryonic mouse and chick skeletal muscle.* Development (Cambridge, England), 1991. **113**(3): p. 1017-29.

102.   Meier, T., et al., *AChR phosphorylation and aggregation induced by an agrin fragment that lacks the binding domain for alpha-dystroglycan.* The EMBO journal, 1996. **15**(11): p. 2625-31.

103. Schaeffer, L., A. de Kerchove d'Exaerde, and J.P. Changeux, *Targeting transcription to the neuromuscular synapse.* Neuron, 2001. **31**(1): p. 15-22.

104. Baldwin, T.J., et al., *Regulation of transcript encoding the 43K subsynaptic protein during development and after denervation.* Development (Cambridge, England), 1988. **104**(4): p. 557-64.

105. Witzemann, V., et al., *Primary structure and functional expression of the alpha-, beta-, gamma-, delta- and epsilon-subunits of the acetylcholine receptor from rat muscle.* European journal of biochemistry / FEBS, 1990. **194**(2): p. 437-48.

106. Glass, D.J., et al., *Kinase domain of the muscle-specific receptor tyrosine kinase (MuSK) is sufficient for phosphorylation but not clustering of acetylcholine receptors: required role for the MuSK ectodomain?* Proceedings of the National Academy of Sciences of the United States of America, 1997. **94**(16): p. 8848-53.

107. Sketelj, J., et al., *Interactions between intrinsic regulation and neural modulation of acetylcholinesterase in fast and slow skeletal muscles.* Cellular and molecular neurobiology, 1991. **11**(1): p. 35-54.

108. Cull-Candy, S.G., R. Miledi, and O.D. Uchitel, *Properties of junctional and extrajunctional acetylcholine-receptor channels in organ cultured human muscle fibres.* The Journal of physiology, 1982. **333**: p. 251-67.

109. Bernheim, L., et al., *Role of nicotinic acetylcholine receptors at the vertebrate myotendinous junction: a hypothesis.* Neuromuscular disorders, 1996. **6**(3): p. 211-4.

110. Bao, Z.Z., et al., *Alpha 7 beta 1 integrin is a component of the myotendinous junction on skeletal muscle.* J Cell Sci, 1993. **106 (Pt 2)**: p. 579-89.

111. Martin, P.T., et al., *Synaptic integrins in developing, adult, and mutant muscle: selective association of alpha1, alpha7A, and alpha7B integrins with the neuromuscular junction.* Dev Biol, 1996. **174**(1): p. 125-39.

112. Williams, P.E. and G. Goldspink, *Longitudinal growth of striated muscle fibres.* J Cell Sci, 1971. **9**(3): p. 751-67.

113. Rupp, F., et al., *Structure and expression of a rat agrin.* Neuron, 1991. **6**(5): p. 811-23.

114. Tsim, K.W., et al., *cDNA that encodes active agrin.* Neuron, 1992. **8**(4): p. 677-89.

115. Sugiyama, J., D.C. Bowen, and Z.W. Hall, *Dystroglycan binds nerve and muscle agrin.* Neuron, 1994. **13**(1): p. 103-15.

116. Santos, A.F. and P. Caroni, *Assembly, plasticity and selective vulnerability to disease of mouse neuromuscular junctions.* J Neurocytol, 2003. **32**(5-8): p. 849-62.

117. Kavran, J.M., et al., *Specificity and promiscuity in phosphoinositide binding by pleckstrin homology domains.* J Biol Chem, 1998. **273**(46): p. 30497-508.

118. Klarlund, J.K., et al., *Distinct polyphosphoinositide binding selectivities for pleckstrin homology domains of GRP1-like proteins based on diglycine versus triglycine motifs.* J Biol Chem, 2000. **275**(42): p. 32816-21.

119. Lemmon, M.A. and K.M. Ferguson, *Molecular determinants in pleckstrin homology domains that allow specific recognition of phosphoinositides.* Biochem Soc Trans, 2001. **29**(Pt 4): p. 377-84.

120. Isakoff, S.J., et al., *The inability of phosphatidylinositol 3-kinase activation to stimulate GLUT4 translocation indicates additional signaling pathways are required for insulin-stimulated glucose uptake.* Proc Natl Acad Sci U S A, 1995. **92**(22): p. 10247-51.

121. Rodrigues, G.A., et al., *A novel positive feedback loop mediated by the docking protein Gab1 and phosphatidylinositol 3-kinase in epidermal growth factor receptor signaling.* Mol Cell Biol, 2000. **20**(4): p. 1448-59.

122. Zhao, M., et al., *Phosphoinositide 3-kinase-dependent membrane recruitment of p62(dok) is essential for its negative effect on mitogen-activated protein (MAP) kinase activation.* J Exp Med, 2001. **194**(3): p. 265-74.

123. Liang, X., et al., *Phosphatidylinositol 3-kinase and Src family kinases are required for phosphorylation and membrane recruitment of Dok-1 in c-Kit signaling.* J Biol Chem, 2002. **277**(16): p. 13732-8.

124. Nobes, C.D. and A. Hall, *Rho, rac, and cdc42 GTPases regulate the assembly of multimolecular focal complexes associated with actin stress fibers, lamellipodia, and filopodia.* Cell, 1995. **81**(1): p. 53-62.

125. Bloch, R.J., *Actin at receptor-rich domains of isolated acetylcholine receptor clusters.* J Cell Biol, 1986. **102**(4): p. 1447-58.

The mitogen-activated protein kinase phosphatase, MKP-1, controls postsynaptic differentiation at nerve-muscle synapses

Gabriela Bezakova[1], C. Florian Bentzinger[1], Marcin Maj[1], Ulrich Certa[2], Hans-Rudolf Brenner[3], Markus A. Ruegg[1]

[1]Biozentrum, University of Basel, CH-4056 Basel, Switzerland;
[2]Roche Center for Medical Genomics, F. Hoffmann-La Roche AG, CH-4070, Basel, Switzerland;
[3]Institute of Physiology, Department of Biomedicine, University of Basel, CH-4056 Basel, Switzerland

2.1 ABSTRACT

Synaptic differentiation requires expression of specific genes and accumulation of distinct proteins on the pre- and postsynaptic sides. Here, we identified and functionally characterized genes induced in soleus muscle by agrin, the organizer of postsynaptic differentiation at the neuromuscular junction (NMJ). We show that signal transduction downstream of agrin involves the mitogen-activated protein kinase (MAPK) pathway, particularly ERK1/2 and JNK. Their activation is ErbB-independent but can be triggered via MuSK signaling probably through the MuSK-associated molecule PAK-1 as its downregulation also inhibits postsynaptic differentiation *in vivo*. Finally, we identify the MAPK phosphatase-1, MKP-1, as a crucial negative feedback control of MAPK signaling that regulates postsynaptic differentiation spatially. Our results provide compelling evidence that the MAPK pathway, which is implicated in synaptic plasticity at neuron-neuron synapses, plays also an important role at the NMJ.

2.2 INTRODUCTION

Neurotransmission at chemical synapses relies on the precise apposition of specialized pre- and postsynaptic structures which contain distinct protein sets according to their synaptic activity (inhibitory versus excitatory). The accumulation of such protein sets is regulated by transcription, translation and aggregation. Additionally, the formation of functionally and molecularly diverse synaptic specializations on a single neuron requires complex regulatory mechanisms for the transcription of specific genes in a single nucleus and the delivery of synthesized products (mRNAs or proteins) to specific synaptic contacts (reviewed in Ref.[1]). Initially, synaptic differentiation is triggered by multiple adhesive interactions between the synapsing cells[1,2] independently of synaptic activity[3].

The NMJ is a peripheral synapse that shares many structural and functional features with central synapses. Because of its relative simplicity and experimental accessibility, the molecular mechanisms underlying NMJ formation have been readily investigated. A key protein involved in the assembly of postsynaptic structures is the <u>mu</u>scle-<u>s</u>pecific receptor tyrosine <u>k</u>inase, MuSK[4], which is activated by the extracellular matrix molecule agrin[5,6]. Agrin comprises several splice variants but only those secreted by the presynaptic motor nerve terminal and anchored in the synaptic basal lamina activate MuSK[7,8]. In addition to agrin-MuSK signaling, the neuregulin-ErbB pathway has long been considered to play an important role in inducing synthesis of AChRs at the NMJ (reviewed in Ref.[9]). However, NMJs of mice in which neuregulin-ErbB signaling in muscle was abrogated are functionally and morphologically normal[10].

Although there is an increasing understanding of the essential molecular components important for the formation of the NMJ, the underlying intracellular signaling pathways remain unclear. Previous studies aimed at identifying transcripts at the mature NMJ revealed a set of candidate genes and several novel synapse-specific proteins[11-13]. Here, we injected recombinant neuronal agrin into adult rat soleus muscle[14] and profiled the transcriptome seven days later. Agrin-induced postsynaptic differentiation induces the transcription of a set of immediate-early genes (IEGs) and engages the mitogen-activated protein kinase (MAPK) pathway and the MAPK-phosphatase MKP-1. Functional analysis shows that MKP-1 is important for the postsynaptic differentiation *in vivo*. Interestingly, the proteins identified in our screen have also been reported to play a key role at excitatory synapses in the brain[15]. Thus, in addition to the well established structural and functional similarities, the formation central synapses and the NMJ also employs common molecular pathways.

2.3 METHODS

Antibodies.

The following sources were used for antibodies: P-ERK1/2 and total ERK1/2 (Invitrogen/BioSource); EGR-1, MKP-1, P-JNK, P-p38, blocking peptide for EGR-1 antibody, blocking peptide for MKP-1 antibody (Santa Cruz); c-Fos (Chemicon); PAK-1 (Cell Signaling); tubulin (Sigma). Antibodies against P-PAK-1 (Thr-423) and against the ε-AChR subunit were kind gifts from Drs. J. Chernoff and J.R. Sanes, respectively.

Induction of postsynaptic structures in soleus muscle.

Agrin-B/z+ and agrin-B/z- were purified from the conditioned media of stably transfected HEK293 cells, as previously described[14]. Animal experiments were carried out on adult male Wistar rats. All surgical procedures were performed under general anesthesia using i.p. injection of Equithesin (0.4 ml/100 g body weight). Independent soleus muscles, 12 for each condition, were injected i.m. with 70 µl of 1 µM agrin-B/z+, 1 µM agrin–B/z- or PBS. After injection, half of the muscles in each group was kept innervated while another half was denervated by removing ~5 mm of the sciatic nerve in the mid thigh[14]. Experiments were approved by the Cantonal Veterinarian Office in Basel. The animals were euthanized 7 days after injections. Excised soleus muscles were either frozen in liquid nitrogen and used for the extraction of total RNA as indicated in **Figure 1a** or pinned down on the Sylgard support in a PBS filled Petri dish, labeled for AChRs with Alexa-bungarotoxin (Invitrogen), fixed with 2% paraformaldehyde and immunostained.

cRNA synthesis and hybridization with the Affymetrix GeneChip.

Pieces of muscle (~50 mg) with highest density of postsynaptic structures (see **Fig. 1a**) were cut on dry ice and total RNA was extracted using TRIzol (Invitrogen) and a FastPrep instrument for homogenization (Qbiogene/BIO101). The integrity of the total RNA was analyzed using an Agilent 2100 Bioanalyzer (Agilent). Ten µg of RNA were used for the synthesis of cDNA and of biotinylated cRNA according to the suppliers protocol (Affymetrix). Affymetrix rat RG-U34A, RG-U34B, and RG-U34C arrays containing 7,000 annotated genes and 17,000 ESTs were hybridized with fragmented biotin-labeled target cRNA, washed and stained using a streptavidin-phycoerythrin (SAPE) conjugate (Molecular Probes). To increase the signal intensity, the antibody amplification protocol was used as recommended by Affymetrix. The arrays were scanned with a confocal scanner (Affymetrix) and the raw data analysis normalization was done using the

Affymetrix Microarray Suite Software (v. 5.0).

GeneSpring analysis.

Raw data were analyzed based on the signal intensities of the corresponding probe sets. Mean values for gene readouts were obtained after normalization to the 50th percentile and after per gene and per chip normalizations. Using Venn diagram function, fold filtering and statistical analysis (two way ANOVA parametric test with $p<0.05$), those genes were selected whose average expression level increased by agrin-B/z+ more than 1.25- or 1.5- fold or decreased more than 1.25- or 1.5-fold in innervated and denervated muscles, respectively, when compared to agrin-B/z- and PBS injected muscles. The hierarchical gene clustering (gene tree) of selected genes was performed according to the software manufacturer's instructions (see **Fig. 1b**).

Histology of muscles from embryonic (E18) and postnatal (P2) tissues.

Mice of appropriate age were euthanized by decapitation. After pinning the tissue onto the Sylgard support, the skin was removed and the tissue was fixed with 4% PFA for 2 hours at room temperature. Fixed tissues were cryoprotected by incubation in 30% sucrose overnight, washed in PBS and mounted in OCT. The muscles of lower limbs were cut to obtain 10 µm longitudinal sections and immunostained.

Immunological staining of muscle whole mounts, cross-sections and C2C12 cells.

Muscles fixed in 2% PFA (see above) were cut into thinner muscle bundles containing ~ 100 fibers. Muscles frozen in isopentane were cut into 10 µm cross-sections. Samples were then permeabilized with 1% Triton/PBS for 30 or 5 min, respectively, washed with 100 mM glycine/PBS for 15 min, blocked with 1% BSA/PBS for 30 min and incubated with specific primary antibody overnight at 4°C. Next day, muscle bundles or cross-sections were washed with 1% BSA/PBS, 3 times for 1 hour or 10 min, respectively, stained with appropriate fluorescently labeled secondary antibodies diluted 1:1,000 for 1 hour at room temperature. After washing 3 times for 1 hour or 10 min, respectively, samples were mounted with Citifluor. C2C12 cells were washed with PBS, stained with Alexa- bungarotoxin for 30 min at 37°C, washed 3 times for 10 min and fixed with 2% PFA. Afterwards, they were processed similarly as muscle cross-sections (see above). All labeled samples were imaged using Leica confocal microscope and 40 – 63x objectives.

C2C12 cell cultures.

C2C12 myoblasts were plated on 3.5 cm dishes coated with 2% gelatin and cultured in Dulbecco's modified Eagle's medium (DMEM) supplemented with 10 % fetal calf serum until 80% confluent. To induce myotube formation, the growth medium was replaced by

the fusion medium containing DMEM supplemented with 2 % horse serum. Approximately 4 days later, when myotubes had formed, 1 nM agrin-B/z+ was added to the culture medium. Cells were harvested after various time intervals and examined by immunostaining or Western blot.

Activation of MuSK in HEK293 cell lines.

HEK293 cells cultured in DMEM supplemented with 10 % fetal calf serum were transfected with an expression constructs encoding full-length mouse MuSK using jetPEI transfection reagent (Qbiogene) according to the manufacturer's instructions. Two days after transfection, the cells were trypsinized and transferred to complete medium containing G418 (600 µg/ml). Several isolated clones were expanded and tested for MuSK expression. One clone with intermediate levels of expression was subsequently used. This clone or wild-type HEK293 cells were then transiently transfected with an expression construct encoding full-length mouse DOK-7 using Lipofectamine2000 transfection reagent (Invitrogen) according to the manufacturer's instructions. One day after transfection, cells were washed twice with ice-cold, serum-free DMEM and then lysed in cold lysis buffer [20 mM HEPES, pH 7.5, 150 mM NaCl, 1 mM EDTA, Protease inhibitor cocktail (Upstate), Phosphatase inhibitor cocktail II (Sigma)]. Cell lysates were incubated on ice for 30 min and centrifuged at 20,000g for 15 min at 4°C. Cleared lysates were incubated for 1 hour at 4°C with anti-MuSK antibodies and then with 50 µl of 50% protein A-Sepharose slurry (GE Healthcare) for 2 hours at 4°C. After centrifugation, beads were washed 3 times with ice-cold lysis buffer, bound proteins were eluted with SDS sample buffer and subjected to analysis by SDS PAGE and Western blot.

Tissue homogenization, immunoprecipitation, SDS PAGE and Western blot.

Muscles frozen in liquid nitrogen were powdered on dry ice, transferred to Dounce homogenizer filled with the cold lysis buffer [20 mM HEPES, pH 7.5, 150 mM NaCl, 1 mM EDTA, Protease inhibitor cocktail (Upstate), Phosphatase inhibitor cocktail II (Sigma)]. Cell lysates were incubated on ice for 30 min and centrifuged at 20,000g for 15 min at 4°C.

Cleared lysates were either diluted with sample buffer and loaded onto a 10% SDS PAGE or they were incubated for 3 hours with a specific primary antibody or control (normal rabbit serum) to immunoprecipitate MKP-1 protein. Antibody-antigen complex was incubated with 50 µl of 50% protein A-Sepharose slurry (GE Healthcare) for 3 hours at 4°C, centrifuged and beads were washed 3 times with ice-cold lysis buffer. Bound proteins eluted with SDS sample buffer were subjected to SDS-PAGE.

Separated proteins were transferred to nitrocellulose membranes (Schleicher & Schuell, Keene, NH). Nitrocellulose blots were incubated for 3 hours in blocking buffer

(5% BSA in PBS containing 0.1% Tween (PBST) or 3% TOP Block in PBST (for anti-phosphotyrosine antibodies) at room temperature. The blots were then incubated in blocking buffer containing specific primary antibodies overnight at 4°C. After washing 3 times for 15 min with PBST, the blots were incubated with HRP-conjugated goat anti-rabbit IgG and washed again 3 times for 15 min with PBST. Immunoreactive bands were visualized with chemiluminescence reagents kit (GE Healthcare).

Plasmids.

Mouse DOK-7 cDNA was derived from mouse gastrocnemius muscle using the forward primer 5'-CCGCTCGAGATGACCGAGGCAGCGC-3' and the reverse primer 5'-CTAGTCTAGAGGGAGGGGAGGGGGCTTTAC-3'. The amplified 1535 bp sequence was subcloned into pCiNeo expression vector (Promega). Rat MKP-1 and PAK-1 cDNAs were derived from rat soleus muscle. To amplify MKP-1, the forward primer 5'-AACCGCACAAGATCGACAGAC-3' and the reverse primer 5'-AACCGCACAAGATCGACAGAC-3' were used. The 1200 bp amplicon was subcloned into pcDNA 3.1 (Invitrogen). PAK-1 was amplified using the forward primer 5' GGAATTCGTGGTGACAATGTCAAATAACGG 3' and the reverse primer 5' CGGGATCCGTGATTGTTCTTGGTTGCCTC 3' excluding stop codon in order to fuse the protein to EGFP and subcloned into pEGFP-N3 vector. Cytoplasmic EGFP construct was from Invitrogen, nuclear targeted construct EGFP-NLS was prepared as described previously[48]. Vectors encoding specific shRNAs were constructed as described elsewhere[26]. The shRNA against CD4 targeted the sequence 494–514 of CD4 (M36850). The shRNA against MKP-1 targeted the sequences 729 – 749 (#1) and 1197 – 1217 (#2) of MKP1 (NM_053769) and the shRNA against PAK-1 targeted the sequences 545 – 565 (#1) and 1525 - 1545 (#2) and 1936-1956 of PAK-1 (NM_017198). The specificity of individual shRNAs was tested by co-transfection of constructs encoding relevant proteins and shRNA into COS7 cells using calcium precipitation. The shRNA construct targeting CD4 was used as a control.

Electroporation of muscle in vivo.

Constructs encoding proteins or shRNAs were electroporated into muscle fibers as described[26]. Briefly, soleus muscle of anesthetized Wistar rats (~160 g of body weight) was exposed and injected with 20 µl of a mixture containig the respective cDNA (2 µg/ml of each construct). The fascia and the skin were sutured and the electroporation was performed using an ECM 830 electroporation system (BTX). Eight pulses lasting 20 ms with the frequency of 1 Hz and the voltage set to 180 V/cm were applied. In some instances, innervation was preserved, while in others the sciatic nerve was cut (see above and results). One week later, soleus muscle was injected with recombinant agrin-B/z+

(see above). After another week the rat was euthanized, the soleus muscle was dissected, stained with Alexa-bungarotoxin and the amount of AChR aggregates in transfected and adjacent, non-transfected fibers was scored and ranked. The fibers with highest density (50 – 100% of AChR aggregates) were ranked as 2, fibers with medium density (10 – 50% aggregates) were ranked as 1 and fibers with less then 10 % aggregates were ranked as 0. The cumulative ranking count of AChRs for a particular condition was divided by the number of counted muscle fibers in given muscle. Transfected fibers were identified by GFP-positive signal and non transfected fibers in their immediate vicinity were used as an additional control when appropriate. Three to eight independently electroporated muscles and 30 – 50 transfected or non-transfected muscle fibers per muscle were evaluated.

Statistics.

Compiled data are expressed as mean ± s.e.m. For statistical comparisons of two conditions, the Student`s t- test was used. For multiple comparisons, a two-way ANOVA followed by parametric tests was applied. The levels of significance are indicated as follows: *** $p < 0.0001$, ** $p < 0.001$, * $p < 0.05$.

2.4 RESULTS

Identification of the transcriptome induced during postsynaptic differentiation

To study the gene program activated during postsynaptic differentiation at the NMJ, we injected recombinant neuronal agrin (agrin-B/z+; Ref.[8]) into innervated and denervated adult rat soleus muscles. As previously shown[14] and schematically drawn in **Figure 1a**, agrin-B/z+ induced the formation of distinct ectopic postsynaptic structures primarily near both ends of the muscle. In contrast, recombinant non-neuronal agrin (agrin-B/z-, inactive splice variant) or PBS did not induce any ectopic postsynaptic structure (**Fig. 1a**). Finally, the same injection protocol was applied to rat soleus muscles where the sciatic nerves were cut immediately after the injections. Muscle denervation upregulates expression of several molecules including MuSK[16] and AChR subunits[17] and thereby facilitates postsynaptic differentiation induced by agrin-B/z+[14]. Accordingly, the number of AChR clusters was much higher in denervated than in innervated muscles (**Fig. 1a**).

Seven days after the injections, RNA probes derived from 36 rat soleus muscles, representing 6 replicates for each of the 6 different treatments, were hybridized to DNA microarrays with about 24'000 oligonucleotide probe sets. Quality control revealed a high integrity of isolated mRNA as the ratios of hybridization signal intensities detected at the 3` and 5` probe sets for β-actin and glyceraldehyde-3-phosphate dehydrogenase (GAPDH) were around 1 in all samples (**Supplementary Fig. 1** online). Additionally, transcription of several genes which served as a control for our experimental setup coincided with previous reports[14,17,18]. For example, the α, β, γ, and δ AChR subunits were markedly upregulated in denervated muscle and transcription of the ε-AChR subunit increased several fold after injection of agrin-B/z+ into both, innervated and denervated muscles (3- and 2-fold above PBS, respectively; **Supplementary Fig. 2a** online). In innervated muscle, AChRs of the mature postsynaptic apparatus typically comprise the ε- but not the γ-subunit[19]. Consistently, ectopic AChR clusters induced by agrin-B/z+ in innervated muscle contained exclusively the ε-subunit. In denervated muscle, only a fraction of AChR clusters was stained for the ε-subunit (**Supplementary Fig. 2b** online), while the rest was positive for the γ-subunit (data not shown).

GeneSpring software was used to detect transcriptional changes induced by agrin-B/z+ (see Methods for details). We obtained a set of genes whose expression was significantly changed after agrin-B/z+ treatment and diverged from control values (PBS and agrin-B/z-) in both, innervated and denervated muscles by more than 25% and 50%,

respectively (**Fig. 1b**, **Supplementary Table 1** and **Supplementary Table 2** online). Upregulation of selected genes was confirmed by quantitative Real Time PCR on independent samples (**Supplementary Fig. 3** online, see also **Supplementary Methods** online for details). Moreover, our candidate list also comprised several genes that have previously been attributed to the NMJ (**Supplementary Table 2** online).
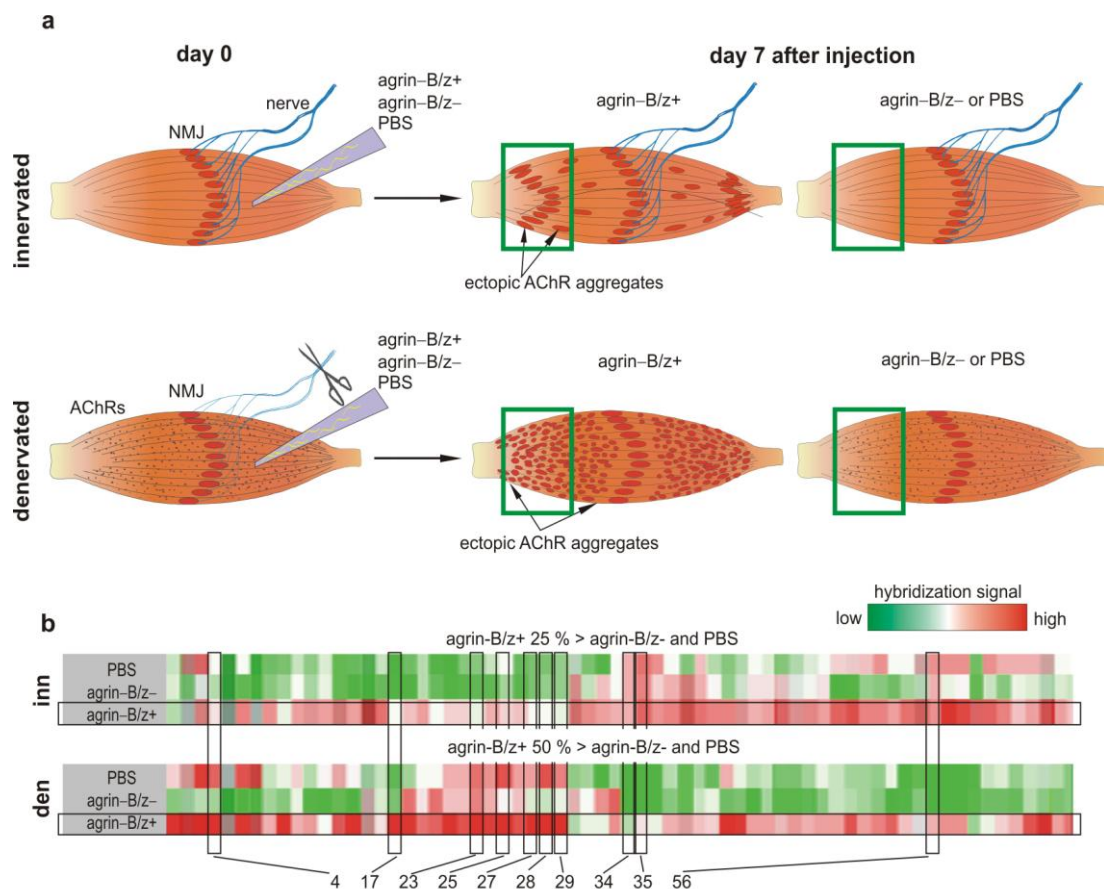
Fig. 1
Bezakova *et al.*

Figure 1 Profiling of synapse-specific gene transcription induced by agrin-B/z+.

(**a**) On day 0, rat soleus muscles were injected either with neuronal agrin-B/z+, agrin-B/z- or PBS. Agents were injected into innervated (upper row) and denervated muscles (lower row) with increased endogenous levels of AChRs (speckles). Seven days after injection, regions with the highest density of postsynaptic structures (green rectangles) were excised without prior visualization of postsynaptic structures and mRNA was isolated (see Methods for detail).

(**b**) Heat-map of genes that are significantly upregulated by agrin-B/z+ by more than 25% in innervated and 50% in denervated muscles when compared to PBS or agrin-B/z-. Genes are sorted by hierarchical clustering (gene tree) according to the intensity of their hybridization signals in all 6 conditions. Each bar represents the mean from 6 replicates. Heat-maps 4, 25, 28 and 29 represent EGR-1; 17 and 27: c-Fos; 34, 35 and 56: MKP-1; 23: ε-AChR subunit. See also **Supplementary Table 1** online for the complete list of genes.

Immediate-early genes are enriched at postsynaptic sites

A first notable result of our screen was that agrin-B/z+ significantly increased transcription of several IEGs such as c-Fos, Jun-B, EGR-1 (NGFI-A, zif268, krox-24 and TIS8), NGFI-B (nurr-77 or NR4A1), MKP-1 (DUSP1), gene-33 (RALT or Mig6), CEPB delta and Btg2 (**Supplementary Table 2** online). These IEGs are also induced by different stimuli in various tissues, the majority of them, however, has not yet been linked to postsynaptic differentiation at the NMJ. We selected and further examined EGR-1, c-Fos and MKP-1 because their expression was increased by agrin-B/z+ injection in several oligonucleotide probe sets (**Supplementary Table 1** online) and because they have been shown to be co-regulated at excitatory glutamatergic synapses[15]. At the NMJs, EGR-1 was found inside of subsynaptic nuclei and in a perinuclear pattern (**Fig. 2a**). Such a perinuclear staining pattern has also been described for the Golgi complex and microtubules[20]. The EGR-1 staining was also detected at the NMJs under YFP-labeled nerve terminals of transgenic mice[21] but was completely abrogated when EGR-1 antibodies were preincubated with the original antigenic peptide (**Supplementary Fig. 4a** and **b** online). Consistent with the microarray expression data, intramuscular injection of agrin-B/z+ increased protein levels of EGR-1 at ectopic sites of AChR clustering (**Fig. 2a**). Here, similarly as at the NMJ, EGR-1 localized to myonuclei and cytoskeleton structures (**Fig. 2a**) that were previously attributed to microtubules[20]. Interestingly, like the ε-AChR subunit, also EGR-1 was expressed at all ectopic AChR clusters in the innervated muscle, whereas some AChR clusters were negative for EGR-1 in denervated muscle (compare **Supplementary Fig. 4c** with **Supplementary Fig. 2b** online). In C2C12 cells, EGR-1 localized to nuclei in myoblasts and myotubes and to agrin-induced AChR aggregates in myotubes (**Supplementary Fig. 4c** online). Another examined IEG was c-Fos. Agrin induces c-Fos expression in CNS neurons[22] and c-Fos has also been implicated in the regulation of the ε-AChR subunit *in vitro*[23]. Antibodies against c-Fos decorated myonuclei throughout the muscle fiber but the myonuclei underneath the NMJ or at ectopic postsynaptic structures induced by agrin-B/z+ were stained more intensely (**Fig. 2b**). In C2C12 cells, nuclear expression of c-Fos increased upon myoblast fusion to myotubes (**Supplementary Fig. 4d** online) and was further enhanced at agrin-induced AChR aggregates (quantitative data not shown). Finally, MKP-1, the third candidate IEG, showed a very similar expression pattern as EGR-1. It was enriched at the NMJ (**Fig. 2c**), localized to nuclei in C2C12 myoblasts and myotubes and was also enriched at agrin-induced AChR aggregates (**Supplementary Fig. 4e** online). In summary, these studies indicate a functional involvement of examined IEGs in agrin-induced postsynaptic differentiation and corroborate our mRNA profiling data on the protein level.
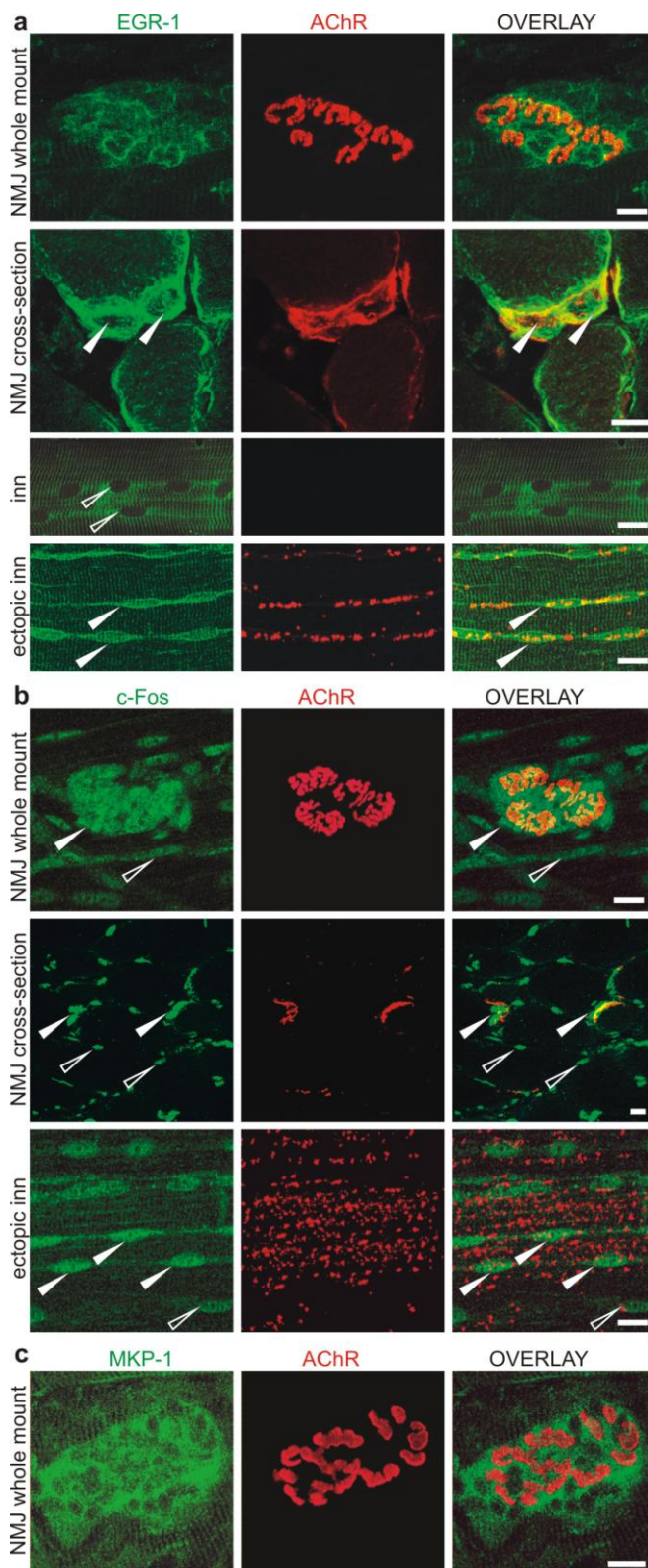
Fig. 2
Bezakova *et al.*

Figure 2 IEGs accumulate at the NMJ and at ectopic postsynaptic structures induced by agrin-B/z+.

(a) EGR-1 (green) is enriched at the NMJ. EGR-1 staining is mainly localized around myonuclei but is also present in subsynaptic myonuclei (arrowheads). The protein is not detected in non-synaptic nuclei of innervated muscle injected with PBS (row 'inn'; empty arrowheads) but is increased in nuclei localized in the vicinity of ectopic postsynaptic structures induced by agrin-B/z+ (row 'ectopic inn'; filled arrowheads).

(b) Staining of c-Fos (green) is found in myonuclei throughout the muscle fibers (empty arrowheads) but is more pronounced in subsynaptic myonuclei (filled arrowheads). Similarly, staining for c-Fos is enhanced in nuclei that are in the vicinity of ectopic postsynaptic structures (filled arrowheads).

(c) MKP-1 (green) is enriched at the NMJ and localizes to transversely oriented stripes throughout the muscle fiber. Note: all NMJs are visualized by rhodamine-labeled α-bungarotoxin (AChR, red). Scale bars, 10 µm.

Figure 2 IEGs accumulate at the NMJ and at ectopic postsynaptic structures induced by agrin-B/z+.

Agrin-induced postsynaptic differentiation involves the MAPK pathway

At central synapses, the MAPK pathway, particularly the extracellular-regulated kinases ERK1 and ERK2[15], induces expression of EGR-1, c-Fos and MKP-1. Moreover, expressed MKP-1 may in turn serve as a negative feedback regulator of the MAPK pathway. Therefore, we asked whether MAPKs localize to the NMJ and whether they can be activated by agrin-B/z+. As shown in **Figure 3a**, phosphorylated ERK1/2 (P-ERK) was enriched at postsynaptic structures of the NMJ. P-ERK was also found in synaptic and non-synaptic myonuclei and, to a lower extent, at cytoskeletal structures throughout the muscle fiber (**Fig. 3a**). P-ERK co-localized precisely with agrin-induced ectopic AChR clusters (**Fig. 3b**) and its total amount was increased by agrin-B/z+ both in innervated and denervated muscle (**Fig. 3c**). Interestingly, the total levels of P-ERK were also increased by denervation alone (**Fig. 3c**).

In muscle cell cultures, the MAPK pathway is activated by neuregulins via ErbB receptors[9]. To test whether the phosphorylation of ERK1/2 *in vivo* requires neuregulin-ErbB signaling, we examined muscles of mice where ErbB2 and ErbB4 receptors were selectively deleted in muscle tissues (herein called ErbB DKO)[10]. Muscles of these mice are normal and the NMJs do not show an apparent phenotype[10]. The expression of P-ERK at the NMJ was also presereved in ErbB DKO (**Fig. 3d**), indicating that neuregulin-ErbB signaling in muscle is also dispensable for ERK1/2 phosphorylation. This finding suggested that agrin-MuSK signaling might be sufficient to activate ERK1/2 at the NMJs. To test this hypothesis, we transfected an expression construct encoding DOK-7 into HEK293 cells that stably express MuSK. DOK-7 acts downstream of agrin-MuSK, binds to MuSK intracellularly and can activate MuSK[24]. While expression of either MuSK or DOK-7 alone did not affect levels of P-ERK, co-expression of both genes markedly boosted ERK1/2 phosphorylation (**Fig. 3e**). Thus, activation of MuSK results in the phosphorylation of ERK1/2 in heterologous cells suggesting that MuSK activation is also responsible for ERK1/2 activation at NMJs.

The finding that P-ERK is found in myonuclei and at AChR-rich sites suggest that it might be involved in both, gene transcription and AChR aggregation. To investigate this we used C2C12 myotubes. Basal levels of P-ERK were low and P-ERK was distributed mainly in the cytosol (**Fig. 3f**; immunofluorescence). Addition of agrin-B/z+ but not agrin-B/z- caused an increase in ERK1/2 phosphorylation after 15 min (**Fig. 3f**; Western blot) and induced the translocation of P-ERK into the nucleus (**Fig. 3f**; immunofluorescence). When C2C12 myotubes were incubated with agrin-B/z+ for 16 hours, P-ERK became aggregated at the plasma membrane and co-localized with AChR clusters (**Fig. 3f**). Hence in cultured muscle cells, agrin-B/z+ affects ERK1/2 phosphorylation in a fast and a

slow manner, which might reflect activation of gene transcription and cytoskeleton remodelling at AChR clusters, respecitively.

MKP-1 is a MAPK phosphatase that can regulate ERK1/2, c-Jun N-terminal kinase (JNK) or p38 depending on the tissue. To test which of the MAPKs is the endogenous substrate for MKP-1, we next examined the distribution of p38 and JNK at NMJs. We found that p38 was phosphorylated along the entire plasma membrane of muscle fiber (**Fig. 4a** and **Supplementary Fig. 5** online) and at the presynaptic nerve terminal as judged from its localization outside of the muscle fiber at the NMJ (**Fig. 4a**; inset). Such expression pattern of p-38 precludes its direct involvement in postsynaptic differentiation. In contrast, P-JNK co-localized with both, AChRs at the NMJ and at agrin-induced ectopic aggregates (**Fig. 4b**). These findings corroborate the role of JNK in the formation of postsynaptic structures *in vivo*[25]. Moreover, P-JNK, like P-ERK, remained highly enriched at NMJs of ErbB DKO mice (**Fig. 4b**). Activation of MuSK by DOK7 in HEK293 cells stably expressing MuSK, however, did not induce major changes in P-JNK levels (data not shown).
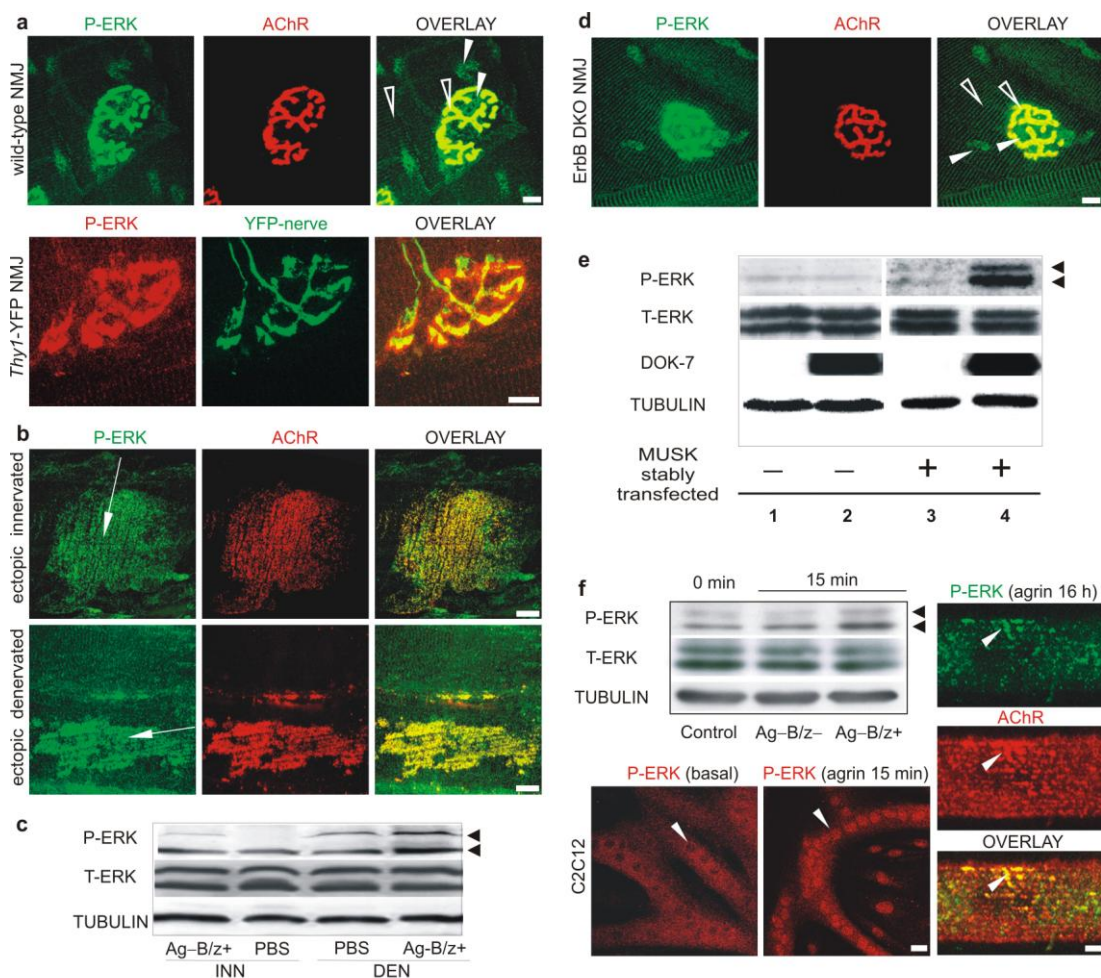
Fig. 3
Bezakova *et al.*

Figure 3 Agrin-MuSK signaling activates ERK1/2 during postsynaptic differentiation.

(a) Phosphorylated ERK1/2 (P-ERK; green or red) is highly enriched at the NMJ (yellow in the overlays), which was labeled either by rhodamine-α-bungarotoxin (AChR, red) or by YFP expressed in motor nerve terminals (YFP-nerve, green). Lower levels of P-ERK are also detected in the myonuclei (filled arrowheads) and at cytoskeletal structures (empty arrowheads).

(b) P-ERK (green) is enriched at ectopic postsynaptic structures (red). Note that in innervated muscle, AChRs and P-ERK are oriented transversely to the muscle axis (arrow, upper row) while their orientation is longitudinal in denervated muscles (arrow, lower row).

(c) P-ERK (arrowheads) is increased in innervated muscle (INN) after injection of agrin-B/z+ (Ag-B/z+). Denervation (DEN) alone increases ERK1/2 phosphorylation and this is further enhanced by injection of agrin-B/z+.

(continued on the next page)

(d) Enrichment of P-ERK at the NMJs is preserved in muscles where ErbB2/ErbB4 receptors were deleted (ErbB DKO). Note that localization of P-ERK to the nuclei (filled arrowheads) and to the cytoskeleton (empty arrowheads) in ErbB DKO and wild-type mice is identical.

(e) Activation of MuSK increases ERK1/2 phosphorylation. Wild-type HEK293 cells (lane 1, 2) or HEK293 cells stably expressing MuSK (lane 3, 4) were transfected with DOK-7 (lane 2, 4) or empty vector (lane 1, 3). Increased phosphorylation of ERK1/2 (arrowheads) is only observed in cells expressing both MuSK and DOK-7.

(f) Incubation of C2C12 myotubes with agrin-B/z+ for 15 minutes increases phosphorylation of ERK1/2 and induces its translocation into nuclei (arrowheads). In myotubes incubated with agrin-B/z+ overnight (agrin 16 h), phosphorylated ERK1/2 co-localizes with AChR clusters at plasma membrane (filled arrowheads). Scale bars, 10 µm.
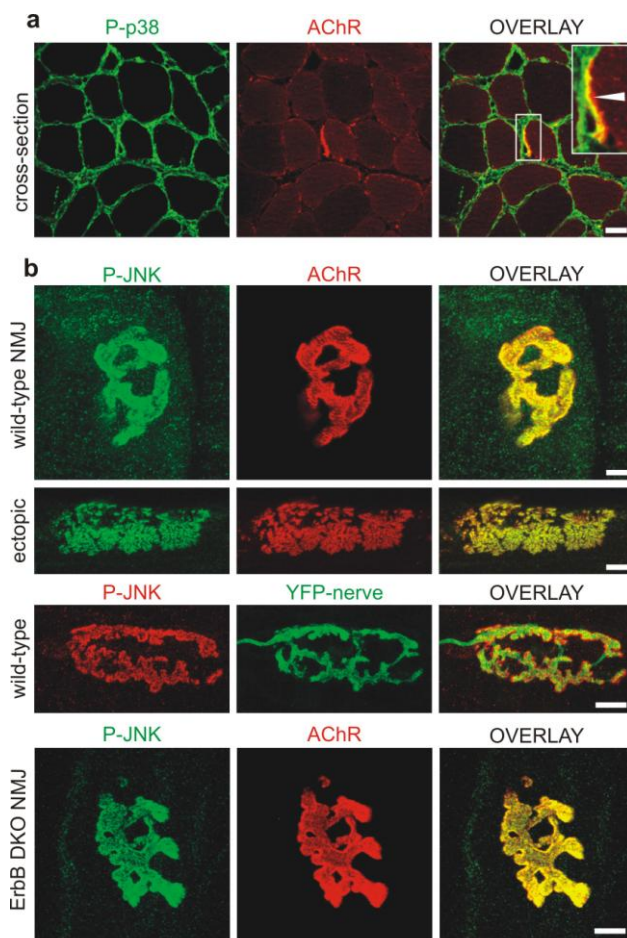
Fig. 4
Bezakova *et al.*

Figure 4 Expression of p38 and JNK.

(a) Phosphorylated p38 MAPK (P-p38; green) is found along the entire muscle fiber and is not confined to the NMJ, which was visualized by rhodamine α-bungarotoxin (AChR, red). Note that P-p38 staining overlaps with AChR staining only outside of the muscle fiber, indicating its presynaptic localization (inset).

(b) Phosphorylated JNK (P-JNK, green or red) is highly enriched at the NMJ and at ectopic postsynaptic structures visualized by rhodamine α-bungarotoxin staining (AChR, red). At the NMJs identified by YFP-labeled motor neurons, P-JNK decorates the area localized under the nerve terminal (third row; YFP-nerve, green). JNK phosphorylation is preserved in muscle lacking ErbB2/ErbB4 receptors (ErbB DKO). Scale bars, 10 μm.

MKP-1 regulates MAPK activation

Regulation of ERK1/2 activity by MKP-1 at glutamatergic synapses[15] and enrichment of ERK1/2 and MKP-1 at the NMJ led us to investigate their relationship in more detail. In muscle, P-ERK precisely co-localized with AChRs in cross-sections (**Fig. 5a**), while antibodies detecting pan-ERK1/2 (called herein total ERK; T-ERK) encircled myofibrils in muscle fibers (**Fig. 5b**). In whole mounts, T-ERK localized to subcellular structures reminiscent of Z-lines (**Fig. 5b**). Co-staining of α-actinin, a Z-line marker, revealed that T-ERK co-aligned around the Z-lines in two parallel stripes while MKP-1 precisely co-localized with Z-lines (**Fig. 5c**). This complementary localization of MKP-1 and T-ERK at the Z-lines suggests that ERK1/2 might be the substrate for MKP-1 in skeletal muscle. Indeed, MKP-1 antibodies but not pre-immune rabbit serum co-immunoprecipitated T-ERK protein from muscle extracts (**Fig. 5d**). Expression of another ERK1/2-selective phosphatase, MKP-3, was also reported at the NMJ[11]. We examined its distribution in cross-sections of rat soleus muscle. However, we neither detected MKP-3 protein at the NMJs (**Fig. 5e**) nor did we observe upregulation of MKP-3 transcription in our original gene expression screen (data not shown). Because of high correlation between expression patterns of MKP-1 and the non-phosphorylated form of ERK1/2, it is then conceivable that in muscle ERK1/2 is rather the substrate for MKP-1 than for MKP-3.

A further detailed examination of MKP-1 expression at the NMJ of wild-type mice revealed that MKP-1 was absent or non-detectable in AChR- and P-ERK-rich regions (**Fig. 5f** and **Supplementary Fig. 6** online). The mutually exclusive localization of MKP-1 and AChRs was also observed in ErbB DKO mice (**Fig. 5f**) and at ectopic postsynaptic structures induced by agrin in innervated muscle where regular stripes of MKP-1 separated transverse strings of AChR aggregates (arrowheads in **Fig. 5g**). Such regular arrangement of MKP-1 was not observed in denervated muscles where AChR aggregates were oriented longitudinally (**Fig. 5g**). Consistently, transcription and translation of MKP-1 was downregulated in one week denervated muscles (see **Supplementary Table 2a** online and **Fig. 5h**). Developmental studies further showed that MKP-1 expression was also undetectable in embryos (E18; **Fig. 5i**), while MKP-1 protein was clearly expressed postnatally (P2; **Fig. 5i**). In conclusion, these observations indicate that high levels of MKP-1 at the NMJs of innervated muscles may restrict activation of the MAPK pathway to the site of innervation and induce compaction of AChRs at the NMJ.
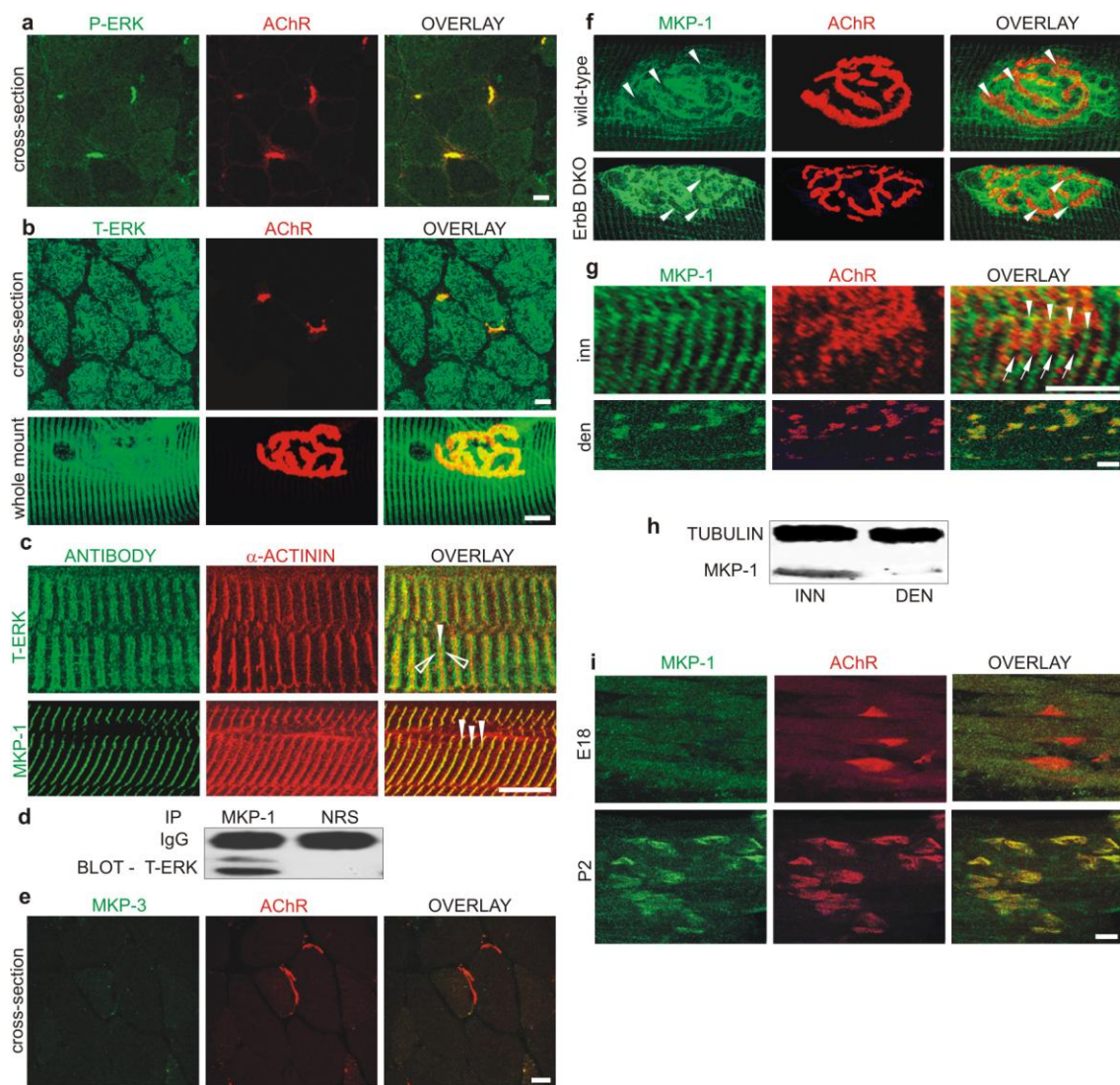
Fig. 5
Bezakova *et al.*

Figure 5 Complementary distributions of P-ERK and MKP-1.

(a) P-ERK (green) localizes to the NMJ, stained with rhodamine α-bungarotoxin (AChR, red).

(b) Antibodies to pan ERK1/2 (T-ERK, green) encircle the myofibrils throughout muscle fiber cross-sections. In whole mounts, T-ERK immunoreactivity is enriched in transverse bands.

(c) T-ERK (green, empty arrowheads) aligns in two parallel stripes around Z-lines, which are visualized with antibodies against α-actinin (red, filled arrowhead). MKP-1 (green, lower row) also localizes to Z-lines (red) throughout the muscle fiber. Note the precise co-localization of MKP-1 and α-actinin (yellow in the overlay and labeled by arrowheads).

(d) T-ERK co-immunoprecipitates from muscle extracts with antibodies to MKP-1 but not with normal rabbit serum (NRS).

(e) MKP-3 is not detected at the NMJ.

(continued on the next page)

(f) MKP-1 staining (green) is enriched at the NMJ and is complementary to the localization of the AChRs (red; arrowheads) in both, wild-type and ErbB DKO muscles.

(g) Agrin-B/z+ induces accumulation of MKP-1 (green) and the formation of ectopic AChR clusters (AChR, red). In innervated muscle (inn), MKP-1(arrowheads) and AChRs (arrows) are oriented transversely to the muscle axis. AChR clusters, however, localize to regions devoid of MKP-1. In denervated (den) muscles, MKP-1 staining is diminished at Z-lines and AChR clusters tend to be oriented more longitudinally.

**(h)** Expression of MKP-1 in innervated muscle (INN) decreases upon denervation after one week (DEN).

(i) Expression of MKP-1 (green) is not detected at the NMJs of muscle from 18-day-old embryos (E18) while MKP-1 accumulation is clearly visible 2 days after birth (P2). Scale bars, 10 µm.

MKP-1 controls postsynaptic differentiation in vivo

To pursue the hypothesis that MKP-1 affects postsynaptic differentiation at the NMJ, we acutely altered expression levels of MKP-1 in muscle in two ways. Firstly, we overexpressed MKP-1 in rat soleus muscles by electroporating expression constructs encoding MKP-1 or cytoplasmic EGFP (control). One week later, we injected the muscles with recombinant agrin-B/z+ and denervated them. After another week, we dissected the muscles and stained AChR clusters and the overexpressed MKP-1. We found that while the number of AChR clusters was similar in both, EGFP-positive and adjacent, non-transfected muscle fibers (**Fig. 6a** and **6b**), muscle fibers that expressed MKP-1 contained much fewer, or no AChR clusters when compared to adjacent, non-transfected fibers (**Fig. 6a** and **b**). Interestingly, the overexpressed MKP-1 protein aligned in muscle fibers in transverse stripes like the endogenous MKP-1 in innervated muscle (**Fig. 6c**; see also **Fig. 5g**). EGFP, as expected, was distributed homogenously throughout the cytosol (**Fig. 6c**). Thus, high levels of MKP-1 prevent the formation of AChR clusters even in denervated muscle. These experiments suggest that, conversely, the low levels of MKP-1 (as found in denervated muscle) may be the basis for the enhanced AChR clustering.

We therefore also tested, secondly, whether acute downregulation of MKP-1 in innervated muscle indeed enhances the formation of ectopic AChR clusters induced by agrin-B/z+. MKP-1 expression was knocked down by RNA interference (RNAi) using shRNA constructs[26]. Two specific shRNA constructs targeting MKP-1 and a control shRNA construct targeting CD4 (**Fig. 6d**) were electroporated into innervated muscle fibers together with an EGFP expression construct containing a nuclear localization signal (NLS-EGFP). To allow the removal of MKP-1 protein, agrin-B/z+ was injected only one week later. After another week, muscles were dissected and stained. There were few or no AChR clusters in non-transfected muscle fibers and in those electroporated with shRNA to CD4 (**Fig. 6e** and **f**). The number of AChR aggregates on muscle fibers expressing shRNA targeting MKP-1 was, however, significantly increased (**Fig. 6e** and **f**). Thus, these data show that downregulation of MKP-1 is sufficient to increase the response of innervated muscle to agrin-B/z+ and corroborate the function of MKP-1 to restrict the postsynaptic structure to the site of innervation.
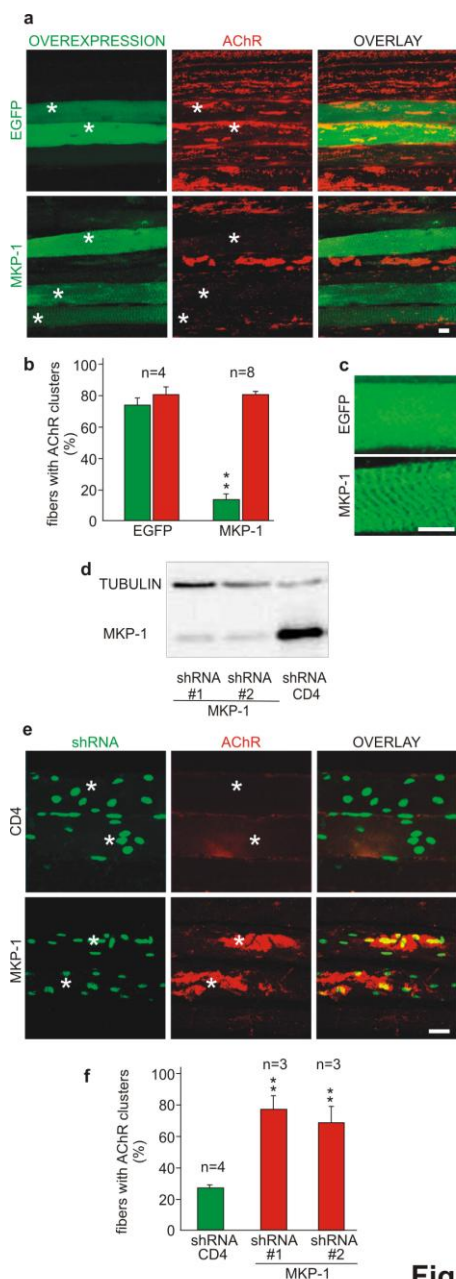
Fig. 6
Bezakova *et al.*

**Figure 6 MKP-1 regulates postsynaptic differentiation.**

(a) Injection of agrin-B/z+ into denervated muscle induces the formation of many AChR clusters (AChR, red) on fibers overexpressing EGFP (first row; green and marked by asterisks) as well as on non-transfected adjacent muscle fibers. In contrast, muscle fibers overexpressing MKP-1 (second row; green and marked by asterisks) contain only few AChR clusters when compared with neighboring, non-transfected fibers.

(continued on the next page)

(b) Quantification of AChR clusters formed on fibers expressing EGFP or MKP-1 (green columns) and on adjacent, non-transfected fibers (red columns). While no significant difference is detected between adjacent non-transfected and EGFP-expressing denervated fibers, MKP-1-positive fibers contain significantly less AChR clusters (**p<0.001).

(c) Overexpressed MKP-1 localizes to regular transverse lines, similar to endogenous MKP-1 protein in innervated muscle fibers(compare with **Fig. 5g**), while EGFP is distributed homogenously in the cytosol.

(d) Western blot analysis of COS7 cells co-transfected with the constructs encoding MKP-1 and the shRNA targeting either MKP-1 or CD4 (control). Both shRNA constructs targeting MKP-1 downmodulate the expression of MKP-1 while the construct targeting CD4 does not have any effect.

(e) Electroporation of innervated muscle fibers with shRNA against CD4 and a nuclearly targeted EGFP (green and marked by asterisks) does not affect the formation of AChR clusters (red) after injection of agrin-B/z+. In contrast, shRNA targeting MKP-1 enhances the formation of AChR clusters after injection of agrin-B/z+.

(f) The number of AChR clusters in innervated muscle fibers expressing shRNA targeting MKP-1 is significantly increased (red column) when compared with muscle fibers expressing shRNA that targets CD4 (green column; **p <0.001). Scale bars, 10 µm.

PAK-1 links agrin-MuSK signaling to MAPK activation

At the NMJ, agrin activates MuSK and the small Rho GTPases Rac1 and Cdc42, which in turn activate p21-activated kinase (PAK-1)[27] and recruit it to the MuSK-dishevelled-1 scaffold[28]. In other cellular systems, activated PAK-1 (P-PAK1) has been shown to anchor components of the MAPK pathway and to activate ERK1/2[29]. Thus it is conceivable that P-PAK-1 may also link the MAPK pathway to the site of agrin-MuSK signaling at the NMJ. Like P-ERK and P-JNK, P- PAK-1 localized to the NMJs of wild-type and of ErbB DKO mice (**Fig. 7a**). Moreover, PAK-1, similar to ERK1/2, also decorated structures reminiscent of the Z-lines (compare **Fig. 7b** to **Fig. 5c**). To assess the functional importance of PAK-1 at the NMJ, we again used RNAi. Three specific shRNA constructs targeting PAK-1 and a control shRNA construct targeting CD4 (**Fig. 7c**) were electroprated into muscle fibers together with an expression plasmid encoding NLS-EGFP. One week after electroporation, agrin-B/z+ was injected and muscles were denervated. After another week, muscles were dissected, stained and the number of muscle fibers expressing ectopic AChR clusters was determined. Many AChR aggregates formed in non-transfected muscle fibers or in those transfected with the control shRNA targeting CD4 (**Fig. 7d** and **e**). In contrast, the number AChR aggregates in fibers transfected with the shRNA targeting PAK-1 was strongly reduced (**Fig. 7d** and **e**). These results indicate that PAK-1 plays an important role in the assembly of postsynaptic structures and are in line with the idea that PAK-1 may serve as a link between the MAPK pathway and the agrin-MuSK scaffold at the NMJ.
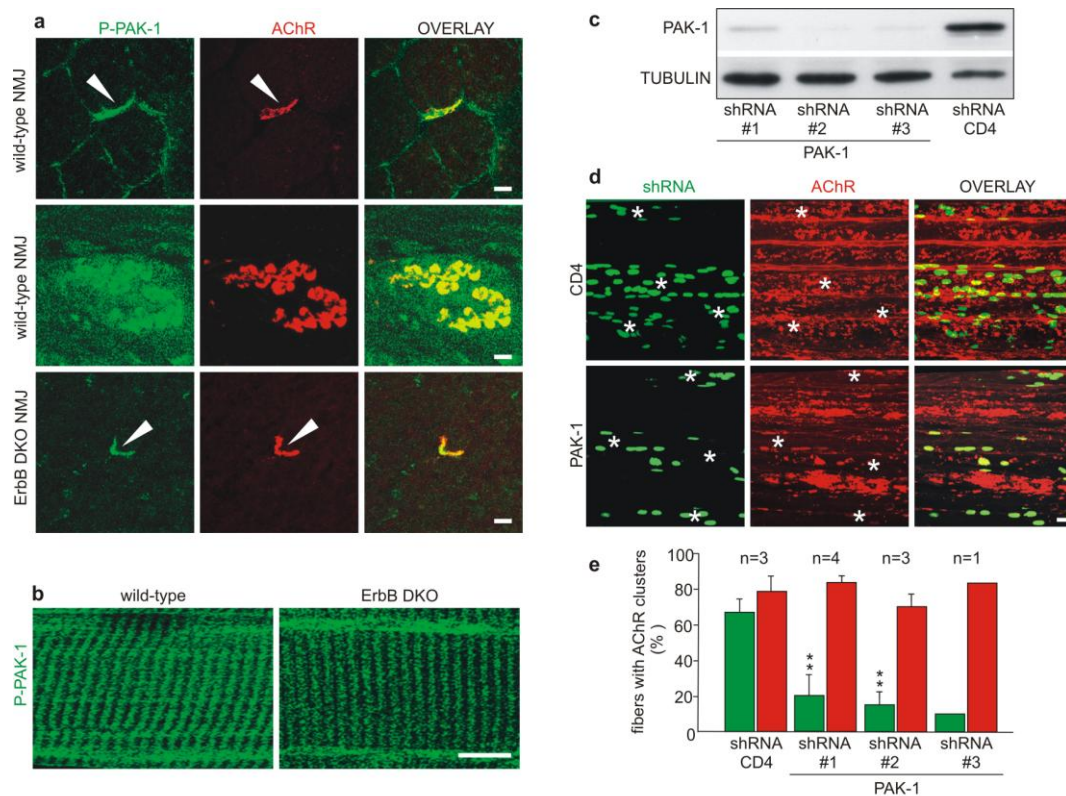
Fig. 7
Bezakova *et al.*

Figure 7 Localization of PAK-1 and its role in postsynaptic differentiation.

(a) Phosphorylated PAK-1 (P-PAK-1, green) is localized to wild-type and ErbB DKO NMJs (arrowheads), labeled by rhodamine α-bungarotoxin staining (AChR, red).

(b) Outside the NMJ, P-PAK-1 localizes to cytoskeletal structures reminiscent of Z-lines. **(c)** Western blot analysis of COS7 cells co-transfected with an expression constructs encoding PAK-1 and shRNA plasmids targeting either PAK-1 or CD4 (control). All three shRNA constructs targeting PAK-1 downmodulate the expression of PAK-1 while the construct targeting CD4 does not have any effect.

(d) Muscle fibers co-electroporated with shRNA targeting CD4 and the nuclearly localized EGFP (green; marked by asterisks), like adjacent, non-transfected muscle fibers, form numerous AChR clusters (red) after injection of agrin-B/z+ into denervated muscle. In contrast, muscle fibers which co-express shRNA targeting PAK-1 and EFGP (green; marked by asterisks), contain none or very few AChR clusters (red).

(continued on the next page)

(e) Quantification of AChR clusters detected on fibers expressing shRNAs targeting CD4 or PAK-1 (green columns) and on adjacent, non-transfected fibers (red columns). No significant difference was seen in denervated muscles fibers that express shRNA against CD4. However, the denervated muscle fibers expressing the shRNA contructs targeting PAK-1 contain significantly less AChR clusters (**$p<0.001$). Scale bars, 10 µm.

2.5   DISCUSSION

Our study addresses several novel aspects as to how agrin-MuSK signaling induces the formation of postsynaptic structures. To identify changes in gene transcription, we used intramuscular injection of agrin-B/z+, an established experimental paradigm that initiates and drives the full postsynaptic program in nerve-free muscle regions[14,18]. Unlike previous approaches, which analyzed transcripts at the endogenous adult NMJs composed of pre- and postsynaptic cells[11-13], transcripts analyzed in our microarray screen originate from ectopically formed postsynaptic structures. Moreover, we collected the samples seven days after treatment when agrin-induced postsynaptic apparatuses still undergo dynamic molecular and structural changes. As we show here, this experimental system allowed us to identify several genes that have not been described at the NMJ. Moreover, we also detected transcripts such as protease nexin-1[30], laminin β2[31] or protein kinase A regulatory subunit α[12,32] whose expression at the NMJ was previously described.

Upregulation of IEGs during postsynaptic differentiation

Several genes identified in our screen such as c-Fos and Jun-B belong to the family of IEGs and have already been implicated in agrin signaling in cortical neurons[22] but also in neuregulin-ErbB signaling in C2C12 cells[23,33]. As their expression in muscles of ErbB DKO was not affected (data not shown), we conclude that their transcription can also be activated by alternative mechanisms.

EGR-1 was one of the most robustly upregulated IEGs. It has been suggested to act downstream of neuregulin-ErbB signaling and has been shown to bind to the so called "neuregulin-1 response element" (NRE) of the ε-AChR promoter[34]. Expression of EGR-1 in muscle is maintained in muscles of ErbB DKO (data not shown) and the EGR-1 protein, like the ε-AChR subunit, accumulates at all ectopic postsynaptic structures induced by agrin-B/z+ in innervated muscle but only in a subset of postsynaptic structures induced in denervated muscle. These results indicate that EGR-1 may indeed be involved in postsynaptic expression of the ε-AChR subunit *in vivo*. However, unlike mice deficient for the ε-AChR subunit[35], mice deficient for EGR-1 are viable and do not show apparent myasthenic syndromes[36]. Thus, other EGR gene family members[37] or the two ETS transcription factors, GA-binding protein (GABP) and/or Erm, which have both been implicated in the regulation of synapse-specific gene transcription *in vivo*[38,39], may compensate for the function of EGR-1.

Agrin-MuSK signaling triggers the MAP kinase pathway at the NMJ

MKP-1 is another IEG whose expression is robustly induced by agrin-B/z+. MKP-1 is known to regulate the activity of all MAPKs therefore we investigated their role in postsynaptic differentiation. We show that phosphorylated forms of ERK and JNK are highly concentrated at postsynaptic structures of the NMJ. Moreover, the preservation of ERK1/2 and JNK phosphorylation of ErbB DKO mice shows that neuregulin-ErbB signaling is not required for ERK1/2 and JNK activation in muscle. Thus, the MAPK pathway, particularly ERK1/2, might be activated by agrin-MuSK signaling instead. We indeed show that DOK-7-induced activation of MuSK in heterologous cells is sufficient to trigger ERK1/2 phosphorylation. We also observe that MAPKs localize to AChR clusters at the NMJ and to subsynaptic myonuclei, which indicates that the MAPK pathway, particularly ERK1/2, is involved in both, the aggregation and the local transcription of postsynaptic proteins (see **Fig. 8)**. Consistent with such dual role of MAPK signaling, addition of agrin-B/z+ to C2C12 myotubes induces rapid phosphorylation and nuclear translocation of ERK1/2, while prolonged incubation of myotubes with agrin-B/z+ results in the translocation of P-ERK to the plasma membrane and to the sites where AChR clusters are formed.

We further suggest that the MAPK signaling is linked to the agrin-MuSK scaffold via the effector protein PAK-1 (see **Fig. 8**). Such function of PAK-1 in postsynaptic differentiation is supported by several lines of evidence. The activated form of PAK-1 is enriched at the NMJ and the knockdown of PAK-1 inhibits agrin-induced formation of postsynaptic structures. Moreover, activated PAK-1 associates with MuSK via dishevelled-1 and its inhibition attenuates agrin-induced AChR clustering in cultured muscle cells[28]. Finally, PAK-1 has been shown to regulate ERK and JNK activation by serving as a scaffold for Raf, MEK and ERK[29] (**Fig. 8**).

Neuregulin-ErbB and agrin-MuSK signaling may converge onto the MAPK pathway

Neuregulin-ErbB signaling induces several aspects of postsynaptic differentiation *in vitro* such as the MAPK activation and transcription of several IEGs[9]. We now show that neuregulin-ErbB signaling is dispensable for the activation of the MAPK pathway at the NMJ and we provide evidence that MAPKs, in particular ERK1/2, can be activated by agrin-MuSK signaling (**Fig. 8**). While inactivation of neuregulin-ErbB signaling in muscle does not cause a neuromuscular phenotype, overexpression of a constitutively active form of the ErbB2 receptor in muscle disperses AChR clusters[40]. One possible explanation for this phenotype is the hyperactivation of MAPK signaling, which would result in a failure to

compact AChR clusters (see **Fig. 8**). It has also been shown that neuregulin-ErbB signaling at the NMJ can be reinforced by a positive feedback loop with the p35/Cdk5 pathway[41]. Interestingly, dispersal of AChR clusters formed in embryonic muscles devoid of agrin-B/z+ is rescued in mutant mice lacking Cdk5[41]. This suggests that reciprocal agrin-MuSK signaling may be required to balance the Cdk5 dispersal activity which may involve p35/Cdk5-neuregulin-ErbB induced activation of MAPK pathway (**Fig. 8**). Moreover, the dispersal of AChR clusters by Cdk5 is also activated by acetylcholine binding to AChRs (**Fig. 8**; Ref[41]). We now suggest that MKP-1 induced by the trophic (agrin) and electrical (ACh) activity of the motor neuron also affects the assembly and dispersal of the AChR clusters at the NMJ through regulation of MAPK pathway.

MKP-1 controls the MAP kinase pathway and regulates postsynaptic differentiation

Upregulation of the dual-specificity phosphatase MKP-1 by neuronal agrin strongly indicates that the MAPK signaling at the NMJ is under a tight spatio-temporal control. As discussed above, such a negative feedback loop of the MAPK pathway may be required to prevent its hyperactivation. Accordingly, the formation of AChR clusters upon denervation of adult muscles and during embryonic muscle development may be facilitated by low levels of MKP-1. Interestingly, genetic ablation of neurotransmission in mutant mice lacking choline acetyl transferase (ChAT) increases the number of AChR clusters in embryonic muscles devoid of agrin[42] that would normally disperse (**Fig. 8**). We hypothesize that this genetically induced denervation of muscle maintains levels of MKP-1 low and sustains MuSK-induced MAPK activation. At the NMJs of innervated muscle, high levels of MKP-1, which are induced by electrical activity and agrin-MuSK signaling, may restrict postsynaptic differentiation and synapse-specific gene transcription to the site of innervation. Both views are supported by independent *in vivo* evidence. First, overexpression of MKP-1 inhibits the formation of ectopic AChR clusters in denervated muscle (where endogenous levels of MKP-1 levels are normally low). Second, knockdown of MKP-1 by RNAi enhances the formation of AChR clusters in innervated muscle (where endogenous levels of MKP-1 levels are normally high). We propose a model in which regulation of the MAPK pathway is important for the establishment and the maintenance of postsynaptic structures *in vivo* (**Fig. 8**).

Finally, if MKP-1 plays an essential role in the spatial control of MAPK activation, one would expect that the NMJs of MKP-1-deficient mice have compromised morphology or function. Although muscle function is altered in such mice[43], we did not observe gross changes in the NMJ morphology (GB, MA Bennett and MAR; unpublished results) suggesting that a chronic absence of MKP-1 during development is compensated by other mechanisms. These may involve upregulation of other MKP family members[11] or

activation of alternative mechanisms, which inhibit activation of the MAPK pathway. Interestingly, p35/Cdk5 has been shown to inhibit ERK1/2 activation in neurons by competing for the same binding site on PAK-1[44] (see **Fig. 8**).   In   conclusion,   we provide compelling evidence that activation of the MAPK pathway and its spatio-temporal control by nerve- and agrin-induced MKP-1 expression is important for the formation of the NMJ. As discussed before, the MAPK pathway has also been shown to induce transcription of MKP-1, c-Fos and EGR-1 during long-term potentiation and subsequent restructuring of central synapses[15]. Moreover, the MAPK pathway is deregulated in the brain of mice that are deficient for agrin[45]. Finally, similar concepts for a regulatory role of dual MAPK phosphatases have also been reported for immunological responses, synapse formation in the brain and learning and memory[46,47]. Thus, a negative feedback loop of MAPK signaling as shown here for MKP-1 may be of general importance for synapse formation and their maintenance.
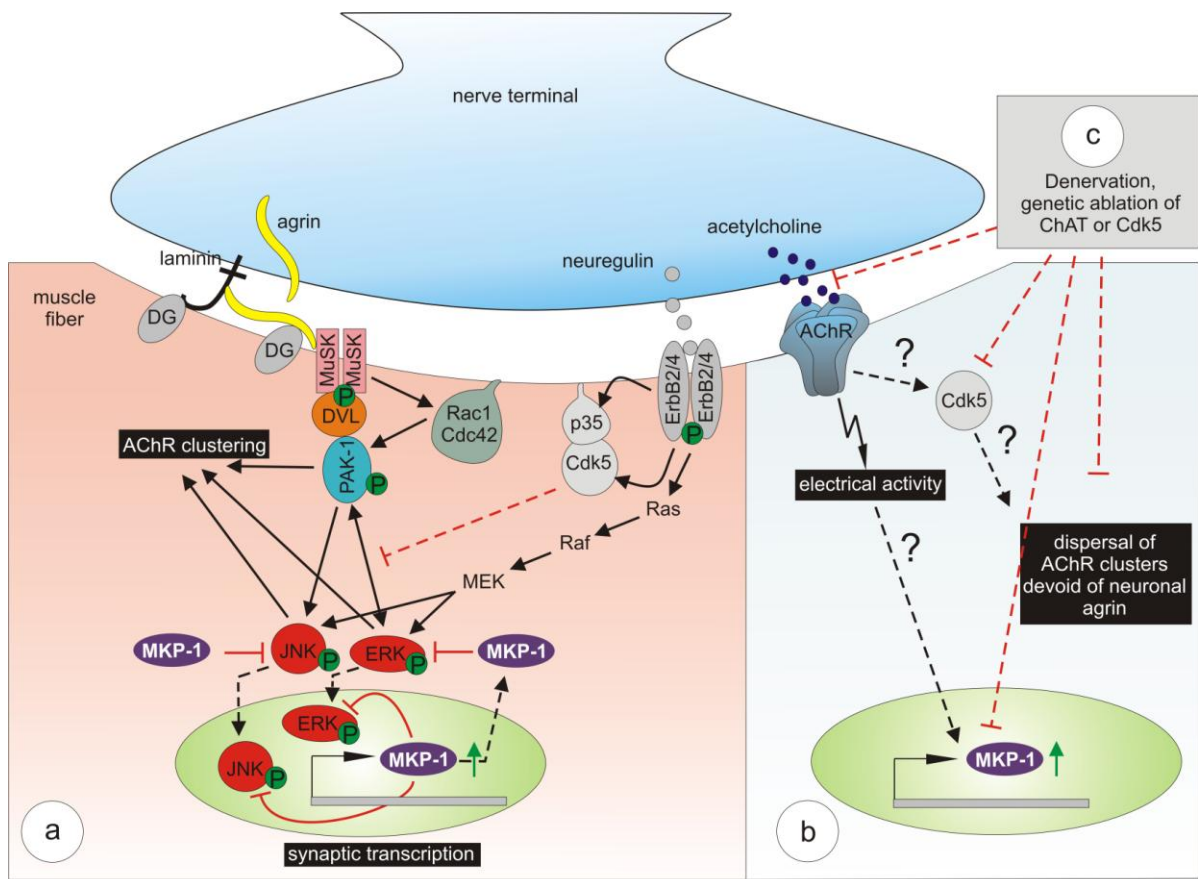
Fig. 8
Bezakova *et al.*

**Figure 8 Schematic representation of agrin-MuSK signaling at the NMJ.**

(a) At the NMJ, agrin released from the presynaptic nerve terminal is incorporated into synaptic basal lamina via its binding to laminin. On muscle membrane, agrin binds to dystroglycan (DG), activates MuSK and induces phosphorylation of p21-activated kinase-1[28] (PAK-1) by engaging the Rho GTPAses Rac1 and Cdc42[27]. Phosphorylated PAK-1 (P-PAK-1) binds to MuSK adaptor dishevelled-1[28](DVL). P-PAK-1 is recruited to the NMJ and serves as a scaffold to activate JNK[27] and ERK1/2[29]. P-ERK and P-JNK may then translocate either to the membrane and participate in the aggregation of synaptic proteins including AChRs or to the subsynaptic myonuclei and induce transcription of synapse-specific genes including MKP-1. MKP-1, in turn, regulates phosphorylation of MAPKs in the nucleus and in the cytosol. At the NMJ, both ERK and JNK can also be activated by neuregulin-ErbB signaling via Ras, Raf, MEK[23,33], although neuregulin-ErbB signaling is not required[10].

(continued on the next page)

(b) Acetylcholine released from the presynaptic nerve terminal opens AChRs and evokes cell depolarization (electrical activity). Electrical activity increases expression of MKP-1 throughout the muscle fiber and inhibits both, activation of MAPKs and formation of AChR clusters in non-synaptic (agrin devoid) regions. ACh also activates Cdk5 which subsequently induces dispersal of non-synaptic AChR aggregates[41]. Note: Cdk5 can affect the postsynaptic differentiation at the NMJ in dual fashion. When interacting with PAK-1 it may compete with ERK1/2 for the same binding site on PAK-1[44] and inhibit activation of ERK1/2 downstream of agrin-MuSK signaling. When interacting with the neuregulin-ErbB pathway, it may enhance MAPK signaling and induce dispersal of AChR aggregates[41]. Accordingly, upregulation of MKP-1 expression by electrical activity and agrin may be a means to efficiently counterbalance activation of ERK and JNK at the NMJ.

(c) Dispersal of non-synaptic AChR aggregates can be prevented by denervation, which lowers MKP-1 expression in muscle, by genetic ablation of ChAT[42] and by blockade of Cdk5 activity in Cdk5 deficient mice or by a Cdk5 inhibitor roscovitin[41].

2.6 SUPPLEMENTARY FIGURES
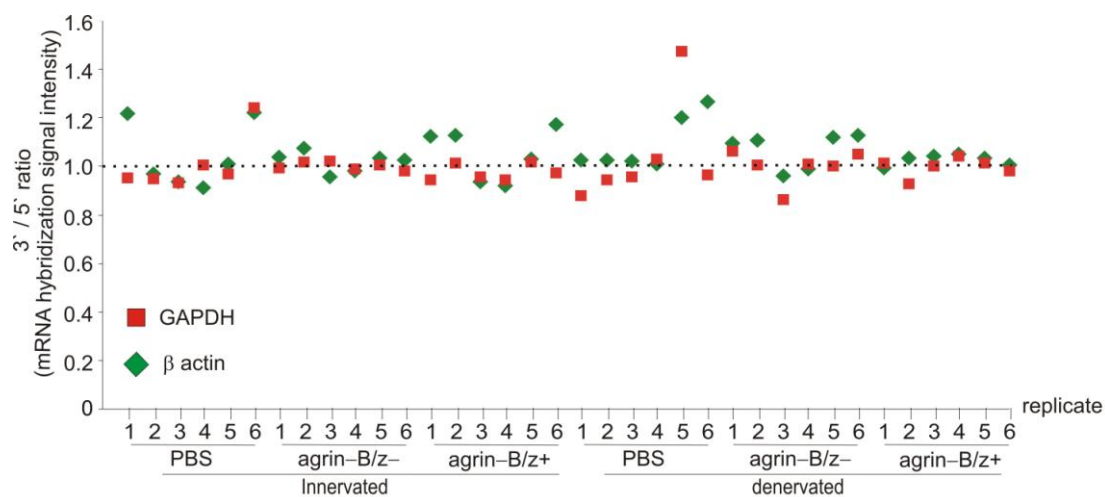
Fig. S1
Bezakova *et al.*

Supplementary Figure 1 Integrity of mRNA isolated from injected muscles.

Probes derived from mRNA isolated from the 6 muscle replicates for each of the 6 conditions were hybridized with Affymetrix GeneChips. Ratio of hybridization signals intensities detected at the probe sets encoding 3'and 5'sequences of β-actin and glyceraldehyde-3-phosphate dehydrogenase (GAPDH) are shown. The ratio for majority of probes is very close to 1, indicating high quality of the isolated mRNA.
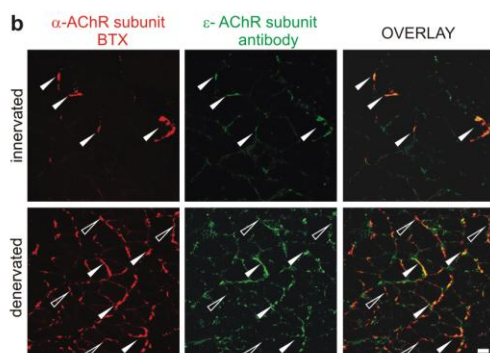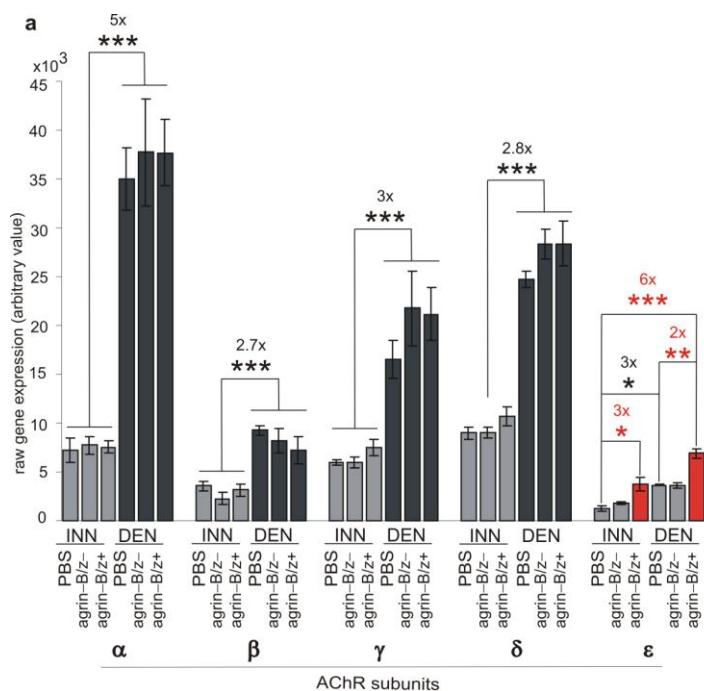
Fig. S2
Bezakova *et al.*

Supplementary Figure 2 Transcription of AChR subunits. (

a) Intensities of hybridization signal for all AChR subunits and the 6 different experimental paradigms. Denervation robustly increases expression of all AChR subunits with the stoichiometry corresponding to AChR. Importantly, injection of agrin-B/z+ causes a significant increase in ε-AChR transcription (red bars). Each bar represents the mean ± s.e.m. (***: p<0.0001; **: p<0.001, *: p<0.02).

(b) Staining of muscle cross-sections with rhodamine-α-bungarotoxin (BTX, red) and with antibodies against the ε-AChR subunit (green) shows their co-localization at ectopic postsynaptic structures in innervated muscle (filled arrowheads). In denervated muscle, only a subset of the ectopic AChR structures contains the ε-AChR subunit (filled arrowheads) while the rest (open arrowheads) expresses reciprocally the γ-AChR subunit (data no shown). Scale bar, 10 μm.
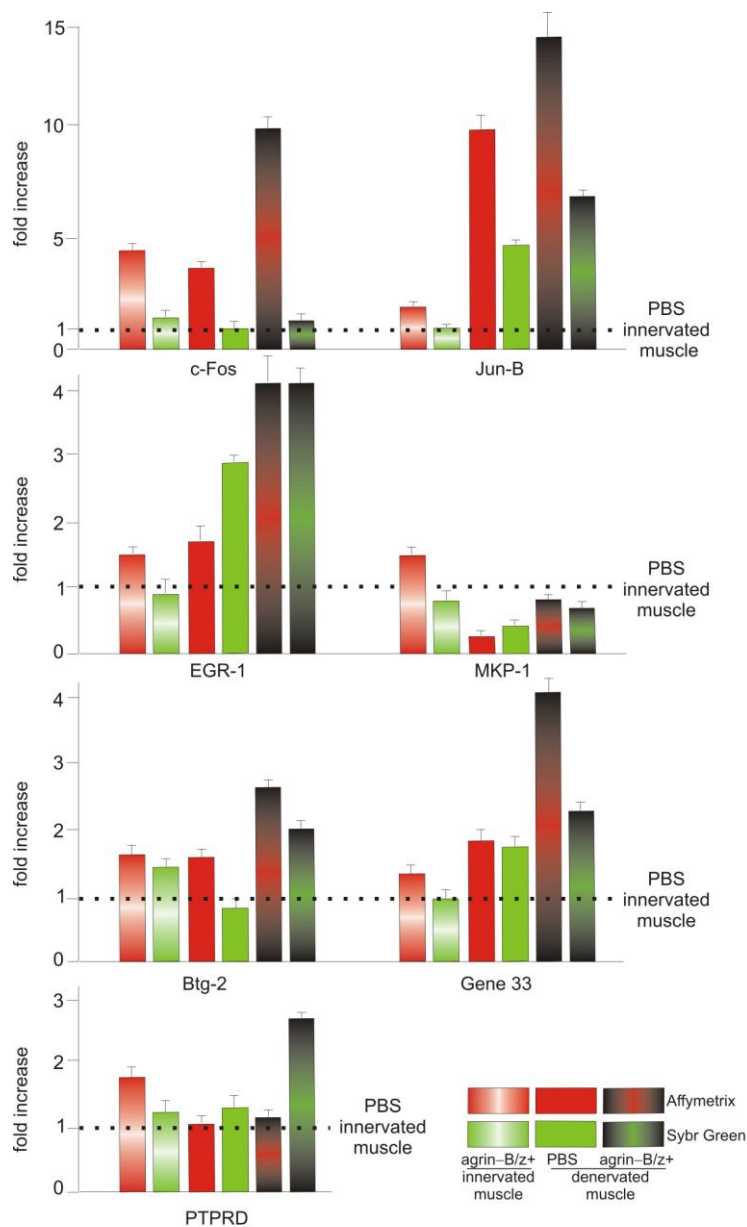
Fig. S3
Bezakova *et al.*

Supplementary Figure 3 Validation of Affymetrix GeneChip data by qRT-PCR. Normalized expression levels of selected genes detected by both, GeneChip hybridization (red bars) and qRT-PCR (green bars). For the majority of genes, data from the GeneChip experiment were confirmed by qRT-PCR. (PTPRD - protein tyrosine phosphatase receptor type D)
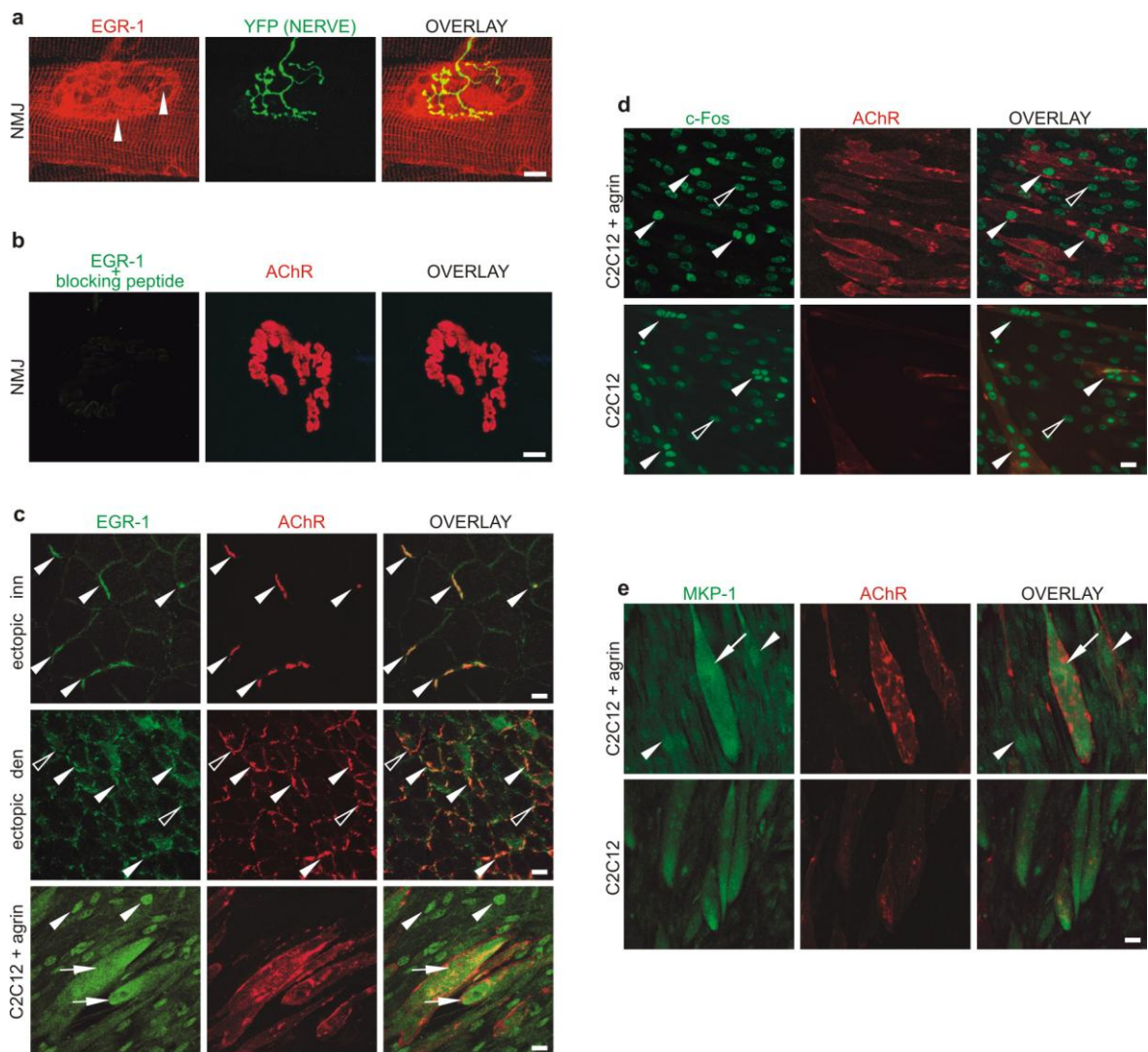
Fig. S4
Bezakova *et al.*

Supplementary Figure 4 Expression of selected IEGs *in vivo* and in cultured C2C12 cells.

(a) EGR-1 (red, arrowheads) accumulates at the NMJ, which is labeled by the YFP-positive motor nerve terminals of *thy1*-YFP transgenic mice (green).

(b) Preincubation of the anti EGR-1 antibody with the original antigenic peptide abolishes EGR-1 staining at the NMJ, labeled by rhodamine-α-bungarotoxin (AChR, red).

(continued on the next page)

(c) In innervated muscle (inn), EGR-1 co-localizes with all agrin-induced ectopic structures (filled arrowheads, first row). In denervated muscle (den), EGR-1 co-localizes only with a subset of ectopic AChR clusters (filled arrowhead, middle row). In C2C12, EGR-1 is found in the nuclei of myoblasts (arrowheads), and localizes to both, nuclei and agrin-induced AChR clusters in myotubes (arrows, bottom row).

(d) C-Fos is expressed in the nuclei of C2C12 myoblasts (empty arrowheads) and the staining intensity increases upon fusion of myoblasts to myotubes (filled arrowheads, second row). C-Fos expression is further slightly increased in the nuclei of myotubes that were treated with agrin-B/z+ overnight (filled arrowheads, first row).

(e) In C2C12 cells, MKP-1 localizes to the nuclei of myoblasts and myotubes (arrowheads) but also to AChR clusters induced by agrin-B/z+ in myotubes (arrow). Scale bar, 10 µm.
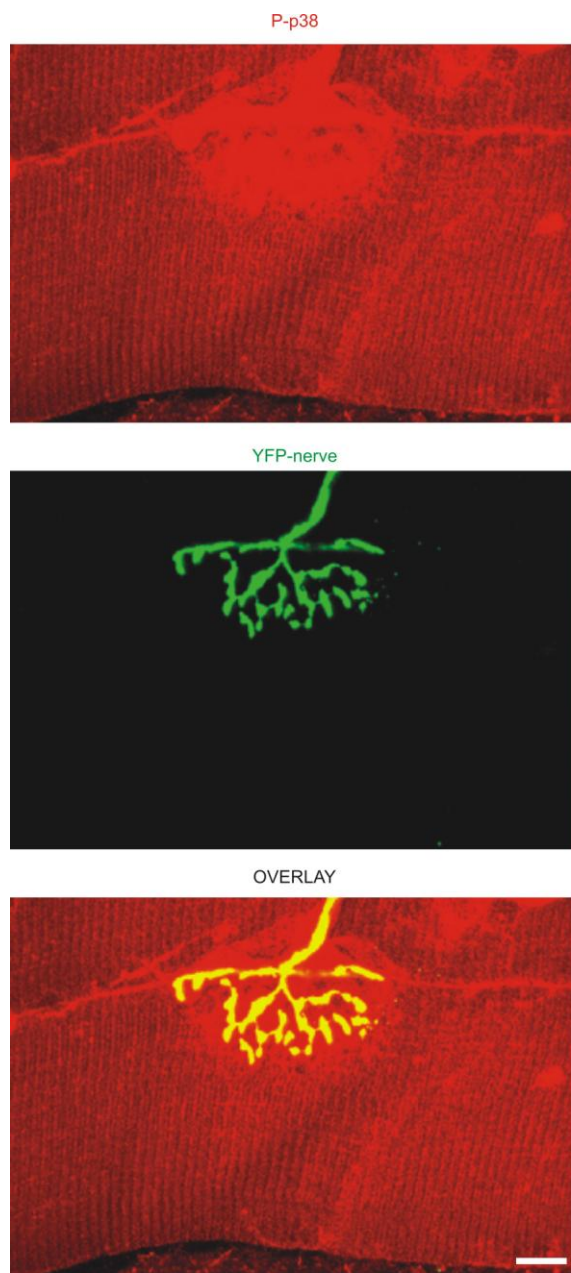
Fig. S5
Bezakova *et al.*

Supplementary Figure 5 Whole mount staining of phosphorylated form of p38 (P-p38) *in vivo.*

P-p38 (red) is abundant in muscle fibers and localizes to the cytoskeleton in a Z-line-like pattern. P-p38 is also expressed in the presynaptic nerve terminal, labeled by YFP expressed in *thy1*-YFP transgenic mice (green, see also **Fig. 5**). Scale bar, 10 µm.
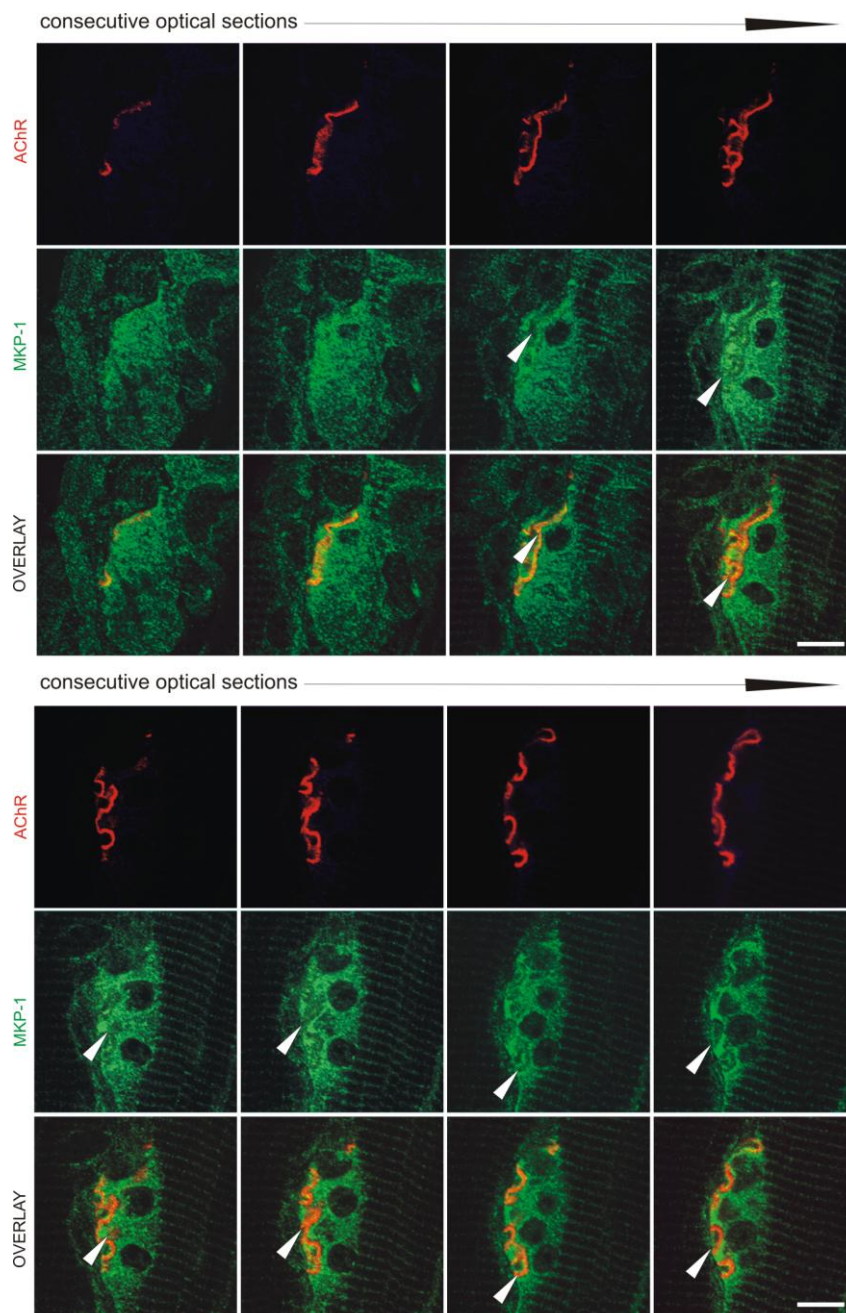
Fig. S6
Bezakova *et al.*

Supplementary Figure 6 Complementary expression of AChR and MKP-1 at the NMJ.

Sequential optical sections spaced 0.5 µm reveal the complementary localization of MKP-1 (green) and AChRs (red, arrowheads). Precise co-localizaion of P-ERK with AChR as observed in **Figure 3** implies the similar complementary distribution between MKP-1 and P-ERK. Scale bar, 10 µm.

Supplementary Table 1

Bar Number	Affymetrix	Short name	Full annotation
1	rc_AA944156_s_at	Btg2	Early induced gene, B-cell translocation gene 2
2	Z11504cds_at	Npy1r; NPY-1	R.rattus mRNA for NPY-1 receptor.
3	rc_AA866414_at	Slc4a1	Solute carrier family 4, member 1, anion exchange protein 1 (kidney band 3)
4	rc_AI176662_s_at	**Egr1**	Early growth response 1
5	rc_AA866291_at		ESTs
6	AB004329_at	Acacb	acetyl-Coenzyme A carboxylase beta
7	rc_AI639284_at		EST, Highly similar to A61404 keratin A, type I - mouse [M.musculus]
8	rc_AI058941_s_at	Ddah1	dimethylarginine dimethylaminohydrolase 1
9	X03347cds_g_at		P75 gag-fos fusion protein (aa 1-554); FBR-murine osteosarcoma provirus genome.
10	rc_AI179075_i_at	Csh1v	Chorionic somatomammotropin hormone 1 variant; Placental lactogen-1
11	rc_AA800026_at		ESTs
12	rc_AA900848_at	Lamb2	Laminin chain beta 2
13	U72632_at	Aoc3	Rattus norvegicus membrane amine oxidase mRNA, partial cds.
14	U65217_i_at		Rattus norvegicus MHC class II antigen RT1.B beta chain mRNA, partial cds
15	AF031880_at	Nfl	neurofilament, light polypeptide
16	S79730_s_at	Pnoc; N23K; Npnc1	endogenous agonist of opioid receptor-like ORL1 receptor; Authors indicate ORL1 receptor agonist peptide is encoded by residues 122-138; Method: conceptual translation with partial peptide sequencing; This sequence comes from Fig. 4; ORL1 receptor agonist
17	X06769cds_at	**C-Fos**	c-fos protein (AA 1-380); Rat c-fos mRNA.
18	M36151cds_s_at		MHC A-beta RT1.B-b cell surface glycoprotein; Rat MHC class II A-beta RT1.B-b-beta gene, partial
19	U75932_at	Prkar1a	Protein kinase, cAMP dependent, regulatory, type 1
20	X14254cds_g_at		invariant chain (AA 1-280); Rat mRNA for MHC class II-associated invariant chain.
21	U07619_at	F3	Coagulation factor III (thromboplastin, tissue factor)
22	rc_AI169756_s_at		ESTs, Highly similar to G33_RAT GENE 33 POLYPEPTIDE [R.norvegicus]
23	X74836cds_s_at	**Chrne**	acetylcholine receptor epsilon
24	M65149_at	Cebpd	CCAAT/enhancerbinding, protein (C/EBP) delta
25	M18416_at	**Egr1**	Early growth response 1
26	X96437mRNA_g_at	PRG1	R.norvegicus PRG1 gene.
27	X06769cds_g_at	**C-Fos**	c-fos protein (AA 1-380); Rat c-fos mRNA.
28	U75397UTR#1_s_at	Krox-24 / **Egr1**	Rattus norvegicus Krox-24 mRNA, 3' untranslated region, partial sequence.
29	AF023087_s_at	nerve growth factor induced factor A **Egr1**	NGFI-A; Rattus norvegicus nerve growth factor induced factor A mRNA, partial 3'UTR.
30	L34074cds_at	Ol1	putative; Rat OL1 receptor gene, complete cds.
31	AF072439_at	Zfp37	zinc finger protein 37
32	rc_AA866231_at		ESTs
33	U31598_s_at	RT1.DMa	similar to mouse H2-M alpha chain encoded by GenBank Accession Number U20306; Rattus norvegicus MHC class II-like alpha chain (RT1.DMa) mRNA, partial cds.
34	S81478_s_at	3CH134/CL100 PTPase **MKP-1**	oxidative stress-inducible protein tyrosine phosphatase; This sequence comes from Fig. 1; 3CH134/CL100 PTPase=oxidative stress-inducible protein tyrosine phosphatase [rats, peritoneal macrophage cDNA library, mRNA, 1912 nt].
35	U02553cds_s_at	Ptpn16 **MKP-1**	protein tyrosine phosphatase, non-receptor type 16
36	AF020210_s_at	DLP1	dynamin-like protein 1; N-terminal region; Rattus norvegicus DLP1 splice variant 4 (DLP1) mRNA,
37	D44481_at	Crk	Rat mRNA for CRK-II, complete cds.
38	AF014827_at	Figf	c-fos induced growth factor (vascular endothelial growth factor D)
39	AF096291_at	Bcl2l2	Bcl-w protein
40	U33540exon_f_at	CYP2B14P	Rattus norvegicus cytochrome P450 (CYP2B14P) pseudogene, exon 1.
41	M24067_at	Serpine1	serine (or cysteine) proteinase inhibitor, clade E (nexin, plasminogen activator inhibitor type 1), member 1
42	X86003_at	NOR-2	neuron-derived orphan receptor
43	J05571_s_at	Mat2a	methionine adenosyltransferase II, alpha
44	U56862_at	Znf146	Pancreas zinc finger protein, see also D1Bda10\2
45	S50461_s_at	G<down>&agr;12z,</down>	signal-transducing G protein alpha 12 subunit; G alpha 12z,=signal-transducing G protein alpha 12 subunit [rats, brain, mRNA Partial, 466 nt].
46	X53565_at	Ttgn1	trans-golgi network protein 1
47	M36317_s_at	Trh; TRH01	Rat thyrotropin-releasing hormone (TRH) precursor mRNA, complete cds.
48	X53363cds_s_at	Calr	calreticulin
49	X63594cds_at	Nfkbia; RL/IF-1	R.rattus RL/IF-1 mRNA.
50	X65454_g_at	Sc65	SC65 synaptonemal complex protein
51	L23148_g_at	Id1	Inhibitor of DNA binding 1, helix-loop-helix protein (splice variation)
52	D00189_at	Atp1a3; Atpa1a3	pot.ORF (1013 AA); Rat mRNA homologous to alpha subunit kidney-type Na+,K+ -ATPase.
53	AF004811_at	Msn	moesin
54	rc_AA957961_at	unr	unr protein
55	rc_AA891242_g_at		ESTs, Weakly similar to MLRV_RAT Myosin regulatory light chain 2, ventricular/cardiac muscle isoform (MLC-2) [R.norvegicus]
56	S74351_s_at	protein tyrosine phosphatase, PTP, CL100, 3CH134 **MKP-1**	This sequence comes from Fig. 2; PTP; CL100; 3CH134; protein tyrosine phosphatase [rats, Wistar, lung, mRNA Partial, 521 nt].
57	U17254_g_at	Nr4a1	immediate early gene transcription factor NGFI-B
58	U17254_at	Nr4a1	immediate early gene transcription factor NGFI-B
59	D16308_at	Ccnd2	Rat mRNA for cyclin D2, complete cds.
60	rc_AI175900_at	Ets1	Ets avian erythroblastosis virus E2 oncogene homolog 1 (tumor progression locus 1)
61	AB009246_at	Scgf	Rattus rattus SCGF mRNA for Stem cell growth factor, complete cds.
62	U44129_at	Lman1	lectin, mannose-binding, 1
63	AB005143_s_at	Ucp2	Uncoupling protein 2, mitochondrial
64	X65454_at	Sc65	SC65 synaptonemal complex protein
65	X63369cds_at	Zfp36; Tis11	R.rattus TIS 11 mRNA.
66	U66479_at	Madh3	MAD (mothers against decapentaplegic, Drosophila) homolog 3

(continued on the next page)

Supplementary Table 1 List of candidate genes that show significant upregulation by agrin-B/z+ sorted by hierarchical gene clustering (gene tree) using GeneSpring software. The graphical interpretation is shown in the heat-map depicted in **Figure 1b**. Genes that have been previously localized to the NMJ are highlighted with yellow color; IEGs are highlighted by light blue (not examined in this study) and dark blue colors (examined further).

Supplementary Table 2a   upregulated genes   1

a		GENES UREGULATED BY AGRIN–B/z+				
			INNERVATED fold change		DENERVATED fold change	
Affymetrix	Short name	Full annotation	normalized to PBS Inn	normalized to agrin-B/z- Inn	normalized to PBS Den	normalized to agrin-B/z- Den
L34074cds_at	Ol1	putative; Rat OL1 receptor gene, complete cds.	1.89	1.56	1.71	1.50
X14254cds_g_at		invariant chain (AA 1-280); Rat mRNA for MHC class II-associated invariant chain.	1.78	1.56	2.23	1.57
AF072439_at	Zfp37	zinc finger protein 37	1.87	1.56	1.68	1.58
rc_AA866231_at		ESTs	2.81	1.56	2.67	1.58
U31598_s_at	RT1.DMa	similar to mouse H2-M alpha chain encoded by GenBank Accession Number U20306; Rattus norvegicus MHC class II-like alpha chain (RT1.DMa) mRNA, partial cds.	1.59	1.56	2.22	1.60
AF031880_at	Nfl	neurofilament, light polypeptide	1.36	5.35	1.87	1.60
U33540exon_f_at	CYP2B14P	Rattus norvegicus cytochrome P450 (CYP2B14P) pseudogene, exon 1.	1.85	1.56	2.36	1.61
S79730_s_at	Pnoc; N23K; Npnc1	endogenous agonist of opioid receptor-like ORL1 receptor; Authors indicate ORL1 receptor agonist peptide is encoded by residues 122-138; Method: conceptual translation with partial peptide sequencing; This sequence comes from Fig. 4; ORL1 receptor agonist	1.33	1.71	1.69	1.68
rc_AI179075_i_at	Csh1v	Chorionic somatomammotropin hormone 1 variant; Placental lactogen-1	1.76	1.56	1.58	1.70
AF096291_at	Bcl2l2	Bcl-w protein	1.64	1.56	1.88	1.75
X63594cds_at	Nfkbia; RL/IF-1	R.rattus RL/IF-1 mRNA.	1.34	2.74	1.91	1.92
rc_AA891242_g_at		ESTs, Weakly similar to MLRV_RAT Myosin regulatory light chain 2, ventricular/cardiac muscle isoform (MLC-2) [R.norvegicus]	1.35	1.56	3.74	1.97
U75932_at	Prkar1a	Protein kinase, cAMP dependent, regulatory, type 1	1.55	1.56	2.07	2.04
L23148_g_at	Id1	Inhibitor of DNA binding 1, helix-loop-helix protein (splice variation)	1.44	1.94	2.08	2.04
rc_AI175900_at	Ets1	Ets avian erythroblastosis virus E2 oncogene homolog 1 (tumor progression locus 1)	1.31	1.79	1.61	2.05
rc_AI058941_s_at	Ddah1	dimethylarginine dimethylaminohydrolase 1	1.66	1.56	1.89	2.06
U56862_at	Znf146	Pancreas zinc finger protein, see also D1Bda10\2	1.69	1.56	1.99	2.07
M36151cds_s_at		MHC A-beta RT1.B-b-beta cell surface glycoprotein; Rat MHC class II A-beta RT1.B-b-beta gene, partial cds.	1.39	1.74	3.37	2.08
D44481_at	Crk	Rat mRNA for CRK-II, complete cds.	1.79	1.56	1.91	2.17
X96437mRNA_g_at	PRG1	R.norvegicus PRG1 gene.	1.45	1.56	2.02	2.19
AB009246_at	Scgf	Rattus rattus SCGF mRNA for Stem cell growth factor, complete cds.	1.33	1.89	1.72	2.21
U07619_at	F3	Coagulation factor III (thromboplastin, tissue factor)	1.28	1.56	2.18	2.25
X53363cds_s_at	Calr	calreticulin	1.60	1.56	1.77	2.29
U44129_at	Lman1	lectin, mannose-binding, 1	1.40	1.56	2.10	2.42
X63369cds_at	Zfp36; Tis11	R.rattus TIS 11 mRNA.	1.45	1.56	2.02	2.44
M65149_at	Cebpd	CCAAT/enhancerbinding, protein (C/EBP) delta	1.39	1.87	2.25	2.47
D00189_at	Atp1a3; Atpa1a3	pot.ORF (1013 AA); Rat mRNA homologous to alpha subunit kidney-type Na+,K+ -ATPase.	1.25	1.99	2.43	2.53
M36317_s_at	Trh; TRH01	Rat thyrotropin-releasing hormone (TRH) precursor mRNA, complete cds.	1.59	1.56	1.98	2.60
X65454_g_at	Sc65	SC65 synaptonemal complex protein	1.35	3.66	2.71	2.68
AF020210_s_at	DLP1	dynamin-like protein 1; N-terminal region; Rattus norvegicus DLP1 splice variant 4 (DLP1) mRNA, partial cds.	1.32	1.56	2.72	2.70
U66479_at	Madh3	MAD (mothers against decapentaplegic, Drosophila) homolog 3	1.44	1.56	2.72	2.72
rc_AA900848_at	Lamb2	Laminin chain beta 2	1.62	1.56	1.46	2.73
Z11504cds_at	Npy1r; NPY-1	R.rattus mRNA for NPY-1 receptor.	1.28	1.81	2.25	2.78
rc_AA957961_at	unr	unr protein	1.29	1.56	2.93	2.78
rc_AA866291_at		ESTs	1.41	1.56	1.61	2.79
AB005143_s_at	Ucp2	Uncoupling protein 2, mitochondrial	1.32	1.56	2.66	2.80
X74836cds_s_at	Chrne	acetylcholine receptor epsilon	2.65	1.56	2.78	2.81
rc_AA800026_at		ESTs	1.72	1.56	2.05	3.27
S50461_s_at	G<down>&agr;12z,</down>	signal-transducing G protein alpha 12 subunit; G alpha 12z,=signal-transducing G protein alpha 12 subunit [rats, brain, mRNA Partial, 466 nt].	2.12	1.56	2.23	3.39
X65454_at	Sc65	SC65 synaptonemal complex protein	1.35	1.56	2.94	3.47
J05571_s_at	Mat2a	methionine adenosyltransferase II, alpha	1.63	1.56	2.00	3.49
rc_AI169756_s_at		ESTs, Highly similar to G33_RAT GENE 33 POLYPEPTIDE [R.norvegicus]	1.33	1.56	3.35	3.62
X86003_at	NOR-2	neuron-derived orphan receptor	1.68	1.56	2.77	3.67
U72632_at	Aoc3	Rattus norvegicus membrane amine oxidase mRNA, partial cds.	1.38	1.56	2.07	4.23
rc_AA866414_at	Slc4a1	Solute carrier family 4, member 1, anion exchange protein 1 (kidney band 3)	1.25	1.73	2.28	4.55
rc_AI176662_s_at	Egr1	Early growth response 1	1.34	1.56	2.73	4.69
AF014827_at	Figf	c-fos induced growth factor (vascular endothelial growth factor D)	2.39	1.56	8.40	4.70
rc_AA944156_s_at	Btg2	Early induced gene, B-cell translocation gene 2	1.62	1.56	3.54	4.80
X06769cds_g_at	C-Fos	c-fos protein (AA 1-380); Rat c-fos mRNA.	1.61	1.56	3.94	4.97

(continued on the next page)

Supplementary Table 2a   upregulated genes   2

Affymetrix	Short name	Full annotation	INNERVATED fold change		DENERVATED fold change	
			normalized to PBS Inn	normalized to agrin-B/z- Inn	normalized to PBS Den	normalized to agrin-B/z- Den
U17254_at	Nr4a1	immediate early gene transcription factor NGFI-B	1.32	1.56	3.56	4.99
AF023087_s_at	nerve growth factor induced factor A **Egr1**	NGFI-A; Rattus norvegicus nerve growth factor induced factor A mRNA, partial 3'UTR.	1.59	1.56	3.86	5.01
M24067_at	Serpine1	serine (or cysteine) proteinase inhibitor, clade E (nexin, plasminogen activator inhibitor type 1), member 1	1.61	1.56	3.56	5.60
U65217_i_at		Rattus norvegicus MHC class II antigen RT1.B beta chain mRNA, partial cds	1.42	4.33	3.45	7.01
S81478_s_at	3CH134/CL100 PTPase **MKP-1**	oxidative stress-inducible protein tyrosine phosphatase; This sequence comes from Fig. 1; 3CH134/CL100 PTPase=oxidative stress-inducible protein tyrosine phosphatase [rats, peritoneal macrophage cDNA library, mRNA, 1912 nt].	1.58	1.56	4.20	7.56
AB004329_at	Acacb	acetyl-Coenzyme A carboxylase beta	1.30	2.03	1.93	7.74
M18416_at	**Egr1**	Early growth response 1	1.34	1.56	5.19	7.88
U75397UTR#1_s_at	Krox-24 / **Egr1**	Rattus norvegicus Krox-24 mRNA, 3' untranslated region, partial sequence.	1.70	1.56	4.62	8.10
U02553cds_s_at	Ptpn16 **MKP-1**	protein tyrosine phosphatase, non-receptor type 16	1.46	1.56	3.82	8.36
X03347cds_g_at		P75 gag-fos fusion protein (aa 1-554); FBR-murine osteosarcoma provirus genome.	1.83	1.56	6.87	8.45
AF004811_at	Msn	moesin	1.41	2.00	2.33	11.56
U17254_g_at	Nr4a1	immediate early gene transcription factor NGFI-B	1.31	1.67	6.16	12.71
rc_AI639284_at		EST, Highly similar to A61404 keratin A, type I - mouse [M.musculus]	2.79	1.56	1.39	12.80
X06769cds_at	**C-Fos**	c-fos protein (AA 1-380); Rat c-fos mRNA.	7.39	1.56	16.15	14.36
X53565_at	Ttgn1	trans-golgi network protein 1	1.78	1.56	2.44	19.56
D16308_at	Ccnd2	Rat mRNA for cyclin D2, complete cds.	1.41	1.84	2.13	27.52
S74351_s_at	protein tyrosine phosphatase, PTP, CL100, 3CH134 **MKP-1**	This sequence comes from Fig. 2; PTP; CL100; 3CH134; protein tyrosine phosphatase [rats, Wistar, lung, mRNA Partial, 521 nt].	1.43	1.56	6.51	28.52

Supplementary Table 2a List of candidate genes that are upregulated by agrin-B/z+.

All the genes listed were significantly changed by more than 25% in innervated and by more than 50% in denervated muscle when compared to PBS and agrin−B/z- injected muscles. Genes are sorted by the ascending fold increase or decrease in the far right columns. Genes that have been previously localized to the NMJ are highlighted with yellow color; IEGs are highlighted by light blue (not examined in this study) and dark blue colors (examined further).

Supplementary Table 2b   downregulated   1

b		GENES DOWNREGULATED BY AGRIN−B/z+				
			INNERVATED fold change		DENERVATED fold change	
Affymetrix	Short name	Full anotation	normalized to PBS Inn	normalized to agrin-B/z- Inn	normalized to PBS Den	normalized to agrin-B/z- Den
rc_AA874805_at		ESTs	0.55	0.59	0.53	0.75
D87515_at	Rnpep	aminopeptidase B	0.57	0.63	0.70	0.74
?322Poly_A_Site#1_s	GHRF	Rat gene for growth hormone-releasing factor (exon 5 and 3' flanking region).	0.46	0.49	0.62	0.72
rc_AA800686_at		ESTs	0.56	0.66	0.59	0.71
rc_AA859519_g_at		ESTs, Highly similar to JC6127 RNA-binding protein type 1 - human [H.sapiens]	0.61		0.56	0.70
rc_AA892860_at		ESTs	0.68	0.70	0.65	0.69
rc_AA875617_at		ESTs, Weakly similar to OAZ2_MOUSE ORNITHINE DECARBOXYLASE ANTIZYME 2 (ODC-AZ 2) (AZ2) (SEIZURE RELATED PROTEIN 15) [M.musculus]	0.58	0.53	0.56	0.69
rc_AA875084_at		ESTs, Highly similar to TLE4_RAT Transducin-like enhancer protein 4 (ESP2 protein) [R.norvegicus]	0.54	0.63	0.46	0.69
rc_AA892550_at		ESTs	0.69	0.69	0.69	0.69
M36453_at	Inha	Inhibin, alpha	0.72	0.63	0.65	0.69
rc_AA799440_g_at		ESTs, Moderately similar to L13 protein [Homo sapiens] [H.sapiens]	0.64	0.67	0.59	0.68
rc_H31323_at		EST	0.71	0.65	0.70	0.68
AF000578_at	Cdc5l	cell division cycle 5-like (S. pombe)	0.59	0.67	0.67	0.68
rc_AA892394_g_at		ESTs, Weakly similar to ELV4_RAT ELAV-like protein 4 (Paraneoplastic encephalomyelitis antigen HuD) (Hu-antigen D) [R.norvegicus]	0.61	0.59	0.65	0.68
rc_AA875129_at		ESTs	0.67	0.63	0.68	0.68
rc_AI233216_at	Glud1	Glutamate dehydrogenase	0.63	0.62	0.71	0.68
rc_H31711_at		ESTs, Weakly similar to S28312 hypothetical protein F02A9.4 - Caenorhabditis elegans [C.elegans]	0.67	0.67	0.67	0.67
rc_AA799575_f_at	Pam	Peptidylglycine alpha-amidating monooxygenase	0.65	0.71	0.65	0.67
rc_AA866364_at		ESTs	0.70	0.69	0.65	0.66
AF009656mRNA_s_at		Rattus norvegicus hypoxanthine guanine phosphoribosyl transferase (hprt) gene, exon 3.	0.66	0.68	0.58	0.66
rc_AA800220_at	Lypla1	Lysophospholipase	0.66	0.59	0.67	0.66
rc_AA799995_g_at	Rpl14	ribosomal protein L14	0.68	0.70	0.66	0.65
rc_AA859931_g_at		ESTs, Moderately similar to hypothetical protein MGC2749 [Homo sapiens] [H.sapiens]	0.63	0.47	0.74	0.65
L20681_at	Ets1	Ets avian erythroblastosis virus E2 oncogene homolog 1 (tumor progression locus 1)	0.61	0.54	0.66	0.65
rc_AA875045_at		ESTs, Highly similar to CNRD_MOUSE Retinal rod rhodopsin-sensitive cGMP 3',5'-cyclic phosphodiesterase delta-subunit (GMP-PDE delta) [M.musculus]	0.60	0.57	0.70	0.65
rc_AI232321_at		ESTs, Highly similar to CGI-150 protein [Homo sapiens] [H.sapiens]	0.72	0.63	0.67	0.65
AB006607_at	Chkl	choline kinase-like	0.62	0.61	0.63	0.64
U32575_g_at	Sec6; rSec6	similar to yeast Sec6p, Swiss-Prot Accession Number P32844; similar to mammalian B94, Swiss-Prot Accession Number Q03169; Method: conceptual translation supplied by author; Rattus norvegicus (rsec6) mRNA, complete cds.	0.72	0.63	0.65	0.64
rc_AA799531_g_at		ESTs, Weakly similar to M18.3.p [Caenorhabditis elegans] [C.elegans]	0.72	0.70	0.61	0.64
rc_AA892390_s_at	Slc11a2	Solute carrier family 11 member 2 (natural resistance-associated macrophage protein 2)	0.54	0.45	0.50	0.64
rc_AA799531_at		ESTs, Weakly similar to M18.3.p [Caenorhabditis elegans] [C.elegans]	0.66	0.62	0.62	0.63
rc_AA799529_at		ESTs	0.71	0.71	0.65	0.63
M31837_at	Igfbp3	insulin-like growth factor-binding protein (IGF-BP3)	0.47	0.66	0.57	0.63
rc_AA892271_at		ESTs	0.69	0.69	0.68	0.63
D37951UTR#1_at	Hivep2	human immunodeficiency virus type I enhancer-binding protein 2	0.68	0.71	0.57	0.63
M81225_at	Fnta	Farnesyltransferase, subunit alpha	0.66	0.69	0.69	0.63
U64030_at	Dut	Deoxyuridinetriphosphatase (dUTPase)	0.63	0.69	0.61	0.63
L34821_at	Aldh5a1	aldehyde dehydrogenase family 5, subfamily A1	0.67	0.68	0.59	0.63
AB006607_g_at	Chkl	choline kinase-like	0.66	0.69	0.61	0.63
rc_AI172097_at	Hsf1	heat shock transcription factor 1	0.61	0.60	0.53	0.63
rc_AA859942_at	Nmt1	Rattus norvegicus mRNA for peptide N-myristoyltransferase 1 (nmt1 gene)	0.69	0.70	0.68	0.63
rc_AA799751_at		ESTs	0.58	0.68	0.57	0.62
rc_AI227608_s_at	Mapt	microtubule-associated protein tau	0.67	0.69	0.62	0.62
AF080468_g_at	G6pt1	glucose-6-phosphatase, transport protein 1	0.63	0.68	0.55	0.62
rc_AI176052_at	Ak3	adenylate kinase 3	0.67	0.72	0.63	0.62
rc_AA799891_g_at	GRASP65	ESTs	0.59	0.57	0.67	0.62
rc_AA875099_s_at	Nup50	Nucleoprotein 50kD	0.69	0.58	0.53	0.62
L07073_at	Ap3m1	adaptor-related protein complex AP-3, mu 1 subunit	0.61	0.62	0.63	0.62
rc_AA866306_at		ESTs	0.57	0.54	0.50	0.62
rc_AA859829_g_at		ESTs	0.71	0.69	0.61	0.62
rc_AA892417_at	Efna1	ephrin A1	0.72	0.66	0.46	0.61
rc_AI171630_s_at	Mapk14	mitogen activated protein kinase 14	0.71	0.68	0.62	0.61
rc_AA893210_at	Copb2	beta prime COP	0.62	0.61	0.62	0.61

(continued on the next page)

Supplementary Table 2b   downregulated   2

Affymetrix	Short name	Full anotation	INNERVATED fold change		DENERVATED fold change	
			normalized to PBS Inn	normalized to agrin-B/z- Inn	normalized to PBS Den	normalized to agrin-B/z- Den
rc_AA892268_at	Ryk	receptor-like tyrosine kinase	0.61	0.67	0.61	0.61
rc_AA799599_at		ESTs	0.70	0.71	0.57	0.61
rc_AA892332_at	Zyx	zyxin	0.67	0.64	0.71	0.61
rc_AA892598_at	Ns	ESTs, Weakly similar to putative nucleotide binding protein, estradiol-induced [Homo sapiens] [H.sapiens]	0.64	0.68	0.51	0.61
rc_AI171562_at	LOC56769	nuclear protein E3-3 orf1	0.66	0.66	0.68	0.61
rc_AI177751_at	Tceb1	elongation factor SIII p15 subunit	0.69	0.63	0.69	0.60
rc_AA893702_s_at	Tcn2p	transcobalamin II precursor	0.63	0.70	0.56	0.60
rc_AA799971_g_at		ESTs, Moderately similar to hypothetical protein FLJ10986 [Homo sapiens] [H.sapiens]	0.63	0.59	0.69	0.60
rc_AI229637_at	Mybbp1a	MYB binding protein (P160) 1a	0.71	0.67	0.59	0.60
L20822_at	Stx5a	syntaxin 5a	0.59	0.63	0.63	0.60
rc_AA799654_g_at		ESTs	0.63	0.72	0.70	0.60
D13907_at	Pmpcb	mitochondrial processing peptidase beta	0.68	0.67	0.61	0.60
Y16774_at	Slc30a4	Dri 27/ZnT4 protein	0.70	0.54	0.75	0.59
rc_AA892297_at	Hdac2	histone deacetylase 2	0.75	0.72	0.54	0.59
rc_AA859899_at	Dmrs91	ESTs	0.71	0.75	0.45	0.59
rc_AA892557_g_at	Srm	ESTs	0.68	0.72	0.58	0.59
rc_AA891666_at	Maged1	melanoma antigen, family D, 1	0.66	0.69	0.69	0.59
rc_AA859909_at		ESTs	0.56	0.59	0.55	0.59
rc_AA892895_i_at	Rps15	ribosomal protein S15	0.60	0.42	0.55	0.59
rc_AA891969_at		ESTs	0.70	0.68	0.57	0.59
rc_AA800044_at		ESTs	0.59	0.67	0.55	0.59
rc_AA891633_f_at	Lypla1	Lysophospholipase	0.74	0.45	0.51	0.58
rc_AA800637_at		ESTs, Highly similar to CCR4-NOT transcription complex, subunit 2; NOT2 (negative regulator of transcription 2, yeast) homolog [Homo sapiens] [H.sapiens]	0.65	0.72	0.58	0.58
rc_AA894101_g_at		ESTs, Moderately similar to PNAD_MOUSE PROTEIN N-TERMINAL ASPARAGINE AMIDOHYDROLASE (PROTEIN NH2-TERMINAL ASPARAGINE DEAMIDASE) (NTN-AMIDASE) (PNAD) (PROTEIN NH2-TERMINAL ASPARAGINE AMIDOHYDROLASE) (PNAA) [M.musculus]	0.68	0.72	0.66	0.58
rc_AI237592_at	dd5	progestin induced protein	0.68	0.71	0.58	0.58
rc_AA800029_at		ESTs, Highly similar to T14792 hypothetical protein DKFZp586G0322.1 - human (fragment) [H.sapiens]	0.69	0.69	0.57	0.58
rc_AA819338_at	Ssr4	signal sequence receptor, delta	0.63	0.72	0.64	0.58
62763complete_seq	Scp2	Sterol carrier protein 2, liver	0.70	0.70	0.60	0.58
rc_AI230260_s_at	Csnk2b	casein kinase II beta subunit	0.69	0.67	0.58	0.58
D00569_g_at	Decr1	2,4-dienoyl CoA reductase 1, mitochondrial	0.64	0.67	0.46	0.57
rc_AA891546_at		ESTs	0.63	0.59	0.66	0.57
X70223_at	Pxmp2	peroxisomal membrane protein 2, 22 kDa	0.60	0.53	0.65	0.57
U95113cds_f_at		similar to Mus musculus H2a pseudogene: GenBank Accession Number X80328; Rattus norvegicus histone H2a gene, complete cds.	0.61	0.61	0.71	0.57
rc_AA891553_at		ESTs, Moderately similar to IF37_MOUSE Eukaryotic translation initiation factor 3 subunit 7 (eIF-3 zeta) (eIF3 p66) [M.musculus]	0.70	0.72	0.53	0.57
X57405_g_at	Notch1; TAN1; NOTCH	R.rattus mRNA homologue of Drosophila notch protein.	0.45	0.31	0.74	0.57
rc_AA800039_s_at		ESTs, Weakly similar to FAF1_MOUSE FAS-associated factor 1 (FAF1 protein) [M.musculus]	0.59	0.66	0.58	0.57
rc_AI012275_at	Tpo1	developmentally regulated protein TPO1	0.63	0.61	0.56	0.56
rc_AI180442_at	Fdps	Farnesyl diphosphate synthase	0.69	0.62	0.70	0.56
rc_AA799464_at		ESTs	0.74	0.67	0.53	0.56
rc_AI237016_at	H2afy	H2A histone family, member Y	0.68	0.66	0.60	0.55
L05541_at		Rattus norvegicus galactose-1-phosphate uridyltransferase gene, complete cds.	0.53	0.38	0.54	0.55
M75168_at	Bat1a	HLA-B associated transcript 1A	0.64	0.68	0.63	0.55
rc_AA891828_g_at	Col1a2	procollagen, type I, alpha 2	0.51	0.64	0.62	0.55
rc_AA800519_at		ESTs	0.71	0.72	0.53	0.54
U11071_i_at		Rattus norvegicus Sprague-Dawley polyadenylate-binding protein-related protein mRNA, 3' end.	0.46	0.23	0.44	0.54
rc_AA946439_at		ESTs, Highly similar to HSRT4 histone H4 - rat [R.norvegicus]	0.57	0.65	0.61	0.54
rc_AA875253_at	Arl1	ADP-ribosylation factor-like 1	0.69	0.67	0.52	0.54
X78606_at	Rab28	RAB28, member RAS oncogene family	0.71	0.74	0.52	0.54
M64986_at	Hmgb1	High mobility group box 1	0.62	0.58	0.64	0.54
rc_AA800218_at		ESTs, Weakly similar to T15476 hypothetical protein C09F5.2 - Caenorhabditis elegans [C.elegans]	0.47	0.49	0.46	0.54
rc_AA892768_at		ESTs, Highly similar to putative breast adenocarcinoma marker (32kD) [Homo sapiens] [H.sapiens]	0.71	0.75	0.53	0.53
AF015728_s_at	Cngb1	rRCNG2ab; Rattus norvegicus cyclic nucleotide-gated cation channel alpha subunit mRNA, partial cds.	0.65	0.49	0.58	0.52
L26267_at	Nfkb1	nuclear factor kappa B p105 subunit	0.66	0.59	0.60	0.52
rc_AI230778_at		ESTs, Highly similar to protein-tyrosine sulfotransferase 2 [Mus musculus] [M.musculus]	0.49	0.50	0.61	0.51
rc_AA859652_at		ESTs	0.39	0.43	0.62	0.50

(continued on the next page)

Supplementary Table 2b   downregulated   3

Affymetrix	Short name	Full anotation	INNERVATED fold change		DENERVATED fold change	
			normalized to PBS Inn	normalized to agrin-B/z- Inn	normalized to PBS Den	normalized to agrin-B/z- Den
rc_AA799732_at		ESTs, Moderately similar to DGC6_MOUSE DGCR6 PROTEIN (DIGEORGE SYNDROME CRITICAL REGION 6 HOMOLOG) [M.musculus]	0.55	0.51	0.46	0.49
rc_AA859898_at		ESTs	0.40	0.22	0.42	0.49
M89953cds_at	Htr1d; 5HT1D	5-HT1D serotonin receptor; putative; Rattus norvegicus 5-HT1D serotonin receptor gene, complete cds.	0.74	0.42	0.50	0.48
rc_AA875438_at		ESTs	0.43	0.35	0.47	0.47
rc_AI171966_at		R.norvegicus mRNA for RT1.Mb	0.70	0.55	0.75	0.46
AF044910_at	Smn	survival motor neuron	0.65	0.63	0.50	0.45
rc_AI013795_at	Dp1	dorsal protein 1	0.75	0.60	0.54	0.45
rc_AA800503_at		ESTs	0.75	0.75	0.42	0.44
rc_AA800176_at		ESTs, Weakly similar to hypothetical protein LOC57019 [Homo sapiens] [H.sapiens]	0.55	0.59	0.46	0.44
rc_AA891735_at		ESTs	0.63	0.42	0.54	0.42
L28801_at	Gtf3c1	general transcription factor III C 1	0.72	0.67	0.41	0.37
rc_AA799396_at		ESTs	0.57	0.51	0.32	0.34
rc_AI639476_s_at		ESTs	0.66	0.57	0.41	0.33
M10094_g_at	RT1Aw2	RT1 class Ib gene	0.75	0.55	0.28	0.29
rc_AA892369_at		ESTs	0.55	0.39	0.44	0.28
M64986_g_at	Hmgb1	High mobility group box 1	0.12	0.13	0.25	0.13
M93017_at	Atp2c1	ATPase, Ca++-sequestering	0.72	0.68	0.00	0.00

Supplementary Table 2b List of candidate genes that are downregulated by agrin-B/z+.

All the genes listed were significantly changed by more than 25% in innervated and by more than 50% in denervated muscle when compared to PBS and agrin−B/z- injected muscles. Genes are sorted by the ascending fold increase or decrease in the far right columns. Genes that have been previously localized to the NMJ are highlighted with yellow color; IEGs are highlighted by light blue (not examined in this study) and dark blue colors (examined further).

2.7   REFERENCES

1. Craig, A.M., Graf, E.R. & Linhoff, M.W. How to build a central synapse: clues from cell culture. *Trends Neurosci* **29**, 8-20 (2006).

2. Washbourne, P.*, et al.* Cell adhesion molecules in synapse formation. *J Neurosci* **24**, 9244-9249 (2004).

3. Verhage, M.*, et al.* Synaptic assembly of the brain in the absence of neurotransmitter secretion. *Science* **287**, 864-869 (2000).

4. DeChiara, T.M.*, et al.* The receptor tyrosine kinase MuSK is required for neuromuscular junction formation in vivo. *Cell* **85**, 501-512 (1996).

5. Glass, D.J.*, et al.* The receptor tyrosine kinase MuSK is required for neuromuscular junction formation and is a functional receptor for agrin. *Cold Spring Harbor Symp Quant Biol* **61**, 435-444 (1996).

6. Gautam, M.*, et al.* Defective neuromuscular synaptogenesis in agrin-deficient mutant mice. *Cell* **85**, 525-535 (1996).

7. McMahan, U.J. The agrin hypothesis. *Cold Spring Harb Symp Quant Biol* **55**, 407-418 (1990).

8. Bezakova, G. & Ruegg, M.A. New insights into the roles of agrin. *Nat Rev Mol Cell Biol* **4**, 295-308. (2003).

9. Schaeffer, L., de Kerchove d'Exaerde, A. & Changeux, J.P. Targeting transcription to the neuromuscular synapse. *Neuron* **31**, 15-22. (2001).

10. Escher, P.*, et al.* Synapses form in skeletal muscles lacking neuregulin receptors. *Science* **308**, 1920-1923 (2005).

11. Nazarian, J., Bouri, K. & Hoffman, E.P. Intracellular expression profiling by laser capture microdissection: three novel components of the neuromuscular junction. *Physiological genomics* **21**, 70-80 (2005).

12. Kishi, M., Kummer, T.T., Eglen, S.J. & Sanes, J.R. LL5beta: a regulator of postsynaptic differentiation identified in a screen for synaptically enriched transcripts at the neuromuscular junction. *J Cell Biol* **169**, 355-366 (2005).

13. Jevsek, M.*, et al.* CD24 is expressed by myofiber synaptic nuclei and regulates synaptic transmission. *Proc Natl Acad Sci U S A* **103**, 6374-6379 (2006).

14. Bezakova, G., Helm, J.P., Francolini, M. & Lomo, T. Effects of purified recombinant neural and muscle agrin on skeletal muscle fibers in vivo. *J Cell Biol* **153**, 1441-1452. (2001).

15. Sgambato, V., Pages, C., Rogard, M., Besson, M.J. & Caboche, J. Extracellular signal-regulated kinase (ERK) controls immediate early gene induction on corticostriatal stimulation. *J Neurosci* **18**, 8814-8825 (1998).

16. Valenzuela, D.M.*, et al.* Receptor tyrosine kinase specific for the skeletal muscle lineage: expression in embryonic muscle, at the neuromuscular junction, and after injury. *Neuron* **15**, 573-584 (1995).

17. Duclert, A. & Changeux, J.P. Acetylcholine receptor gene expression at the developing neuromuscular junction. *Physiol Rev* **75**, 339-368 (1995).

18. Jones, G*., et al.* Induction by agrin of ectopic and functional postsynaptic-like membrane in innervated muscle. *Proc Natl Acad Sci U S A* **94**, 2654-2659 (1997).

19. Brenner, H.R., Witzemann, V. & Sakmann, B. Imprinting of acetylcholine receptor messenger RNA accumulation in mammalian neuromuscular synapses. *Nature* **344**, 544-547 (1990).

20. Ralston, E., Lu, Z. & Ploug, T. The organization of the Golgi complex and microtubules in skeletal muscle is fiber type-dependent. *J Neurosci* **19**, 10694-10705 (1999).

21. Feng, G*., et al.* Imaging neuronal subsets in transgenic mice expressing multiple spectral variants of GFP. *Neuron* **28**, 41-51 (2000).

22. Smith, M.A. & Hilgenberg, L.G. Agrin in the CNS: a protein in search of a function? *Neuroreport* **13**, 1485-1495. (2002).

23. Si, J., Wang, Q. & Mei, L. Essential roles of c-JUN and c-JUN N-terminal kinase (JNK) in neuregulin-increased expression of the acetylcholine receptor epsilon-subunit. *J Neurosci* **19**, 8498-8508 (1999).

24. Okada, K*., et al.* The muscle protein Dok-7 is essential for neuromuscular synaptogenesis. *Science* **312**, 1802-1805 (2006).

25. Lacazette, E., Le Calvez, S., Gajendran, N. & Brenner, H.R. A novel pathway for MuSK to induce key genes in neuromuscular synapse formation. *J Cell Biol* **161**, 727-736 (2003).

26. Kong, X.C., Barzaghi, P. & Ruegg, M.A. Inhibition of synapse assembly in mammalian muscle in vivo by RNA interference. *EMBO reports* **5**, 183-188 (2004).

27. Weston, C., Yee, B., Hod, E. & Prives, J. Agrin-induced acetylcholine receptor clustering is mediated by the small guanosine triphosphatases Rac and Cdc42. *J Cell Biol* **150**, 205-212. (2000).

28. Luo, Z.G*., et al.* Regulation of AChR clustering by Dishevelled interacting with MuSK and PAK1. *Neuron* **35**, 489-505 (2002).

29. Sundberg-Smith, L.J., Doherty, J.T., Mack, C.P. & Taylor, J.M. Adhesion stimulates direct PAK1/ERK2 association and leads to ERK-dependent PAK1 Thr212 phosphorylation. *J Biol Chem* **280**, 2055-2064 (2005).

30. Akaaboune, M*., et al.* Developmental regulation of the serpin, protease nexin I, localization during activity-dependent polyneuronal synapse elimination in mouse skeletal muscle. *J Comp Neurol* **397**, 572-579 (1998).

31. Martin, P.T., Ettinger, A.J. & Sanes, J.R. A synaptic localization domain in the synaptic cleft protein laminin b2 (s-laminin). *Science* **269**, 413-416 (1995).

32. Imaizumi-Scherrer, T., Faust, D.M., Benichou, J.C., Hellio, R. & Weiss, M.C. Accumulation in fetal muscle and localization to the neuromuscular junction of cAMP-dependent protein kinase A regulatory and catalytic subunits RIa and Ca. *J Cell Biol* **134**, 1241-1254 (1996).

33. Altiok, N., Altiok, S. & Changeux, J.P. Heregulin-stimulated acetylcholine receptor gene expression in muscle: requirement for MAP kinase and evidence for a parallel inhibitory pathway independent of electrical activity. *Embo J* **16**, 717-725 (1997).

34. Fromm, L. & Rhode, M. Neuregulin-1 induces expression of Egr-1 and activates acetylcholine receptor transcription through an Egr-1-binding site. *J Mol Biol* **339**, 483-494 (2004).

35. Witzemann, V.*, et al.* Acetylcholine receptor e-subunit deletion causes muscle weakness and atrophy in juvenile and adult mice. *Proc Natl Acad Sci USA* **93**, 13286-13291 (1996).

36. Lee, S.L., Tourtellotte, L.C., Wesselschmidt, R.L. & Milbrandt, J. Growth and differentiation proceeds normally in cells deficient in the immediate early gene NGFI-A. *J Biol Chem* **270**, 9971-9977 (1995).

37. O'Donovan, K.J., Tourtellotte, W.G., Millbrandt, J. & Baraban, J.M. The EGR family of transcription-regulatory factors: progress at the interface of molecular and systems neuroscience. *Trends Neurosci* **22**, 167-173 (1999).

38. O'Leary, D.A.*, et al.* Targeting of the ETS factor GABPalpha disrupts neuromuscular junction synaptic function. *Mol Cell Biol* **27**, 3470-3480 (2007).

39. Hippenmeyer, S., Huber, R.M., Ladle, D.R., Murphy, K. & Arber, S. ETS transcription factor Erm controls subsynaptic gene expression in skeletal muscles. *Neuron* **55**, 726-740 (2007).

40. Ponomareva, O.N.*, et al.* Defective neuromuscular synaptogenesis in mice expressing constitutively active ErbB2 in skeletal muscle fibers. *Mol Cell Neurosci* **31**, 334-345 (2006).

41. Lin, W.*, et al.* Neurotransmitter acetylcholine negatively regulates neuromuscular synapse formation by a Cdk5-dependent mechanism. *Neuron* **46**, 569-579 (2005).

42. Misgeld, T.*, et al.* Roles of neurotransmitter in synapse formation: development of neuromuscular junctions lacking choline acetyltransferase. *Neuron* **36**, 635-648 (2002).

43. Wu, J.J.*, et al.* Mice lacking MAP kinase phosphatase-1 have enhanced MAP kinase activity and resistance to diet-induced obesity. *Cell metabolism* **4**, 61-73 (2006).

44. Nikolic, M., Chou, M.M., Lu, W., Mayer, B.J. & Tsai, L.H. The p35/Cdk5 kinase is a neuron-specific Rac effector that inhibits Pak1 activity. *Nature* **395**, 194-198 (1998).

45. Ksiazek, I.*, et al.* Synapse loss in cortex of agrin-deficient mice after genetic rescue of perinatal death. *J Neurosci* **27**, 7183-7195 (2007).

46. Jeffrey, K.L., Camps, M., Rommel, C. & Mackay, C.R. Targeting dual-specificity phosphatases: manipulating MAP kinase signalling and immune responses. *Nature reviews* **6**, 391-403 (2007).

47. Thomas, G.M. & Huganir, R.L. MAPK cascade signalling and synaptic plasticity. *Nat Rev Neurosci* **5**, 173-183 (2004).

48. Jones, G., Moore, C., Hashemolhosseini, S. & Brenner, H.R. Constitutively active MuSK is clustered in the absence of agrin and induces ectopic postsynaptic-like membranes in skeletal muscle fibers. *J Neurosci* **19**, 3376-3383 (1999).

Muscle-wide secretion of a miniaturized form of neural agrin rescues focal neuromuscular innervation in agrin mutant mice

Shuo Lin[1], Marcin Maj[1], Gabriela Bezakova[1], Josef P. Magyar[2], Hans Rudolf Brenner[3] and Markus A. Ruegg[1]

[1]Biozentrum, University of Basel, Klingelbergstrasse 70, 4056 Basel, Switzerland

[2]Santhera Pharmaceuticals, Hammerstrasse 47, 4410 Liestal, Switzerland

[3]Institute of Physiology, Dept. of Biomedicine, University of Basel, 4056 Basel, Switzerland

3.1 ABSTRACT

Agrin and its receptor MuSK are required and sufficient for the formation of the postsynaptic apparatus at the neuromuscular junction (NMJ). In the current model the local deposition of agrin by the nerve and the resulting local activation of MuSK is responsible for creating and maintaining the postsynaptic apparatus including clusters of acetylcholine receptors (AChRs). Concomitantly, the release of acetylcholine (ACh) and the resulting depolarization disperses those postsynaptic structures that are not apposed by the nerve and thus not stabilized by agrin-MuSK signaling. Here we show that a miniaturized form of agrin, consisting of the laminin-binding and the MuSK-activating domains, is sufficient to fully restore NMJs in agrin mutant mice when expressed by developing muscle. Mice expressing this mini-agrin are fertile and can survive for at least one year. The innervation band in these mice is substantially widened, but the number of non-synaptic AChR clusters declines during development and the size and the number of nerve-associated AChR clusters increases. The factor responsible for the differential stabilization of AChRs that are apposed by nerve terminals appears to be ACh, as incubation with the agonist carbachol reduces the loss of AChR clusters in organotypic cultures of the diaphragm. Our results show that agrin function in NMJ development requires only two small domains, and that this function does not depend on local deposition of agrin at synapses, and suggest a novel local function of ACh to stabilize postsynaptic structures.

3.2 INTRODUCTION

One of the fundamental questions in neuroscience is how synapse formation between neurons and their targets is controlled during development. Current evidence indicates that initial stages of target recognition and of synapse formation are driven by cell adhesive interactions and that later stages require electrical activity (1, 2). The easy accessibility of the neuromuscular junction (NMJ) for experimental manipulation, has allowed investigating synapse formation at both the molecular and physiological levels. Based on knockout experiments in mice NMJ formation critically depends on agrin, an extracellular matrix molecule released by the nerve (3), the receptor tyrosine-kinase MuSK, which is activated by agrin (4), the low-density lipoprotein receptor-related protein 4 (5) and the two intracellular adaptor molecules Dok-7 (6) and rapsyn (7), which bind to activated MuSK and the acetylcholine receptor (AChR), respectively. Of these molecules, agrin and its signal-transducing receptor MuSK are the most upstream components to initiate postsynaptic differentiation. Agrin's synapse-inducing activity is regulated by alternative mRNA splicing. In particular, only certain splice variants that differ within the most carboxy-terminal laminin G (LG)-like domain at a site called B in chick (8) or z in rodents (9) are capable of inducing AChR aggregation (10, 11) and MuSK activation (12). Importantly, active agrin isoforms are released by motor neurons whereas non-neuronal cells including muscle fibers synthesize splice variants that lack the inserts at the B/z site (13).

According to the agrin hypothesis (14), agrin released from growth cones of motor neurons initiates a signaling cascade that results in the formation of the entire postsynaptic apparatus. In accordance with this, either agrin (15, 16) or a constitutively active form of MuSK (17) is capable of inducing new postsynapses when applied to non-synaptic regions of adult muscle. However, the finding that developing muscle of mice lacking motor neurons or agrin still forms AChR clusters in the region where synapses are normally made (18-20) has challenged the traditional view that agrin is required for initiating postsynaptic differentiation (see also 21). Moreover, the neurotransmitter acetylcholine (ACh) has been shown to disperse AChR clusters that are not contacted by motor neurons (22, 23). Thus, the current concept is that agrin stabilizes pre-existing AChR clusters rather than to induce new ones in developing muscle and thereby counteracts the dispersing activity of ACh (21).

Here we report on transgenic mice that express a miniaturized version of an agrin isoform, which is synthesized by motor neurons, in skeletal muscle fibers. We show that

mini-agrin is sufficient to fully restore NMJ formation in agrin-deficient mice. Unexpectedly, although mini-agrin is expressed along the entire myofibers, AChR clusters become restricted to the sites of nerve contact during development. We provide evidence that this restriction is mediated by ACh, which besides dispersing non-synaptic AChR clusters (22, 23), stabilizes those that appose the nerve terminal.

3.3 MATERIALS AND METHODS

Mice.

Transgenic mice expressing c-mag$_{B8}$ were generated as described (1) using the chick N257C21B8_myc construct, which has been described elsewhere (2). The cDNA encoding mouse mini-agrin (m-mag$_{z8}$) was obtained by RT-PCR on mRNA isolated from mouse spinal chord. The entire construct was sequenced and inserted into the tetO7-CMV promoter by replacing the cDNA construct described elsewhere (3). MCK-tTA mice (4) were obtained from N. Raben (National Institutes of Health, Bethesda, MD). Transgenic founders were identified by Southern blot analysis and PCR. The following primers were used for PCR genotyping: 5' ACC CAG CCC CTC AGT ACA TGT and 5' CTT CTG TTT TGA TGC TCA GC for c-mag$_{B8}$; 5' CCA ATG TGA CCG CTA GCG AGA AG and 5' CTG TAG GCC TCC AAG CCA CA for m-mag$_{z8}$. Previously described primers and procedures were used to identify mice that express tTA (3) or YFP 5 or that are deficient for agrin (6).

Antibodies.

Antibodies directed against chick agrin (7), mouse agrin (8) and MuSK (9) were raised in our laboratory and have been characterized previously. To avoid reactivity with mouse tissue of anti-mouse secondary antibodies, anti-myc antibody 9E10 (10) was biotinylated with biotin-NHS according to the manufacturer's procedure. Other antibodies used were from the following commercial sources: rabbit antibodies against synaptophysin (Dako) or neurofilament (Sigma). Secondary antibodies were coupled to either Cy3 (Jackson ImmunoResearch) or Alexa-488 (Invitrogen).

Immunoblot and quantification.

Frozen tissues were pulverized on a metal plate cooled in liquid nitrogen and resuspended in protein extraction buffer [80 mM Tris-HCl pH 6.8, 10 mM EDTA, 2% SDS and 1:50 diluted mix protease inhibitors (Sigma)]. 10 µg of protein was separated on a 7.5% SDS–PAGE and immunoblotted. Expression levels of the transgenes were quantified by measuring the intensity of the band after subtracting the background in the same blot. For normalization, the intensity of the actin band after Ponceau S staining (Sigma) was used.

Quantitative analysis of synaptic AChR cluster bands.

For measuring the width of the synaptic band in the diaphragm, images of whole mounts such as those shown in SI Figs. 7-10 were analyzed by AnalySIS software (Soft Imaging System). By using the "measuring Area/Perimeter tool", the periphery of the region comprising AChR clusters contacted by motor nerves was outlined manually and the area of this outline was determined. The average width of the synaptic band was calculated by dividing its length.

Organotypic culture of E14.5 diaphragms.

The method of culturing E14.5 diaphragms ex vivo has been described (32). Briefly, diaphragms with ribcages were incubated in M199 medium supplemented with 5% horse serum and penicillin/streptomycin in an atmosphere of 95% O_2 and 5% CO_2 at 37°C. Carbachol (Sigma) was used at a concentration of 0.1 mM. After 18 hours, diaphragms were fixed in 4%PFA, stained with Alexa-555-α-bungarotoxin and mounted. At the middle of each hemidiaphragm, three confocal stacks were recorded with the 40x objective and 0.5 μm z-steps. The number and volume of AChR clusters (> 10 μm^3) were quantified as described below.

Image acquisition and processing.

Diaphragms were analyzed with a confocal laser scanning microscope (Leica TCS SPE). Images were recorded with HC_PL_APO 20x/nA 0.7 (506514) or ACS_APO 40x/nA 1.15 (507901) objectives with 1 μm and 0.5 μm z-steps, respectively. Images were recorded with the same laser power and the same parameter setting. For quantification of AChR clusters, three to eight image stacks with 20x objective in the middle of the hemidiaphragm (as illustrated in SI Fig. 8-10) were analyzed with Imaris software (Version x64 5.7.2, Bitplane AG). The threshold intensity was set by visual inspection so that the size of the AChR clusters and the nerve was similar to what is shown in the image stack. Only particles that were bigger than 30 μm^3 were included. AChR clusters were then separated manually into two categories based on the colors. Nerve-associated clusters appeared yellow while non-synaptic clusters were red. The total number and the volume of AChR clusters of the two categories were determined by the Imaris program.

3.4 RESULTS

Transgenic expression of a miniaturized form of neural agrin in skeletal muscle.

We have previously shown that a miniaturized form of neural agrin containing the eight amino acid insert at the B/z site is sufficient to induce postsynapse-like structures when expressed in non-synaptic regions of the adult soleus muscle (24). To further study this phenomenon, we generated several transgenic mouse lines. Transgenes were derived from full-length chick or mouse agrin$_{B/z8}$ (see Fig. 1A for domain organization) and consisted of the amino-terminal domain that confers binding to laminins (25) and the most carboxy-terminal LG domain that is sufficient to activate MuSK (12). Between the domains, one follistatin-like repeat was inserted to allow independent folding and the transgenic proteins were myc-tagged. Expression of the cDNAs encoding chick mini-agrin (c-mag$_{B8}$) or mouse mini-agrin (m-mag$_{z8}$) was under the control of the promoter elements of muscle creatine kinase (Fig. 1A). While c-mag$_{B8}$ was constitutively expressed (see also 26), expression of m-mag$_{z8}$ could be suppressed by doxycycline in the drinking water (tet-off system; see 27 for further details). For both constructs, several mouse lines were established, which expressed the transgenes at different levels (Fig. 1B, C). In the current studies, we mainly used the non-inducible line c-mag$_{B8}$ and two m-mag$_{z8}$ lines without the addition of doxycycline. As expected for the MCK promoter (28, 29), c-mag$_{B8}$ was expressed as early as embryonic day 13.5 (SI, Fig. 6). In adult muscle, c-mag$_{B8}$ was not enriched at NMJs unlike endogenous agrin (SI, Fig. 6C, D). A similar expression pattern of the transgene was observed in each of the tet-off lines that expressed m-mag$_{z8}$ in the absence of doxycycline (data not shown).

To test whether overexpression of mag$_{B/z8}$ induces the formation of ectopic postsynaptic structures, we examined hindlimb and diaphragm muscles in adult animals. In line with previous results (24), all these muscles contained ectopic AChR clusters. We noticed, however, a large difference between muscles to form ectopic AChR aggregates. For example, soleus muscle contained many ectopic AChR clusters (Fig. 1D) while extensor digitorum longus (EDL) contained only very few (Fig. 1E). Quantification revealed that the average number of ectopic AChR clusters per muscle fiber ranged from 2 (soleus) to 0.1 (EDL) (Fig. 1F). This 20-fold difference in the responses of soleus and EDL muscles was not due to differences in levels of the c-mag$_{B8}$ (Fig. 1B, C). Moreover, the order of responsiveness was the same in all the transgenic lines irrespective of the levels of mag$_{B/z8}$ (data not shown). Denervation of hindlimb muscles resulted in the

formation of an exuberant number of AChR clusters in both muscles, and the difference in cluster number between muscles was abrogated (data not shown). These results thus indicate that the intrinsic sensitivity to ectopic expression of $mag_{B/z8}$ differs greatly between muscles.
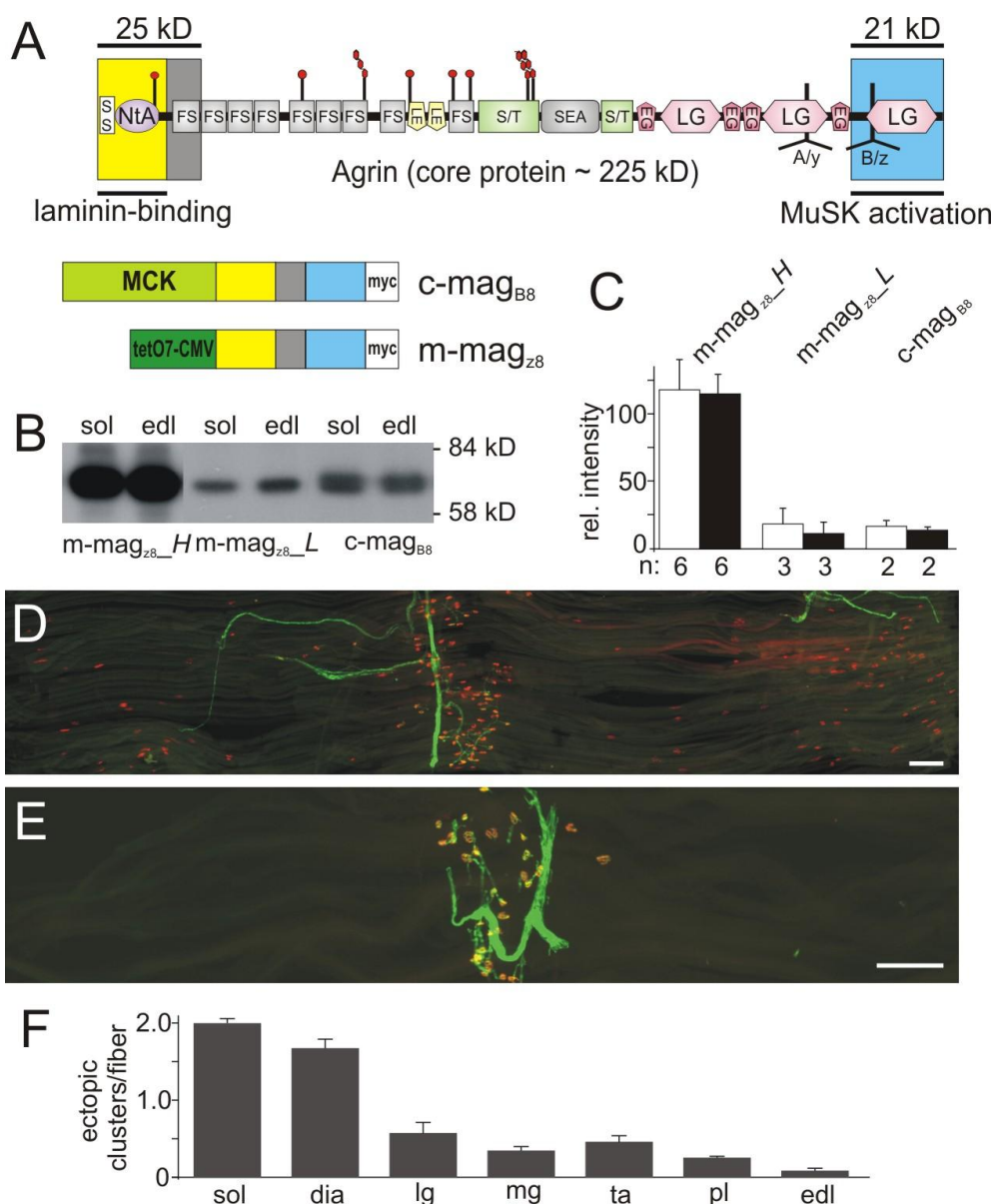
Figure 1 (80x97 mm)

Fig. 1. Transgenic expression of a miniaturized form of neural agrin induces the formation of non-synaptic AChR clusters.

(A) Top: Schematic presentation of the protein domains of agrin and the localization of the alternative mRNA splice sites A/y and B/z (modified from 13). Bottom: Schematic representation of mini-agrin constructs used. Promoters are shown in green, the domains included in the mini-agrin were derived from either chick (c-mag$_{B8}$) or mouse agrin (m-mag$_{z8}$).

(continued on the next page)

Both mini-agrins include a myc-tag at the C-terminus (white) for detection. MCK represent the 1.3 kb fragment of the human muscle creatine kinase (MCK) promoter as described (26). TetO7-CMV represents the tetracycline-responsive promoter. After mating such a transgenic mouse with a MCK-tTA mouse (43), the m-magz8 is expressed exclusively in skeletal muscle as described elsewhere (27).

(B) Western blot analysis of muscle extracts of 6 week-old mice from different transgenic lines using anti-myc antibodies. Line m-mag$_{z8}$_*H* expresses high levels while lines m-mag$_{z8}$_*L* and c-mag$_{B8}$ express moderate levels of the transgene.

(C) Quantification of the signals observed in Western blots. Soleus muscles are represented by open bars, EDL muscles by filled bars. Relative intensity represents mean ± SD. Number of samples measured (n) is given.

(D, E) Single fiber layer bundles of soleus *(D)* or EDL *(E)* muscles isolated from 6 week-old c-mag$_{B8}$ transgenic mice. AChRs are stained with Alexa-555-α-bungarotoxin (red) and motor nerves are labeled by YFP (44). While many ectopic AChR clusters are seen in the soleus muscle (*D*), only few can be detected in EDL.

(F) Quantification of the number of ectopic AChR clusters per NMJ. Numbers represent mean ± SEM; N = 3 mice. In each mouse between 87 and 424 muscle fibers were examined. Note that there is a large difference in the response of a muscle to c-mag$_{B8}$. Abbreviations: sol: soleus; dia: diaphragm; lg: lateral gastrocnemius; mg: medial gastrocnemius; ta: tibialis anterior; pl: plantaris; edl: extensor digitorum longus. Scale bars: 250 µm.

Mini-agrin expressed by skeletal muscle is sufficient to drive synapse formation in the absence of endogenous agrin.

We have previously shown that expression of full-length chick agrin in motor neurons is capable of preventing the perinatal death of agrin-deficient mice (30). The relatively low number of ectopic postsynapses, the fact that the innervation band remained localized in the center of the muscle and the lack of an overt phenotype in the transgenic mice led us to test whether NMJs would still form in the absence of any nerve-derived agrin. To investigate this, we mated the transgenic mice with heterozygous agrin-deficient mice (20) to obtain lines that are deficient for agrin and express $mag_{B/z8}$ in skeletal muscle ($mag_{B/z8}$; *agrn*$^{-/-}$). Such mice were born alive and could not be distinguished from their littermate controls (Fig. 2A; see also SI Video). While some mice developed symptoms such as kyphosis, signs of muscle fibrillation and eventually died early, the majority was fertile and lived for a prolonged time, the oldest being now 1 year old (Fig. 2B). NMJs in the $mag_{B/z8}$; *agrn*$^{-/-}$ mice were localized to the central region of the muscle both in soleus (Fig. 2C) and EDL (Fig. 2D). At higher magnification, the NMJs of the $mag_{B/z8}$; *agrn*$^{-/-}$ (Fig. 2E and F) mice looked remarkably similar to those of control littermates (inserts in Fig. 2E and F). In summary, these experiments show that uniform expression of mini-agrin in skeletal muscle restores the formation of nerve-muscle synapses, notably of presynaptic nerve terminals. Interestingly, the rescue is superior to that obtained by the expression of full-length agrin in motor neurons (30).

A

B

line	born	fertile	mice died <3 mo.	age reached
c-mag$_{B8}$; *agrn*$^{-/-}$	60	yes	5%	9 mo.
m-mag$_{z8}$_*H*; *agrn*$^{-/-}$	15	yes	0	12 mo.
m-mag$_{z8}$_*L*; *agrn*$^{-/-}$	18	yes	12%	12 mo.

C

D

E

F
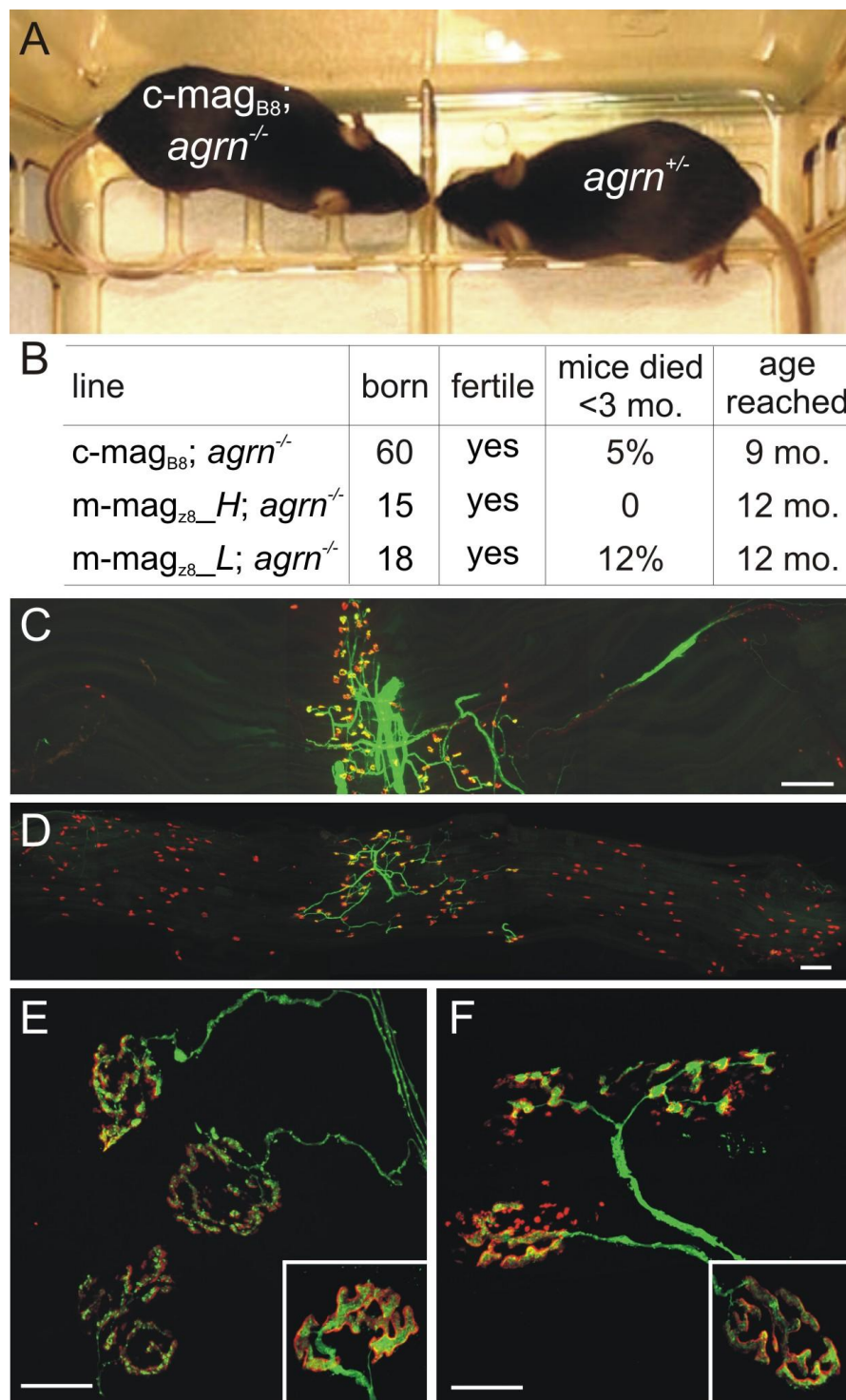
Figure 2 (83x130 mm)

(continued on the next page)

Fig. 2. Transgenic expression of mag$_{B/z8}$ in muscle restores NMJ function and prevents perinatal death of agrin mutant mice.

(A) Photograph of two 8 week-old littermates. No difference is seen between c-mag$_{B8}$; *agrn*$^{-/-}$ and a control (*agrn*$^{+/-}$) littermate.

(B) Summary of the overall phenotype of rescued mice using three different transgenic mouse lines. Number of mice born is given for each line. A low percentage of the rescued mice shows motor deficits and eventually dies before the age of three months (4th column). The current age of the oldest mice is given (5th column). See also SI Video for locomotory behavior.

(C, D) Low magnification images of EDL *(C)* and soleus *(D)* muscle from a 7 week-old m-mag$_{z8}$; *agrn*$^{-/-}$ mouse. AChRs are visualized by Alexa-555-α-bungarotoxin (red), motor nerves by YFP (green). Scale bar: 250 µm.

(E, F) Confocal images of NMJs of m-mag$_{z8}$; *agrn*$^{-/-}$ mice in the EDL *(E)* and soleus *(F)* muscle. For comparison, NMJs of control mice are shown in the inserts. NMJs of rescued mice appear slightly more fragmented. Scale bar: 50 µm.

Development of NMJs.

We next examined the development of the NMJ between embryonic day 13.5 (E13.5) and embryonic day 18.5 (E18.5). For comparison with other studies addressing NMJ development (e.g. 20, 31), we focused on the diaphragm muscle. To minimize biological variation, we always compared mice of the different genotypes from the same litter. As controls, we used mice that were not transgenic and carried at least one wild-type allele for *agrn* ($agrn^{+/?}$). These were compared with agrin-deficient ($agrn^{-/-}$), transgenic control ($mag_{B/z8}$; $agrn^{+/?}$) and transgenic, agrin-deficient mice ($mag_{B/z8}$; $agrn^{-/-}$). Diaphragms were isolated from embryos and both the presynaptic nerve terminals and postsynaptic AChR clusters were visualized in whole mount preparations (see SI, Figs. 7 – 10).

At E13.5, the motor nerves had entered the diaphragm and only few branches emerged (SI; Fig. 7). Diaphragms from mice expressing $mag_{B/z8}$ contained more AChR clusters than those from control and agrin-deficient mice (Fig. 3A), but most of them were not contacted by nerve terminals (Fig. 3A). At E14.5, motor nerves had branched further (SI, Fig. 8). The number, intensity and the fraction of the AChR clusters associated with presynaptic nerve terminals had increased in all genotypes except in $agrn^{-/-}$ mice (SI, Fig. 8; Fig. 3B). In transgenic mice, however, non-synaptic AChR clusters remained more frequent than in controls (Fig. 3B). At E16.5, the majority of AChR clusters in control mice were confined to a central band where they were contacted by nerves (Fig. 3C and SI, Fig. 9) whereas in agrin-deficient mice only remnants of AChR clusters were detected (Fig. 3C), and motor nerves continued to grow towards the tendon (SI, Fig. 9). Nerve association of AChR clusters was also increased in $mag_{B/z8}$ transgenic mice although the number of nerve-free AChR clusters remained substantial (Fig. 3C; SI, Fig. 9). At E18.5, NMJ maturation was further advanced in control mice (Fig. 3D; SI, Fig. 10), whereas most AChR clusters had disappeared from $agrn^{-/-}$ diaphragms (Fig. 3D). In contrast in $mag_{B/z8}$ transgenic mice, irrespective of whether they were deficient for endogenous agrin or not, many of the AChR clusters were contacted by the motor nerve terminals (Fig. 3D). Unlike control diaphragms, however, those expressing mini-agrin still contained non-synaptic AChR clusters, and their innervation band appeared wider than in controls (SI, Fig. 10).

To quantify the influence of the ectopic expression of mini-agrin on motor innervation, we determined its effect on the width of the synaptic band. A widening by $mag_{B/z8}$ could be resolved as early as E14.5 and was even more pronounced at E18.5 (Fig. 4A). Interestingly, the widening of the synaptic band was largely due to the expression of $mag_{B/z8}$, as only a small additional increase was seen in $mag_{B/z8}$; $agrn^{-/-}$ mice (Fig. 4A).
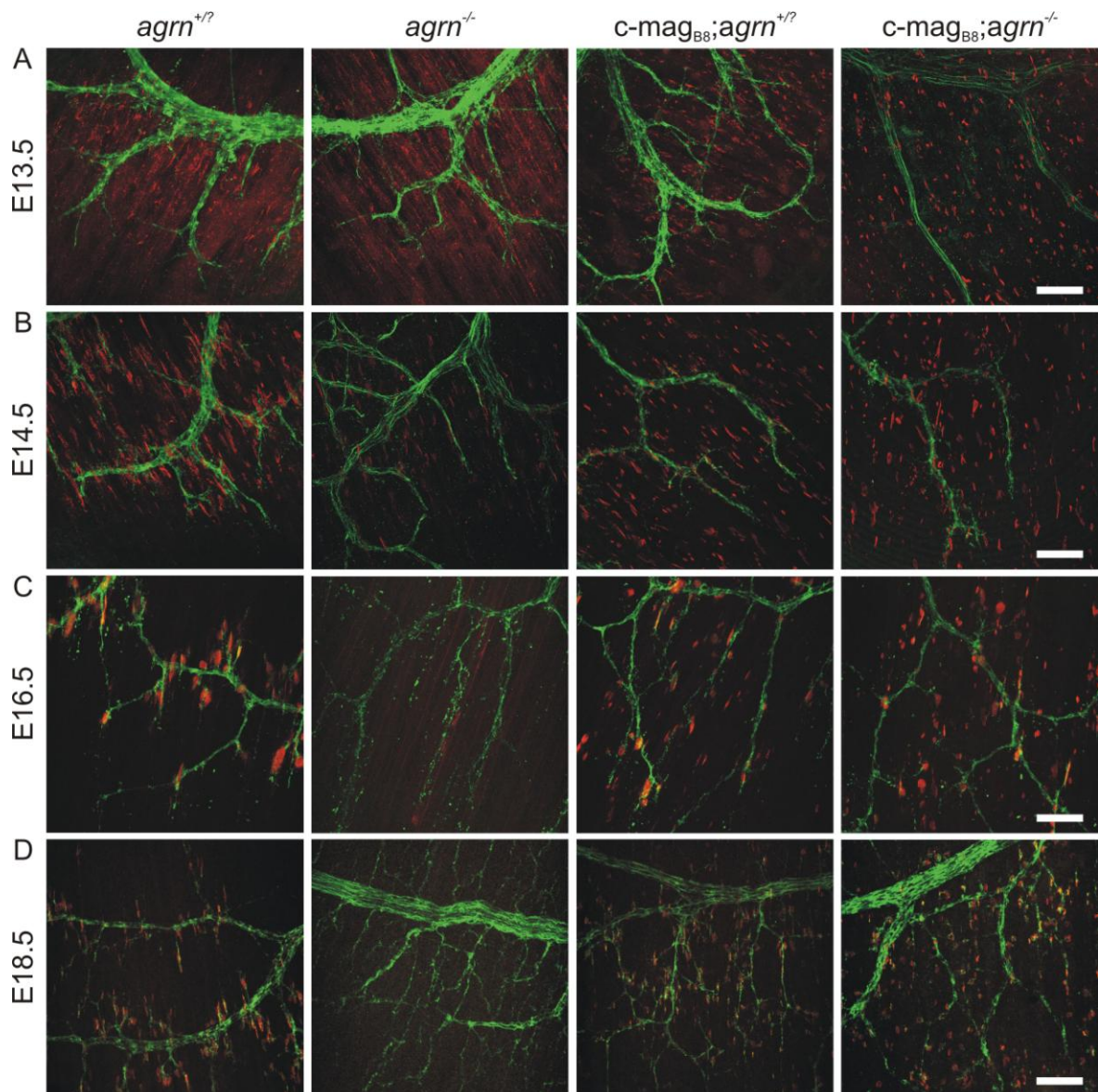
Figure 3 (87x87 mm)

Fig. 3. Confocal images of diaphragms from E13.5 to E18.5 mice of the different genotypes indicated at the top.

The entire thickness of the diaphragms were scanned with either a 40x (*A-C*) or a 20x (*D*) objective. Images were recorded from whole mounts as shown in SI Figs. 7-10. Scale bars: 50 µm *(A-C)* and 100 µm *(D)*.

AChR clusters that are contacted by the nerve are stabilized.

The current model proposes that neural agrin deposited at the site of innervation stabilizes AChR clusters while ACh acts as a dispersal factor to remove non-synaptic AChR clusters that are devoid of neural agrin (21). Since mini-agrin is secreted throughout the entire length of the muscle fibers in the $mag_{B/z8}$ transgenic mice, all AChR clusters, irrespective of whether they are innervated should be stable. To test this, we systematically recorded confocal stacks through the entire thickness of hemidiaphragms from developmental time points (see detailed description in "Materials and Methods" and SI, Figs. 8 – 10). For each stack, the total number of AChR clusters, the number of clusters contacted by nerve terminals, and the volume of the clusters were determined. The number of AChR clusters per stack was higher in $mag_{B/z8}$ transgenic mice than in controls at each developmental time point (Fig. 4B). In control mice, the percentage of synaptic AChR clusters steadily increased over time to reach close to 100% by E18.5 (Fig. 4C) and the number of non-synaptic AChR clusters decreased (SI, Fig. 11). In $mag_{B/z8}$; *agrn*$^{+/?}$ mice, the percentage of synaptic AChR clusters also increased (Fig. 4C) and the number of non-synaptic clusters decreased over time (SI, Fig. 11). Importantly, a similar increase in the number of synaptic and a decrease of non-synaptic AChR clusters was seen in the $mag_{B/z8}$; *agrn*$^{-/-}$ mice (Fig. 4C; SI, Fig. 11). Nerve-associated (i.e. synaptic) AChR clusters were also significantly larger than those that were not innervated and the difference became more pronounced at later developmental time points (Fig. 4D). Thus, even when nerve terminals do not secrete agrin, those AChR clusters that are contacted by nerve terminals are selectively stabilized although this process is slower in $mag_{B/z8}$ transgenic mice than in control mice. These results strongly suggest that nerve terminals release a factor different from agrin that selectively stabilizes AChR clusters.
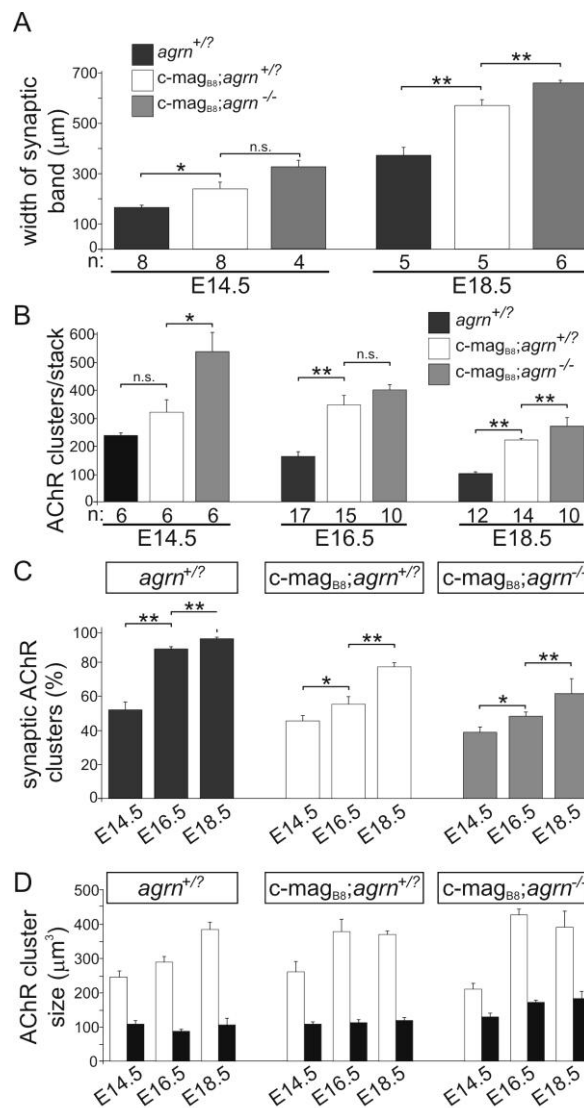
Figure 4 (81x154 mm)

Fig. 4. Quantification of the width of the synaptic band *(A)*, of the number of AChR clusters *(B)*, the percentage of synaptic AChR clusters *(C)* and the size of synaptic (open bars) and non-synaptic (filled bars) AChR clusters *(D)*.

For each parameter, diaphragms from at least three mice were examined. Numbers represent mean ± SEM from one stack of confocal images through the entire hemidiaphragm. For each hemidiaphragm, three to eight stacks of confocal images were measured (see SI, Fig. 8 – 10 as examples). Numbers of stacks measured (n) are given *(A, B)*. *P*-values (two tailed Student's t-test): **: $p \leq 0.01$; *: $p \leq 0.05$; n.s.: $p > 0.05$. For experimental details see Materials and Methods.

Carbachol stabilizes synaptic AChR clusters.

A candidate for a nerve-derived factor could be the neurotransmitter itself. To test for this, we made use of an *ex vivo* preparation of diaphragms isolated from E14.5 embryos. In this experimental paradigm, the number AChR clusters is determined after culturing the entire diaphragms for 18 hours at 37°C (SI, Fig. 12; 32). In diaphragms from control mice, most of the AChR clusters were lost after 18 hours incubation (SI, Fig. 12; Fig. 5A). Diaphragms from agrin mutant mice had fewer AChR clusters, and almost none were left after incubation (SI, Fig. 12; Fig. 5A). In contrast, diaphragms that continued to synthesize $mag_{B/z8}$ (i.e. that were derived from $mag_{B/z8}$; $agrn^{+/?}$ or $mag_{B/z8}$; $agrn^{-/-}$ mice) showed a massive increase in the number of AChR clusters (Fig. 5A). To test the influence of AChR activation on AChR cluster stability, we incubated diaphragms for 18 hours in the presence of the AChR agonist carbachol (CCh). Conspicuously, culturing control diaphragms in the presence of 0.1 mM CCh increased the fraction of AChRs remaining by 2.4 fold, i.e. from 21 to 51%. Interestingly, this is equal to the fraction of AChR clusters that had been contacted by nerves before incubation (see Fig. 4B). In contrast, CCh did not affect AChR cluster number in $agrn^{-/-}$ and in $mag_{B/z8}$ transgenic diaphragms (SI, Fig. 12; Fig. 5A). Finally, unlike cluster number, cluster size was not affected by CCh (Fig. 5B). These results show that an excess of exogenous agrin is sufficient to saturate AChR aggregation. In control diaphragms, CCh has a local stabilizing effect on those AChR clusters that are formed during development by the action of neural agrin. As a consequence, rescued AChR clusters in control diaphragms are localized in the central region where motor nerves have innervated the muscle and deposited neural agrin (see SI, Fig. 12A). Conversely, and consistent with the idea that neural agrin is necessary for this stabilizing function, CCh does not prevent AChR cluster loss in $agrn^{-/-}$ diaphragms.
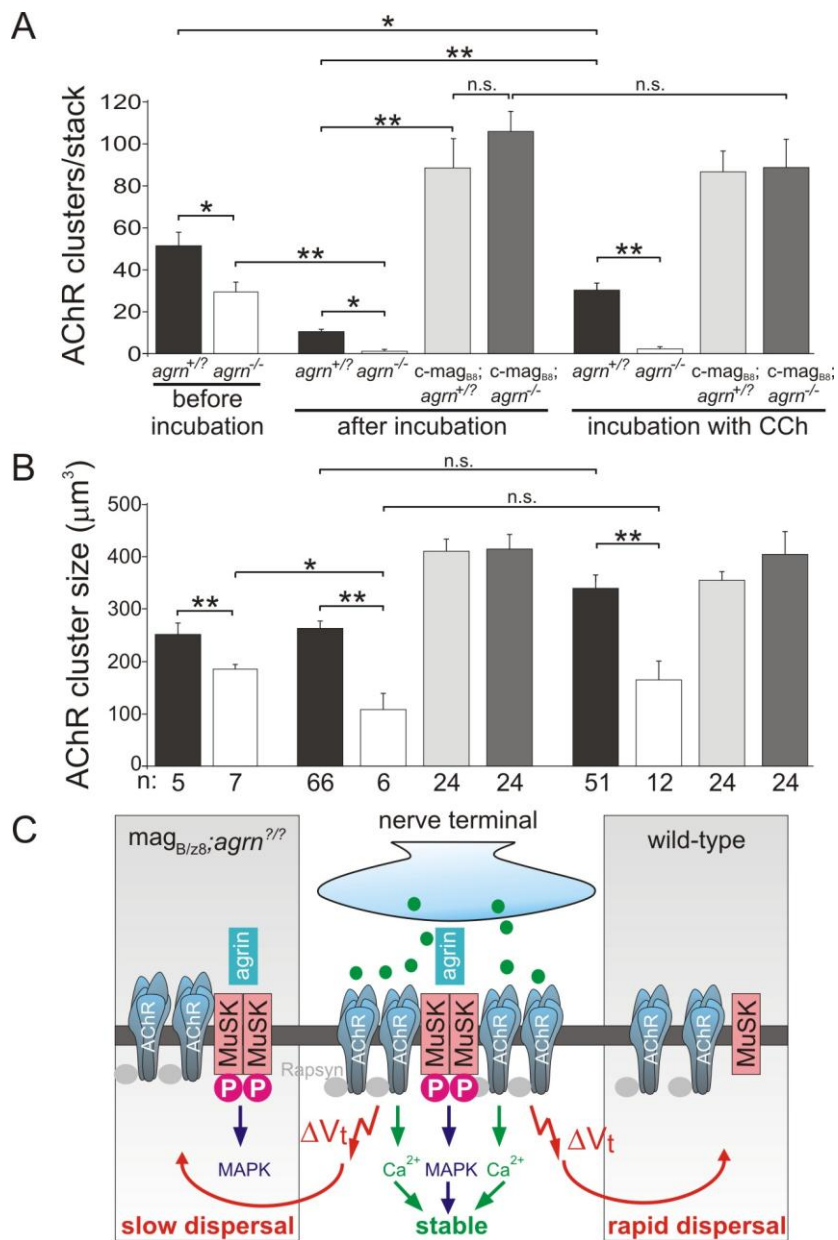
Figure 5 (84x126 mm)

Fig. 5. Carbachol stabilizes AChR clusters in the presence of agrin.

Quantification of the number *(A)* and the size *(B)* of AChR clusters present after overnight cultivation of diaphragms isolated from E14.5 embryos from different genotypes. Carbachol (CCh) was added at a final concentration of 0.1 mM. Data represent ± SEM from 4 independent experiments (N = 5 – 66). *P*-values (one tailed Student's t-test): **: $p \leq 0.01$; *: $p \leq 0.05$; n.s.: not significant. For images of AChR clusters in these experiments, see also SI, Fig. 12.
(continued on the next page)

(C) Proposed model for the action of acetylcholine to stabilize AChR clusters. At the NMJ, release of agrin causes MuSK dimerization and phosphorylation. This activates intracellular signaling pathways such as the mitogen-activated protein kinase (MAPK) pathway (GB, MAR, unpublished observation). Release of ACh from the presynaptic nerve terminal depolarizes the muscle fiber (ΔV_t) and disperses aneural AChR clusters (red arrow) as proposed by others (23, 31). ACh also causes the opening of AChRs and stabilizes them at sites of agrin-MuSK signaling. Dispersal of aneural AChR clusters in wild-type mice, which are not stabilized by agrin-MuSK signaling is fast (right part of the scheme). In $mag_{B/z8}$ transgenic mice, aneural AChR clusters are stabilized by agrin-MuSK signaling (left part of the scheme) but most of them still disperse slowly as they lack the local ACh signal from the nerve terminal. One possibility for the stabilizing function of ACh on postsynaptic structures is the local influx of Ca^{2+} via AChRs that could act in parallel with agrin-MuSK signaling.

3.5 DISCUSSION

Our work provides new insights into several aspects of how NMJs form during development and, in particular, of how agrin-MuSK signaling regulates this process. The staring point of our work was the observation that mice overexpressing mag$_{B/z8}$ did not show a strong phenotype despite the presence of some ectopic AChR clusters in the skeletal muscle. We also observed a large difference in the response of muscles to the expression of mag$_{B/z8}$, suggesting that muscles differ greatly in their capability of responding to neural agrin. A similar difference in response to innervation has been described previously (33). In that work, muscles like soleus or diaphragm were categorized as "delayed synapsing" (DeSyn) while EDL and gastrocnemius muscles were characterized as "fast synapsing" (FaSyn). We find now that DeSyn muscles respond well to the mini-agrin transgene while FaSyn muscles respond poorly. One possible explanation for such a muscle-intrinsic difference to respond to innervation and to neural agrin is a difference in the expression of molecules involved in agrin-MuSK signaling, such as MuSK itself, Dok-7 (6) or Lrp4 (5). Indeed, MuSK expression is substantially lower in the less-responsive EDL than in the highly responsive soleus (SL, MM and MAR, unpublished observation).

Agrin domains sufficient for postsynaptic differentiation.
Agrin is a large heparan sulfate proteoglycan that has been shown to bind to several cell surface receptors (integrins, α-dystroglycan and N-CAM), to growth factors (FGF), and extracellular matrix (ECM) molecules (laminins, other heparan sulfate proteoglycans). The fact that the miniaturized form of neural agrin consisting solely of the laminin-binding (25) and the MuSK-activating domains (10, 12) can rescue the perinatal death caused by agrin deficiency strongly argues that none of the other interactions of full-length agrin are required for its function in the initial development of NMJs. Of particular interest is the fact that our work provides the first *in vivo* evidence that induction of postsynaptic structures during development does not require binding of neural agrin to α-dystroglycan, unlike what previous work had postulated (34).

Our data also show that presynaptic differentiation is not a direct consequence of the accumulation of agrin at nerve-muscle contacts as had been postulated (35, 36). Instead, presynapses are rather formed as a consequence of the accumulation of other factor(s) that become concentrated in response to agrin-MuSK signaling during postsynaptic differentiation. Consistent with this idea, motor nerves continue to grow in MuSK-deficient

mice (4) and overexpression of MuSK in skeletal muscle, which causes its self-activation and the formation of AChR postsynapses is sufficient to induce presynaptic differentiation in *agrn*$^{-/-}$ mice and thus prevents perinatal death (37). Factors that have been shown to accumulate during postsynaptic differentiation and have been implicated to induce presynaptic differentiation are FGFs, laminin-β2 and collagen α(IV) chains (38). Alternatively, activation of MuSK alone could be sufficient to induce presynaptic specialization. A direct feedback of activated MuSK to motor neurons has indeed been described *in vitro* (39).

The central region of the muscle is more responsive to mini-agrin during development.

Although there is no difference in the level of expression of mag$_{B/z8}$ between the central and the most lateral part of the muscle fibers, the AChR clusters induced are localized in the central region. This preferential localization is most likely based on a high concentration of MuSK in the central portion of the muscle (37). In support of this idea, AChR clusters are scattered along the entire muscle fiber in adult mice that overexpress both mag$_{B/z8}$ and MuSK in skeletal muscle (MM, SL and MAR, unpublished observation). Nevertheless, the synaptic band in the mag$_{B/z8}$ transgenic mice became significantly widened (Fig. 4A). There are several reasons that may underlie this effect. For example, high concentrations of mag$_{B/z8}$ should allow MuSK activation in regions where expression of this receptor tyrosine kinase is low. Activation of MuSK would then trigger transcriptional changes that allow recruitment of more MuSK (17). Thus, the region of the muscle in which AChRs can be clustered and stabilized by innervation is wider in mag$_{B/z8}$ transgenic mice. Such a widening of the innervation band was also observed in mice overexpressing MuSK (37), suggesting that activated MuSK and neural agrin are in an equilibrium and that perturbation of this equilibrium causes a change in the width of the innervation band. Alternatively, the widening of the synaptic band might be based on the insufficient presence of a stop signal for presynaptic axons. We believe this explanation is less likely, as widening of the synaptic band is also observed in mag$_{B/z8}$; *agrn*$^{+/?}$ mice that still express endogenous full-length agrin (Fig. 4A).

ACh released from motor nerve terminal stabilizes AChR clusters.

Although the innervation band becomes wider in mag$_{B/z8}$; *agrn*$^{-/-}$ mice, motor neurons nevertheless stop and form proper NMJs. Further, the number of non-synaptic AChR clusters decreases, the proportion of nerve-contacted AChR clusters increases during development (Fig. 4B, C), and the volume of nerve-contacted AChR clusters is significantly larger than that of non-synaptic ones (Fig. 4D). Thus, nerve-contacted postsynapses are preferentially maintained in mag$_{B/z8}$; *agrn*$^{-/-}$ animals while those that are

not innervated are eliminated, indicating that the motor nerve terminal produces factors in addition to agrin that stabilize synaptic AChR clusters during development. Our data now indicate that such a factor might be ACh itself as addition of the AChR agonist CCh stabilizes AChR clusters in cultured, denervated diaphragm muscle (Fig. 5A). In current models, the only role of ACh was that of a dispersal activity for spontaneously formed AChR clusters (Fig. 5C). In these models, the local deposition of agrin in synaptic basal lamina and thus activation of MuSK counteracted the dispersal activity of ACh. As the number of synaptic AChR clusters still increases in $mag_{B/z8}$; *agrn$^{+/?}$* and $mag_{B/z8}$; *agrn$^{-/-}$* mice, although all AChR clusters are stabilized by $mag_{B/z8}$, we propose a model in which local signaling pathways activated by ACh contribute to the stabilization of synaptic AChR clusters (Fig. 5 C). One possibility is that the opening of AChRs by ACh causes the local influx of calcium (40). As calcium has been shown to be required for agrin-induced AChR clustering and cluster maintenance *in vitro* (41), the high calcium concentration in conjunction with activation of agrin-MuSK signaling could result in sustained stabilization of postsynaptic structures (Fig. 5C). According to our model, aneural postsynaptic structures in wild-type mice will disperse rapidly because they lack both the local calcium influx and agrin-MuSK signaling. Aneural AChR clusters in $mag_{B/z8}$ transgenic mice will disperse only slowly because they are partially protected by the active agrin-MuSK signaling (Fig. 5C). Nevertheless, our data show that these aneural AChR clusters are still removed and we suggest that this is due to the lack of a local calcium influx (Fig. 5C). Interestingly, an influence of calcium influx through AChR channels on innervation has been suggested previously: changing the dynamics of AChR-mediated calcium influx by genetically engineering fetal-type AChRs to adopt the ion conductance properties of adult-type AChRs causes a widening of the synaptic band (40, 42). In summary, our work has uncovered a new role of the ACh in the stabilization of postsynaptic receptors. A dual role of neurotransmitters to locally stabilize the postsynaptic receptor clusters that are apposed by a nerve terminal and to destabilize those that are not innervated by the appropriate presynaptic nerve terminal may also be involved in synapse formation and selective synapse elimination in the CNS.

3.6 SUPPLEMENTARY FIGURES
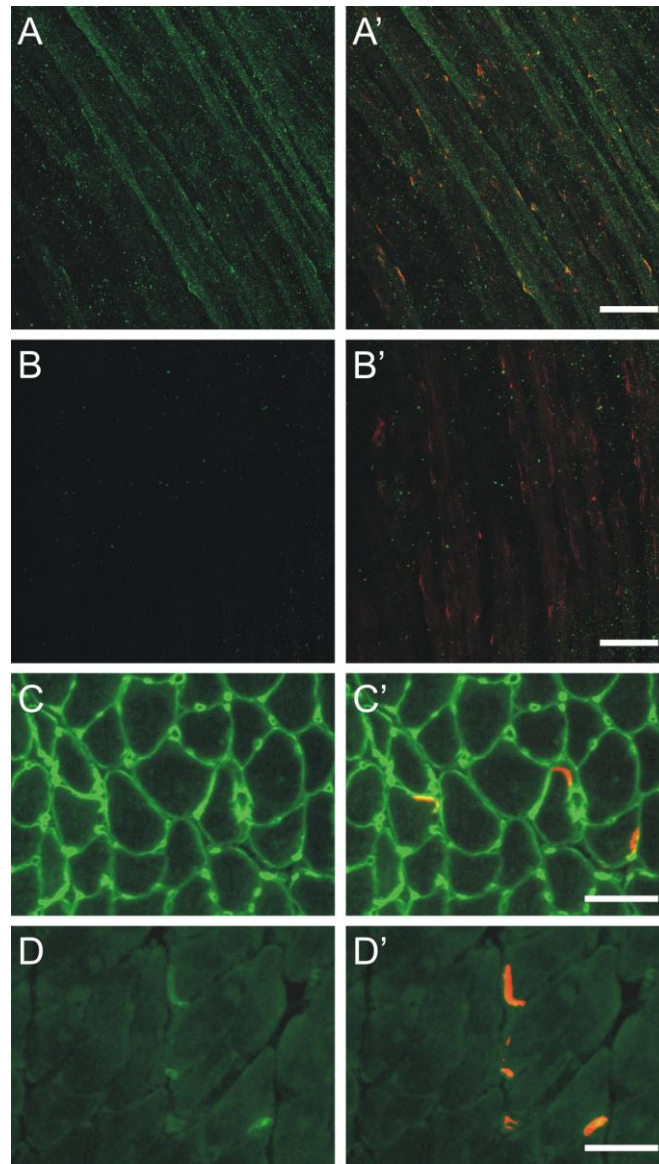
SI Figure 6
scale bar: 50 μm (A and B) and 25 μm (C and D)

SI Fig. 6. Expression of c-mag$_{B8}$ in embryonic and adult muscle. *(A, B)* Whole mounts of diaphragm muscles from E13.5 c-mag$_{B8}$ transgenic *(A, A')* or wild-type *(B, B')* mice. Muscles were stained with an antibody raised against chick agrin (10) followed by an Alexa-488 conjugated secondary antibody (green; *A, B*).

(continued on the next page)

AChRs were visualized with Alexa-555-α-bungarotoxin (red; *A', B'*). The transgenic protein is detected already at E13.5 (compare A to B). *(C, D)* Cross-sections of soleus muscle from 6 week-old c-mag$_{B8}$ transgenic (*C, C'*) or wild-type (*D, D'*) mice. Staining procedure was the same as described above. The transgenic protein is detected in the muscle basal lamina without a particular enrichment at AChR clusters. Note: immunoreactivity in wild-type mice originates from the cross-reactivity of the antiserum with mouse agrin. Scale bars: 50 µm (*A, B*) and 25 µm (*C, D*).
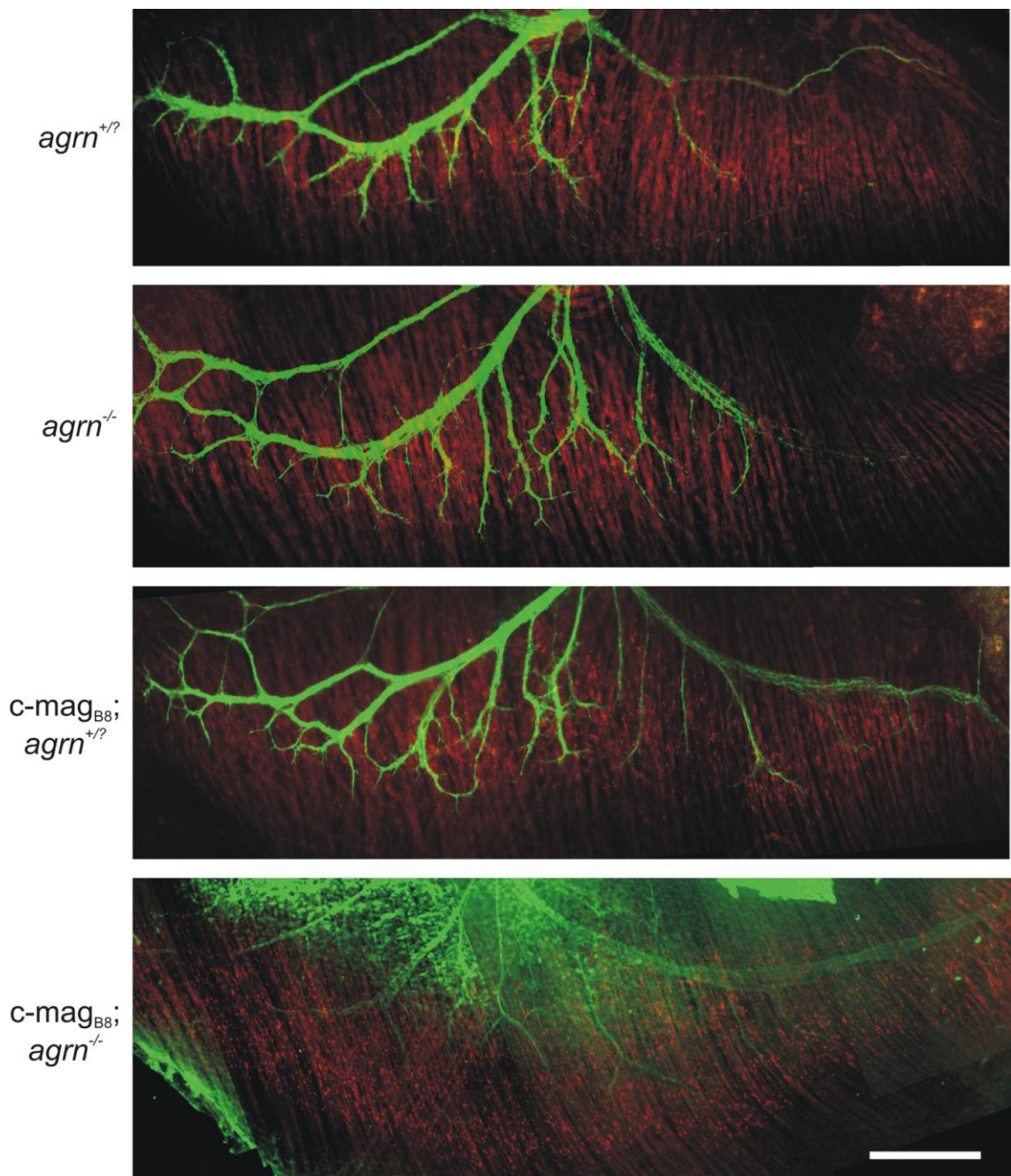
SI Figure 7
scale bar: 250 μm
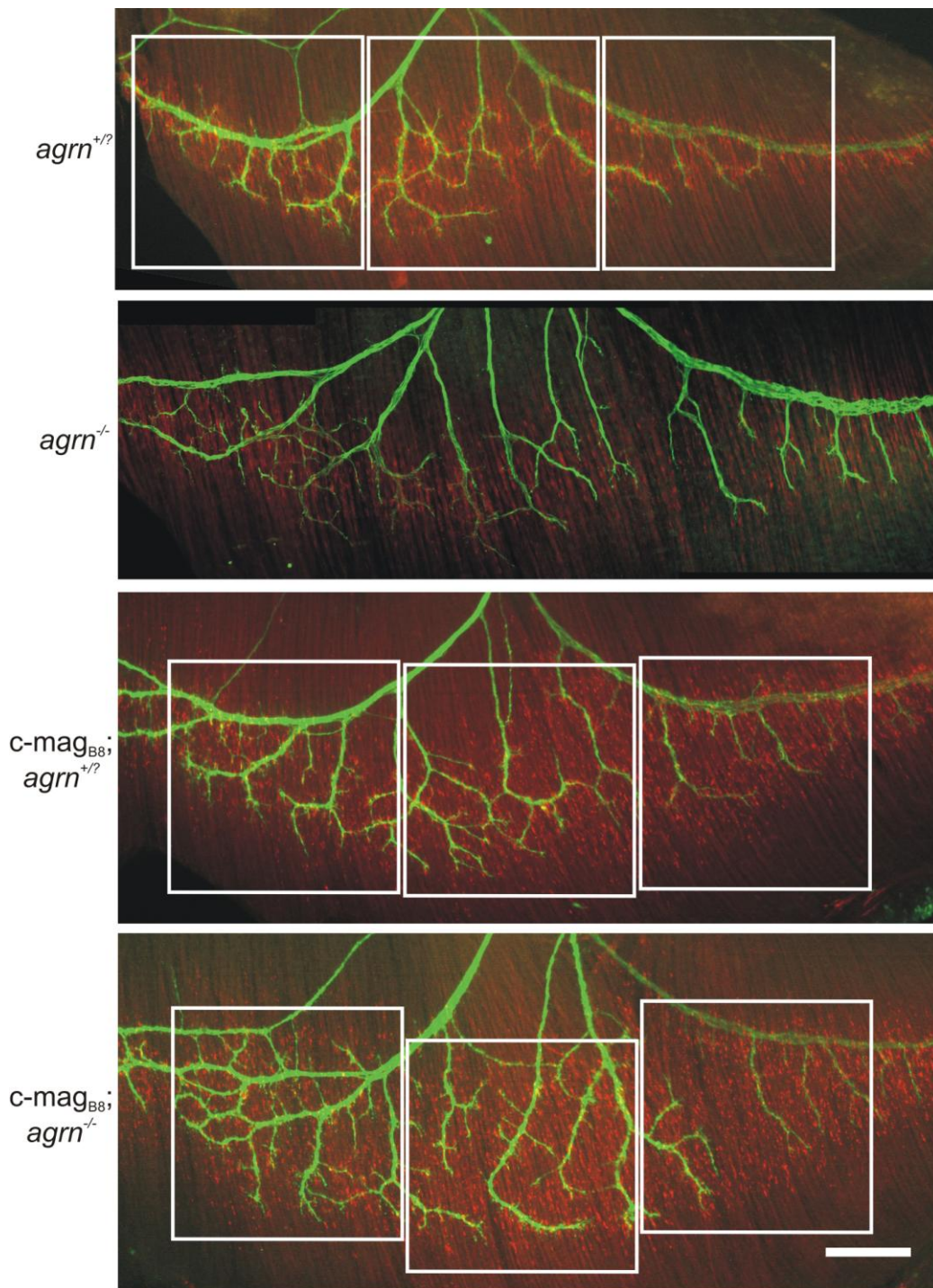
SI Figure 8
scale bar: 250 μm

SI Figure 9
scale bar: 250 μm
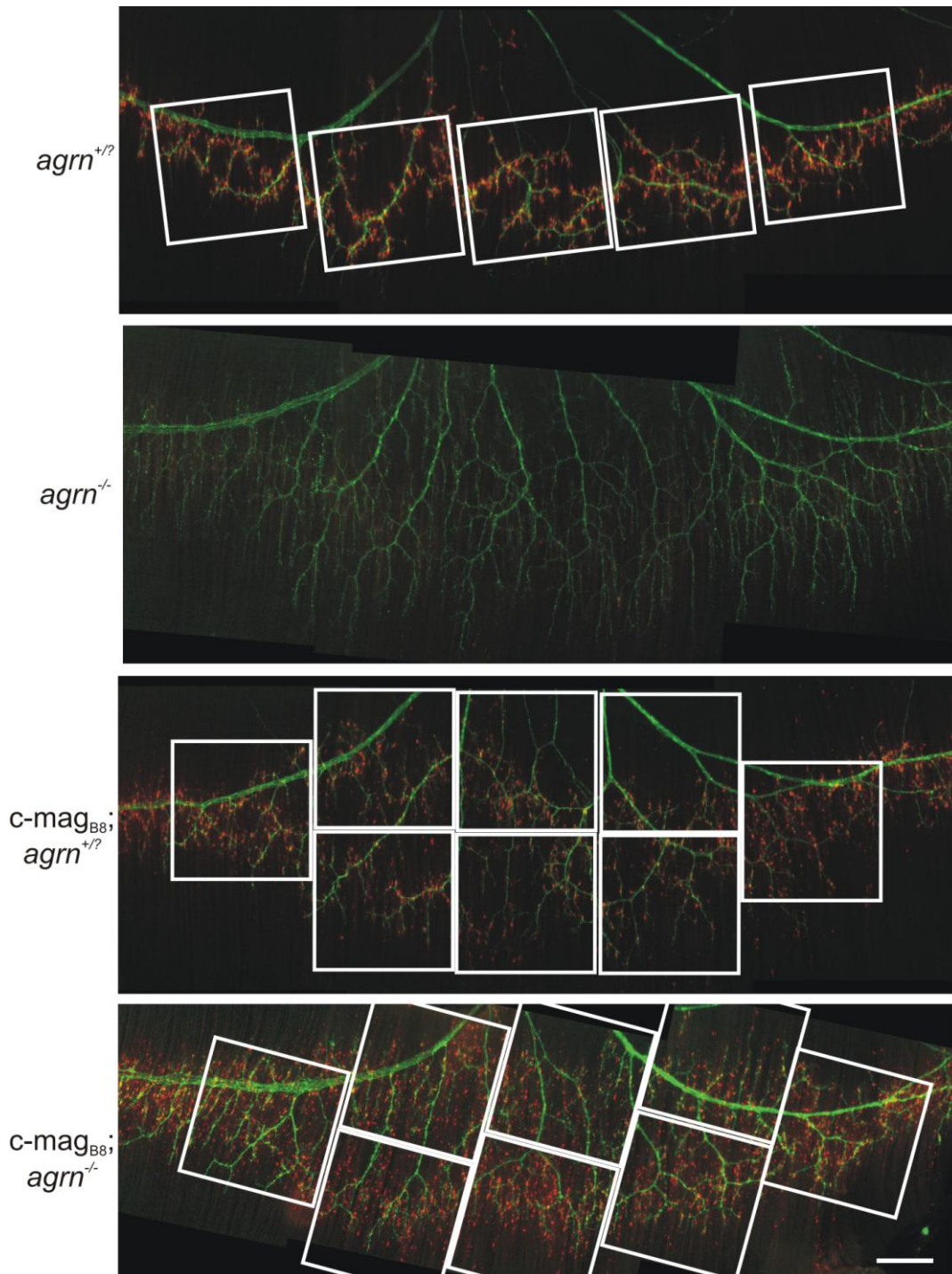
SI Figure 10
scale bar: 250 μm
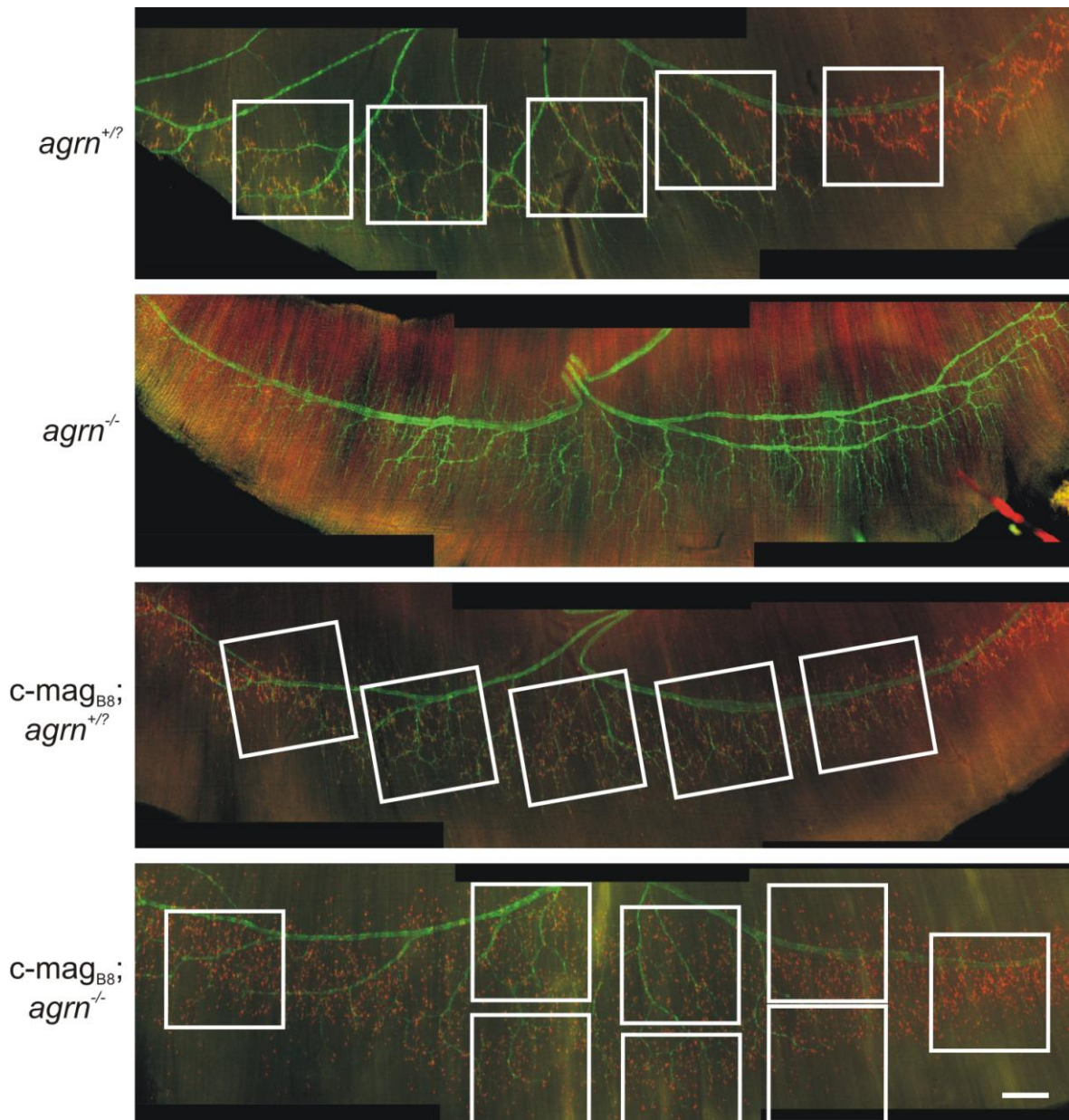
SI Figs. 7-10. Whole mounts of diaphragm muscles from E13.5 to E18.5. AChR clusters were visualized by Alexa-555-α-bungarotoxin. Motor neurons are visualized either by YFP expression or by an antibody mixture against neurofilament and synaptophysin. White frames indicate the regions used for quantification as shown in Fig. 4 and SI Fig. 11. Scale bars: 250 μm.
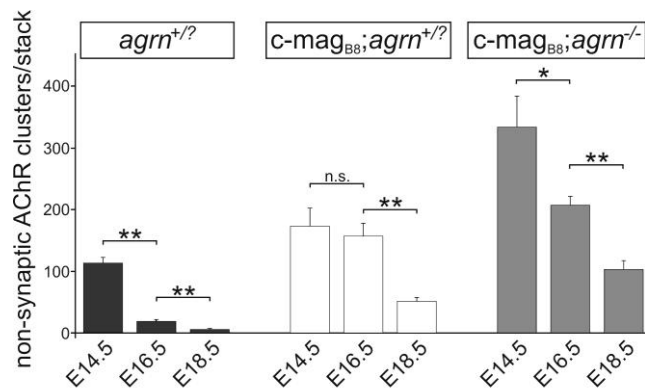
SI Figure 11

SI Fig. 11. Absolute number of non-synaptic AChR clusters per stack. Quantification and parameters were set the same as in Fig. 4.
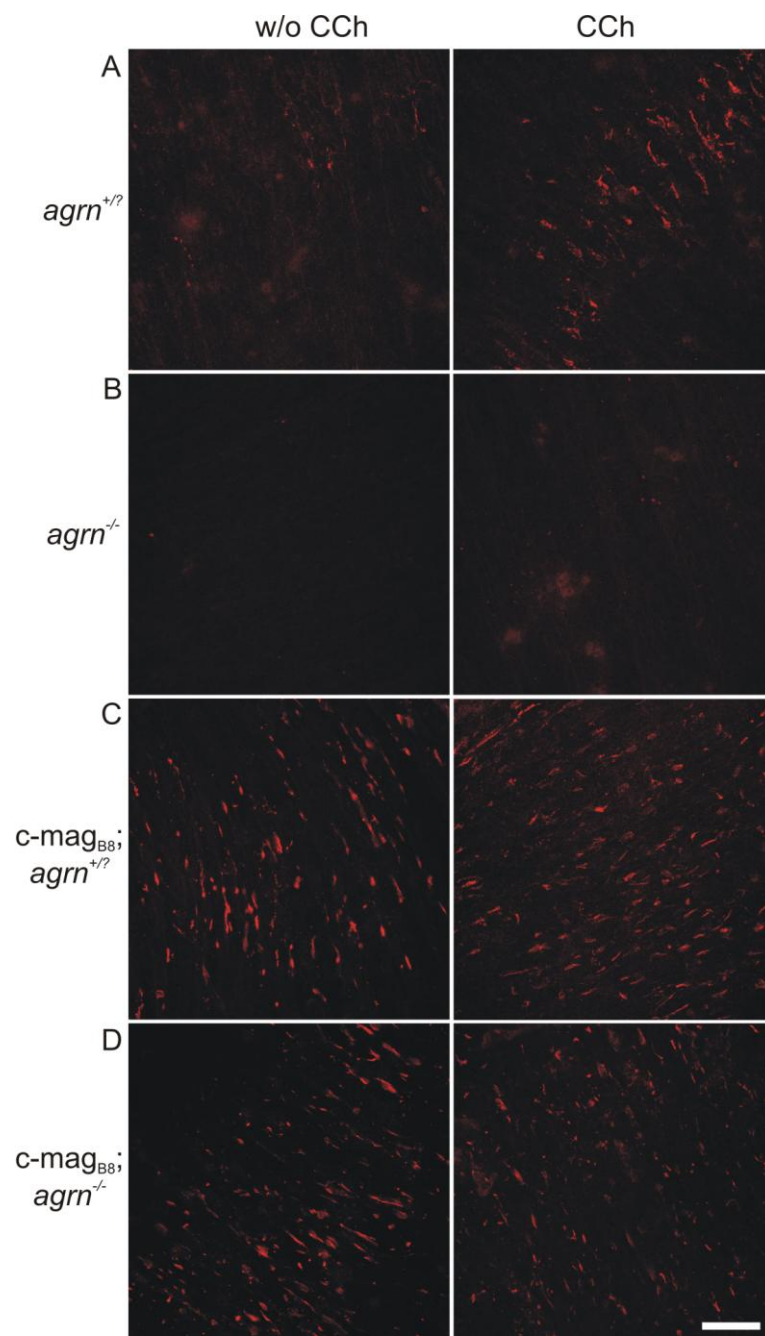
SI Figure 12
scale bar: 50 μm

SI Fig. 12. Confocal images of E14.5 diaphragms after 18 hours cultivation. Whole mounts of diaphragm muscles were incubated with or without carbachol (CCh). AChR clusters, visualized by Alexa-555-α-bungarotoxin, were recorded with a 40x objective through the entire thickness of the muscles. Three image stacks from each hemidiaphragm in the central

3.7 REFERENCES

1. Tada T, Sheng M (2006) Molecular mechanisms of dendritic spine morphogenesis. *Curr Opin Neurobiol* 16:95-101.

2. Dalva MB, McClelland AC, Kayser MS (2007) Cell adhesion molecules: signalling functions at the synapse. *Nat Rev Neurosci* 8:206-220.

3. Gautam M*, et al.* (1996) Defective neuromuscular synaptogenesis in agrin-deficient mutant mice. *Cell* 85:525-535.

4. DeChiara TM*, et al.* (1996) The receptor tyrosine kinase MuSK is required for neuromuscular junction formation in vivo. *Cell* 85:501-512.

5. Weatherbee SD, Anderson KV, Niswander LA (2006) LDL-receptor-related protein 4 is crucial for formation of the neuromuscular junction. *Development* 133:4993-5000.

6. Okada K*, et al.* (2006) The muscle protein Dok-7 is essential for neuromuscular synaptogenesis. *Science* 312:1802-1805.

7. Gautam M*, et al.* (1995) Failure of postsynaptic specialization to develop at neuromuscular junctions of rapsyn-deficient mice. *Nature* 377:232-236.

8. Ruegg MA*, et al.* (1992) The agrin gene codes for a family of basal lamina proteins that differ in function and distribution. *Neuron* 8:691-699.

9. Rupp F*, et al.* (1992) Structure and chromosomal localization of the mammalian agrin gene. *J Neurosci* 12:3535-3544.

10. Gesemann M, Denzer AJ, Ruegg MA (1995) Acetylcholine receptor-aggregating activity of agrin isoforms and mapping of the active site. *J Cell Biol* 128:625-636.

11. Burgess RW, Nguyen QT, Son YJ, Lichtman JW, Sanes JR (1999) Alternatively spliced isoforms of nerve- and muscle-derived agrin: their roles at the neuromuscular junction. *Neuron* 23:33-44.

12. Scotton P*, et al.* (2006) Activation of muscle-specific receptor tyrosine kinase and binding to dystroglycan are regulated by alternative mRNA splicing of agrin. *J Biol Chem* 281:36835-36845.

13. Bezakova G, Ruegg MA (2003) New insights into the roles of agrin. *Nat Rev Mol Cell Biol* 4:295-308.

14. McMahan UJ (1990) The agrin hypothesis. *Cold Spring Harb Symp Quant Biol* 55:407-418.

15. Jones G*, et al.* (1997) Induction by agrin of ectopic and functional postsynaptic-like membrane in innervated muscle. *Proc Natl Acad Sci U S A* 94:2654-2659.

16. Cohen I, Rimer M, Lomo T, McMahan UJ (1997) Agrin-induced postsynaptic apparatus in

skeletal muscle fibers in vivo. *Mol. Cell. Neurosci.* 9:237-253.

17. Jones G, Moore C, Hashemolhosseini S, Brenner HR (1999) Constitutively active MuSK is clustered in the absence of agrin and induces ectopic postsynaptic-like membranes in skeletal muscle fibers. *J Neurosci* 19:3376-3383.

18. Harris AJ (1981) Embryonic growth and innervation of rat skeletal muscles. III. Neural regulation of junctional and extra-junctional acetylcholine receptor clusters. *Philos Trans R Soc Lond B Biol Sci* 293:287-314.

19. Yang X, Li W, Prescott ED, Burden SJ, Wang JC (2000) DNA topoisomerase IIbeta and neural development. *Science* 287:131-134.

20. Lin W*, et al.* (2001) Distinct roles of nerve and muscle in postsynaptic differentiation of the neuromuscular synapse. *Nature* 410:1057-1064.

21. Kummer TT, Misgeld T, Sanes JR (2006) Assembly of the postsynaptic membrane at the neuromuscular junction: paradigm lost. *Curr Opin Neurobiol* 16:74-82.

22*.* Misgeld T*, et al.* (2002) Roles of neurotransmitter in synapse formation: development of neuromuscular junctions lacking choline acetyltransferase. *Neuron* 36:635-648.

23. Brandon EP*, et al.* (2003) Aberrant patterning of neuromuscular synapses in choline acetyltransferase-deficient mice. *J Neurosci* 23:539-549.

24. Meier T*, et al.* (1998) A minigene of neural agrin encoding the laminin-binding and acetylcholine receptor-aggregating domains is sufficient to induce postsynaptic differentiation in muscle fibres. *Eur J Neurosci* 10:3141-3152.

25. Denzer AJ, Brandenberger R, Gesemann M, Chiquet M, Ruegg MA (1997) Agrin binds to the nerve-muscle basal lamina via laminin. *J Cell Biol* 137:671-683.

26. Moll J*, et al.* (2001) An agrin minigene rescues dystrophic symptoms in a mouse model for congenital muscular dystrophy. *Nature* 413:302-307.

27. Meinen S, Barzaghi P, Lin S, Lochmuller H, Ruegg MA (2007) Linker molecules between laminins and dystroglycan ameliorate laminin-alpha2-deficient muscular dystrophy at all disease stages. *J Cell Biol* 176:979-993.

28. Jaynes JB, Chamberlain JS, Buskin JN, Johnson JE, Hauschka SD (1986) Transcriptional regulation of the muscle creatine kinase gene and regulated expression in transfected mouse myoblasts. *Mol Cell Biol* 6:2855-2864.

29. Sternberg EA*, et al.* (1988) Identification of upstream and intragenic regulatory elements that confer cell-type-restricted and differentiation-specific expression on the muscle creatine kinase gene. *Mol Cell Biol* 8:2896-2909.

30. Ksiazek I*, et al.* (2007) Synapse loss in cortex of agrin-deficient mice after genetic rescue of perinatal death. *J Neurosci* 27:7183-7195.

31. Misgeld T, Kummer TT, Lichtman JW, Sanes JR (2005) Agrin promotes synaptic differentiation by counteracting an inhibitory effect of neurotransmitter. *Proc Natl Acad Sci U S A* 102:11088-11093.

32.   Lin S, Landmann L, Ruegg MA, Brenner HR (2008) The role of nerve- vs. muscle-derived factors in mammalian neuromuscular junction formation. *J. Neurosci.* in press.

33.   Pun S*, et al.* (2002) An intrinsic distinction in neuromuscular junction assembly and maintenance in different skeletal muscles. *Neuron* 34:357-370.

34.   Gee SH, Montanaro F, Lindenbaum MH, Carbonetto S (1994) Dystroglycan-a, a dystrophin-associated glycoprotein, is a functional agrin receptor. *Cell* 77:675-686.

35.   Campagna JA, Ruegg MA, Bixby JL (1995) Agrin is a differentiation-inducing "stop signal" for motoneurons in vitro. *Neuron* 15:1365-1374.

36.   Chang D, Woo JS, Campanelli J, Scheller RH, Ignatius MJ (1997) Agrin inhibits neurite outgrowth but promotes attachment of embryonic motor and sensory neurons. *Dev Biol* 181:21-35.

37.   Kim N, Burden SJ (2008) MuSK controls where motor axons grow and form synapses. *Nat Neurosci* 11:19-27.

38.   Fox MA*, et al.* (2007) Distinct target-derived signals organize formation, maturation, and maintenance of motor nerve terminals. *Cell* 129:179-193.

39.   Dimitropoulou A, Bixby JL (2005) Motor neurite outgrowth is selectively inhibited by cell surface MuSK and agrin. *Mol Cell Neurosci* 28:292-302.

40.   Villarroel A, Sakmann B (1996) Calcium permeability increase of endplate channels in rat muscle during postnatal development. *J Physiol* 496 (Pt 2):331-338.

41.   Megeath LJ, Fallon JR (1998) Intracellular calcium regulates agrin-induced acetylcholine receptor clustering. *J Neurosci* 18:672-678.

42.   Koenen M, Peter C, Villarroel A, Witzemann V, Sakmann B (2005) Acetylcholine receptor channel subtype directs the innervation pattern of skeletal muscle. *EMBO reports* 6:570-576.

43.   Ghersa P*, et al.* (1998) Highly controlled gene expression using combinations of a tissue-specific promoter, recombinant adenovirus and a tetracycline- regulatable transcription factor. *Gene Ther* 5:1213-1220.

44.   Feng G*, et al.* (2000) Imaging neuronal subsets in transgenic mice expressing multiple spectral variants of GFP. *Neuron* 28:41-51.

Synapse loss in cortex of agrin-deficient mice after genetic rescue of perinatal death

Iwona Ksiazek,[1] Constanze Burkhardt,[1] Shuo Lin,[1] Riad Seddik,[2] Marcin Maj,[1] Gabriela Bezakova,[1] Mathias Jucker,[3] Silvia Arber,[1,4] Pico Caroni,[4] Joshua R. Sanes,[5] Bernhard Bettler,[2] and Markus A. Ruegg[1]

[1]Biozentrum, University of Basel, Switzerland

[2]Institute of Physiology, Department of Clinical-Biological Sciences, University of Basel, Switzerland

[3]Department of Cellular Neurology, Hertie-Institute of Clinical Brain Research, Tübingen, Germany,

[4]Friedrich Miescher Institute, Switzerland,

[5]Department of Molecular and Cellular Biology, Harvard University, Cambridge, MA, USA

Cellular/Molecular

Synapse Loss in Cortex of Agrin-Deficient Mice after Genetic Rescue of Perinatal Death

Iwona Ksiazek,[1] Constanze Burkhardt,[1] Shuo Lin,[1] Riad Seddik,[2] Marcin Maj,[1] Gabriela Bezakova,[1] Mathias Jucker,[3] Silvia Arber,[1,4] Pico Caroni,[4] Joshua R. Sanes,[5] Bernhard Bettler,[2] and Markus A. Ruegg[1]

[1]Biozentrum and [2]Institute of Physiology, Department of Clinical-Biological Sciences, University of Basel, CH-4056 Basel, Switzerland, [3]Department of Cellular Neurology, Hertie-Institute of Clinical Brain Research, D-72076 Tübingen, Germany, [4]Friedrich Miescher Institute, CH-4058 Basel, Switzerland, and [5]Department of Molecular and Cellular Biology, Harvard University, Cambridge, Massachusetts 01238

Agrin-deficient mice die at birth because of aberrant development of the neuromuscular junctions. Here, we examined the role of agrin at brain synapses. We show that agrin is associated with excitatory but not inhibitory synapses in the cerebral cortex. Most importantly, we examined the brains of agrin-deficient mice whose perinatal death was prevented by the selective expression of agrin in motor neurons. We find that the number of presynaptic and postsynaptic specializations is strongly reduced in the cortex of 5- to 7-week-old mice. Consistent with a reduction in the number of synapses, the frequency of miniature postsynaptic currents was greatly decreased. In accordance with the synaptic localization of agrin to excitatory synapses, changes in the frequency were only detected for excitatory but not inhibitory synapses. Moreover, we find that the muscle-specific receptor tyrosine kinase MuSK, which is known to be an essential component of agrin-induced signaling at the neuromuscular junction, is also localized to a subset of excitatory synapses. Finally, some components of the mitogen-activated protein (MAP) kinase pathway, which has been shown to be activated by agrin in cultured neurons, are deregulated in agrin-deficient mice. In summary, our results provide strong evidence that agrin plays an important role in the formation and/or the maintenance of excitatory synapses in the brain, and we provide evidence that this function involves MAP kinase signaling.

Key words: neuromuscular synapse; gene expression; excitatory synapse; MuSK; spines; MAP kinase

Introduction

The molecular mechanisms involved in the formation of the postsynaptic apparatus are well understood at the neuromuscular junction (NMJ), where spinal motor neurons synapse on muscle fibers. The most important players involved in NMJ development are the motor neuron-released molecule agrin and the muscle-specific proteins MuSK, acetylcholine receptor (AChR), and rapsyn (McMahan, 1990; Sanes and Lichtman, 2001; Bezakova and Ruegg, 2003). The receptor tyrosine kinase MuSK is the signaling receptor activated by agrin, and rapsyn is a cytosolic adaptor molecule that links MuSK signaling to AChR clustering. Although agrin is not required to form AChR aggregates before innervation, motor neuron-derived agrin is required to induce and maintain the AChR aggregates that are closely associated with the nerve terminal and that persist after the onset of electrical activity (Sanes and Lichtman, 2001; Bezakova and Ruegg, 2003). Consistent with this concept, agrin-deficient mice die at

birth because of respiratory failure. Similarly, inactivation of MuSK or rapsyn causes respiratory failure.

Formation of synapses in the CNS shares many features with the NMJ. For example, neurotransmitter release is not required to form both presynaptic and postsynaptic specializations (Verhage et al., 2000), suggesting that adhesive interactions are responsible for synapse assembly. Indeed, several adhesion molecules have now been implicated in synapse formation in the brain (for review, see Akins and Biederer, 2006). Although agrin is also expressed in the brain, its role is controversial. For example, synaptic deficits in agrin-deficient mice have only been observed in the PNS (Gingras et al., 2002) but not in embryonic brain. Although cortical neurons from heterozygous and homozygous agrin knock-out mice are more resistant to damage triggered by excitatory neurotransmitters (Hilgenberg et al., 2002), synapses still form in such neurons (Li et al., 1999; Serpinskaya et al., 1999). These experiments thus indicate that agrin signaling is not required for the formation of neuron-to-neuron synapses.

In contrast, there is evidence that agrin may have a function at neuron-to-neuron synapses. Most importantly, acute suppression of agrin expression by antisense oligonucleotides impairs synapse formation and dendritic development in cultured hippocampal neurons (Ferreira, 1999; Bose et al., 2000). Moreover, agrin added to cultured neurons activates signaling pathways that are known to be involved in synapse function, such as the transcription factor cAMP response element-binding protein

(CREB) (Ji et al., 1998), the immediate-early gene c-*fos* (Hilgenberg et al., 1999), or the mitogen-activated protein (MAP) kinase pathway (Karasewski and Ferreira, 2003; Hilgenberg and Smith, 2004). Finally, alternative splicing of the agrin transcript generates a protein isoform that is inserted into plasma membranes as a type II transmembrane protein (Burgess et al., 2000; Neumann et al., 2001). This form is highly expressed in neurons. Thus, unlike the situation at the NMJ, agrin expressed in CNS neurons does not require a structured basement membrane.

To clarify the role of agrin in the formation of synapses in the CNS, we now examined the brain of agrin-deficient mice in which perinatal death was prevented by the transgenic expression of agrin in motor neurons. We find that there is a loss of synapses in the cortex of these rescued mice and that agrin loss selectively affects excitatory but not inhibitory synapses. These results are thus the first to provide strong evidence for a role of agrin in the formation and/or the maintenance of excitatory synapses in the brain.

Materials and Methods

Generation of Tg/agrn$^{-/-}$ mice. The cDNA encoding the 9-kb-long promoter region of mouse Hb9 was cloned into pBluescript (pBS). To release the final Hb9-agrin construct (see Fig. 1*a*) from the pBS backbone, we first inserted an additional *Pac*I restriction site at the 5′ end of the pBS-Hb9 construct by adaptor ligation. The cDNA encoding full-length chick agrin was inserted downstream of this construct by *Asc*I/*Xba*I double digestion. The final construct was then released by *Pac*I digestion and injected into oocytes. Transgenic mice were identified by PCR and Southern blot analysis using primers and probes from the 3′ untranslated region of chick agrin mRNA. From six transgenic founders, three permanent lines were established that expressed chick agrin. Each of the transgenic lines was mated with heterozygous agrin-deficient mice (Lin et al., 2001), giving birth to transgenic heterozygous agrin-deficient mice (*Tg/agrn$^{+/-}$*). These mice were then mated with heterozygous agrin-deficient mice. The line that gave rise to surviving *Tg/agrn$^{-/-}$* mice first was used for the analysis described here. For most experiments, 6- to 7-week-old mice of both genders were used. Control animals were usually littermates of the same age. Whenever possible, these animals were wild type or transgenic for Hb9-agrin. In a few cases, heterozygous agrin knock-out mice were used.

Antibodies. Anti-agrin antibodies included rabbit antisera raised against the C-terminal half of chick (Gesemann et al., 1995) or mouse (Eusebio et al., 2003) agrin and the mouse monoclonal antibody 5B1 (Reist et al., 1987). Antibodies to the α1 or the α2 subunits of GABA$_A$ receptors were raised in guinea pigs and were a kind gift from J.-M. Fritschy (University of Zurich, Zurich, Switzerland). Anti-MuSK antibodies were raised against the extracellular domain of mouse MuSK that had been expressed in 293 EBNA cells (Invitrogen, San Diego, CA) as a His-tagged fusion protein and were purified from culture medium using a Ni-column. This antiserum recognizes MuSK in Western blots and immunohistochemistry (see supplemental Fig. 2, available at www.jneurosci.org as supplemental material). All of the other antibodies used were from the following commercial sources: rabbit antibodies against synaptophysin (Dako, High Wycombe, UK), neurofilament (Sigma, St. Louis, MO), S-100 (Dako), glial fibrillary acidic protein (Dako), and SynGAP (Affinity Bioreagents); and mouse monoclonal antibodies against CaMKIIα (calcium/calmodulin-dependent protein kinase IIα; 6G9; Affinity Bioreagents, Golden, CO), gephyrin (Mab7a; Connex, Martinsried, Germany), phospho-c-jun N-terminal kinase (JNK; Cell Signaling Technology, Danvers, MA), mitogen-activated protein kinase kinase 7 (MKK7; 611246; BD Biosciences, Franklin Lakes, NJ), NR1 (54.1; PharMingen, San Diego, CA), synaptophysin (MAB5258; Chemicon, Temecula, CA), and postsynaptic density protein-95 (PSD-95; K28/86; Upstate Biotechnology, Lake Placid, NY). Detection was done using the appropriate, affinity-purified secondary antibodies coupled to either Cy3 (Jackson ImmunoResearch, West Grove, PA) or Alexa 488 (Invitrogen).

Stereological analysis. The analysis was performed as described previously (Calhoun et al., 1998). Briefly, mice were perfused with 0.1 M PBS, pH 7.4, followed by 4% paraformaldehyde (PFA) in PBS, and the brains were dehydrated in ethanol (70, 83, and 96% for 1 h each). After 15 min in 100% ethanol, the brains were kept in a 1:1 cedarwood oil/ethanol mixture and then in cedarwood oil at 60°C, each for 1 h. Excess oil was removed by immersion in a 1:1 cedarwood oil/methyl salicylate mixture overnight and in 100% methyl salicylate for 1 h. Brains were embedded into paraffin using standard procedures, and 25-μm-thick coronal sections were cut using a rotatory microtome. Total numbers of neocortical neurons and synaptophysin-positive puncta were counted on cresyl violet- and synaptophysin-stained sections, respectively. A systematic random series of every 20th section throughout the entire cortex was selected, yielding 10–15 sections per animal. To stain for synaptophysin, sections were quenched with 0.3% H$_2$O$_2$ in methanol, followed by blocking in 5% goat serum. Sections were incubated with primary antibodies overnight at 4°C and then with biotinylated secondary antibodies, ABC solution (Vector Laboratories, Burlingame, CA), and 0.08% diaminobenzidine/0.03% H$_2$O$_2$ in PBS. Quantification was performed by estimating the volume of the cortex according to the Cavalieri method (grid point area, 500 μm^2) and multiplying it by the numerical density, which was determined by counting objects within three-dimensional optical dissectors (16 μm^3 for boutons, 4200 μm^3 for neurons), systematically spaced throughout the neocortex. On average, 75 ± 23 and 103 ± 21 dissectors per mouse were counted for synapses and neurons, respectively. Only cells with a typical neuronal morphology (clear nucleolus or discrete, darkly stained synaptophysin-positive boutons) were counted (100×; 1.3 numerical aperture objective; on-screen magnification, 2759×). Analysis was performed with stereological software (SPA, Alexandria, VA).

Golgi–Cox impregnation. Freshly isolated brains were impregnated in a 15:5:4 mixture of potassium dichromate, mercuric chloride, and potassium chromate solutions (5% each) for 3 weeks in the dark. After dehydration in ethanol (70% for 12 h, 96 and 100% for 24 h each), brains were impregnated with celloidin solution (2, 4, and 8% for 24, 48, and 72 h, respectively) and cut into 80- to 100-μm-thick coronal sections, which were then processed for Golgi–Cox staining. Staining was visualized by incubation in 25% NH$_4$OH for 30 min, followed by 0.5% phenylenediamine for 4 min, 1% Dektol (Eastman Kodak, Rochester, NY) for 2 min, 5% fixative solution (G305) for 5 min, and acetate buffer at pH 4.1 for 5 min. After dehydration in ethanol, sections were mounted, and well impregnated pyramidal neurons were reconstructed using Neurolucida software.

Locomotion. Exploratory locomotion was examined in an open-field test. Mice were placed into a new cage, and the time they spent moving during the first 10 min was measured manually.

Immunohistochemistry. Double immunofluorescence for excitatory synaptic markers was performed by the antigen-unmasking method with pepsin pretreatment (Watanabe et al., 1998). Other stainings on brain tissue were performed as described previously (Fritschy et al., 1998). Whole-mount staining of muscle was performed as described previously (Bezakova and Lomo, 2001). Cultured neurons were washed with PBS, fixed with 4% PFA in PBS, permeabilized with 0.1% Triton X-100, and blocked with 10% fetal calf serum in PBS for 1 h at room temperature. Cells were incubated with primary antibodies overnight at 4°C, washed, and further incubated with secondary antibodies for 2 h at room temperature. All images were analyzed using fluorescence or confocal laser-scanning microscopy (Leica, Nussloch, Germany) and the appropriate imaging software.

Immunoelectron microscopy. Mice were perfused with PBS, followed by 4% PFA in PBS. Cortices were postfixed in the same fixative overnight, followed by 0.5% OsO$_4$ for 30 min. After dehydration in ethanol (50 and 70% for 10 min each), tissue was infiltrated with a 2:1 mixture of ethanol and LR White, followed by pure LR White (1 h each), and polymerized at 70°C for 24 h. Sixty-nanometer-thick microtome sections were first incubated with agrin antiserum (1:500) and then with 10 nm gold-coupled secondary antibodies (1:20). For quantification, all gold particles within 100 nm of the middle of the synaptic cleft of randomly selected synapses were counted.

Electrophysiological measurements. Recordings were made from visu-

ally identified pyramidal neurons located in layer II/III of the motor cortex. Slices were prepared from 4- to 5-week-old mice. Parasagittal slices (300 μm thick) were cut with a Leica VT1000S in ice-cold artificial CSF (aCSF) containing (in mM) 119 NaCl, 1 NaH$_2$PO$_4$, 26.2 NaHCO$_3$, 2.5 KCl, 2.5 CaCl$_2$, 1.3 MgCl$_2$, and 11 glucose, pH 7.3, equilibrated with 95% O$_2$/5% CO$_2$. Slices were then kept in oxygenated aCSF at room temperature for at least 1 h before starting recordings at 30–32°C. Pyramidal neurons were visualized using an infrared-sensitive camera (Hitachi, Tokyo, Japan) and oblique illumination optics (BX51WI; Olympus, Tokyo, Japan). Synaptic activity was recorded from cortical pyramidal cells by a whole-cell voltage-clamp technique using an Axopatch 200B amplifier (Molecular Devices, Union City, CA). Patch electrodes (3–5 MΩ) were filled with a solution containing (in mM) 135 CsMeSO$_4$, 8 NaCl, 10 HEPES, 0.5 EGTA, 4 Mg-ATP, and 0.3 Na-GTP, pH 7.25 (adjusted with CsOH). Series resistance was not compensated. Currents were digitized at 20 kHz using a Digidata 1322A interface (Molecular Devices) driven by pClamp 9.2 software (Molecular Devices). Slices were continuously superfused (1.5–2 ml/min) with oxygenated aCSF supplemented with 0.5 μM TTX (Latoxan, Valence, France) to record miniature EPSCs (mEPSCs) and miniature IPSCs (mIPSCs). mEPSCs and mIPSCs were recorded at a holding potential of -70 and 0 mV, respectively. All mEPSCs were measured in the presence of 100 μM picrotoxin (a selective GABA$_A$ receptor antagonist; Sigma), and mIPSCs were measured in the presence of 2 mM kynurenic acid (a selective glutamate receptor antagonist; Sigma). The detection and analysis of miniature currents were achieved by the Minianalysis software (version 6.0.3; Synaptosoft, Decatur, GA). For statistical analysis, the one-way ANOVA test was used. All values are given as mean $\pm$ SEM.

Preparation of brain lysates, brain membranes, synaptic plasma membranes, and immunoblotting. For total brain lysates, tissue was homogenized in radioimmunoprecipitation assay buffer (150 mM NaCl, 50 mM Tris-HCl, pH 8.0, 1% NP-40, 0.5% sodium deoxycholate, and 0.1% SDS; 3 ml/g tissue) with a protease inhibitor mixture on ice. Samples were centrifuged at 10,000 $\times$ g for 10 min at 4°C, and supernatants were collected. For brain membranes, cortices were homogenized with a glass-Teflon homogenizer in 10 vol of ice-cold 10 mM Tris-HCl, pH 7.4, containing 320 mM sucrose and protease inhibitors. The homogenate was centrifuged at 700 $\times$ g for 10 min at 4°C, and the pellet was resuspended and spun again at 700 $\times$ g. Supernatants were combined and centrifuged at 37,000 $\times$ g at 4°C for 40 min. This high-speed pellet (P2) was resuspended in 10 mM Tris-HCl, pH 7.4, containing protease inhibitors. Protein concentration was determined using the BCA protein assay (Pierce, Rockford, IL). Further purification of synaptic plasma membranes (SPMs) was performed as described previously (Jones and Matus, 1974). Separation of proteins by SDS-PAGE was done using 7.5% or 4–8% polyacrylamide gels.

Microarray analysis. Total RNA was prepared by Trizol extraction (Sigma) from triplicate samples of cortices of 4-week-old $Tg/agrn^{-/-}$ and control littermates. For microarray analysis, RNA was reverse transcribed using Superscript II reverse transcriptase (Invitrogen) and oligo-dT as primers. Resulting cDNA was used as a template for the production of biotin-labeled cRNA using a RNA transcript labeling kit (Affymetrix, Santa Clara, CA). Finally, the labeled cRNA was purified using RNeasy spin columns (Qiagen, Chatsworth, CA), fragmented, and hybridized to Affymetrix Mouse Genome 430 2.0 Arrays, as recommended by the manufacturer. Raw expression signals for each transcript were computed using the algorithm implemented in MAS 5.0 (Affymetrix). The robust multichip average method, implemented as a part of the BioConductor package affy, was used for data normalization, background correction, and summarization. The hybridization signal intensity was analyzed with Gene Spring 6.1 software (Silicon Genetics, Fremont, CA). In this study, the fold-change analysis method was used to select genes differentially expressed in each genotype. The increase or decrease in mRNA level was considered reliable if the difference in hybridization signal intensity between a control and $Tg/agrn^{-/-}$ samples yielded at least a twofold change ($<$0.5 or $>$2.0) as described previously (Soriano et al., 2000; Matzilevich et al., 2002). For each genotype, three gene chips were used. Only genes showing a less than twofold or more than twofold change

in at least 83% (five of six) of comparisons were selected as differentially expressed for further analysis. The fold-change value for each gene was calculated based on the mean and SD of comparisons that had the highest, more reliable, individual fold-change values. These selected genes were then subjected to extensive, gene-by-gene literature research and divided into functional classes based on their putative functions reported in the literature.

RNA extraction and reverse transcription-PCR for MuSK. Total RNA was extracted from 50 mg of cortex tissue using 1 ml of TRI reagent and the Fast Prep FP120 apparatus (Savant, Hicksville, NY) for homogenization. Residual proteins were extracted by chloroform. RNA was precipitated with isopropanol, washed with ice-cold 75% ethanol, and recentrifuged for 5 min at 7500 $\times$ g (4°C). The RNA pellet was air dried and dissolved in 80 μl of DEPC-treated water. Single-stranded cDNA was prepared from 5 μg of total RNA using SuperScript II Reverse Transcriptase (Invitrogen) according to the supplier's instruction. PCR was performed for 33 cycles using the forward primer 5′-CTGGATCAAGGGGGACAAT-3′and the reverse primer 5′-CTCT-GGTACCGGAAGGGAGA-3′. PCR products were analyzed on a 2% agarose gel.

Results

Restoration of nerve–muscle synapse in agrin-deficient mice

Neural agrin secreted from motor neurons is required for the formation of NMJs (Gautam et al., 1996; Burgess et al., 1999). Because neural agrin injected into muscle is sufficient to induce postsynaptic structures (Cohen et al., 1997; Jones et al., 1997), we hypothesized that neural agrin released from motor neurons in otherwise agrin-deficient mice might prevent the perinatal death. To test this idea, we generated transgenic (Tg) mice that express the cDNA encoding neural chick agrin under the control of the 9 kb promoter region of the motor neuron-specific homeobox transcription factor Hb9 (Arber et al., 1999; Thaler et al., 1999) (Fig. 1a). Using antibodies that recognize chick but not mouse agrin, we found that NMJs of Tg mice were positive for the transgene (Fig. 1b) and that the transgene did not alter the structure of the NMJs (see supplemental Fig. 1, available at www.jneurosci. org as supplemental material). In a few muscles, such as soleus or the diaphragm, chick agrin was also detected in extrasynaptic regions, and these agrin deposits often induced aggregation of AChRs at nonsynaptic sites (Fig. 1b), as does neural agrin injected into the muscle (Bezakova et al., 2001). The Tg mice were then bred with heterozygous agrin knock-out mice (Lin et al., 2001) to generate offspring that were homozygous for the agrin deletion and expressed the transgene (called herein $Tg/agrn^{-/-}$). $Tg/agrn^{-/-}$ mice were born with the expected Mendelian frequency and, in contrast to agrin-deficient mice, were able to move and breathe. NMJs of 6- to 7-week-old $Tg/agrn^{-/-}$ mice looked normal in most muscles including extensor digitorum longus (EDL) or tibialis anterior (TA) (Fig. 1c). In some muscles, such as soleus and diaphragm, AChR clusters were found throughout the entire muscle, and the motor nerve terminals strongly sprouted (soleus) (Fig. 1c). These muscles also atrophied, indicative of denervation. $Tg/agrn^{-/-}$ mice were also considerably smaller than their control littermates (Hausser et al., 2006), and half of the mice had died after 50 d (Fig. 1d). Death was often preceded by impairment of locomotory behavior (Fig. 1e) and some fibrillation (data not shown), suggesting that neuromuscular defects may contribute to lethality but central defects may also play a role. For our analysis of the brain phenotype (see below), we took 30- to 50-d-old mice that did not show signs of fibrillation or locomotory impairment.

Agrin localizes to excitatory but not inhibitory synapses in the brain

Agrin staining in the brain is most prominent in the blood vessels and in pial basement membranes (Barber and Lieth, 1997; Halfter et al., 1997). Moreover, neurons in the CNS have been shown to express mRNA encoding agrin isoforms that contain amino acid inserts at the B/z site (O'Connor et al., 1994; Stone and Nikolics, 1995). Because we focused in this work on the role of agrin at synapses, we first examined the distribution of agrin in different regions of the adult brain that are rich in synapses using antibodies raised against mouse agrin (Eusebio et al., 2003). We examined the neuropil of the CA3 region, the dentate gyrus, and the cortex, where we found agrin-like immunoreactivity associated in puncta (Fig. 2a). In agreement with other studies, the strongest immunoreactivity was found in blood vessels (Fig. 2a, arrow). In $Tg/agrn^{-/-}$ mice, the antiserum stained neither blood vessels nor the puncta (Fig. 2a), confirming the specificity of the anti-mouse agrin antiserum. As shown in Figure 2b, agrin-positive puncta (red) often overlapped with staining obtained with antibodies against the presynaptic marker synaptophysin (green). This colocalization of agrin- and synaptophysin-like immunoreactivity (Fig. 2b, arrowheads), together with the fact that the synaptophysin-positive puncta outnumbered those for agrin, indicates that agrin is localized to a subset of synapses. As shown in Figure 2c, agrin-like immunoreactivity was detected in brain homogenates (lysate) and in subcellular fractions enriched for SPMs that were isolated by differential centrifugation in a sucrose gradient, according to Jones and Matus (1974). Agrin-like immunoreactivity migrated on SDS-PAGE as a smear with an apparent molecular mass between 400 and 600 kDa (Fig. 2c, arrowhead). As observed in other tissues, the anti-agrin antibodies also recognized several smaller bands (Fig. 2c, asterisks) that are likely the product of proteolytic degradation. In summary, our results indicate that agrin in the adult brain is localized to synapses and that the synaptically localized agrin is also a proteoglycan as it is in other tissues (Tsen et al., 1995).

To assure that the agrin-immunoreactive puncta indeed represented synapses, we also used postembedding immunoelectron microscopy. First, we confirmed that the anti-agrin antiserum was also specific in immunoelectron microscopy. To this end, we examined blood vessels, which are strongly positive for agrin (Fig. 2a), and compared the staining in the basal lamina of wild-type and $Tg/agrn^{-/-}$ mice. Indeed, many immunogold particles were found in wild-type controls but not in $Tg/agrn^{-/-}$ mice (Fig. 3a). In the cerebral cortex from wild-type controls, agrin immunostaining was associated with both presynaptic and postsynaptic membranes, and it often appeared within the synaptic cleft (Fig. 3b). We could not detect any preference of the gold particles to either the presynaptic or the postsynaptic site of the synapses, which is probably attributable to the fact that agrin is a large,
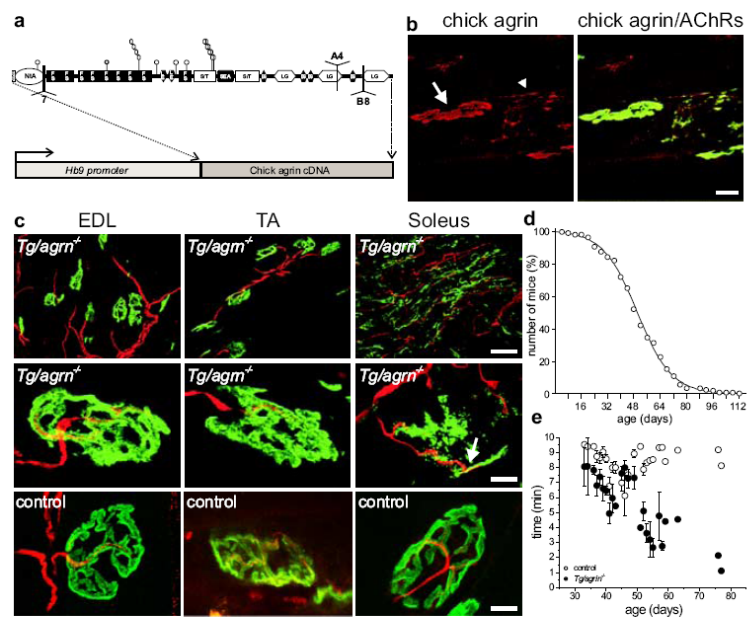

Figure 1. Characterization of mice used in this study. *a*, Schematic representation of neural chick agrin (top) and of the DNA construct (bottom) used to generate $Tg/agrn^{-/-}$ mice. A 9-kb-long genomic region encoding the promoter of the motor neuron-specific homeobox gene Hb9 was cloned upstream of the agrin cDNA. *b*, Soleus muscle from Tg mice stained for chick agrin (red) and AChRs (green). At the NMJ, the transgenic chick agrin (arrow) colocalized with AChR clusters (right, merge in yellow). Deposits of chick agrin immunoreactivity were also detected outside of the NMJ (arrowhead), and they often induced ectopic postsynaptic-like structures as indicated by aggregation of AChRs. Scale bar, 10 μm. *c*, NMJs of $Tg/agrn^{-/-}$ and control mice stained with anti-neurofilament antibodies (red) and α-bungarotoxin to label AChRs (green). Muscle fibers are properly innervated in EDL and TA muscles but not in soleus where AChRs are spread throughout the muscle. Moreover, motor neurons sprouted exuberantly and eventually left the muscle denervated. Occasionally, AChR clusters were matched by a nerve terminal (arrow). Scale bars: top row, 40 μm; middle and bottom rows, 10 μm. *d*, Survival analysis of $Tg/agrn^{-/-}$ mice. The mean survival time of the mice was 50 d. Note the rather large variation in survival time. *e*, Exploratory locomotion of $Tg/agrn^{-/-}$ (filled circles) and control (open circles) mice. There is no difference between the two genotypes, except at a higher age (>50 d) at which $Tg/agrn^{-/-}$ are close to dying.

95-nm-long particle as determined by rotary shadowing (Denzer et al., 1998). Thus, depending on the plane of the section, agrin could be at either side of the synapse. In contrast to the staining in wild-type mice, only few immunogold particles were detected in sections from $Tg/agrn^{-/-}$ mice (Fig. 3b). To get a quantitative measure for the synaptic localization of agrin, we counted the immunogold particles within a 100-nm-wide area (i.e., the size of agrin) surrounding the synaptic cleft. This quantification yielded an average of 1.4 gold particles per synapse (Fig. 3c). In contrast, $Tg/agrn^{-/-}$ mice contained only ∼0.6 gold particles in synaptic regions, which is not significantly different from the number of particles in nonsynaptic regions of control mice (Fig. 3c). From these results, we conclude that agrin is indeed enriched at synapses.

During these electron microscopic studies, we noticed that agrin-like immunogold particles were predominantly associated with asymmetric (excitatory) but not with symmetric (inhibitory) synapses. To validate this impression, we stained cross sections from cerebral cortex for agrin and for the α2 subunit of the GABA_A receptors. Strong immunoreactivity for both proteins was detected around the soma and in the neuropil (Fig. 3d). However, the dot-like staining for either protein did not overlap significantly (Fig. 3d, merge). The same results were obtained in other regions of the brain, including hippocampus and dentate gyrus (data not shown). Similarly, agrin-like immunoreactivity did not colocalize with gephyrin (data not shown), an adaptor
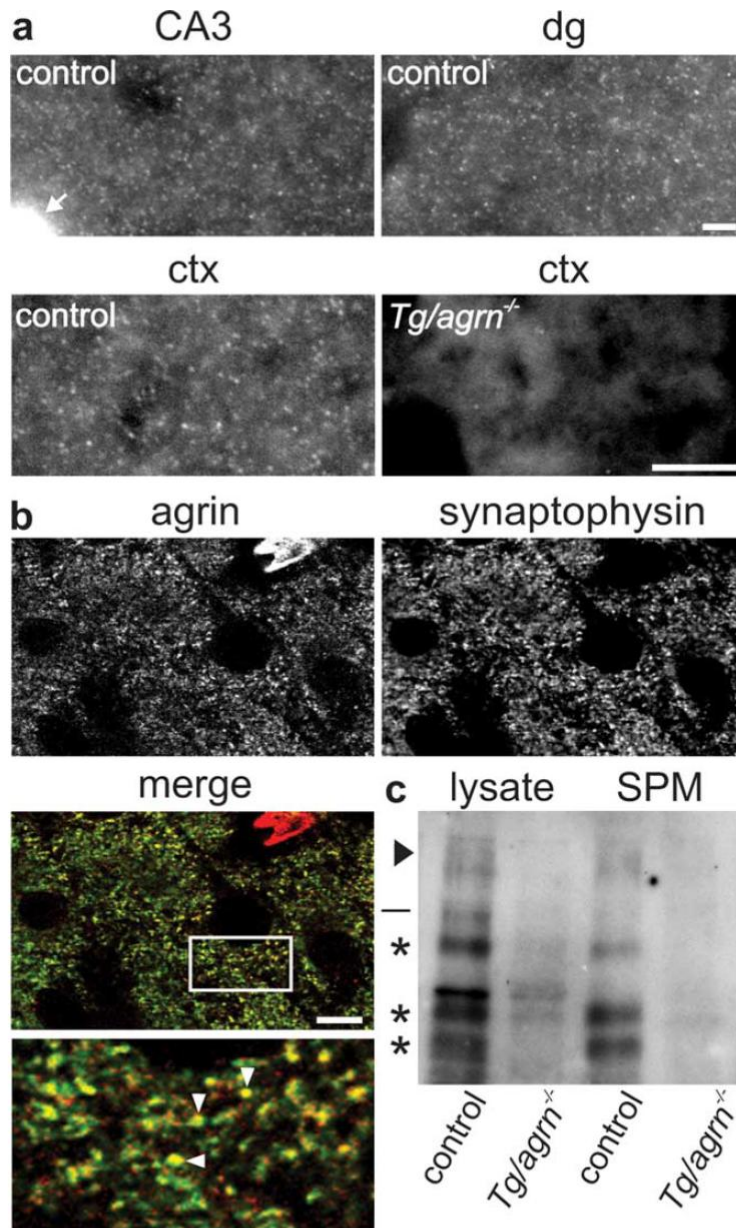
Figure 2. Agrin-like immunoreactivity in the brain. *a*, In control animals, agrin staining is most prominent in blood vessels (arrow). Agrin-like protein also shows a dot-like pattern in the CA3 region of the hippocampus, the dentate gyrus (dg), and the cerebral cortex (ctx). No agrin-like immunoreactivity was detected in agrin-deficient mice (*Tg/agrn⁻/⁻*; ctx). *b*, Sections of cerebral cortex of control mice were stained with antibodies against agrin (red) and the presynaptic marker synaptophysin (green). The bottom picture represents a higher-power view of the framed region. A fraction of the synaptophysin-positive puncta is also positive for agrin-like immunoreactivity (see examples highlighted by arrowheads). *c*, Western blot analysis using anti-agrin antibodies of crude brain lysates (lysate) and of preparations enriched for SPMs. Agrin-like protein in control mice appears as a smear with an apparent molecular mass of 400 – 600 kDa (arrowhead) and in several smaller bands (asterisks). None of these bands were visible in samples isolated from *Tg/agrn⁻/⁻* mice. The line indicates marker size of 250 kDa. Scale bars, 20 μm.

protein required for the clustering of glycine and GABA$_A$ receptors. Moreover, GABA$_A$ receptor α2 subunit and gephyrin remained coclustered in *Tg/agrn⁻/⁻* mice (data not shown). In contrast, the staining for PSD-95, a marker for excitatory syn-

apses (for review, see Kim and Sheng, 2004), showed some overlap with the puncta that were positive for agrin-like immunoreactivity (Fig. 3*e*, arrowheads). Colocalization between agrin and PSD-95 was not seen in all cases, and the PSD-95-positive puncta outnumbered those positive for agrin (Fig. 3*e*, arrow). These experiments are thus strong evidence that agrin localizes to a subset of excitatory but not inhibitory synapses in the adult mouse cortex.

The number of synapses is reduced in *Tg/agrn⁻/⁻* mice

Next, we examined how agrin deficiency affected the brain. As shown in Figure 4, *a* and *b*, the overall morphology of the brain as visualized in serial cresyl violet-stained paraffin sections was unchanged. Likewise, no significant change in the overall morphology of pyramidal neurons in the hippocampus could be detected by Golgi impregnation (Fig. 4*c,d*). Thus, unlike other main components of the pial basement membranes, such as perlecan or some of the laminin chains (Miner et al., 1998; Costell et al., 1999; Halfter et al., 2002), agrin seems not to be essential for the development of the laminar structure of the brain and for the proper differentiation of neurons.

Next, we wanted to see whether synapse number and/or structure was affected. One complication in determining synapse number is the fact that *Tg/agrn⁻/⁻* mice are significantly smaller than control mice. Because size differences can be caused by either changes in cell number or in cell volume, we first quantified the total number of neurons in the cortex using cresyl violet-stained sections in combination with modern, unbiased stereology (Calhoun et al., 1998). As shown in Figure 4*e*, neuronal cell bodies (arrowheads) were smaller and more densely packed in *Tg/agrn⁻/⁻* mice, which resulted in a significantly higher density of neurons in *Tg/agrn⁻/⁻* mice (Fig. 4*f*). Because the total volume of the cortex, as determined by stereology, was smaller in *Tg/agrn⁻/⁻* mice (Fig. 4*g*), the total number of neurons in the entire cortex of *Tg/agrn⁻/⁻* mice remained the same as in control mice (Fig. 4*h*). By using the same method of unbiased stereology in combination with staining for the presynaptic marker protein synaptophysin, we then determined the density of synaptophysin-positive puncta in a given volume. As shown in Figure 4*i*, this parameter was the same in *Tg/agrn⁻/⁻* and control mice. Because the total volume of the cortex is considerably smaller in *Tg/agrn⁻/⁻* mice than in con-
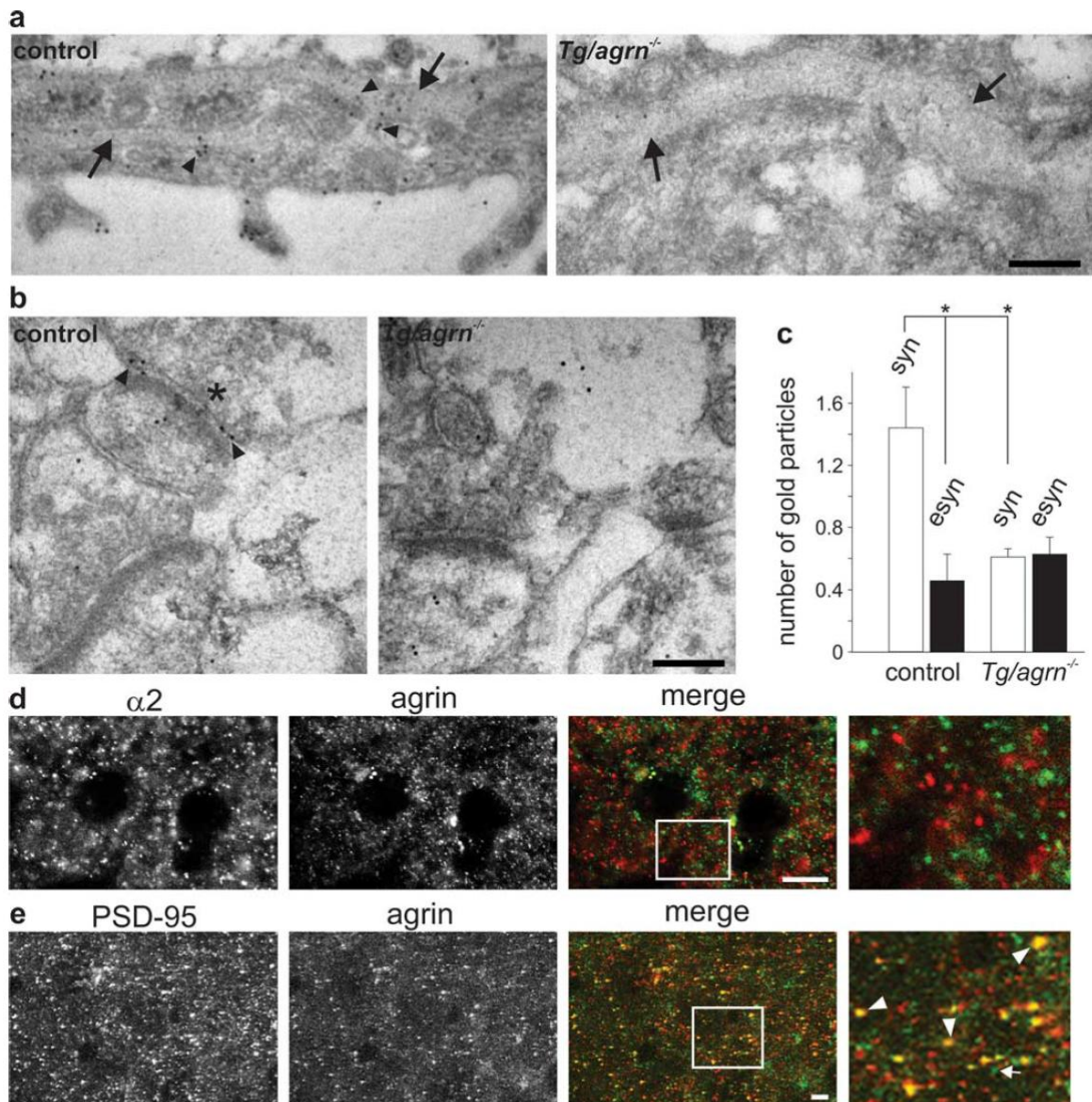
Figure 3. Agrin-like immunoreactivity in the cerebral cortex is enriched at synapses and is localized to a subset of excitatory synapses. *a*, Basal lamina surrounding blood vessels (arrows) contained agrin-like immunoreactivity (arrowheads) in control but not in $Tg/agrn^{-/-}$ mice. Note that the basal lamina of $Tg/agrn^{-/-}$ mice was often thicker than that of control mice. *b*, Agrin immunogold particles (arrowheads) were found near presynaptic (asterisk) and postsynaptic membranes and within the synaptic cleft. *c*, Quantification of the distribution of agrin immunogold particles. In control mice, the number of gold particles was significantly higher at synaptic (syn) than at extrasynaptic (esyn) regions. No synaptic enrichment was detected in $Tg/agrn^{-/-}$ mice (*$p < 0.001$, Mann–Whitney test; $n = 4$ from two different mice per genotype and counting between 35 and 80 synapses per experiment). Error bars indicate mean ± SE. *d*, Staining of sections from wild-type cortex for the $GABA_A$ $\alpha2$ subunit (green) and agrin (red). The puncta are primarily non-overlapping (merge). Right, High-power view of the boxed area. *e*, Considerable overlap of the punctate staining for the PSD-95 (green) and agrin (red) was observed in control mice. Right, High-power view of the boxed area. Examples for the colocalization between agrin and PSD-95 are indicated by arrowheads; lack of colocalization is shown with an arrow. Scale bars: *a, b*, 200 nm; *d, e*, 10 μm.

trol mice (Fig. 4*j*), the total number of presynaptic terminals in the cortex of $Tg/agrn^{-/-}$ mice is ~30% lower than in controls (Fig. 4*k*). Thus, cortices of $Tg/agrn^{-/-}$ mice have the same total number of neurons but only 70% of the number of presynaptic terminals. These results are thus evidence that the number of synapses per neuron is significantly lower in agrin-deficient cortices.

Agrin affects dendrite length and spine number in cortical pyramidal neurons

To examine whether postsynaptic elements were also affected, we analyzed individual pyramidal neurons of the cortex. To this end, neurons were visualized by Golgi staining. As noted in Figure 4, the overall structure of the neurons did not differ between mu-
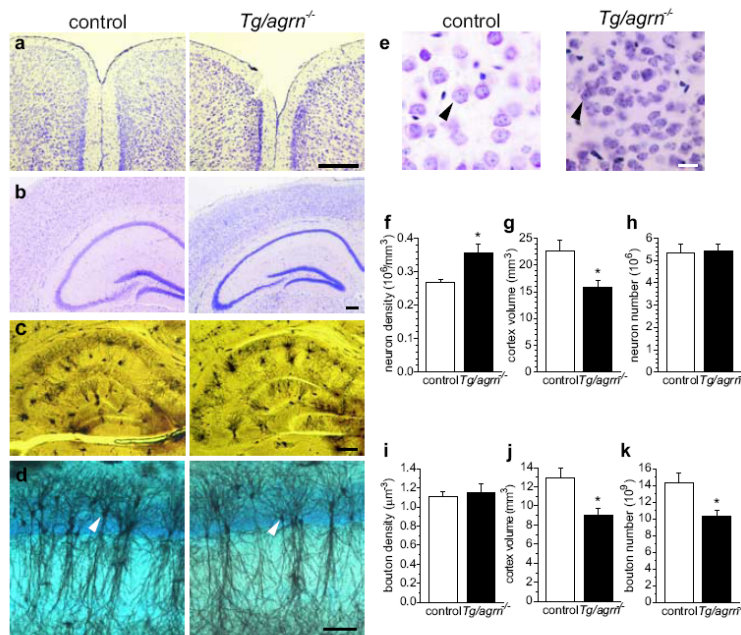
Figure 4. Brain phenotype of adult $Tg/agrn^{-/-}$ mice. **a, b,** Cresyl violet staining of cortical hemispheres (**a**) and of cortex and hippocampus (**b**) does not reveal any overt difference between $Tg/agrn^{-/-}$ and control mice. **c, d,** Similarly, the gross morphology of the different neuronal cell types was unchanged as observed in Golgi-stained sections from hippocampus. In **d,** CA1 hippocampal neurons (arrows) were stained with Golgi impregnation (black) and cresyl violet (blue). **e,** Neuronal cell bodies were considerably bigger and less packed in control mice compared with $Tg/agrn^{-/-}$ mice (arrowheads). **f– h,** Stereological quantification of the number of neurons. **f,** The density of neurons is significantly higher in $Tg/agrn^{-/-}$ than in control mice. **g,** In contrast, the total volume of the cortex is significantly smaller in $Tg/agrn^{-/-}$ than in control mice. **h,** Based in these two parameters, the number of neurons in the cortex remains constant. **i– k,** Stereological quantification of synapse number after staining for synaptophysin. **i,** The density of synaptic boutons is the same in control and $Tg/agrn^{-/-}$ mice. **j, k,** Because of the significant decrease in the total volume of the cortex (**j**), the total number of boutons in the cortices of $Tg/agrn^{-/-}$ mice decreases by 30%. (**k**). Asterisks indicate a significant difference between the two groups of mice (p value at least < 0.02; $n = 5$ or 6 mice for each group). Note that the difference in the cortex volume measured in cresyl violet- and synaptophysin-stained sections is caused by different tissue shrinkage during the experimental procedure. Values in **g, h, j,** and **k** are calculated for one hemisphere. Error bars indicate mean ± SE. Scale bars: **a– c,** 200 μm; **d,** 100 μm; **e,** 30 μm.
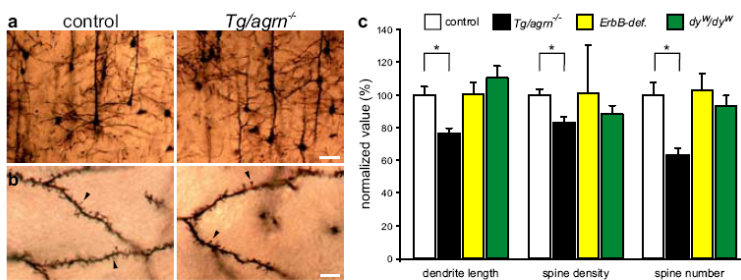
Figure 5. The number of spines is decreased in $Tg/agrn^{-/-}$ mice but not in other mouse models. **a,** Overall morphology of pyramidal neurons localized to layer II/III of the motor cortex from control and $Tg/agrn^{-/-}$ mice visualized by Golgi impregnation. **b,** High-magnification images of dendritic spines in which individual spines (arrowheads) can be clearly identified. **c,** Measurement of the total length of the dendrites (dendrite length), average density of spines (spine density), and the total number of spines (spine number) in cortical neurons after reconstruction using a Neurolucida camera (see also supplemental Fig. 2, available at www.jneurosci.org as supplemental material). The values for all these parameters were significantly lower in neurons from $Tg/agrn^{-/-}$ mice compared with control mice. In contrast, values do not differ from controls in neurons of mice that are either deficient for ErbB2 and ErbB4 in skeletal muscle (ErbB-def.) or deficient for laminin-α2 (dy^{W}/dy^{W}). For each genotype, at least three mice were examined, and 10 neurons each were reconstructed. Data represent mean ± SE ($n \geq 3$) where the values of the control mice were set to 100%. Asterisks denote significant differences ($p < 0.01$, Mann–Whitney test). Scale bars: **a,** 50 μm; **b,** 10 μm. See Table 1 for details and for additional parameters. See Material and Methods for experimental details.

tants and controls (Fig. 5a). Examination at high power suggested, however, that the density of the spines (Fig. 5b, arrowheads) was lower than in control mice. To measure different dendritic parameters and to quantify them, we next reconstructed individual neurons using a Neurolucida camera (see examples in supplemental Fig. 2, available at www.jneurosci.org as supplemental material). As shown in Figure 5c and in Table 1, dendrite length and spine density was significantly lower in pyramidal neurons from $Tg/agrn^{-/-}$ mice. This resulted in a 30% loss of postsynaptic spines per neuron compared with control mice (Fig. 5c). No significant alterations could be found in the number of primary dendrites, the number of dendritic branching points, and the length of the postsynaptic spines (Table 1). Despite the change in synapse number, the remaining synapses in $Tg/agrn^{-/-}$ mice were morphologically indistinguishable from synapses in control littermates, as revealed by electron microscopy (supplemental Fig. 3, available at www.jneurosci.org as supplemental material). Together with the data presented in Figure 4, these results indicate that pyramidal neurons in the cortex of $Tg/agrn^{-/-}$ mice have ∼30% less presynaptic and postsynaptic specializations than controls.

To ask whether the changes in synapse number are a direct consequence of agrin deficiency and not secondary to neuromuscular problems, changes in organ size, or overall health, we also measured dendrite length and spine number in pyramidal neurons in the cortex of two additional mouse models. The first model, called dy^{W}/dy^{W}, carries a targeted deletion of the $lama2$ gene and represents a model for MDC1A congenital muscle dystrophy (Kuang et al., 1998). Laminin-α2-like immunoreactivity and its integrin receptors have been localized to spines in hippocampal neurons (Tian et al., 1997; Shi and Ethell, 2006). Moreover, dy^{2J}/dy^{2J} mice, which also carry a mutation in the $lama2$ gene but display a milder form of MDC1A, show deficits in long-term synaptic plasticity in Purkinje cells (Anderson et al., 2005). Most importantly, dy^{W}/dy^{W} mice are small, strongly impaired in their locomotory activity, and often die at the age of ∼8 weeks (Moll et al., 2001). The second mouse model carries a muscle-specific deletion of the two neuregulin receptors ErbB2 and ErbB4 (Escher et al., 2005). These mice weigh ∼30% less than control littermates but have a normal locomotory activity and do not die prematurely. Thus, both of these mouse models reiterate some of the pheno-

Table 1. Quantification of neuronal complexity

	Control	$Tg/agrn^{-/-}$
Number of primary dendrites per neuron	5.6 ± 0.30	5.5 ± 0.31
Branching points per 100 μm of dendrite	1.10 ± 0.04	1.17 ± 0.04
Length of dendrites (μm)	1491 ± 73	1134 ± 50*
Spine length (μm)	1.841 ± 0.006	1.731 ± 0.006
Spine density (μm^{-1})	0.83 ± 0.028	0.69 ± 0.028*
Spine number per dendrite	401 ± 30.5	253 ± 17.6*

Morphology of cortical pyramidal neurons in 7-week-old mice. Values derive from at least three mice of each genotype and the full reconstruction of 10 neurons from each mouse. Values are mean ± SE. *$p < 0.01$ compared with control. For details, see also supplemental Fig. 2 (available at www.jneurosci.org as supplemental material) and Materials and Methods.

types that are also found in the $Tg/agrn^{-/-}$ mice and are therefore appropriate models to check whether the synaptic phenotype observed in $Tg/agrn^{-/-}$ mice is a direct consequence of the loss of agrin. As shown in Figure 5c, neither the length of the dendrites nor the density of spines in dy^W/dy^W or ErbB-deficient mice was significantly different from control mice.

Agrin deficiency affects the function of excitatory but not inhibitory synapses

Because our results strongly indicate that the synapse number in $Tg/agrn^{-/-}$ is lower, we next asked whether synaptic functions were affected. To test this, we measured the frequency and amplitude of mEPSC and mIPSC currents of pyramidal neurons in layer II/III of the motor cortex using whole-cell patch-clamp recordings. mEPSCs were recorded in the presence of TTX (0.5 μM) and picrotoxin (100 μM) to block action potential firing and GABA$_A$ activity, respectively. mIPSCs were recorded in the presence of TTX and the glutamate receptor antagonist kynurenic acid (2 mM). As shown in Figure 6a–c, we found a significant decrease in the mEPSC frequency in $Tg/agrn^{-/-}$ compared with littermate controls, consistent with a decrease in the number of glutamatergic synapses. mEPSCs were completely blocked by the application of 2 mM kynurenic acid, both in $Tg/agrn^{-/-}$ and control littermates ($n = 5$ and $n = 7$ for $Tg/agrn^{-/-}$ and control mice, respectively), thus confirming that mEPSCs are mediated by glutamate receptors. The amplitudes of mEPSCs were similar between control and $Tg/agrn^{-/-}$ mice (Fig. 6c), suggesting that the responsiveness and number of postsynaptic glutamate receptors are not altered. Neither the mean mIPSC frequency (Fig. 6e) nor amplitude (Fig. 6f) differed between the $Tg/agrn^{-/-}$ and control mice. In both types of mice, mIPSCs were abolished by the application of 100 μM picrotoxin, indicating that mIPSCs are mediated by the activation of GABA$_A$ receptors ($n = 6$ and $n = 5$ for $Tg/agrn^{-/-}$ and control mice, respectively). In summary, the decrease in the mEPSC frequency and the absence of changes in inhibitory synaptic transmission is consistent with a selective loss of excitatory synapses in $Tg/agrn^{-/-}$ mice.

The receptor tyrosine kinase MuSK is localized to CNS synapses

At the NMJ, the receptor tyrosine kinase MuSK is required for agrin-induced signaling (Glass et al., 1996). Using Northern blot analysis, MuSK is not detected in rat brain (Valenzuela et al., 1995). In contrast, transcripts for MuSK were found in the brain of other species (Ganju et al., 1995; Fu et al., 1999; Garcia-Osta et al., 2006). Because agrin signaling in the brain might be mediated by MuSK, we looked at the expression of MuSK on the mRNA and protein level. Reverse transcription (RT), followed by PCR on RNA isolated from cortices of wild-type mice, revealed a product of the expected size (Fig. 7a, ctx). This product was specific because it was absent when the reverse transcriptase was omitted
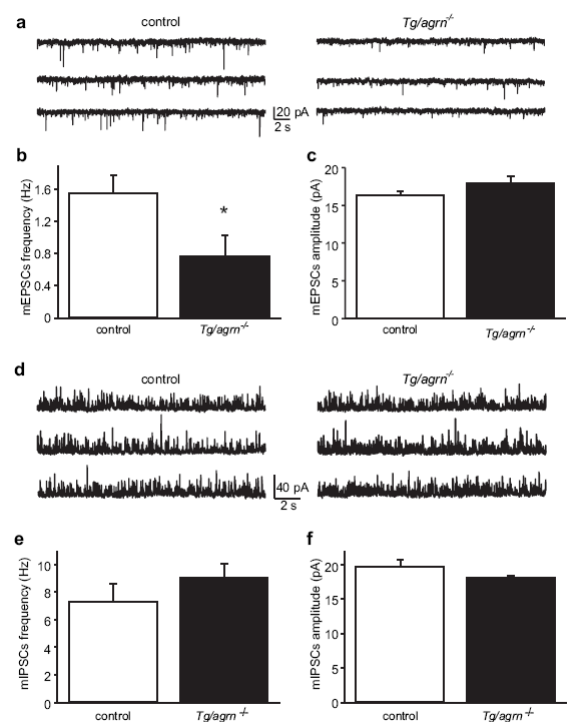
Figure 6. Spontaneous miniature currents recorded in layer II/III pyramidal neurons of the motor cortex from $Tg/agrn^{-/-}$ and control littermates. **a**, Representative recordings of pharmacologically isolated mEPSCs in pyramidal neurons of control and $Tg/agrn^{-/-}$ mice. mEPSCs were recorded at a holding potential of -70 mV in the presence of 1 μM TTX and 100 μM picrotoxin. **b, c**, The frequency of mEPSCs was significantly reduced in $Tg/agrn^{-/-}$ mice compared with control littermates (control: 1.56 ± 0.22 Hz, $n = 17$; $Tg/agrn^{-/-}$: 0.77 ± 0.26 Hz, $n = 12$; $p < 0.05$, ANOVA test). In contrast, the amplitude of the mEPSCs did not differ between control (16.42 ± 0.47 pA; $n = 17$) and $Tg/agrn^{-/-}$ (17.99 ± 0.85 pA; $n = 12$) mice. **d**, Representative mIPSCs recorded in control and $Tg/agrn^{-/-}$ mice at a holding potential of 0 mV and in the presence of 1 μM TTX and 2 mM kynurenic acid. **e, f**, Neither the frequency nor the amplitude of the mIPSCs was changed between controls (frequency, 7.28 ± 1.13 Hz; amplitude, 19.77 ± 0.94 pA; $n = 12$) and $Tg/agrn^{-/-}$ mice (frequency, 8.99 ± 1.21 Hz; amplitude, 18.12 ± 0.31 pA; $n = 12$). Control mice were always littermates of $Tg/agrn^{-/-}$ mice. Data are represented as means ± SE.

(Fig. 7a, neg) and was also detected in skeletal muscle (Fig. 7a, sm). Using a newly raised antiserum against the extracellular domain of mouse MuSK, which recognizes MuSK in Western blots and immunohistochemistry (supplemental Fig. 4, available at www.jneurosci.org as supplemental material) (Scotton et al., 2006), we detected MuSK-like protein in fractions enriched for membranes in brains of wild-type mice (Fig. 7b). In contrast, preimmune serum did not detect any such band. In cross sections from the cortex of wild-type mice, MuSK-like protein was detected as puncta (Fig. 7c). Importantly, these MuSK-positive puncta partially overlapped with puncta positive for PSD-95 (Fig. 7c, yellow color in the merged images). Preimmune serum did not stain (Fig. 7d). Quantitative assessment showed that 14.6 ± 1.9% (mean ± SE; $n = 8$) of the PSD-95-positive puncta were also positive for MuSK and that 23.0 ± 3.0% (mean ± SE; $n = 8$) of the MuSK-positive puncta were also positive for PSD-95. In contrast, preimmune serum hardly stained any puncta (~10 times fewer than immune serum), and of those, only 2.4 ± 0.7% overlapped with PSD-95. Because the anti-agrin and anti-MuSK antibodies were both raised in rabbits, we could not perform
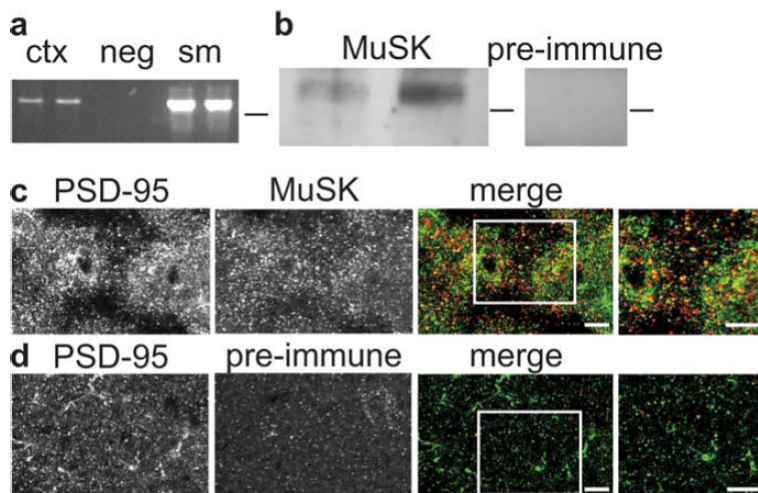
Figure 7. MuSK is expressed in the brain and is localized to a subset of excitatory synapses. *a*, RT-PCR of RNA from cortex (ctx), negative control (neg), and skeletal muscles (sm) of adult mice. MuSK mRNA is clearly detected in mouse cortex although at lower levels than in skeletal muscle. *b*, In Western blot analysis of P2 brain membranes, anti-MuSK antiserum but not preimmune serum detects a protein with an apparent M_r of 115 kDa. Lines indicate 100 kDa marker band. *c*, Sections from wild-type cortex stained for MuSK (red) and PSD-95 (green). MuSK partially colocalizes with PSD-95-positive synapses (merge; yellow). Right, Higher-power view of the boxed area. *d*, No specific signal was detectable in cortical sections from wild-type mice that were stained with MuSK preimmune serum (red) and PSD-95 (green). Right, Higher-power view of the boxed area. Scale bars, 20 μm.

colocalization studies. The finding that agrin (Fig. 3*e*) and MuSK both colocalize with PSD-95 suggests, however, that they probably also colocalize. We additionally tried to detect the two homologs of MuSK, Ror1, and Ror2, but the commercial antibodies were not sensitive enough to detect any staining (data not shown).

Alterations in the MAP kinase pathway
To get some understanding of the molecular mechanisms that may underlie the synaptic changes in the cortex, we next quantified the amount of synaptic marker proteins in the cortices of control and $Tg/agrn^{-/-}$ mice. In 7-week-old mice, no change in expression levels of markers for inhibitory synapses, such as the α1 subunit and gephyrin was observed (Fig. 8*a*). Similarly, the amount of the NMDA receptor subunit NR1, of PSD-95, and of CAMKII was not changed (Fig. 8*a*). In strong contrast, a substantial increase of the synaptic GTPase-activating protein SynGAP was detected (Fig. 8*b*). Interestingly, SynGAP levels were not altered in cortices isolated from dy^W/dy^W mice, consistent with the lack of synaptic phenotype in these mice. The increase in SynGAP levels of $Tg/agrn^{-/-}$ mice was even more pronounced in fractions enriched for synaptic membranes (Fig. 8*b*), indicating that these alteration are synapse specific.

To avoid any bias in our approach, we also examined gene expression in cortices of 4-week-old control and $Tg/agrn^{-/-}$ mice on a genome-wide scale using the Affymetrix Mouse Genome 430 2.0 Array. Of the >39,000 transcripts, 255 were significantly regulated at least twofold (supplemental Table 1, available at www.jneurosci.org as supplemental material). The majority of the regulated genes falls into the class of signal transduction, followed by genes involved in cell communication (Fig. 8*c*). The fact that most of the gene families are represented in the 255 genes suggests that agrin affects many pathways. Moreover, agrin deficiency is likely to influence gene expression not only in neurons but also in non-neuronal cells (e.g., glial cells and blood vessels).

One of the candidates identified, MKK7, has been shown to be involved in agrin signaling at the NMJ (Lacazette et al., 2003). Moreover, the MAP kinase pathway has been implicated in the response of cultured neurons to agrin (Karasewski and Ferreira, 2003; Hilgenberg and Smith, 2004). We therefore concentrated our work on characterizing this pathway. The amount of MKK7 on the mRNA (data not shown) and the protein level was considerably lower in brain extracts from $Tg/agrn^{-/-}$ mice than in control or dy^W/dy^W mice (Fig. 8*d*). Moreover, the JNK, which is the main substrate for MKK7, became phosphorylated in cultured hippocampal neurons by the addition of neural agrin (data not shown). In summary, these results strongly suggest that agrin can activate the MAP kinase pathway in neurons and that the lack of agrin deregulates this pathway through changes of some of its regulators, such as SynGAP and MKK7.

Discussion
We show that transgenic expression of neural agrin in motor neurons in agrin-deficient mice is sufficient to assemble a functional NMJ and to prevent perinatal death. Thus, agrin expressed by the muscle is not required for the formation of functional NMJs. We observed, however, that the extent to which NMJs were restored greatly differed between individual muscles. Because we did not detect differences in the levels of expression of the transgene between the motor neurons innervating the different muscles (I. Ksiazek and M. A. Ruegg, unpublished observation), our results suggest that there are muscle-intrinsic differences that influence their response to neural agrin. Interestingly, the muscles where synapses were not well restored (such as soleus and diaphragm) were those that have recently been found to be "delayed synapsing" (Pun et al., 2002). Thus, differential responsiveness to neural agrin might be the basis for the phenomenon of delayed synapsing during muscle innervation in the embryo.

Agrin deficiency affects excitatory but not inhibitory synapses
In our current work, we focus on the phenotype of $Tg/agrn^{-/-}$ mice in the brain. We find a highly significant loss of synapses in the cortex. This conclusion is based on the decrease in the total number of presynaptic terminals detected in cortex (Fig. 4) and a decrease in the density of postsynaptic spines and the length of dendrites (Fig. 5). This loss in synapses is unlikely attributable to the smaller size or the premature death of the $Tg/agrn^{-/-}$ mice because synapse number was not changed in the cortex of dy^W/dy^W or ErbB-deficient mice (Fig. 5). Importantly, our electrophysiological studies on acute cortical slices show that the frequency but not the amplitude of mEPSCs is strongly altered in $Tg/agrn^{-/-}$ mice. In contrast, the mIPSC frequency and amplitudes remain normal in $Tg/agrn^{-/-}$ mice, revealing that functional alterations are confined to excitatory synapses.

The presumed loss of excitatory synapses in the agrin-deficient mice, as observed with electrophysiology, is also consistent with the localization of agrin to excitatory (PSD-95 positive) but not inhibitory synapses in wild-type mice (Fig. 3). These
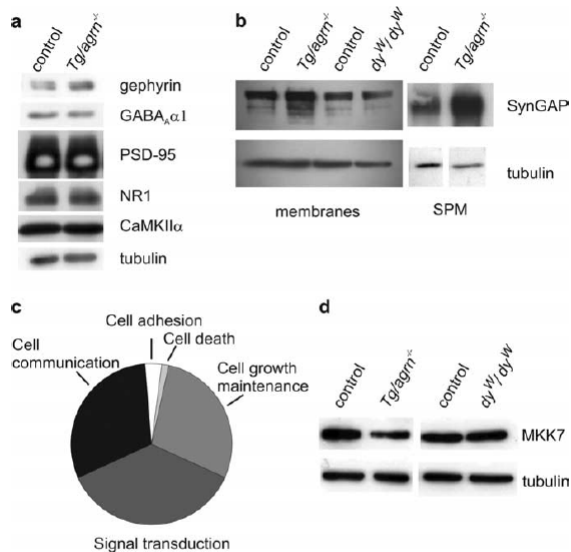
Figure 8. Agrin affects the MAP kinase pathway. *a*, Western blot analysis from P2 membranes isolated from cortices of 6- to 7-week-old mice. No change in the levels of several synaptic proteins was observed. *b*, Compared with wild-type controls, the amount of SynGAP was higher in P2 membrane fractions and in fractions enriched for synaptic membranes (SPM) isolated from cortices of $Tg/agrn^{-/-}$ mice. Such change was not detected in dy^W/dy^W mice. *c*, GeneChip analysis on cortices from 4-week-old control and $Tg/agrn^{-/-}$ mice. Genes with at least twofold altered expression levels in $Tg/agrn^{-/-}$ compared with controls are classified into groups by their biological function. *d*, MKK7 is downregulated in $Tg/agrn^{-/-}$ but not in dy^W/dy^W mice.

results were unexpected because previous antisense experiments provided evidence for a role of agrin at inhibitory synapses (Ferreira, 1999). In addition, α-dystroglycan, which is probably the most abundant agrin-binding protein (Gesemann et al., 1998), colocalizes with a subset of GABA$_A$ receptors (Brunig et al., 2002; Levi et al., 2002). Thus, the finding that agrin does not colocalize with inhibitory synapses and that deletion of the agrin gene does not affect the function of inhibitory synapses strongly suggests that the binding of agrin to α-dystroglycan might be compensated for by other α-dystroglycan-binding molecules of the extracellular matrix, in particular by the neurexins (Sugita et al., 2001), perlecan, or the laminins (Talts et al., 1999). Our observation that the pial basement membrane, the glia limitans, and the laminar structures of the cortex are also not affected in $Tg/agrn^{-/-}$ mice is consistent with such a compensatory mechanism because brain-specific inactivation of α-dystroglycan disrupts these structures (Moore et al., 2002).

Receptors that may mediate agrin signaling

There are several candidate receptors for agrin in the CNS. One of those is the receptor tyrosine kinase MuSK that mediates the postsynapse-inducing activity of agrin at the NMJ. We find that MuSK is also expressed in cortex and that the protein, like agrin, partially overlaps with PSD-95-positive puncta (Fig. 7). Our data are also supported by the recent report showing that MuSK is expressed in brain (Garcia-Osta et al., 2006). At the NMJ, MuSK can only be activated by agrin splice variants that are released from the nerve terminal (called neural agrin) but not by those synthesized by non-neuronal tissue including muscle (called non-neuronal or muscle agrin), which are also inactive in inducing AChR aggregation (for review, see Bezakova and Ruegg,

2003). Previous work has shown that mRNA encoding neural agrin is expressed in noncholinergic neurons of the brain (O'Connor et al., 1994; Stone and Nikolics, 1995). Thus, it may well be that the loss of synapses in the cortex of $Tg/agrn^{-/-}$ mice is only attributable to the loss of neural agrin. Consistent with the possibility that agrin could signal through MuSK, knock-down of MuSK expression by antisense oligonucleotides in rat brain leads to impairment of memory consolidation and of the induction and maintenance of long-term potentiation (Garcia-Osta et al., 2006). This activity of MuSK appears to involve phosphorylation of CREB and upregulation of expression of CCAAT enhancer-binding protein β. Phosphorylation of CREB has been shown to be induced only by neural but not by non-neuronal forms of agrin (Ji et al., 1998), and it is known to be downstream of the MAP kinase pathway (for review, see Thomas and Huganir, 2004), which is also perturbed in the cortex of $Tg/agrn^{-/-}$ mice (see discussion below). Thus, our results would be in agreement with the possibility that agrin also acts via MuSK at excitatory synapses in the brain.

Other candidate receptors that have been suggested to mediate agrin signaling in the brain are the two MuSK homologs Ror1 and Ror2, which are both highly expressed in developing and adolescent brain (Yoda et al., 2003). Our own attempts to localize Ror1 and Ror2 to synapses in the mouse brain were not successful (data not shown), which might be because of low sensitivity of the antibodies used. No gross morphological abnormalities in the nervous system were observed for Ror1- or Ror2-deficient mice (Yoda et al., 2003). In addition, Ror1 and Ror2 are rather enriched at growth cones than at synapses in developing hippocampal neurons (Paganoni and Ferreira, 2003), and they have been implicated in affecting neurite outgrowth (Paganoni and Ferreira, 2005). Finally, Ror2 was shown to be involved in the formation of filopodia induced by wnt5a (Nishita et al., 2006). Thus, the current data make MuSK a more likely candidate receptor for agrin than Ror1 or Ror2.

Another particularly attractive candidate receptor for agrin is the α3 subunit of the Na$^+$/K$^+$-ATPase (NKA) that was recently shown to bind both neural and non-neuronal splice variants of agrin (Hilgenberg et al., 2006). The α3 subunit of NKA is localized to synapses in cultured cortical neurons, and agrin binding to α3NKA inhibits its function and therefore causes a slight depolarization of the cell. Thus, the lack of agrin could result in reduced neuronal activity and reduced responsiveness of neurons to excitatory input. The fact that we find a strong decrease in the frequency of the mEPSC but not the mIPSC would then suggest that the function of agrin to antagonize α3NKA is selective for excitatory synapses or that α3NKA expression is restricted to excitatory synapses. Whether an increased activity of α3NKA because of the lack of its endogenous antagonist agrin will result in a lower number of synapses remains unknown.

Agrin deficiency deregulates MAP kinase signaling

Several lines of evidence suggest that agrin activates the MAP kinase pathway in cultured neurons (Karasewski and Ferreira, 2003; Hilgenberg and Smith, 2004). Moreover, one of its downstream targets, CREB, becomes phosphorylated after the addition of agrin (Ji et al., 1998). We now find strong evidence that MAP kinase signaling is indeed altered in the brain of $Tg/agrn^{-/-}$ mice because they show a strong increase in the amount of the Ras GTPase-activating protein SynGAP and a reduction in MKK7 mRNA and protein. SynGAP has been shown to dampen MAP kinase signaling (Komiyama et al., 2002), and neurons cultured from SynGAP-deficient mice have more AMPA receptor clusters (Kim et al., 2003). Interestingly, transfection of constructs encod-

ing green fluorescent protein–SynGAP into neuronal cultures causes a strong decrease in the frequency of the mEPSCs and a dampening of extracellular signal-regulated kinase (ERK) activation compared with control cultures. Conversely, SynGAP-deficient neurons show an increase in the frequency of the mEP-SCs and increased ERK activation (Rumbaugh et al., 2006). Thus, upregulation of SynGAP in the *Tg/agrn*$^{-/-}$ mice could lower the activity of MAP kinases and subsequently result in less synapses. Similarly, the decrease in MKK7, which is also highly enriched in postsynaptic density fractions (Collins et al., 2005), is likely to dampen signaling via the MAP kinase.

Although it is unknown how agrin activates MAP kinase signaling in the brain, we have recently found that both ERK and JNK are phosphorylated at the NMJ or at ectopic postsynaptic structures induced by the injection of recombinant agrin into muscle (G. Bezakova and Ruegg, unpublished data). Importantly, phosphorylation of JNK and ERK at the NMJ is a direct consequence of the activation of MuSK by agrin because it does not require ErbB-signaling (Bezakova and Ruegg, unpublished data). Thus, the capability of agrin to activate MAP kinase signaling in neurons could also be mediated by MuSK. Alternatively, binding of agrin to α3NKA could trigger Ca^{2+} signaling in neurons (Hilgenberg et al., 2006), which in turn can activate the MAP kinase pathway.

Other pathways that might be regulated by agrin

Our gene expression studies in *Tg/agrn*$^{-/-}$ mice show that expression of the GTPase-activating RANGAP domain-like 1 protein (also called TULIP1 or GARNL1 (Schwarzbraun et al., 2004) is increased by >20-fold. Although the function of GARNL1 is not known, it is highly expressed in brain, and it is a close homolog of tuberous sclerosis complex (TSC) 1 and TSC2. TSC1/2 have been shown to control cell size by inhibiting the mammalian target of rapamycin (mTOR) pathway (Inoki et al., 2005). The annotated gene, the expression level of which is >20-fold lower in *Tg/agrn*$^{-/-}$ mice than in control mice, is the ribosomal protein S6, a substrate of S6 kinase 1, which is activated by mTOR. These results suggest that agrin deficiency might affect protein translation via the mTOR pathway. Changes in protein synthesis might be the reason for the smaller size of the neurons in *Tg/agrn*$^{-/-}$ mice.

In conclusion, our work provides for the first time evidence that agrin does play a role in the formation and/or maintenance of CNS synapses *in vivo*. The synaptic deficits are detectable only in adolescent and adult mice, whereas neurons from agrin-deficient mice still form synapses in culture (Li et al., 1999; Serpinskaya et al., 1999) and the brain of agrin-deficient embryos have no synaptic defects (Gautam et al., 1996). Interestingly, a similar situation was reported for the development of the NMJ, where AChR clusters form in cultured myotubes independent of agrin and where AChR clusters are detected in embryos that are deficient for agrin, or where innervation of the muscle by the motor neuron has been prevented by genetic ablation (Lin et al., 2001; Yang et al., 2001). Thus, in both systems, the function of agrin at synapses may become only apparent when synapses are fully functional.

References

Akins MR, Biederer T (2006) Cell-cell interactions in synaptogenesis. Curr Opin Neurobiol 16:83–89.

Anderson JL, Head SI, Morley JW (2005) Synaptic plasticity in the dy2J mouse model of laminin alpha2-deficient congenital muscular dystrophy. Brain Res 1042:23–28.

Arber S, Han B, Mendelsohn M, Smith M, Jessell TM, Sockanathan S (1999) Requirement for the homeobox gene Hb9 in the consolidation of motor neuron identity. Neuron 23:659–674.

Barber AJ, Lieth E (1997) Agrin accumulates in the brain microvascular basal lamina during development of the blood-brain barrier. Dev Dyn 208:62–74.

Bezakova G, Lomo T (2001) Muscle activity and muscle agrin regulate the organization of cytoskeletal proteins and attached acetylcholine receptor (AchR) aggregates in skeletal muscle fibers. J Cell Biol 153:1453–1463.

Bezakova G, Ruegg MA (2003) New insights into the roles of agrin. Nat Rev Mol Cell Biol 4:295–308.

Bezakova G, Helm JP, Francolini M, Lomo T (2001) Effects of purified recombinant neural and muscle agrin on skeletal muscle fibers in vivo. J Cell Biol 153:1441–1452.

Bose CM, Qiu D, Bergamaschi A, Gravante B, Bossi M, Villa A, Rupp F, Malgaroli A (2000) Agrin controls synaptic differentiation in hippocampal neurons. J Neurosci 20:9086–9095.

Brewer GJ, Torricelli JR, Evege EK, Price PJ (1993) Optimized survival of hippocampal neurons in B27-supplemented Neurobasal, a new serum-free medium combination. J Neurosci Res 35:567–576.

Brunig I, Scotti E, Sidler C, Fritschy JM (2002) Intact sorting, targeting, and clustering of gamma-aminobutyric acid A receptor subtypes in hippocampal neurons in vitro. J Comp Neurol 443:43–55.

Burgess RW, Nguyen QT, Son YJ, Lichtman JW, Sanes JR (1999) Alternatively spliced isoforms of nerve- and muscle-derived agrin: their roles at the neuromuscular junction. Neuron 23:33–44.

Burgess RW, Skarnes WC, Sanes JR (2000) Agrin isoforms with distinct amino termini. Differential expression, localization, and function. J Cell Biol 151:41–52.

Calhoun ME, Kurth D, Phinney AL, Long JM, Hengemihle J, Mouton PR, Ingram DK, Jucker M (1998) Hippocampal neuron and synaptophysin-positive bouton number in aging C57BL/6 mice. Neurobiol Aging 19:599–606.

Cohen I, Rimer M, Lomo T, McMahan UJ (1997) Agrin-induced postsynaptic apparatus in skeletal muscle fibers in vivo. Mol Cell Neurosci 9:237–253.

Collins MO, Husi H, Yu L, Brandon JM, Anderson CN, Blackstock WP, Choudhary JS, Grant SG (2006) Molecular characterization and comparison of the components and multiprotein complexes in the postsynaptic proteome. J Neurochem 97]Suppl 1]:16–23.

Costell M, Gustafsson E, Aszodi A, Morgelin M, Bloch W, Hunziker E, Addicks K, Timpl R, Fassler R (1999) Perlecan maintains the integrity of cartilage and some basement membranes. J Cell Biol 147:1109–1122.

Denzer AJ, Schulthess T, Fauser C, Schumacher B, Kammerer RA, Engel J, Ruegg MA (1998) Electron microscopic structure of agrin and mapping of its binding site in laminin-1. EMBO J 17:335–343.

Escher P, Lacazette E, Courtet M, Blindenbacher A, Landmann L, Bezakova G, Lloyd KC, Mueller U, Brenner HR (2005) Synapses form in skeletal muscles lacking neuregulin receptors. Science 308:1920–1923.

Eusebio A, Oliveri F, Barzaghi P, Ruegg MA (2003) Expression of mouse agrin in normal, denervated and dystrophic muscle. Neuromuscul Disord 13:408–415.

Ferreira A (1999) Abnormal synapse formation in agrin-depleted hippocampal neurons. J Cell Sci 112:4729–4738.

Fritschy JM, Weinmann O, Wenzel A, Benke D (1998) Synapse-specific localization of NMDA and GABA(A) receptor subunits revealed by antigen-retrieval immunohistochemistry. J Comp Neurol 390:194–210.

Fu AK, Smith FD, Zhou H, Chu AH, Tsim KW, Peng BH, Ip NY (1999) Xenopus muscle-specific kinase: molecular cloning and prominent expression in neural tissues during early embryonic development. Eur J Neurosci 11:373–382.

Ganju P, Walls E, Brennan J, Reith AD (1995) Cloning and developmental expression of Nsk2, a novel receptor tyrosine kinase implicated in skeletal myogenesis. Oncogene 11:281–290.

Garcia-Osta A, Tsokas P, Pollonini G, Landau EM, Blitzer R, Alberini CM (2006) MuSK expressed in the brain mediates cholinergic responses, synaptic plasticity, and memory formation. J Neurosci 26:7919–7932.

Gautam M, Noakes PG, Moscoso L, Rupp F, Scheller RH, Merlie JP, Sanes JR (1996) Defective neuromuscular synaptogenesis in agrin-deficient mutant mice. Cell 85:525–535.

Gesemann M, Denzer AJ, Ruegg MA (1995) Acetylcholine receptor-aggregating activity of agrin isoforms and mapping of the active site. J Cell Biol 128:625–636.

Gesemann M, Brancaccio A, Schumacher B, Ruegg MA (1998) Agrin is a high-affinity binding protein of dystroglycan in non-muscle tissue. J Biol Chem 273:600–605.

Gingras J, Rassadi S, Cooper E, Ferns M (2002) Agrin plays an organizing role in the formation of sympathetic synapses. J Cell Biol 158:1109–1118.

Glass DJ, Bowen DC, Stitt TN, Radziejewski C, Bruno J, Ryan TE, Gies DR, Shah S, Mattsson K, Burden SJ, DiStefano PS, Valenzuela DM, DeChiara TM, Yancopoulos GD (1996) Agrin acts via a MuSK receptor complex. Cell 85:513–523.

Halfter W, Schurer B, Yip J, Yip L, Tsen G, Lee JA, Cole GJ (1997) Distribution and substrate properties of agrin, a heparan sulfate proteoglycan of developing axonal pathways. J Comp Neurol 383:1–17.

Halfter W, Dong S, Yip YP, Willem M, Mayer U (2002) A critical function of the pial basement membrane in cortical histogenesis. J Neurosci 22:6029–6040.

Hausser HJ, Ruegg MA, Brenner RE, Ksiazek I (2006) Agrin is highly expressed by chondrocytes and is required for normal growth. Histochem Cell Biol 127:363–374.

Hilgenberg LG, Smith MA (2004) Agrin signaling in cortical neurons is mediated by a tyrosine kinase-dependent increase in intracellular Ca2+ that engages both CaMKII and MAPK signal pathways. J Neurobiol 61:289–300.

Hilgenberg LG, Hoover CL, Smith MA (1999) Evidence of an agrin receptor in cortical neurons. J Neurosci 19:7384–7393.

Hilgenberg LG, Ho KD, Lee D, O'Dowd DK, Smith MA (2002) Agrin regulates neuronal responses to excitatory neurotransmitters in vitro and in vivo. Mol Cell Neurosci 19:97–110.

Hilgenberg LG, Su H, Gu H, O'Dowd DK, Smith MA (2006) Alpha3Na+/K+-ATPase is a neuronal receptor for agrin. Cell 125:359–369.

Inoki K, Corradetti MN, Guan KL (2005) Dysregulation of the TSC-mTOR pathway in human disease. Nat Genet 37:19–24.

Ji RR, Bose CM, Lesuisse C, Qiu D, Huang JC, Zhang Q, Rupp F (1998) Specific agrin isoforms induce cAMP response element binding protein phosphorylation in hippocampal neurons. J Neurosci 18:9695–9702.

Jones DH, Matus AI (1974) Isolation of synaptic plasma membrane from brain by combined flotation-sedimentation density gradient centrifugation. Biochim Biophys Acta 356:276–287.

Jones G, Meier T, Lichtsteiner M, Witzemann V, Sakmann B, Brenner HR (1997) Induction by agrin of ectopic and functional postsynaptic-like membrane in innervated muscle. Proc Natl Acad Sci USA 94:2654–2659.

Karasewski L, Ferreira A (2003) MAPK signal transduction pathway mediates agrin effects on neurite elongation in cultured hippocampal neurons. J Neurobiol 55:14–24.

Kim E, Sheng M (2004) PDZ domain proteins of synapses. Nat Rev Neurosci 5:771–781.

Kim JH, Lee HK, Takamiya K, Huganir RL (2003) The role of synaptic GTPase-activating protein in neuronal development and synaptic plasticity. J Neurosci 23:1119–1124.

Komiyama NH, Watabe AM, Carlisle HJ, Porter K, Charlesworth P, Monti J, Strathdee DJ, O'Carroll CM, Martin SJ, Morris RG, O'Dell TJ, Grant SG (2002) SynGAP regulates ERK/MAPK signaling, synaptic plasticity, and learning in the complex with postsynaptic density 95 and NMDA receptor. J Neurosci 22:9721–9732.

Kuang W, Xu H, Vachon PH, Liu L, Loechel F, Wewer UM, Engvall E (1998) Merosin-deficient congenital muscular dystrophy. Partial genetic correction in two mouse models. J Clin Invest 102:844–852.

Lacazette E, Le Calvez S, Gajendran N, Brenner HR (2003) A novel pathway for MuSK to induce key genes in neuromuscular synapse formation. J Cell Biol 161:727–736.

Levi S, Grady RM, Henry MD, Campbell KP, Sanes JR, Craig AM (2002) Dystroglycan is selectively associated with inhibitory GABAergic synapses but is dispensable for their differentiation. J Neurosci 22:4274–4285.

Li Z, Hilgenberg LG, O'Dowd DK, Smith MA (1999) Formation of functional synaptic connections between cultured cortical neurons from agrin-deficient mice. J Neurobiol 39:547–557.

Lin W, Burgess RW, Dominguez B, Pfaff SL, Sanes JR, Lee KF (2001) Distinct roles of nerve and muscle in postsynaptic differentiation of the neuromuscular synapse. Nature 410:1057–1064.

Matzilevich DA, Rall JM, Moore AN, Grill RJ, Dash PK (2002) High-density microarray analysis of hippocampal gene expression following experimental brain injury. J Neurosci Res 67:646–663.

McMahan UJ (1990) The agrin hypothesis. Cold Spring Harb Symp Quant Biol 55:407–418.

Miner JH, Cunningham J, Sanes JR (1998) Roles for laminin in embryogenesis: exencephaly, syndactyly, and placentopathy in mice lacking the laminin alpha5 chain. J Cell Biol 143:1713–1723.

Moll J, Barzaghi P, Lin S, Bezakova G, Lochmuller H, Engvall E, Muller U, Ruegg MA (2001) An agrin minigene rescues dystrophic symptoms in a mouse model for congenital muscular dystrophy. Nature 413:302–307.

Moore SA, Saito F, Chen J, Michele DE, Henry MD, Messing A, Cohn RD, Ross-Barta SE, Westra S, Williamson RA, Hoshi T, Campbell KP (2002) Deletion of brain dystroglycan recapitulates aspects of congenital muscular dystrophy. Nature 418:422–425.

Neumann FR, Bittcher G, Annies M, Schumacher B, Kroger S, Ruegg MA (2001) An alternative amino-terminus expressed in the central nervous system converts agrin to a type II transmembrane protein. Mol Cell Neurosci 17:208–225.

Nishita M, Yoo SK, Nomachi A, Kani S, Sougawa N, Ohta Y, Takada S, Kikuchi A, Minami Y (2006) Filopodia formation mediated by receptor tyrosine kinase Ror2 is required for Wnt5a-induced cell migration. J Cell Biol 175:555–562.

O'Connor LT, Lauterborn JC, Gall CM, Smith MA (1994) Localization and alternative splicing of agrin mRNA in adult rat brain: transcripts encoding isoforms that aggregate acetylcholine receptors are not restricted to cholinergic regions. J Neurosci 14:1141–1152.

Paganoni S, Ferreira A (2003) Expression and subcellular localization of Ror tyrosine kinase receptors are developmentally regulated in cultured hippocampal neurons. J Neurosci Res 73:429–440.

Paganoni S, Ferreira A (2005) Neurite extension in central neurons: a novel role for the receptor tyrosine kinases Ror1 and Ror2. J Cell Sci 118:433–446.

Pun S, Sigrist M, Santos AF, Ruegg MA, Sanes JR, Jessell TM, Arber S, Caroni P (2002) An intrinsic distinction in neuromuscular junction assembly and maintenance in different skeletal muscles. Neuron 34:357–370.

Reist NE, Magill C, McMahan UJ (1987) Agrin-like molecules at synaptic sites in normal, denervated, and damaged skeletal muscles. J Cell Biol 105:2457–2469.

Rumbaugh G, Adams JP, Kim JH, Huganir RL (2006) SynGAP regulates synaptic strength and mitogen-activated protein kinases in cultured neurons. Proc Natl Acad Sci USA 103:4344–4351.

Sanes JR, Lichtman JW (2001) Induction, assembly, maturation and maintenance of a postsynaptic apparatus. Nat Rev Neurosci 2:791–805.

Schwarzbraun T, Vincent JB, Schumacher A, Geschwind DH, Oliveira J, Windpassinger C, Ofner L, Ledinegg MK, Kroisel PM, Wagner K, Petek E (2004) Cloning, genomic structure, and expression profiles of TULIP1 (GARNL1), a brain-expressed candidate gene for 14q13-linked neurological phenotypes, and its murine homologue. Genomics 84:577–586.

Scotton P, Bleckmann D, Stebler M, Sciandra F, Brancaccio A, Meier T, Stetefeld J, Ruegg MA (2006) Activation of muscle-specific receptor tyrosine kinase and binding to dystroglycan are regulated by alternative mRNA splicing of agrin. J Biol Chem 281:36835–36845.

Serpinskaya AS, Feng G, Sanes JR, Craig AM (1999) Synapse formation by hippocampal neurons from agrin-deficient mice. Dev Biol 205:65–78.

Shi Y, Ethell IM (2006) Integrins control dendritic spine plasticity in hippocampal neurons through NMDA receptor and Ca2+/calmodulin-dependent protein kinase II-mediated actin reorganization. J Neurosci 26:1813–1822.

Soriano MA, Tessier M, Certa U, Gill R (2000) Parallel gene expression monitoring using oligonucleotide probe arrays of multiple transcripts with an animal model of focal ischemia. J Cereb Blood Flow Metab 20:1045–1055.

Stone DM, Nikolics K (1995) Tissue- and age-specific expression patterns of alternatively spliced agrin mRNA transcripts in embryonic rat suggest novel developmental roles. J Neurosci 15:6767–6778.

Sugita S, Saito F, Tang J, Satz J, Campbell K, Sudhof TC (2001) A stoichiometric complex of neurexins and dystroglycan in brain. J Cell Biol 154:435–445.

Talts JF, Andac Z, Gohring W, Brancaccio A, Timpl R (1999) Binding of the G domains of laminin alpha1 and alpha2 chains and perlecan to heparin, sulfatides, alpha-dystroglycan and several extracellular matrix proteins. EMBO J 18:863–870.

Thaler J, Harrison K, Sharma K, Lettieri K, Kehrl J, Pfaff SL (1999) Active

suppression of interneuron programs within developing motor neurons revealed by analysis of homeodomain factor HB9. Neuron 23:675–687.

Thomas GM, Huganir RL (2004) MAPK cascade signalling and synaptic plasticity. Nat Rev Neurosci 5:173–183.

Tian M, Hagg T, Denisova N, Knusel B, Engvall E, Jucker M (1997) Laminin-alpha2 chain-like antigens in CNS dendritic spines. Brain Res 764:28–38.

Tsen G, Halfter W, Kroger S, Cole GJ (1995) Agrin is a heparan sulfate proteoglycan. J Biol Chem 270:3392–3399.

Valenzuela DM, Stitt TN, DiStefano PS, Rojas E, Mattsson K, Compton DL, Nunez L, Park JS, Stark JL, Gies DR, Thomas S, Le BMM, Fernald AA, Copeland NG, Jenkins NA, Burden SJ, Glass DJ, Yancopoulos GD (1995) Receptor tyrosine kinase specific for the skeletal muscle lineage: expression in embryonic muscle, at the neuromuscular junction, and after injury. Neuron 15:573–584.

Verhage M, Maia AS, Plomp JJ, Brussaard AB, Heeroma JH, Vermeer H, Toonen RF, Hammer RE, van den Berg TK, Missler M, Geuze HJ, Sudhof TC (2000) Synaptic assembly of the brain in the absence of neurotransmitter secretion. Science 287:864–869.

Watanabe M, Fukaya M, Sakimura K, Manabe T, Mishina M, Inoue Y (1998) Selective scarcity of NMDA receptor channel subunits in the stratum lucidum (mossy fibre-recipient layer) of the mouse hippocampal CA3 subfield. Eur J Neurosci 10:478–487.

Yang X, Arber S, William C, Li L, Tanabe Y, Jessell TM, Birchmeier C, Burden SJ (2001) Patterning of muscle acetylcholine receptor gene expression in the absence of motor innervation. Neuron 30:399–410.

Yoda A, Oishi I, Minami Y (2003) Expression and function of the Ror-family receptor tyrosine kinases during development: lessons from genetic analyses of nematodes, mice, and humans. J Recept Signal Transduct Res 23:1–15.

CHAPTER III

APPENDIX

Curriculum Vitae

Name:	Maj Marcin
Home Address:	Rodersdorferstrasse 11,
	4055 Basel, Switzerland
Telephone:	0041 61 3222187, 0041 76 474 87 61
Company Name:	Department of Neurobiology/Pharmacology,
	Biozentrum, University of Basel, Switzerland
	Klingelbergstrasse 50-70, 4056 Basel, Switzerland
Telephone:	+41 61 2672216, +41 76 474 87 61
e-mail address:	marcin.maj@unibas.ch
Birthday:	January 6th, 1975
Nationality:	Polish
Marital Status:	Married, 1 child

Education

May 2003 – present

PhD student

Department of Neurobiology/Pharmacology, Biozentrum, University of Basel, Switzerland (Prof. M. Rüegg Lab)

June 2001

Degree: Master of Sciences, Biology
(Grade 4;   5=maximum)

Thesis: "Seizure-induced changes in the ARPP-21 biosynthesis in rat hippocampus."
(Prof. H. Lach Lab)

September 1996 – June 2001

Student of Biology, Pedagogical Academy, Kraków, Poland

June 1996

Degree: Medical Analysis Technician
(Grade 5;   5=maximum)

September 1994 – June 1996

Student of Medical Analysis, Medical College, Kraków, Poland

May 1994

High School Diploma,
(Grade 5;   5=maximum)

September 1990 – June 1994

M. Sklodowska – Curie High School, Skawina,

Poland

Professional experience

Maj 2003 - present	***PhD student***
	Department of Neurobiology/Pharmacology, Biozentrum, University of Basel, Switzerland (Prof. M. Rüegg Lab)
September 2002 – April 2003	**Research assistant**
	Department of Molecular Neuropharmacology, Institute of Pharmacology, Polish Academy of Sciences, Kraków, Poland, headed by Prof. R. Przewlocki
September 2001 – August 2002	***Trainee***
	Novartis Institutes for BioMedical Research, Neuroscience Research Department, Novartis Pharma AG, Basel, Switzerland (Dr. P.J. Flor Lab)
May 2001 – August 2001	***Research assistant***
	Department of Molecular Neuropharmacology, Institute of Pharmacology, Polish Academy of Sciences, Kraków, Poland, headed by Prof. R. Przewlocki
September 1996 – May 2001	***Engineer and Technician***
	Department of Molecular Neuropharmacology, Institute of Pharmacology, Polish Academy of Sciences, Kraków, Poland, headed by Prof. R. Przewlocki

Scholarships / Awards

IAESTE foreign exchange scholarship for Novartis Pharma AG, Basel

Courses attended

1.   28th – 29th November 2001, FMI Basel, FMI Radiation Safety Course
2.   8th – 12th March 2004, University of Zürich, Introductory Course in Laboratory Animal Science (LTK Module 1E)

Languages:

Polish: Native

English: Fluent

German: Basic

Work Experience / Technical Skills

Molecular Biology

- Extraction of total RNA from several tissues (e.g. brain, muscles, *in vitro* cultures)
- Reverse Transcription and Real Time PCR
- Radioactive labeling of DNA and RNA probes for *in situ* hybridization
- *In situ* hybridization technique
- Cloning of native and chimera proteins cDNA, DNA mutations

Biochemistry

- Extraction of proteins from several tissues (e.g. brain, muscles, *in vitro* cultures)
- Large scale protein expression and purification
- TAP tag purification for protein - protein interactions
- Membrane preparation for functional studies
- Immunoprecipitations
- Surface proteins biotinylation
- Western Blott, 2D gel electrophoresis

Cellular Biology

Mammalian cell culture of various cell lines including CHO, HEK, COS-1, C2C12, Sol-8, C2Y, NIH3T3

Transient and stable expression of expression plasmids in mammalian cells

Animal Handling / Histology

Handling of laboratory animals (mice, rats, rabbits, guinea pigs) (LTK Module 1E)

Intraperitoneal, subcutaneous, intramuscular injections

Preparation of muscles from *post mortem* animals (soleus, TA, EDL, gastrocnemius, diaphragm)

Electroporation of expression plasmids into muscles

Sciatic nerve cut and crush experiments

Seizures experiments using kainic acid (KA) and pentylenetetrazole (PTZ)

Work with cryostat microtome, light and confocal microscope, computer imaging analyzer (MCID system)

Immunostainings

Pharmacology

Functional characterization of cloned glutamate receptors by calcium measurements using recombinant mammalian cells; determination of EC_{50} / IC_{50} values of various compounds

Radioligand-binding assays

Publications

1. Smialowska M., Bajkowska M., Przewlocka B., **Maj M.,** Turchan J., Przewlocki R.
   Effect of 6-hydroxydopamine on neuropeptide Y (NPY) and corticotropin releasing factor
   (CRF) expression in rat amygdala.
   Neuroscience 1999;94:1125-32

2. Calbet M., Guadano-Ferraz A., Spier D. A., **Maj M.,** Sutcliffe J. G., Przewlocki R., de Lecea L.
   Cortistatin and somatostatin mRNAs are differentially regulated in response to kainate
   Molecular Brain Research 1999;72:55-64

3. Smialowska M., Bajkowska M., Hellig M., Obuchowicz E., Turchan J., **Maj M.,** Przewlocki R.
   Pharmacological studies on the monoaminergic influence on the synthesis and expression of
   Neuropeptide Y and Corticotropin Releasing Factor in rat brain Amygdala
   Neuropeptides 2001;35:82-91

4. Chadzinska M., **Maj M.**, Scislowska-Czarnecka A., Przewlocka B., Plytycz B.
   Expression of Proenkephalin (PENK) mRNA in Inflammatory Leukocytes During Experimenta
   Peritonitis in Swiss Mice
   Polish Journal of Pharmacology 2001; 53:715-718

5. Przewlocka B., Sieja A., Starowicz K., **Maj M.**, Bilecki W., Przewlocki R.
   Knockdown of spinal opioid receptors by antisense targeting beta-arrestin reduces morphine
   tolerance and allodynia in rat.
   Neurosci Letters 2002; 325(2):107-10

6. Borghi V., Przewlocka B., Labuz D., **Maj M.**, Obara I., Pavone F.
   Formalin-induced pain and mu-opioid receptor density in brain and spinal cord are modulated
   by A1 and A2a adenosine agonists in mice.
   Brain Research 2002; 956(2):339-48.

7. Turchan J., **Maj M**., Przewlocka B., Przewlocki R.
   Effect of cocaine and amphetamine on biosynthesis of proenkephalin and prodynorphin in
   some regions of the rat limbic system.
   Polish Journal of Pharmacology 2002; 54:367-372

8. **Maj. M.,** Turchan J., Śmiałowska M., Przewłocka B
   Morphine and cocaine influenced CRF biosynthesis in the rat amygdala

Neuropeptides. 2003; 37(2):105-10

9. Turchan J., **Maj M.,** Przewłocka B.

The effect of drugs of abuse on NMDAR1 receptor expression in the rat limbic system

Drug Alcohol Depend. 2003; 72(2):193-6

10. Maj M., Bruno V., Dragic Z., Yamamoto R., Battaglia G., Inderbitzin W., Stoehr N., Stein T., Gasparini F., Vranesic I., Kuhn R., Nicolettiand F., Flor P. J.

(-)-PHCCC, a positive allosteric modulator of mGluR4: Characterization, mechanism of action, and neuroprotection

Neuropharmacology 2003; 45(7):895-906

11. Ksiazek I, Burkhardt C, Lin S, Seddik R, **Maj M**, Bezakova G, Jucker M, Arber S, Caroni P, Sanes JR, Bettler B, Ruegg MA.

Synapse loss in cortex of agrin-deficient mice following genetic rescue of perinatal death

J Neurosci. 2007 27(27):7183-95.

12. Gabriela Bezakova, C. Florian Bentzinger, **Marcin Maj**, Ulrich Certa, Hans-Rudolf Brenner, Markus A. Ruegg

The mitogen-activated protein kinase phosphatase, MKP-1, controls postsynaptic differentiation at nerve-muscle synapses **(submitted)**

13**.** Shuo Lin, **Marcin Maj**, Gabriela Bezakova, Josef P. Magyar, Hans Rudolf Brenner and Markus A. Ruegg

Muscle-wide secretion of a miniaturized form of neural agrin rescues focal neuromuscular innervation in agrin mutant mice **(submitted)**

14. **Maj M.,** Lin S., Ruegg M.A.

MuSK alone is sufficient to respond to neural agrin in muscle (**in preparation)**

References and Letters of Recommendation (upon request):

Dr. Peter J. Flor

Novartis Institutes for BioMedical Research, Neuroscience Research Department,

Novartis Pharma AG, K-125.6.08, CH-4002 Basel, Switzerland

Tel: 0041-61-6964218

Fax: 0041-61-6962809

e-mail: peter_josef.flor@pharma.novartis.com

Prof. Ryszard Przewlocki

Department of Molecular Neuropharmacology,

Institute of Pharmacology, Polish Academy of Sciences,

Smetna St 12, 31-343 Kraków, Poland

Tel: 0048-12-6623218,

Fax: 0048-12-6374500

e-mail: nfprzewl@cyf-kr.edu.pl

Prof. Markus A. Rüegg

Department of Neurobiology/Pharmacology,

 Biozentrum, University of Basel,

Klingelbergstrasse 50-70, 4056 Basel Switzerland

Tel: 0041612672225

e-mail: markus-a.ruegg@unibas.ch

Acknowledgment

First of all, I would like to express my deepest sense of gratitude to my supervisor Prof. Markus A. Ruegg for his patient guidance, encouragement and excellent advices throughout this study.

Prof. Martin Spiess and Dr. Thomas Meier deserve also special thanks as my thesis committee members.

I am deeply and forever indebted to my family for their unflagging love and support throughout my life. Especially, I would like to thank my parents Janusz and Wiesława. I am also very grateful to my sister Joanna.

My sincere thanks go to my wife Katarzyna for her love and patience during the PhD period. One of the best experiences that we lived through in this period was the birth of our son, Grzegorz, who provided an additional and joyful dimension to our life mission. All I have achieved until now including my private and professional life would not be possible without them.

Finally, it gives me a great pleasure to express my cardinal thanks to the present and former members of Prof. Ruegg's lab, (especially Dr. Patrick Scotton, Dr. Shuo Lin, Dr. Gabriela Bezakova, Alexander Kriz, Filippo Oliveri), and all the people working with me during my PhD study.

Last but not least, thanks be to God for giving me my life and for guiding me through all the days in the past five years. May your name be exalted, honored, and glorified. "Bądź wywyższony, Boże, ponad niebo, a Twoja chwała ponad całą ziemię!" (Ps. 57;12)